Insight into the role of the Dual Specificity Phosphatase 3 in non-alcoholic fatty liver disease and insulin resistance

Sophie Jacques

Promotor : Souad Rahmouni, PhD
Co-promotor : Cécile Oury, PhD

University of Liège
Faculty of Medicine
Laboratory of Animal Genomics
GIGA-Research

Thesis submitted in partial fulfillment of the requirements for the degree of Doctor in Biomedical and Pharmaceutical Sciences

Academic year 2020-2021

ACKNOWLEDGEMENTS

Cette thèse n'aurait pas vu le jour sans le soutien de nombreuses personnes, que je tiens à remercier.

Je tiens tout d'abord à remercier ma promotrice, Souad Rahmouni. Souad, merci de m'avoir accueillie dans ton laboratoire, et de m'avoir permis de mener à bien ce projet. Merci de m'avoir encadrée, et d'avoir cru en moi, jusqu'à la dernière minute. Tes conseils et ta confiance ont été deux moteurs importants pour moi. Je suis heureuse d'avoir pu travailler avec toi, j'ai appris énormément. Je tiens également à te remercier pour toutes les opportunités que tu m'as présentées, que ce soit au niveau des congrès, du choix des expériences, ou pour mon futur.

J'aimerais remercier Michel Georges de m'avoir accueillie au sein de son laboratoire et de m'avoir permis d'y poursuivre mon projet de thèse.

Je tiens également à remercier ma co-promotrice, Cécile Oury, qui m'a accueillie dans son laboratoire et au sein de son équipe durant une période de ma thèse. Merci pour vos conseils, notamment lors des réunions de mon comité de thèse.

Merci aux autres membres de mon comité de thèse : Ingrid Struman, Nor Eddine Sounni et Emmanuel Dejardin. Merci pour vos conseils et votre guidance au cours de ces cinq années de thèse. Merci également aux membres invités, Nicolas Paquot et Michel Moutschen. Merci d'avoir pris le temps de me donner votre vision clinique de mon projet.

La réalisation de ce travail n'aurait pas été possible sans le soutien financier du Fond National de la Recherche Scientifique (F.R.S.-FNRS), du Télévie, de l'ULiège et de la Fondation Léon-Frédéricq.

Merci également à tous les membres des différentes plateformes du GIGA, qui m'ont permis de construire ce projet. Merci à Manu, François et Alexandra pour les productions virales. Merci à Chantal Humblet, Tiffany et Hülya pour tout le travail d'histologie effectué ! Merci à Sandra et Jean-Jacques de m'avoir guidée dans l'utilisation des microscopes. Merci Alex pour les analyses informatiques. Merci à Lati, Manon et Emilie pour le séquençage et vos bons conseils. Merci à Arnaud et

Alice, pour votre aide précieuse dans l'analyse du RNAseq. Merci à tous les membres de l'animalerie. J'aimerais également remercier Philippe Delvenne et Partick Collins d'avoir pris le temps d'analyser et de scorer mes échantillons.

Une thèse, c'est aussi l'occasion de créer des liens avec nos collègues, ces personnes sans qui le travail serait beaucoup moins marrant. Maud, merci de m'avoir encadrée lors de mes premiers pas dans le laboratoire. Arash, thank you for sharing a piece of this project with me. J'ai apprécié travailler avec vous ! Merci à tous les membres du LTH de m'avoir accueillie dans votre laboratoire, et pour tous les conseils que vous avez pu me donner. Nathalie, Odile, Nicolas, Lucy, Laurence, Céline[2], Alex, Alexia, Maxime, merci pour toutes les fois où je suis venue vous demander de l'aide. Et ensuite, j'ai rencontré toute une nouvelle et grande équipe. Myriam, merci de m'avoir accueillie dans cette nouvelle équipe. Merci pour ta gentillesse et pour les expériences de dernière minute. Marie, tes bavardages et ta bonne humeur vont me manquer ! Merci d'avoir été ma victime pour les westernblot. Hélène, merci pour tes analyses du RNAseq et ta disponibilité. Tu m'as été d'une aide précieuse ! Yumie, Sam, Samira, Nicolas merci pour votre bonne humeur, votre présence et votre soutien. Merci également à Vincent, Jérôme et Virginie pour votre aide et vos conseils. Et merci à tous les membres du laboratoire de génomique animale. Ça a été un plaisir de travailler avec vous et de partager les activités de labo avec vous !

Et puis il y a les amis, qui pendant 5 ans ont entendu parler de cette thèse et m'ont encouragée. Les amis sans qui je ne serais sûrement pas arriver jusqu'ici.

Merci aux SBIMettes d'avoir été là tout au long de ce parcours. Stella, je suis tellement heureuse que tu aies été au GIGA pendant une bonne partie de ma thèse ! Ton amitié et ta folie m'ont été très précieuses. Merci pour les (nombreuses) pauses thé. Megan, merci de m'avoir écoutée pendant nos sorties courses, qui m'ont fait un bien fou ! Même celles de 6h du matin, mêmes celles sous la neige. Justine, merci pour ta bonne humeur et tes expressions uniques. Odile, tu as été une présence calme et rassurante. Yas, même si tu as fui à l'autre bout du monde, merci pour ton soutien sans frontière. Tout ce parcours n'aurait pas été pareil sans vous.

Merci à Fallone, Lola et Anaïs. Même si vous n'avez aucune idée de ce que je fais, vous avez vécu cette thèse avec moi. Merci pour vos encouragements et votre soutien.

Merci pour les soupers, les escapades, les soirées karaoké, les pique-niques. Merci d'être là depuis autant d'années. Fallone, j'ai bien cherché, et j'ai un peu trouvé.

Merci à Fiona et Margot, mes deux pharmaciennes préférées. Merci pour votre présence et tous les pique-niques, les soupers, les soirées, le verre en terrasse.

Finalement, un énorme merci à ma famille et à ma belle-famille. Je ne vous dirai jamais assez merci pour tous vos encouragements, votre soutien, votre présence. Merci d'avoir cru en moi. Souvent plus que moi-même. Papa, Maman, merci de m'avoir permis d'être là où je suis aujourd'hui. Bertrand, merci pour tout. Merci d'avoir vécu (subi ?) cette thèse avec moi. Merci de m'avoir écoutée, de m'avoir poussée en avant et d'y avoir cru jusqu'au bout.

ABSTRACT

Non-alcoholic fatty liver disease (NAFLD) is the most common chronic liver disease in Western countries. It encompasses a broad spectrum of liver conditions ranging from simple steatosis to the more severe and progressive disease, non-alcoholic steatohepatitis (NASH) that can lead to hepatocellular carcinoma (HCC). Obesity and related metabolic syndrome and insulin resistance are important risk factors for the development of NAFLD, NASH and HCC. We investigated the impact of DUSP3 deficiency in metabolic syndrome manifestations and in HCC using a knockout (KO) mouse model. While aging, DUSP3-KO mice became obese and exhibited insulin resistance. These phenotypes were exacerbated under HFD and were accompanied by NAFLD and associated liver damages. In addition, DEN administration combined to HFD led to a rapid HCC development compared to WT mice. DUSP3-KO mice had more serum triglycerides, cholesterol, AST and ALT than control WT mice under both regular chow diet (CD) and HFD. The level of fasting insulin was higher compared to WT mice, though, fasting glucose as well as glucose tolerance were similar to those of control mice. At the molecular levels, HFD led to a decrease of DUSP3 expression at both protein and RNA levels. Under CD, DUSP3 deletion was associated with increased phosphorylation of the insulin receptor (IR) and subsequently, with higher activation of the downstream signaling pathway. The difference of IR phosphorylation was maintained between mutant and WT mice under HFD. However, IR downstream signaling pathway was equally activated in both groups of mice. Liver RNA sequencing and differential expression genes analysis demonstrated the effect of the diet on the expression of several genes, including genes from lipid metabolism. Gene set enrichment analysis highlighted pathways specifically regulated in DUSP3-KO mice, such as fatty acid metabolism and DNA repair pathways.

Collectively, our results support a new role for DUSP3 in obesity, insulin resistance, NAFLD and liver damage.

RÉSUMÉ

La maladie du foie gras non alcoolique (NAFLD en anglais) est la pathologie affectant le foie la plus répandue dans les pays occidentaux. Elle comprend un large spectre de pathologies hépatiques, allant de la simple stéatose à une forme plus sévère de la maladie, la stéatose hépatite non alcoolique (NASH en anglais). Cette dernière peut évoluer vers un carcinome hépatocellulaire (CHC). L'obésité, ainsi que le syndrome métabolique et la résistance à l'insuline qui y sont associés, sont des facteurs de risque importants pour le développement du NAFLD, NASH et CHC. Nous avons étudié l'impact de l'absence de DUSP3 dans les manifestations du syndrome métabolique et dans le développement du HCH en utilisant un modèle de souris déficientes pour cette phosphatase (souris DUSP3-KO). En vieillissant, les souris DUSP3-KO deviennent obèses et présentent une résistance à l'insuline. Ce phénotype est exacerbé par une nourriture riche en graisse (HFD) et est accompagné du développent d'une stéatose hépatique, ainsi que les lésions hépatiques associées. De plus, l'administration du carcinogène DEN combinée à la HFD entraînait un développement rapide du CHC chez les souris DUSP3-KO, en comparaison des souris contrôles (WT). Les souris DUSP3-KO présentaient également des niveaux sanguins plus élevés de triglycérides, de cholestérols, d'AST et d'ALT, par rapport aux souris WT, aussi bien lorsqu'elles étaient nourries avec une nourriture classique (CD) qu'avec une HFD. Le niveau d'insuline à jeun dans le sang était plus élevé chez les souris DUSP3-KO, comparées au souris WT, bien que le niveau de glucose à jeun ainsi que la tolérance au glucose étaient similaires à ceux du groupe de souris contrôles. Au niveau moléculaire, la HFD entraînait une diminution de l'expression de DUSP3, tant au niveau protéique qu'au niveau de l'ARN. Sous CD, la délétion de DUSP3 était associée avec une augmentation de la phosphorylation du récepteur à l'insuline, et consécutivement, avec une activation plus importante des voies de signalisation en aval. La différence de phosphorylation du récepteur à l'insuline était maintenue entre les souris mutantes et les souris WT sous HFD. Cependant, les voies de signalisation en aval du récepteur à l'insuline étaient activées de manière similaire dans les deux groupes de souris. Le séquençage des ARN messagers extraits des foies des souris et une analyse de l'expression différentielle des gènes ont souligné l'effet de la nourriture sur

l'expression de différents gènes, y compris l'expression de gènes impliqués dans le métabolisme lipidique. Une analyse de l'enrichissement d'ensembles de gènes a souligné certaines voies de signalisation spécifiquement régulées chez les souris DUSP3-KO, telles que la voie du métabolisme des acides gras ou encore la voie de la réparation de l'ADN.

En conclusion, ces résultats supportent un nouveau rôle pour DUSP3 dans l'obésité, la résistance à l'insuline, le NAFLD et les lésions hépatiques.

ABBREVIATIONS

18F-FDG	Fluorodeoxyglucose F 18
AAV	Adeno-associated virus
A-DUSP	Atypical dual specificity phosphatase
ALD	Alcoholic liver disease
ALT	Alanine aminotransferase
AMPK	AMP-activated protein kinase
AST	Aspartate aminotransferase
AT	Adipose tissue
ATM	Ataxia Telangiectasia Mutated
ATP	Adenosine triphosphate
BAD	BCL2-associated agonist of cell death
BAT	Brown adipose tissue
bFGF	Basic fibroblast growth factor
BMI	Body mass index
CD	Chow diet
cDNA	complementary DNA
ChREBP	Carbohydrate-responsive element binding protein
CRP	c-reactive protein
CT	Computed tomography
CTC	Circulating tumor cells
DAB	3'-Diaminobenzidine
DAMPs	Danger-associated molecular patterns
DAPI	4′,6-diamidino-2-phenylindole
DDR	DNA damage response
DEN	Diethylnitrosamine
DNA	Deoxyribonucleic acid
DNL	*De novo* lipogenesis
DUSP	Dual specificity phosphatase
eGFP	Enhanced green fluorescent protein
EGFR	Epidermal growth factor receptor
ER	Endoplasmic reticulum
ERK	Extracellular-signal-regulated kinases
FA	Fatty acid
FAK	Focal adhesion kinase
FASN	Fatty acid synthase
FDR	False Discovery Rate
FFA	Free fatty acid
GCK	Glucokinase
GKS3	Glycogen synthase kinase 3

GSEA	Gene set enrichment analysis
GWAS	Genome wide association studies
H&E	Hematoxylin and eosin
HCC	Hepatocellular carcinoma
HDL	High-density lipoprotein
HFD	High fat diet
HnRNP	Heterogeneous nuclear ribonucleoprotein
HOMA-IR	Homeostatic model assessment for insulin resistance
HRP	Horseradish peroxidase
HSC	Hepatic stellate cells
IFN	Interferon
IGF	Insulin-like growth factor
IL	Interleukin
IR	Insulin receptor
IRES	Internal ribosome entry site
IRS	Insulin receptor substrate
JNK	c-Jun N-terminal kinases
KDM2A	Histone lysine demethylase
KGFR	Keratinocyte growth factor receptor
KO	Knockout
LDL	Low-density lipoprotein
LEPR	Leptin receptor
LLC	Lewis Lung Carcinoma
LPS	Lipopolysaccharide
MAPK	Mitogen-activated protein kinases
MBOAT7	Membrane bound O-acyltransferase domain-containing 7
MCD	Methionine/choline deficient
MEK	Mitogen-activated protein kinase kinase
MKP	MAP kinase phosphatase
mRNA	Messenger RNA
mTORC	Mammalian target of rapamycin
NAFLD	Nonalcoholic fatty liver disease
NASH	Nonalcoholic steatohepatitis
NMR	Nuclear magnetic resonance
NPM	Nucleophosmin
NSCLC	Non-small cell lung cancer
NUCL	Nucleolin
OGTT	Oral glucose tolerance test
PAMPs	Pathogen-associated molecular protein
PBS	Phosphate buffer saline
PCA	Principal component analysis
PCR	Polymerase chain reaction

PDGFR	Platelet-derived growth factor receptor
PDK1	Pyruvate dehydrogenase kinase 1
PET	Positron emission tomography
PI3K	Phosphoinositide 3-kinase
PKC	Protein kinase C
PNPLA3	Patatin-like phospholipase domain-containing 3
PPM	Protein phosphatase metal
PPP	Phosphoprotein phosphatase
p-Ser	Phospho-serine
PSTP	Protein serine/threonine phosphatase
PTEN	Phosphatase and tensin homolog
p-Thr	Phospho-threonine
PTP	Protein tyrosine phosphatase
PTP1B	Protein tyrosine phosphatase 1B
p-Tyr	Phospho-tyrosine
RNA	Ribonucleic acid
ROS	Reactive oxygen species
shRNA	Short hairpin RNA
SREBF	Sterol regulatory element-binding factor
STAT	Signal transducer and activator of transcription
TBG	Thyroxine-binding globulin
TCPTP	T cell protein tyrosine phosphatase
TCR	T-cell receptor
TG	Triglycerides
TLR	Toll-like receptor
TM6SF2	Transmembrane 6 superfamily member 2
TNF	Tumor necrosis factor
Tyk2	Tyrosine Kinase 2
UPR	Unfolded protein response
VHR	VH1-related phosphatase
VLDL	Very-low-density-lipoprotein
VRK3	Vaccinia-related kinase 3
WAT	White adipose tissue
WHO	World health organization
WT	Wild type

TABLE OF CONTENTS

ACKNOWLEDGEMENTS ..... **I**

ABSTRACT ..... **V**

RÉSUMÉ ..... **VII**

ABBREVIATIONS ..... **IX**

TABLE OF CONTENTS ..... **XIII**

INTRODUCTION **1**

1. Protein tyrosine phosphatases **1**
1.1 Definition and classification 1
1.2 DUSP3 2
1.2.1 DUSP3 substrates 3
1.2.2 Regulation of DUSP3 phosphatase activity 4
1.2.3 Physiological roles of DUSP3 5
1.2.4 DUSP3 in diseases 6

2. Obesity and associated pathologies **7**
2.1 Definition and prevalence of obesity 7
2.2 Metabolic syndrome 8
2.3 Insulin resistance 9
2.3.1 Insulin and insulin signaling pathway 10
2.3.2 Insulin resistance pathophysiology 12
2.4 Type 2 diabetes 14
2.5 Nonalcoholic fatty liver disease and NALFD-induced hepatocellular carcinoma 14
2.5.1 Definition and prevalence of NAFLD 14
2.5.2 Definition and prevalence of HCC 16
2.5.3 Mechanisms and pathogenesis of NAFLD and NAFLD-induced HCC 19
2.5.3.1 Sources of fatty acids in the liver 19
2.5.3.2 Insulin 22
2.5.3.3 ER stress 23
2.5.3.4 DNA damage and cell death 23
2.5.3.5 The inflammasome 24
2.5.3.6 Inflammation and immune cells 25
2.5.3.7 Microbiome 27
2.5.3.8 Fibrogenesis 28
2.5.3.9 Genetics and epigenetics 29

2.5.4 Diagnosis and management 31
2.6 Protein tyrosine phosphatases in NAFLD and HCC 33
2.6.1 Cys-based PTP, class I, subclass I 33
2.6.2 DUSPs (cys-based PTPs, class I, subclass II) 34
2.6.2.1 MKPs 34
2.6.2.2 A-DUSPs 35
2.6.2.3 Other DUSPs 36

OBJECTIVES 39

MATERIALS AND METHODS 43
Mice 43
Obesity model 43
MicroCT imaging 44
Glucose tolerance assay 45
^{18}F-FDG biodistribution 45
DEN-induced hepatocarcinogenesis mouse model 45
shRNA lentiviral plasmids and HepG2 transduction 46
Ectopic xenograft of HepG2 cells in NOD/SCID mice 47
Adeno-associated virus production and *in vivo* reconstitution of DUSP3 expression in the liver of DUSP3-KO mice 47
Serological analysis 49
HOMA-IR 50
Proliferation assay 50
Adipocytes size assessment 50
Liver histology 50
Immunohistochemistry 52
Immunofluorescence staining 53
Tissue homogenization and Western blot 53
RNA extraction 54
RNA sequencing 54
Differential gene expression analysis 54
Gene Set Enrichment Analysis (GSEA) analysis 55
qRT-PCR 55
Statistical analysis 56

RESULTS 59
DUSP3-KO mice become obese while aging 59
DUSP3 deletion promotes fat accumulation in mice body 61
DUSP3-KO mice show modifications in serum triglycerides, cholesterol and CRP concentrations 63
DUSP3 deletion promotes NAFLD, NASH, fibrosis and HCC under HFD 65
DUSP3 deletion promotes leukocytes infiltration in the liver under HFD 69
DUSP3 deficiency exacerbates HFD-induced insulin resistance 71

DUSP3 deletion does not modify glucose distribution 75
DUSP3 expression is reduced under HFD and its genetic deletion enhances IR phosphorylation and signaling.....77
Analysis of differential gene expression by RNA sequencing 80
DUSP3 deletion promotes HCC development in an *in vivo* model of carcinogenesis 94
DUSP3 deletion alters cholesterol but not triglycerides metabolism under HFD .99
DUSP3 deletion promotes insulin resistance in DEN-induced hepatocarcinogenesis.....101
DUSP3 deletion does not affect HepG2 cells growth 101
Liver-specific DUSP3 expression in DUSP3-KO mice 103
DUSP3 reconstitution in the liver does not alter triglycerides or cholesterol metabolism 107
DUSP3 reconstitution in the liver increased fasting insulin concentration 109
DUSP3 expression reconstitution in the liver does not affect the number of tumors in DEN-induced hepatocarcinogenesis model.....110

DISCUSSION AND PERSPECTIVES.....117

SUPPLEMENTARY DATA.....131

1. Supplementary figures.....131

2. Supplementary tables.....133

REFERENCES.....149

Introduction

INTRODUCTION

1. Protein tyrosine phosphatases

1.1 Definition and classification

Reversible phosphorylation of proteins regulates numerous signaling pathways and cellular processes, such as migration, proliferation, differentiation, immunity and apoptosis. Phosphorylation is controlled by two major actors: protein kinases, which transfer phosphate from ATP to the substrate and by protein phosphatases, which reverse this action. Phosphorylation is an efficient way to control cellular response to diverse signals. Indeed, this mechanism is fast, it does not involve new protein synthesis and it is easily reverted [1].

Protein phosphatases are historically classified into two groups based on their substrate specificity: the protein serine/threonine phosphatases (PSTPs) family and the protein tyrosine phosphatases (PTPs) family. PSTPs include the phosphoprotein phosphatases (PPPs) class and the protein phosphatases metal (PPMs) class. We will not discuss this family as it is not the focus of our research.

PTPs were classified by Alonso *et al.* in subfamilies on the basis of the amino acid sequences of their catalytic domains (Figure I.1): the cysteine-based phosphatases, containing a conserved catalytic motif CXXXXXR, the aspartic-based phosphatases and the histidine-based phosphatases [2,3]. Cys-based phosphatases are grouped into three classes and six subclasses. The human extended PTP family contains 125 proteins, of which 40 are selective for phospho-tyrosine.

Most of the identified PTP are part of the class I. VH1-like or dual-specificity phosphatases (DUSPs) constitute the largest and most heterogeneous group among the class I of cysteine-based PTPs. Compared to the classical PTPs, DUSPs display a broader and shallower catalytic pocket, allowing them to dephosphorylate both phospho-tyrosine (p-Tyr) and phospho-serine/phospho-threonine (p-Ser/p-Thr) residues [4], but also non-peptidic substrates such as phospho-inositides [5], messenger RNA [6] and glycans [7]. DUSPs can be divided into seven groups based on the presence of specific domains and sequence similarity [2]: slingshots, PRLs,

CDC14s, phosphatase and tensin homolog (PTENs), myotubularins, MAP kinase phosphatases (MKPs) and atypical (A-DUSPs). MKPs and A-DUSPs are part of the two major families and are evolutionary and structurally related. MKPs inactivate the mitogen-activated protein kinases (MAPKs) by dephosphorylation. The MKPs have an overlapping and distinct sub-cellular localization, expression pattern, and substrate specificity toward the MAPK family members [8]. A-DUSPs form a group of 20 members. They contain the consensus DUSP catalytic domain but lack the N-terminal CH2 domain found in MKPs. The relationship between A-DUSPs and MAPK is complex and not well defined. However, it has been demonstrated that A-DUSPs have a vast range of substrate specificity and physiological roles.

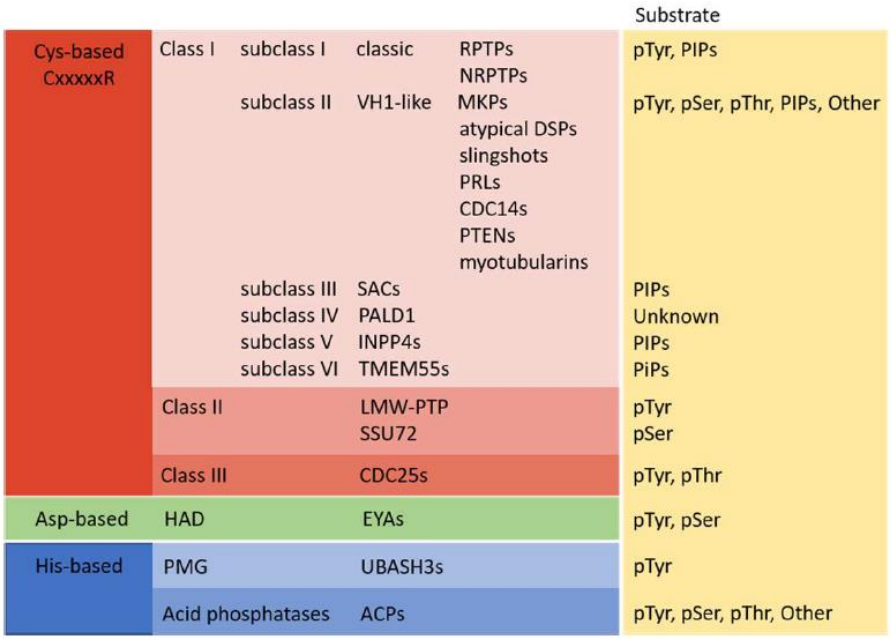

Figure I.1. Protein tyrosine phosphatases (PTPs) classification. PTPs are grouped based on their nucleophilic catalytic residue: Cys-based PTPs, Asp-based PTPs and His-based PTPs. The generic substrates targeted by each family are indicated in the right column. Adapted from [2].

1.2 DUSP3

In 1992, Ishibashi *et al.* identified a new PTP using an expression cloning strategy [9]. The protein was named VH1-related phosphatase (VHR) due to its resemblance with the Vaccinia virus protein VH1. VHR/DUSP3 is a small A-DUSP with only 185 amino acids and a molecular weight of 21 kDa. It is encoded by the *DUSP3* gene located on chromosome 17q21 in humans, and on chromosome 11 in mice. DUSP3 is

relatively conserved during evolution. Indeed, the human and mouse protein share a 92.98% sequence identity. DUSP3 is ubiquitously expressed in the body, though it is highly expressed in platelets and macrophages [10]. Its phosphatase activity can target both p-Ser/p-Thr and p-Tyr residues, with a preference for p-Tyr residues. Moreover, DUSP3 seems to target preferentially bi-phosphorylated residues over mono-phosphorylated ones [11].

1.2.1 DUSP3 substrates

In their first *in vitro* study, Ishibashi *et al.* showed that DUSP3 can dephosphorylate platelet-derived growth factor receptor (PDGFR), epidermal growth factor receptor (EGFR), keratinocyte growth factor receptor (KGFR) and insulin receptor (IR). Since then, other targets have been reported (Figure I.2) including the MAPKs ERK1/2 [12–14], c-Jun N-terminal kinase (JNK) [13,15] and to a lesser extent p38 MAPK [16]. Hoyt *et al.* showed that DUSP3 selectively dephosphorylates tyrosine-phosphorylated STAT5 after activation by IFN-α and β. This leads to the inhibition of STAT5 function [17]. However, this study was not confirmed by other investigators including our host laboratory. ErbB2 was also reported as a potential DUSP3 substrate in non-small cell lung cancer (NSCLC) H1299 cells [18]. Panico and Forti designed a proteomic study that led to the discovery of three additional new substrates, namely nucleolin (NUCL), nucleophosmin (NPM) and heterogeneous nuclear ribonucleoprotein (HnRNP) C1/C2. These three proteins have previously been linked to DNA damage response (DDR) and repair [19]. DUSP3 was also shown to be involved in protein kinase C (PKC) signaling in HUVEC cells. Its downregulation in these cells led to a hyper-phosphorylation of PKC at basal level and after bFGF stimulation [20]. More recently, Chen *et al.* revealed new physiological substrates of DUSP3 in both mouse embryonic fibroblasts and lung epithelial cells derived from DUSP3 knockout (DUSP3-KO) mice: EGFR and focal adhesion kinase (FAK) [21].

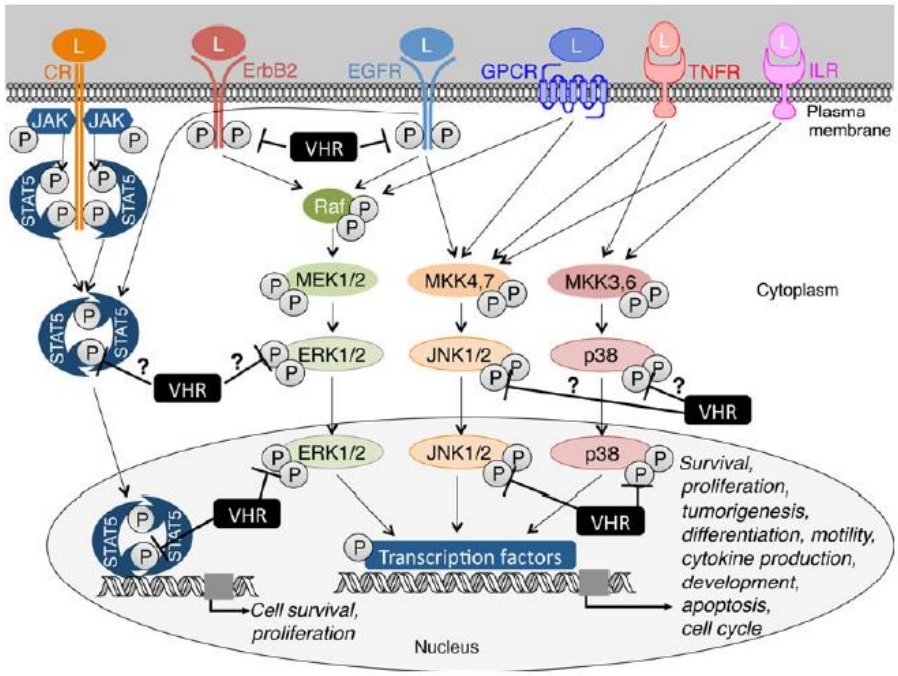

Figure I.2. Reported potential physiological substrates of DUSP3 (STAT5, ERK1/2, JNK1/2, p38, EGFR, ErbB2) and their involvement in different pathways (simplified). The question marks signify that it is unclear if DUSP3 acts on the MAPKs ERk1/2, JNK1/2 and p38 also in the cytoplasm in addition to the nucleus. L (ligand) = hormones, growth factors, cytokines, interleukins, stress stimuli, lipopolysaccharide, mitogens, GPCR activation (corresponding to the receptors); ILR = interleukin receptor; TNFR = tumor necrosis factor receptor; GPCR = G-protein coupled receptor; CR = cytokine receptor. Adapted from [22].

1.2.2 Regulation of DUSP3 phosphatase activity

A few processes have been proposed for the regulation of DUSP3 activity. One of them is the negative regulation by oxidation. Indeed, PTPs are sensitive to oxidation of their catalytic cysteine. It was demonstrated *in vitro* that the oxidation of DUSP3 by H_2O_2 leads to reversible inactivation of the phosphatase [23]. This theory was later confirmed *in vivo* by Wentworth *et al*. who showed that commensal bacteria-induced generation of reactive oxygen species (ROS) can lead to the direct oxidative inactivation of DUSP3 phosphatase activity against ERK1/2 [24]. However, DUSP3 is resistant to irreversible oxidative damage [23]. A possible explanation for this resistance could be the formation of dimers. Indeed, it was shown that DUSP3 can form dimers, which could block its active site and protect it from over-oxidation [25]. This dimerization has also been proposed as a novel negative regulatory mechanism,

since the formation of dimers results in a reduced catalytic activity of the phosphatase [25]. Moreover, in a cancer-related study, *DUSP3* gene was identified as a target of the histone lysine demethylase KDM2A. DUSP3 expression was increased in KDM2A knockdown NSCLC cells, leading to a decrease of ERK1/2 activity [14]. However, it is unclear whether this repression is specific to the pathological context or if it is a physiological mechanism of DUSP3 regulation.

In T cells, upon TCR stimulation by antigen, DUSP3 is phosphorylated at Tyr138 by the protein tyrosine kinase ZAP-70 [26]. This event subsequently inhibits ERK2 and JNK MAPKs activity. It is possible that this phosphorylation enhances the phosphatase activity of DUSP3, probably by affecting its protein-protein interaction, its cellular localization or its substrate targeting. Similarly, the tyrosine kinase Tyk2 is required for the phosphorylation at Tyr138 of DUSP3 and subsequently, its activation in HEK293T cells [17]. Moreover, it was demonstrated in neuronal cell lines that Vaccinia-related kinase 3 (VRK3) suppresses ERK activity through direct binding of DUSP3 [27]. This interaction between VRK3 and DUSP3 enhances DUSP3 phosphatase activity by mechanisms independent of its kinase activity [27].

1.2.3 Physiological roles of DUSP3

DUSP3 regulates cell-cycle progression by modulating ERK and JNK activation in a cell-cycle phase-dependent manner and is itself modulated during the cell cycle [28]. DUSP3 downregulation by RNA interference in HeLa cells stops cell proliferation and cell cycle progression in G1/S and G2/M transition and induces senescence initiation. It was later demonstrated that DUSP3 plays a role in the control of ERK1/2 activity in dividing HeLa cells to facilitate normal spindle assembly [29]. Using the DUSP3 knockout mouse, Amand *et al*. showed that DUSP3 is also a key player in tubulogenesis by regulating the bFGF-induced endothelial cell sprouting through the PKC signaling pathway [20]. Another function of DUSP3 was revealed in platelet activation and thrombosis. Musumeci *et al.* demonstrated that DUSP3 plays a key role in arterial thrombosis through a mechanism involving GPVI and CLEC-2 signaling pathways, but is dispensable for primary hemostasis [30]. DUSP3 also participates in regulating the formation and disassembly of focal adhesion via its action on FAK [21]. Moreover, pharmacological inhibition of DUSP3 in HeLa and MeWo tumor cell lines

and in normal human cell lines increases their sensitivities to gamma ionizing radiation [31]. This indicates a potential role for DUSP3 in DNA repair.

1.2.4 DUSP3 in diseases

DUSP3 is downregulated in some human cancers, such as breast cancer and NSCLC. In breast cancer, it was shown that its expression was decreased upon overexpression of breast cancer 1 (BRCA1)-IRIS. This downregulation correlates with the activation of cyclin D1 expression and provides a growth advantage to tumor cells [32]. In NSCLC, the reduced expression of DUSP3 improved ErbB signaling, causing cancer progression [18]. Moreover, as previously mentioned, in another model of NSCLC, the repression of DUSP3 by KDM2A methylation was associated with tumorigenesis and metastasis [14]. Using a Lewis Lung Carcinoma (LLC) cells experimental metastasis model, Vandereyken *et al.* showed that DUSP3 can also act as an anti-metastatic agent by regulating the migration of monocytes and macrophages to the site of metastasis [33].

On the other hand, DUSP3 is overexpressed in prostate cancer and in several cervix cancer cell lines and *in situ* in cervical cancer. An overexpression of DUSP3 was observed in human prostate cancer, conferring cancer cells a JNK-mediated resistance to apoptosis [34]. In cervix cancer cell lines, the overexpression of DUSP3 may facilitate the cancer cell proliferation by preventing the activation of ERK and JNK [35]. Due to its role in angiogenesis, DUSP3 may also play a role in angiogenesis in cancer. After injection of LLC, DUSP3 knockout mice presented reduced hemoglobin content in the tumors compared to control mice [20]. LLC tumors size in the knockout mice was reduced. This suggests that DUSP3-deficiency leads to a defective tumor-induced angiogenesis.

Altogether, these results suggest that DUSP3 exerts both tumor-suppressive and oncogenic activities depending on the cell types or the model used to study DUSP3. DUSP3 targets different substrates depending on the cell type, thus DUSP3 could have different effects in tumor development. This contradictory role is not unique to DUSP3 and was also reported for other PTP. For example, Shp2 was described as both a tumor-suppressor in HCC and a proto-oncogene in leukemogenesis [36]. The

underlying mechanisms for these paradoxical effects are not fully understood either. Shp2 acts to mediate pro-survival and mitogenic signals both in hepatocytes and in hematopoietic cells. Activating mutation of Shp2 have been found in leukemogenesis. On the other hand, removal of Shp2 in hepatocytes causes chronic hepatic damage and injury, leading to tumorigenesis. Further investigations are therefore required to better understand the molecular and cellular mechanisms, and the conditions in which DUSP3 plays as a proto-oncogene or as a tumor-suppressor molecule.

Besides its role in cancer, DUSP3 also displays a role in acute inflammation. DUSP3-KO mice are protected from sepsis and septic shock through a mechanism involving M2-like macrophage polarization and a reduction of TNF-α production [10]. Another study reported that DUSP3 deletion confers resistance to lipopolysaccharide (LPS)-induced lethality and to polymicrobial-induced septic shock in female mice but not in males, showing that sepsis resistance is gender dependent [37]. The role of female sex hormones in the phenotype was highlighted using bone marrow transplantation and ovariectomized mice. In ovariectomized and male mice the dominance of M2-like macrophages observed in DUSP3-KO female mice was lost. This confirmed the role of M2-like macrophages in sepsis tolerance. In DUSP3-KO female peritoneal macrophages stimulated *ex vivo* by LPS, ERK1/2, PI3K and Akt were hypo-phosphorylated [37].

2. Obesity and associated pathologies

2.1 Definition and prevalence of obesity

Over the last decades, overweight and obesity have become a major health issue worldwide. Overweight is defined as abnormal or excessive fat accumulation that presents a risk to health. A person with a body mass index (BMI, defined as the weight in kilograms divided by the square height in meters, kg/m^2) over 25 is considered overweight, and over 30 is considered obese. Overweight and obesity are associated with hyperplasia and hypertrophy of adipocytes. Obesity occurs when an imbalance between energy intake and energy expenditure leads to an increase in body weight. But the exact cause of obesity is unknown. It appears to be a complex link between biologic, psychological and behavioral factors. Risk factors include genetic factors,

physical inactivity, diet, socioeconomic factors, medications, medical conditions and gut microbiome [38].

Obesity is a worldwide epidemic that has reached incredible proportions, in developed countries as well as in developing countries [39]. According to the World Health Organization (WHO), there were 1.9 billion overweight adults worldwide in 2016, and of these, 650 million were obese [40]. 340 million children were considered overweight or obese in 2016.

Obesity is an independent risk factor for excess morbidity and mortality. People with a higher BMI have a greater risk of all-cause mortality [41]. Overweight and obesity are also associated with an increased risk for multiple morbidities. Indeed, raised BMI is a major risk factor for disease such as cardiovascular diseases, diabetes, musculoskeletal disorders and some cancers, including esophageal adenocarcinoma, pancreatic, liver, colorectal, breast, endometrial and kidney cancers [42].

2.2 Metabolic syndrome

Metabolic syndrome, also known as syndrome X, is not a single disease but a clustering of individual risk factors for diseases, mainly cardiovascular diseases. Metabolic syndrome has had different names and definitions over the past decades. It was first described as a combination of hypertension, hyperglycemia, and obesity. Now it is defined as “a constellation of an interconnected physiological, biochemical, clinical, and metabolic factors that directly increases the risk of atherosclerotic cardiovascular disease, type 2 diabetes mellitus, and all-cause mortality” [43]. The International Diabetes Federation and other organizations worked together to define the criteria for clinical diagnosis. These factors include elevated waist circumference, elevated triglycerides (TGs), reduced high-density lipoprotein (HDL), elevated blood pressure and elevated fasting glucose (Table I.1) [44]. The presence of any 3 out of 5 of those risk factors constitutes a diagnosis of metabolic syndrome.

Measure	Categorical points
Elevated waist circumference	≥ 94 cm in men ≥ 80 cm in women
Elevated triglycerides	≥ 150 mg/dL
Reduced HDL cholesterol	< 40 mg/dL in men < 50 mg/dL in women
Elevated blood pressure	Systolic ≥ 130 and/or diastolic ≥ 85 mm Hg
Elevated fasting glucose	≥ 100 mg/dL

Table I.1. *Criteria for metabolic syndrome diagnosis.*

The incidence of metabolic syndrome parallels the incidence of obesity. Between 20 and 45% of the population present metabolic syndrome [45]. However, obesity is not always associated with metabolic syndrome. Metabolically healthy obese individuals have high level of insulin sensitivity and do not have hypertension and hyperlipidemia or other features of the syndrome [46]. Metabolic syndrome is associated with a higher risk of developing cardiovascular diseases, diabetes and some cancers [47], including liver cancer. Metabolic syndrome is also associated with non-alcoholic fatty liver disease (NAFLD). In a cross-sectional study from Mexico, 87% of males and 76% of females with metabolic syndrome presented NAFLD [48]. There are several hypotheses concerning the mechanisms for the pathophysiology of the metabolic syndrome, including low-grade chronic inflammation. However, the most widely accepted is the presence of insulin resistance [49].

2.3 Insulin resistance

Prolonged caloric excess in obese individuals disrupt the intricate balance between energy storage and consumption, leading to desensitization of tissues to insulin action and the development of insulin resistance. Insulin resistance is a condition in which a normal insulin concentration does not adequately produce a normal insulin response in the target tissues, such as adipose tissue, muscle and liver [50]. Under these circumstances, pancreatic beta cells secrete more insulin, a condition called hyperinsulinemia, to overcome the hyperglycemia. This hyperinsulinemia compensates for insulin resistance to some biological actions of insulin (normoglycemia) but it may cause an increased activity of insulin in some tissues that

are still sensitive to insulin. Insulin resistance and hyperinsulinemia, along with other obesity-related factors, were linked to the development of several types of cancers [51]. The mechanisms linking insulin resistance and the development of cancer are still poorly understood. One of the current explanation is linked to hyperinsulinemia. Indeed, insulin has a well-known mitogenic effect and the presence of increased levels of insulin could stimulate cancer cells development [52]. Moreover, insulin resistance is commonly associated with obesity and a low-grade inflammatory state. This environment could also play a role in malignant transformation and cancer progression [53].

2.3.1 Insulin and insulin signaling pathway

Insulin is a peptide hormone produced in the β cells of Langerhans islets and secreted by the pancreas. Its role is to maintain normal blood glucose levels by facilitating cellular glucose uptake, regulating carbohydrate, lipid and protein metabolism. Insulin acts on adipose tissues, muscles and the liver (Figure I.3). In the postprandial state, insulin controls the synthesis and storage of lipids in the liver by stimulating *de novo* lipogenesis (DNL), by suppressing fatty acid oxidation, and by promoting TG esterification and secretion [54]. It also plays a role in promoting cell division and growth through mitogenic effects [55]. Insulin is also a growth factor for hepatocytes, promoting their division through G1/S and G2/M transitions and their survival [56].

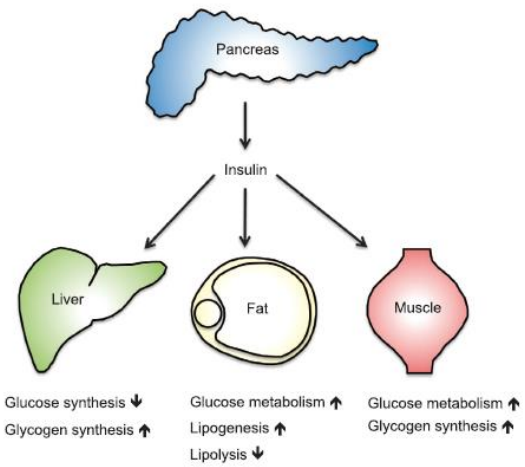

Figure I.3. *Role of insulin in the control of whole-body metabolism.* Adapted from [51].

In the liver, insulin mediates its biological effects via binding to a heterotetrameric α2β2 tyrosine kinase receptor expressed at the plasma membrane of hepatocytes, called insulin receptor (IR). Binding of insulin to its receptor leads to tyrosine auto-phosphorylation of the receptor and tyrosine phosphorylation of cytosolic substrates: insulin receptor substrate (IRS)-1 and 2. The activation of IRS1/2 activates a complex network of intracellular pathways, including the two most studied: phosphatidylinositol 3-kinase (PI3K)/Akt and rat sarcoma-mitogen-activated protein kinase (Ras)/MAPK (Figure I.4) [57]. Akt is central for metabolism regulation and multiple targets of Akt are involved in insulin action. Upon activation, IRS1/2 recruit PI3K, which phosphorylates phosphatidylinositol (3,4)-biphosphate (PIP2) to generate phosphatidylinositol (3,4,5)-triphosphate (PIP3) [58]. This leads to the recruitment of pyruvate dehydrogenase kinase 1 (PDK1) and Akt. Akt is then phosphorylated by PDK1 and mammalian target of rapamycin (mTORC2). Akt then signals to multiple downstream pathways to control several functions. Akt phosphorylates and inhibits the glycogen synthase kinase 3 (GSK3), which is a negative regulator of lipogenesis and glycogen synthesis [59]. Akt also induced the activation of mammalian target of rapamycin complex 1 (mTORC1) which phosphorylates the sterol regulatory element-binding factor 1c (SREBF 1c) [60]. This protein is a transcription factor that induces the transcription of genes involved in lipogenesis and represses those involved in lipolysis. The PI3K/Akt pathway also mediates mitogenic effects of insulin, via S6 kinase and 4E binding proteins (4EBPs) [61]. Moreover, the activation of BCL2-associated agonist of cell death (BAD) represses the cellular apoptotic program. The Ras-MAPK/ERK signaling pathway rather controls cellular proliferation. SH2 domain-containing adaptor (SHC) interacts with activated IR and recruits growth factor receptor bound 2 – son of sevenless (GRB2-SOS) complex [62]. SOS activates Ras, which recruits and activates Raf. Raf phosphorylates and activates MEK, which activates MAPK/ERK. Activated ERK translocate to the nucleus where it phosphorylates transcription factors implicated in cell growth, proliferation, differentiation and survival.

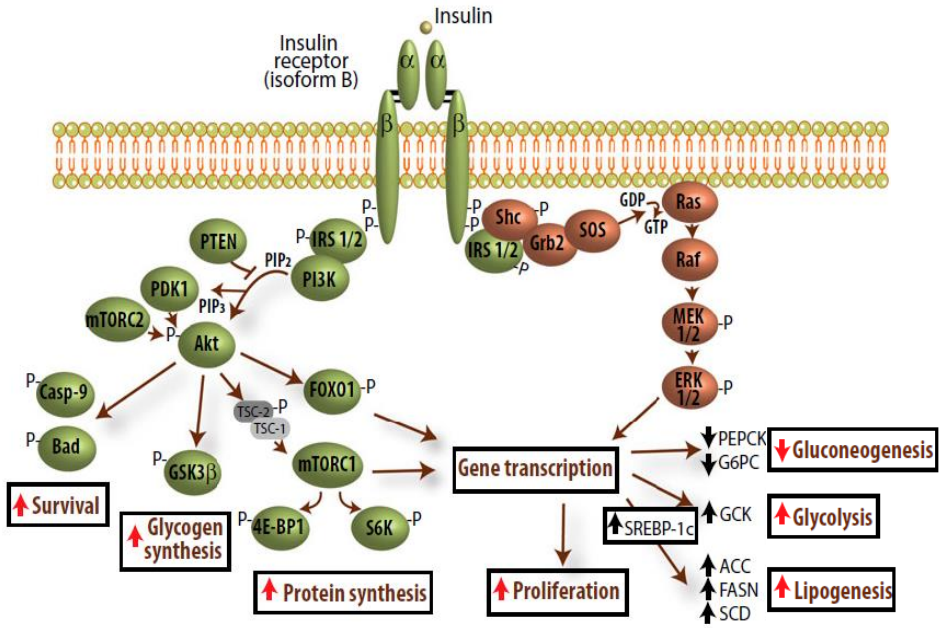

Figure I.4. *Insulin signaling in hepatocytes.* Upon insulin binding, auto-phosphorylation of the insulin receptor leads to recruitment and phosphorylation of IRS1/2. IRS proteins recruit and activate PI3K, which phosphorylates PIP2 to generate PIP3. PDK1 is then activated by PIP3, which phosphorylate Akt along with mTORC2. Activated Akt signals via phosphorylation to control multiple metabolic processes in liver. The MAPK pathway rather controls cellular proliferation. Adapted from [63].

2.3.2 Insulin resistance pathophysiology

Insulin resistance and hyperinsulinemia in obesity are due to several confounding factors and a complex interplay between many tissues. Even though the mechanisms have not been fully understood, it is now recognized that the major factors are changes in the adipose tissue (AT) biology, disruption of the normal endocrine function of adipocytes and deregulated lipolysis [51]. AT is the main energy reserve of the body and is composed of two major types: white adipose tissue (WAT) and brown adipose tissue (BAT). BAT is mainly responsible for heat production in infants but BAT depots are also found in adults. Most of the body fat is stored in WAT, where energy is stored by adipocytes as TGs. TGs are broken down into glycerol and free fatty acids (FFAs) via lipolysis when there is energetic demand. Adipocytes then release glycerol and FFAs into the blood where they are capture mainly by the liver and muscles. In obese patients, an expansion of the adipose tissue results in an increase in circulating FFAs levels and their uptake by the muscles and liver. The excessive accumulation of FFAs in these tissues lead to lipotoxicity and development of insulin resistance [64].

In addition to fat storage, adipocytes are also secretory cells. They produce hormones and cytokines called adipokines [65]. Leptin was the first one discovered. Leptin is a hormone that acts in the hypothalamus to repress appetite, and in the AT and the liver to stimulate lipolysis and inhibit lipogenesis. Leptin levels are increased in obesity and subcutaneous fat has been showed to play a major role in leptin levels [66]. Adiponectin is also produced by adipocytes and induces glucose uptake and lipolysis, and inhibits gluconeogenesis and promotes FFAs oxidation in the liver and muscles. Expression of adiponectin decreases with the increase in adiposity [66]. Adipocytes also produce pro-inflammatory cytokines, such as interleukin 6 (IL-6) and TNFα. In obese patients and rodents, enlarged adipocytes overexpress TNFα which is thought to play an important role in the development of insulin resistance [67].

Defective intracellular signaling can cause insulin resistance. IRS is an important element in the insulin signaling pathway. IRS proteins can be regulated by decreased levels of protein expression. Hyperinsulinemia is known to decrease the expression of IRS1 and 2 in cell-culture models as well as in mice tissues [68]. Two mechanisms have been proposed. First, hyperinsulinemia induces degradation of IRS1 and inhibits the synthesis of IRS2 at the transcriptional level [68]. Second, suppressor of cytokines signaling (SOCS) proteins might induce ubiquitin-mediated degradation of IRS1/2 [69]. Decreased levels of IRS proteins certainly contribute to insulin resistance in rodents and humans [70]. Moreover, decreased hepatic IRS1 correlates with increased expression of genes that are involved in gluconeogenesis, whereas downregulation of hepatic IRS2 leads to increased expression of genes involved in lipogenesis [71]. Akt plays a central role in insulin signaling. Akt2-deficient mice show insulin resistance and develop diabetes [72]. This could be due to the inability of insulin to induce glucose metabolism and decreased hepatic glucose output. Likewise, a mutation in the kinase domain of Akt2 has been found to cause severe insulin resistance and diabetes in humans [73].

In a context of over-nutrition and obesity, the accumulation of glucose, fatty acids (FAs) and amino acids can suppress the activity of AMP-activated protein kinase (AMPK) and contributes to insulin resistance [74]. AMPK is a Ser/Thr protein kinase that works as a central sensor of metabolic signals. It responds to low glucose levels

via a high AMP/ATP ratio [75]. When activated, AMPK inhibits *de novo* synthesis of FAs, cholesterol and TGs, and activates FAs uptake and FA β-oxidation. AMPK also plays an important role in glucose metabolism by stimulating glucose uptake and glycolysis and inhibiting glycogen synthesis. Insulin inhibits AMPK by inducing its direct phosphorylation by Akt [76]. In insulin resistance, AMPK is inhibited by hyperinsulinemia and excessive nutrient accumulation [77].

2.4 Type 2 diabetes

Type 2 diabetes is a metabolic disease defined by chronic hyperglycemia. This disorder is due to insulin resistance in the skeletal muscles, the adipose tissue and the liver, which increases the demand for insulin in insulin-target tissues. When the pancreas is unable to produce enough insulin to compensate this demand, hyperglycemia appears [78]. The prevalence of diabetes has been rising these last two decades. According to the WHO, the global prevalence of diabetes among adults over 18 was of 4.7% in 1980 and was of 8.5% in 2014. 422 million people were suffering of diabetes in 2014, of which 90% with type 2 diabetes. Risk factors associated with the disease include genetics, obesity, low physical activity, unhealthy diet, age, ethnicity, high blood pressure and impaired glucose tolerance. The link between obesity and diabetes is still unclear but several mechanisms have been proposed, such as dysregulation of adipokines, reticulum endoplasmic (ER) stress, chronic low grade inflammation and lipotoxicity [79].

2.5 Nonalcoholic fatty liver disease and NALFD-induced hepatocellular carcinoma

2.5.1 Definition and prevalence of NAFLD

With the rise of obesity, NAFLD is reaching epidemic proportions [80]. NAFLD is one of the most important causes of liver disease worldwide. This disorder is characterized by excess accumulation of fat in hepatocytes (>5% fat content in the liver, called steatosis). Steatosis alone is referred as nonalcoholic fatty liver (NAFL). NAFL is generally considered a non-progressive disease. In presence of additional factors, cell death and inflammation can occur and lead to nonalcoholic steatohepatitis

(NASH) [81]. NASH is the most severe form of NAFLD and is characterized by the presence of hepatocellular ballooning, Mallory-Denk bodies, inflammation and various degrees of fibrosis. NAFLD is not only a disease of the obese, but is typically associated with metabolic dysfunction. The metabolic comorbidities associated with NAFLD are hyperlipidemia (69.2%), obesity (51.3%), metabolic syndrome (42.5%), hypertension (39.3%) and type 2 diabetes (22.5%) [82]. NALFD and alcoholic fatty liver disease (AFLD) share some histological features. However, patients with NAFLD are usually obese, do not consume excess alcohol and are insulin resistant, compare to patients with AFLD [83]. Adverse hepatic outcomes of NASH may include liver failure, cirrhosis and hepatocellular carcinoma (HCC). Cardiovascular diseases and malignancy are other adverse outcomes.

The presence of NAFLD can be assessed by ultrasonography or nuclear magnetic resonance (NMR) spectroscopy. The global prevalence of NAFLD in adults is estimated to be 24% [82], with the highest average rates reported in South America (31%) and the Middle East (32%), followed by Asia (27%), the USA (24%) and Europe (23%) (Figure I.5). The prevalence of NAFLD varies between ethnic groups. This variation can be explained by differences in lifestyle, access to healthcare, the prevalence of metabolic syndrome, and genetics, such as a polymorphism of the patatin-like phospholipase domain-containing 3 (PNPLA3) gene [81]. Because imaging can only detect fatty liver but not fibrosis or inflammation, the prevalence of NASH and related liver fibrosis in the population is unclear. Although the prevalence of NASH is the general population is not available, it is estimated to be between 1.5% to 6.5% worldwide, depending on the studies [84,85].

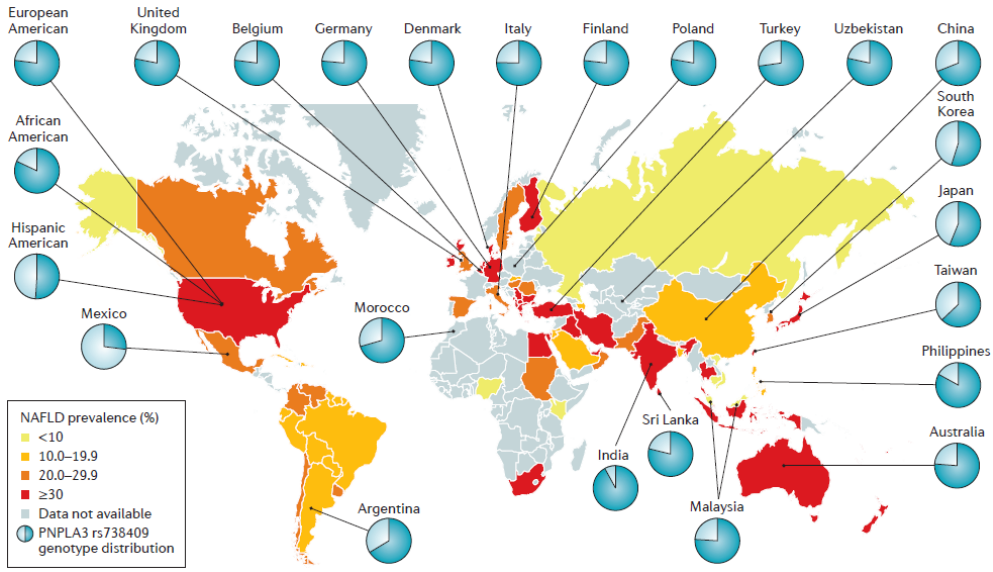

Figure I.5. *Worldwide estimated prevalence of NAFLD and distribution of PNPLA3 genotypes.* Adapted from [80].

NAFLD is currently the most common cause of liver disease in Western countries. In Europe, the presence of NAFLD is growing parallel to the prevalence of obesity. Even though the prevalence varies depending on the technique used to detect NAFLD, it is estimated that approximatively a quarter of Europe is affected. In 2016, a meta-analysis reported an average prevalence of 23.71% in Europe, varying from 5 to 44% between countries [82]. Fatty liver has been reported in 40-80% of patients with type 2 diabetes and 30-90% of obese patients [86]. In the meta-analysis of 2016, the prevalence of NASH in Europe among patients with NAFLD was 69.25%. Hepatic complications represent the third most common cause of death in patients with NAFLD or NASH, after cardiovascular events and malignancies [87].

2.5.2 Definition and prevalence of HCC

Hepatic complications of NAFLD include the development of HCC, which is the most frequent malignant liver tumor worldwide, accounting for 70-85% of all liver cancer [88]. HCC is estimated to be the fourth most common cause of cancer-related death overall worldwide [39], the incidence of which has increased by threefold in North America and several European countries in the last three decades [82]. High-quality studies evaluating the association between HCC and NAFLD are currently lacking. By using the United States Surveillance, Epidemiology, and End results (US SEER)-

Medicare database, a recent study showed that among the patients with HCC, NAFLD was the most common underlying etiology (26.14%), followed by hepatitis C viral infection (14.47%) [89].

The exact pathogenesis of HCC in NAFLD is not fully understood. However, some risk factors and mechanisms that can potentially promote HCC in patients with NASH have been described (Figure I.6). The accumulation of lipids in hepatocytes of patients with NAFLD and the presence of metabolic dysfunctions, such as insulin resistance, lead to numerous modifications in the hepatic cells: formation of ROS, inflammation, cell death and ER stress. As a consequence, hepatic stellate cells (HSC) are activated and produce extracellular matrix, leading to hepatic fibrosis. This accumulation of extracellular matrix modifies the hepatic architecture [90]. The subsequent development of nodules of regenerating hepatocytes leads to cirrhosis. Cirrhosis induces hepatocellular dysfunction and increases intrahepatic resistance to blood flow. Cirrhosis creates a permissive milieu for the development of HCC. However, although cirrhosis creates a permissive environment for the development of HCC, it is now estimated that 10-75% of HCC cases occur in non-cirrhotic NAFLD [91,92].

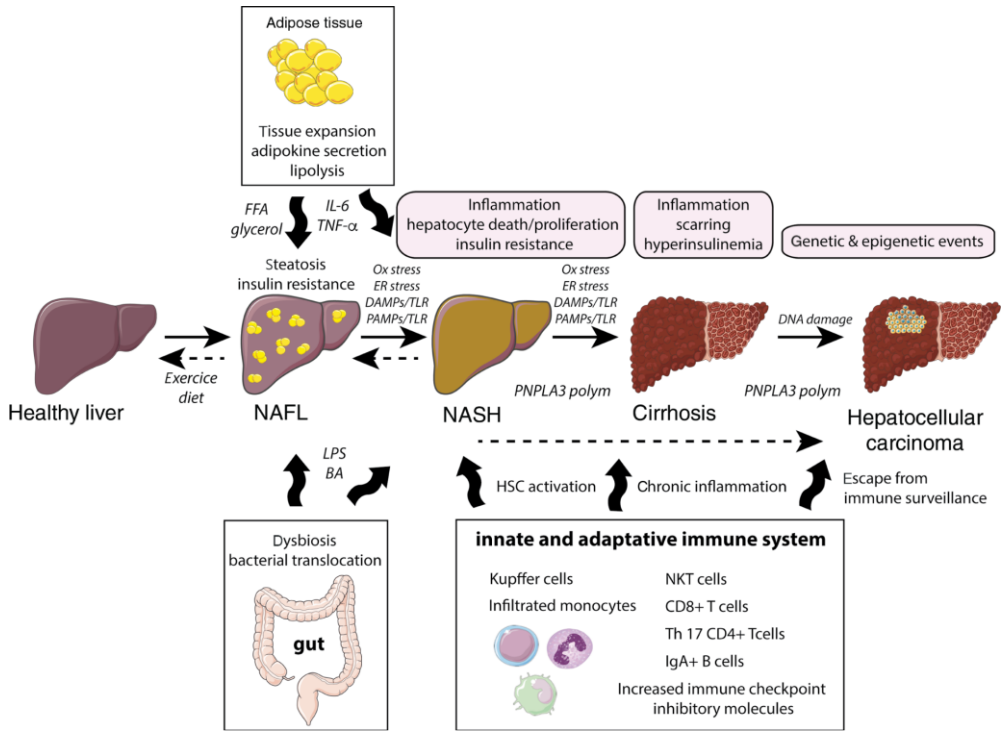

Figure I.6. *Schematic representation of the natural history of HCC in a NAFLD context*. In a context of metabolic imbalance and genetic predisposition, multiple parallel hits coming from adipose tissue and gut converge to the liver and initiate tissue injury. Lipotoxicity, ER stress and oxidative stress are key players in the initiation of hepatocytes death and the release of DAMPs and PAMPs, initiating a cycle of pro-inflammatory response. The recruitment of Kupffer cells and other immune cells trigger the release of pro-inflammatory and pro-fibrogenic cytokines and chemokines. Hepatic stellate cells (HSC) are subsequently activated and produce extracellular matrix, leading to fibrosis and cirrhosis. This environment leads to cellular stress, DNA damage, epigenetic modifications in liver cells. Adapted from [93].

Some risk factors that can potentially promote HCC in patients with NASH have been described. Diabetes and obesity are key players in the development of HCC. It was shown that a combination of type 2 diabetes and obesity can double the risk for HCC [94,95]. It was also noted that, compared to women, men have an increased incidence of NASH-related HCC [92]. Sedentary lifestyle, with low levels of physical activity [96] and high intake of carbohydrates [97] are risk factors for the development of NAFLD and HCC. In this context, Park *et al.* showed that obesity-promoted HCC development was dependent on increased production of pro-inflammatory cytokines IL-6 and TNFα, leading to hepatic inflammation and activation of the oncogenic transcription factor STAT3 [98].

2.5.3 Mechanisms and pathogenesis of NAFLD and NAFLD-induced HCC

Twenty years ago, Day and James [99] proposed the 'two-hit' hypothesis to explain the pathogenesis of NAFLD. This hypothesis proposed that accumulation of lipids in the liver is the 'first hit', which sensitized the liver to a 'second hit' of oxidative stress due to lipotoxicity and subsequent inflammation. It is now clear that this hypothesis is an over-simplification of the pathogenesis and that NAFLD is a complex disease. The mechanisms implicated include a range of environmental factors, such as diet, lifestyle and microbiota, but also genetic and epigenetic background.

2.5.3.1 Sources of fatty acids in the liver

In the setting of obesity, several factors lead to accumulation of fat in the liver. The liver receives fatty acids trough the blood, the majority of which are produced in adipose tissue by lipolysis of TGs, a process regulated by the action of insulin on adipocytes [100]. Weight gain is associated with an expansion of adipose tissue, that leads to a dysfunction of the adipocytes. Such dysfunction results in local inflammation and upregulation of cytokines promoting insulin resistance. Such resistance compromises the ability of adipose tissue to store lipids, resulting in the release of FFAs into the circulation [101]. The liver is then exposed to an increased amount of FFAs as well as high levels of insulin. Hepatocytes take up these FFAs through the fatty acids transport protein 5 (FATP5) [102] and CD36 [103], that are upregulated in obesity. The accumulation of fatty acids in hepatocytes stimulates the synthesis of TGs. Moreover, Samuel *et al.* showed that this fat-induced hepatic insulin resistance is due to the activation of PKCε by diacylglycerol [104]. Activated PKCε then binds to and inhibits insulin receptor tyrosine kinase activity.

The second major source of fatty acids is their synthesis from the liver itself by *de novo* lipogenesis (DNL). Insulin and glucose upregulate the enzymes responsible for DNL through the action of two transcription factors: carbohydrate-responsive element binding protein (ChREBP) and SREBF1 [105]. DNL is not a major source of hepatic lipids in the normal liver, but in the setting of obesity and insulin resistance, it can contribute up to 25% of total hepatic lipid storage [106,107]. It may seem paradoxical that DNL would be upregulated in hepatocytes if the uptake of fatty acids makes them

insulin resistant. An explanation was proposed by Li *et al.* who showed that insulin resistance in hepatocytes manifests downstream of the insulin receptor [108]. Another explanation could be the possibility that DNL is induced by insulin-independent pathways [109].

Dietary fats and sugars are also substrates for hepatic TGs synthesis. Sugars are converted to fatty acids via DNL, and fats are taken up by the liver with adipose tissue-derived fatty acids. Around 14% of the TGs in liver come from the diet [107] .

TGs not exported from the liver into the blood as very-low-density lipoprotein (VLDL) form lipid droplets in hepatocytes, which are a characteristic of NAFLD. The liver response to these lipotoxic lipids is vast: ER stress, dysfunctional unfolded protein response (UPR), inflammasome activation, activation of apoptotic pathways and inflammation (Figure I.7).

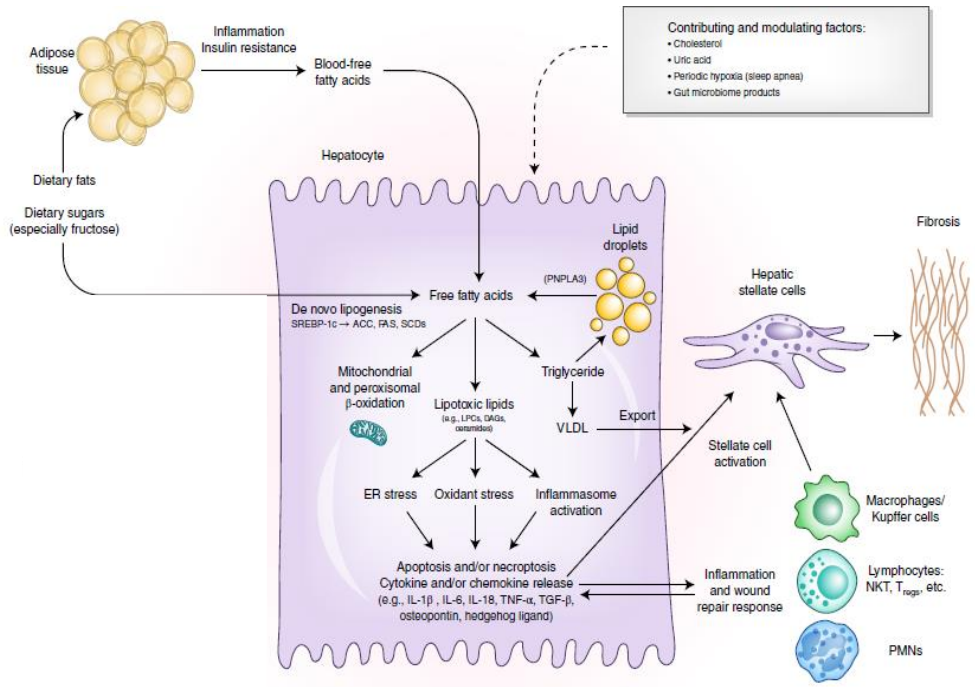

Figure I.7. *The substrate-overload liver injury model of NAFLD pathogenesis.* FFAs are central to the pathogenesis of NAFLD. The major contributors to the FFAs flux in the liver are: FFAs that originate from lipolysis in adipose tissue, *de novo* lipogenesis in the live and nutrients from the diet. The two major fates of fatty acids in hepatocytes are mitochondrial oxidation and transformation in TGs that can be exported into the blood as VLDL or stored in lipid droplets. Lipid droplet containing TGs undergoes regulated lipolysis to release fatty acids. PNPLA3 participates in this lipolytic process. When this mechanism is overwhelmed, fatty acids can contribute to the formation of lipotoxic species that leads to ER stress, oxidant stress and inflammasome activation. These processes are responsible for the phenotype of NASH with hepatocellular injury, inflammation, stellate cells activation and progressive accumulation of excess extracellular matrix. Adapted from [100].

As already mentioned, AMPK is a key player in lipid metabolism. Interestingly, Garcia *et al.* generated a genetically engineered mouse model where AMPK can be activated *in vivo* in mice in a spatially and temporally restricted manner [110]. In this model, they showed that liver-specific AMPK activation reprograms lipid metabolism, reduces liver steatosis, and decreases expression of inflammation and fibrosis genes. The reduction of lipid in the liver was due to a promotion of FA oxidation and an inhibition of DNL.

2.5.3.2 Insulin

Hyperinsulinemia has been identified as a risk factor for NAFLD and HCC development [111,112]. Insulin resistance is a major feature of NASH so it may seem paradoxical to link hyperinsulinemia to HCC. But, as already discussed, insulin resistance is not absolute but pathway selective, and some pathways remain responsive to insulin. The preservation of some insulin signaling pathways may provide a selective advantage for premalignant hepatocytes by promoting metabolism, proliferation and survival [63]. The insulin signaling pathway is activated in human HCC due to overexpression of signaling components or due to the loss of negative regulators. It was reported that the insulin receptor is overexpressed in 40% of 85 HCC investigated tumors compared to adjacent non-tumor tissues [113]. This increase is accompanied by a modification of the relative expression of the two IR isoforms IR-A and IR-B. IR-A (the fetal isoform of IR) is upregulated while the expression of IR-B (the adult isoform of the receptor) is downregulated, suggesting that the increase in IR-A/IR-B ratio is a possible mechanism for hepatocarcinogenesis. Consistently, a high IR-A/IR-B ratio is associated with a poor prognosis in patients [114]. Moreover, ectopic overexpression of IR-A in human HCC cell lines promotes a migratory/invasive phenotype of these cells. IR-A displays 1.8-fold higher affinity for insulin than IR-B and can also binds proinsulin and insulin-like growth factor-II (IGF-II) [115]. Pro-insulin is found at high level in the plasma of insulin resistant patients [116]. IGF-II is a growth factor peptide produced by the liver mainly in fetus and early after birth, and at a lesser level in adults. IGF-II is overexpressed in HCC. Indeed, Martinez-Quetglas *et al.* reported that 15% of human HCC tissues expressed increased levels of IFG-II compared to non-tumor liver tissues [117]. Methylation at the fetal promoters of IGF-II was reduced in the HCC samples that overexpressed IGF-II. The expression of IRS 1 and 2 is frequently increased in HCC tumors compared to adjacent non-tumor liver tissue [118,119]. It was reported that the loss of negative regulators of insulin signaling, such as SOCS proteins [120–122], growth factor receptor-bound protein 14 (GRB14) [123] and PTEN [124], is also frequently observed in human HCC.

2.5.3.3 ER stress

The ER is the main cellular compartment involved in secretory and transmembrane protein folding, calcium homeostasis and lipid biogenesis. The accumulation of TGs in hepatocytes in NAFLD is associated with dysfunction of the ER, inducing ER stress [125]. Chronic ER stress can affect hepatic lipid metabolism directly by inducing DNL, and indirectly via the alteration of VLDL secretion, insulin signaling and autophagy. In MUP-uPA mice fed HFD, is was shown that ER stress increased lipogenesis, oxidative stress and lipotoxic hepatocyte death [126]. This led to the induction of inflammatory TNF-α-producing macrophages that contribute to HCC growth in this model.

Chronic ER stress also causes the accumulation of unfolded proteins in the ER, triggering an evolutionary conserved response, called the unfolded protein response (UPR). UPR is an adaptive signaling pathway used to restore normal ER function [127]. In case of severe or persistent ER stress, the UPR can cause steatosis aggravation, insulin resistance, inflammation, inflammasome activation and, ultimately, hepatocyte death [125]. In patients and mice with NASH, markers of ER stress and UPR have been found [128].

2.5.3.4 DNA damage and cell death

Hepatocyte injury is a hallmark of NASH and can be caused by several mechanisms. First, the strain put on mitochondria to metabolize the excess of fatty acids leads to mitochondrial uncoupling, the production of ROS and the activation of JNK [129]. This leads to mitochondrial damage and cell death. Fatty acids can also kill hepatocytes trough the activation of death receptors. A number of death receptors, such as FAS [130], death receptor 5 [131] and tumor necrosis factor receptor superfamily member 1A [132] are upregulated on hepatocytes in the setting of steatosis. The activation of these receptors seems to activate hepatocyte apoptosis.

ROS production can also damage DNA. The abundance of ROS, together with the presence of chronic inflammation, have been associated with cancers [133,134]. ROS produced by macrophages and neutrophils recruited in the context of NAFLD can induce DNA damage and probably play a role in the development of HCC [135,136].

In this context, the response to DDR determines if a mutation has pathogenic consequences. Daugherity *et al.* studied the role of DNA damage checkpoint kinase Ataxia Telangiectasia Mutated (ATM) is NAFLD development by using ATM knock-out mice fed HFD for 8 weeks. They found that ATM was activated by oxidative stress and contributes to NAFLD progression by promoting liver fibrosis and apoptosis [137]. Moreover, in human liver specimens, a reduction in nucleotide excision repair capacity has also been associated with reduced DNA damage recognition and DDR in the presence of steatosis and hepatic inflammation, potentially contributing to HCC risk [138].

Lipid peroxidation, a normal cellular process which become significant under oxidative stress, generates aldehydes. One of the most abundant and cytotoxic aldehyde produced is *Trans*-4-hydroxy-2-nonenal (4-HNE). Cell exposition to 4-HNE causes a mutation in the *p53* gene, in a mutational hotspot, particularly in HCC [139]. Another mechanism linking oxidative stress and HCC development involves the nuclear respiratory factor 1 (Nrf1), which is a transcription factor involved in oxidative stress response [140]. Xu *et al.* showed that mice with a somatic inactivation of *nrf1* in the liver developed steatosis, inflammation and fibrosis, leading to hepatic cancer development. These results demonstrate that Nrf1 has a protective function against oxidative stress and a potential function in lipid homeostasis in the liver [141].

2.5.3.5 The inflammasome

It was recently suggested that hepatocytes inflammasome activation might link metabolic stress to NASH. The inflammasome is a cytoplasmic complex of multiple proteins that responds to danger-associated molecular patterns (DAMPs) and to pathogen-associated molecular protein (PAMPs). In NASH, DAMPs include fatty acids produced by DNL, and PAMPs are the products of gut microbiota that are delivered to the liver in portal circulation [142]. In mouse, activation of the inflammasome in the liver leads to expression of pro-inflammatory cytokines (IL-1β and IL-18) and promotes apoptosis through caspase-1 activation.

2.5.3.6 Inflammation and immune cells

NASH is characterized by the recruitment of immune cells into the liver, where they become activated and have the capacity to release molecules that cause inflammation (Figure I.8) [143]. At early stage, inflammatory response may be important for healing and tissue repair. However, a dysregulated immune response can lead to disease progression. Moreover, both innate [144] and adaptive [145] immunities play a role in the progression of the disease. Liver macrophages are a heterogeneous population which includes Kupffer cells and bone marrow monocyte-derived macrophages. In mouse, Kupffer cells play a role in the setting of the disease through increased production of TNFα and CCL2 [146]. Moreover, in rats, the depletion of Kupffer cells attenuates NAFLD development and hepatic insulin resistance [147]. This could be due to the activation of NLRP3 inflammasome which promotes IL-1β secretion, fueling the progression of NASH [148]. Furthermore, Kupffer cells-derived factors facilitate the infiltration of bone marrow-derived monocytes into the liver which contribute to the progression of NASH [149]. The infiltration of neutrophils into the liver also contributes to the progression of NASH via the secretion of cytokines and active molecules, such as elastase [150], myeloperoxidase [151] and extracellular traps [152]. T-helper (Th) have been shown to participate in the pathology. Indeed, NASH is characterized by an excessive Th1-derived cytokines (INFγ) and a deficiency in Th2-derived cytokines (IL-4, IL-5 and IL-13) production [153]. Th-17 cells accumulate in the liver and act on macrophages and stellate cells, inducing inflammation and fibrosis. Removing cytotoxic $CD8^+$ T cells results in decreased steatosis, insulin resistance, inflammation and hepatic stellate cells activation in mice and humans [154,155].

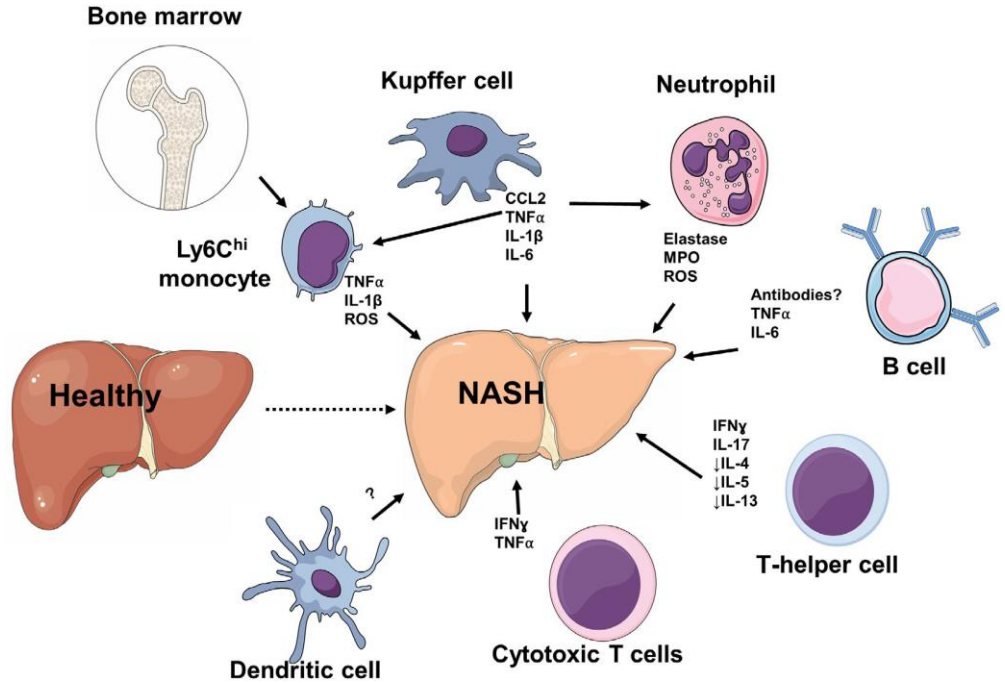

Figure I.8. *Immune dysregulation in NASH development.* Kupffer cells (KCs) activation results in release of pro-inflammatory cytokines, leading to the recruitment of bone-marrow-derived monocytes and neutrophils, further contributing to the inflammatory response. Activated neutrophils promote NASH by releasing elastase, MPO and ROS. B cells can produce TNFα and IL-6. NASH is characterized by excessive Th17- and Th1-derived IFNγ and IL-17 and a deficiency in Th-2 derived cytokines. Cytotoxic $CD8^+$ T cells are supported by type I IFN responses and lead to the production of IFNγ and TNFα. The role of dendritic cells is still unclear. Adapted from [143].

HCC development in the context of NAFLD is intimately associated with complex changes in the immuno-metabolic compartment. Indeed, recent studies have shown that the liver pro-inflammatory microenvironment present in NASH is crucial for NASH to HCC progression [156]. Different cell types are involved. It has been shown in a diethylnitrosamine (DEN) carcinogen-induced HCC mouse model that pro-inflammatory activation of Kupffer cells, and notably myeloid cell receptor TREM-1 expression, is important in HCC development [157]. Moreover, recent data identified interaction between Kupffer cells and platelets as an important initiating factor for liver inflammation [158]. In a long-term choline-deficient high fat diet mouse model, it was shown that the activation of intrahepatic $CD8^+$ T cells and natural killer T cells lead to NASH-induced HCC [159]. In this model, the activation of the immune cells initiates release of soluble mediators, such as LIGHT (a member of TNF family), that facilitates the NASH-to-HCC transition. $CD4^+$ T cells however inhibit HCC initiation

and mediate tumor regression [160,161]. Pre-malignant senescent hepatocytes secrete chemokines and cytokines and are subject to immune-mediated clearance. This clearance critically depends on an intact $CD4^+$ T cell-mediated adaptive immune response, in a specific antigen-dependent manner. Therefore, senescence surveillance is important for tumor suppression in vivo and depends on an efficient immune surveillance [161]. Moreover, by using a series of different NAFLD and HCC mouse models, Ma *et al.* described that NASH induces a selective loss of intrahepatic $CD4^+$ T cells [162]. This results in an acceleration of tumor development in liver-specific MYC transgenic mice fed a methionine-choline-deficient diet. B cells have recently been investigated during NASH and NASH-to-HCC transition. In both human and mice with NASH, resident IgA+-PDL1+ cells (PDL1, programmed cell death 1 ligand 1) accumulate in the liver. This phenomenon suppresses the efficient immune response from $CD8^+$ T cells in the context of NASH-induced liver cancer [163]. These findings suggest that, in the liver, inflammation-induced suppression of cytotoxic $CD8^+$ T lymphocytes activation is a tumor-promoting mechanism. Moreover, NK cells, a group of innate immune cells that show cytolytic activity against tumor cells, perform anti-tumor functions through surveillance. This surveillance is crucial in combatting HCC. However, the number of NK cells is reduced in HCC conditions [156]. The production of IFNγ is also impaired due to an increased number of T_{regs} [164].

2.5.3.7 Microbiome

Interactions between the intestine and the liver, called the gut-liver axis, is a relatively new additional contributor to NAFLD. A specific microbial signature has not yet been linked to NAFLD, but studies showed that NAFLD patients have a different composition of the gut microbiota from healthy individuals [165]. Some families of bacteria have been shown to be increased or decreased in NAFLD patients compared to healthy individuals. Moreover, Le Roy *et al.* demonstrated that, in rodent, it is possible to transfer propensity to develop NAFLD features by transplanting gut microbiota from mice with or without NAFLD to germ free mice [166]. One possible explanation is that an altered microbiome (dysbiosis) may affect the intestinal barrier and enable the translocation of bacteria or bacterial products, such as endotoxin [167].

Lipopolysaccharides are potent inducer of inflammation via binding to toll-like receptor (TLR)-4 in hepatocytes and Kupffer cells. Levels of LPS are increased in the portal vein of NASH patients through mechanisms involving small bacterial overgrowth, increased intestinal permeability, tight junction alteration and bacterial translocation [168,169]. This create a pro-inflammatory environment in the liver. Dysbiosis can also lead to the degradation of beneficial nutrients, such as choline, which are important for the maintenance of hepatic lipid homeostasis [81]. Moreover, microbiome study could potentially be used as a diagnostic method. Indeed, Nelson *et al.* conducted a study on stool microbiome from 86 liver biopsy-proven NAFLD patients [170]. They identified 37 bacterial species allowing them to distinguish moderate NAFLD from advanced fibrosis. Although the data do not demonstrate causality, they suggest that microbial biomarkers could be used as non-invasive approaches to determine stage of liver disease.

Modification of the microbiota can also influence HCC development. Indeed, mice housed in germ-free conditions developed less tumors than mice housed in conventional conditions [171]. Dysbiosis could also promote hepatocarcinogenesis by modifying bile acid metabolism. Primary bile acids are signaling molecules synthesized in perivenous hepatocytes and are metabolized as secondary bile acids by intestinal bacteria in the small intestine [172]. These molecules are important for the maintenance of a healthy gut microbiota, insulin sensitivity, innate immunity and balanced lipid and carbohydrate metabolisms. Dysbiosis can modify the production of secondary bile acids, which return to the liver and lead to liver inflammation. High level of secondary bile acids, such as deoxycholic acid and lithocholic acid in the liver can induce hepatocyte DNA damage, cell death and inflammation, promoting carcinogenesis [173–175].

2.5.3.8 Fibrogenesis

Hepatic fibrosis, caused by the accumulation of extracellular matrix in the liver, is associated with poor outcome in NASH [176]. The main process in fibrogenesis is the activation of resident hepatic stellate cells by a number of compounds that are present in a diseased fatty liver. DAMPs produced by dying hepatocytes can activate stellate cells. Free cholesterol upregulates the expression of TLRs on stellate cells, amplifying

hepatic fibrosis [177]. Oxidative stress can also activate stellate cells by inducing the production of ROS by the stellate cells via the enzyme NADPH oxidase 2 [178]. In mouse, there is an increased signaling by the transcriptional activator TAZ in NASH hepatocytes [179]. This pathway promotes the secretion of Indian Hedgehog ligand resulting in paracrine fibrogenic signaling in stellate cells.

2.5.3.9 Genetics and epigenetics

A substantial proportion of the overweight population is at risk of NAFLD, but only a minority of people with NAFLD will progress to more advanced disease, including hepatocellular carcinoma (HCC). The reasons for this are not fully understood yet. However, studies in twins or families with different ancestry (Hispanic [180,181], European [182], African [183]) have shown a substantial heritable component to the disease, ranging from 22 to 38%. These studies clearly suggest that genetic factors contribute at least partially to determine how individuals respond to caloric excess and the development of associated pathologies.

Genome Wide Association Studies (GWAS) allowed the identification of a number of genetic polymorphisms involved in NAFLD. The first GWAS in NAFLD patients was published in 2008 [184]. This study detected that one variant in the gene *PNPLA3,* the rs738409 C>G single nucleotide polymorphism (SNP), encoding an I148M missense mutant, was strongly associated with accumulation of fat in hepatocytes, in a cohort of more than 2.000 ethnically diverse patients. This association remained significant after adjustment for BMI, diabetes, alcohol intake and ethnicity. In obesity and insulin resistance, the expression of PNPLA3 is induced in hepatocytes, hepatic stellate cells and adipocytes, and is localized on the surface of lipid droplets [185,186]. PNPLA3 protein has intrinsic lipase activity on TGs, phospholipids and retinyl esters. This hydrolase activity could not be present in the I148M variant. The wild-type protein is rapidly degraded, but the mutant one cannot be ubiquitylated and degraded and thus it accumulates on the surface of lipid droplets [187,188]. These defects promote lipid droplets accumulation in the liver. Patients with I148M *PNPLA3* polymorphism have also more than threefold increased risk to develop HCC [189,190]. Study in a European NAFLD cohort with or without HCC has demonstrated that PNPLA3 mutation induced HCC is independent of potential

cofounders such as gender, age, BMI, presence of type 2 diabetes and the presence of fibrosis or cirrhosis [189]. Using whole-exome sequencing, several other driver mutations implicated in HCC promotion have been identified in different genes including *TERT* (promoter mutation), *TP53* (somatic R249S mutation), *CTNNB1* (large deletions of exon 3) and *ARID1A* (mutations in exon 1) [191].

GWAS has allowed the identification of other variants, such as rs585442926 in the gene transmembrane 6 superfamily member 2 (*TM6SF2*). This gene is involved in hepatic lipid metabolism. Indeed, the encoded TM6SF2 protein is involved in the enrichment of TGs in VLDL secreted from hepatocytes [192]. The rs585442926 C>T polymorphism in this gene leads to a loss-of-function of TM6SF2, which leads to higher TG content in hepatic lipid droplets and lower circulating lipoproteins [193]. A third variant found to be associated with NAFLD is the *GCKR* (rs1260326). The glucokinase regulator (GCKR) regulates *de novo* lipogenesis by controlling the influx of glucose in hepatocytes and, consequently, the flow of substrate for lipogenesis. The variant rs1260326 leads to decreased circulating fasting glucose and insulin levels, and hepatic fat accumulation by blocking fatty acid oxidation [194]. The common rs641738 C>T variant of membrane bound O-acyltransferase domain-containing 7 (MBOAT7) has been linked to downregulation of MBOAT7 protein. Such decrease in protein expression is implicated in NAFLD development during obesity and insulin resistance, by altering phospholipid remodeling in lipid droplets [195]. Finally, variation in *17-beta hydroxysteroid dehydrogenase 13* (*HSD17B13*) has been linked to protection against the development of hepatic inflammation and fibrosis [196–198]. HSD17B13 enzyme localizes on lipid droplets in hepatocytes. The mutant was shown to reduce progressive liver damage but to not decrease hepatic steatosis [198].

A recent genome-wide DNA methylation analysis suggested that NASH-specific DNA methylation pattern may participate in hepatocarcinogenesis [199]. Two non-coding microRNA have also been implicated in the transition from NASH to HCC: miR-122 and miR-34a. miR-122 is liver-specific and play a role in cholesterol metabolism and hepatocyte differentiation. miR-122 is down-regulated in the liver of NASH patients [200] and is associated to progression of HCC in mice [201]. On the

contrary, miR-34a is up-regulated in NASH patients and mice fed high-fat diet [200]. Its inhibition inhibits tumor development [202].

2.5.4 Diagnosis and management

Most NAFLD patients are asymptomatic or complain about nonspecific symptoms: sleep disturbances, fatigue, or abdominal pain. The diagnostic of NAFLD is complicated because no specific marker is currently available. The different steps of the diagnosis should include evaluation of personal and family history, assessment of metabolic syndrome, oral glucose tolerance test, liver tests, and imaging techniques. Liver tests can show increased levels of alanine aminotransferase (ALT) and/or aspartate aminotransferase (AST). The insulin sensitivity can be measured using the homeostatic model assessment for insulin resistance (HOMA-IR) [203]. Ultrasound-based technique can be used based on the principle that ultrasound energy is more attenuated by fat than by non-fatty tissues [204]. Magnetic resonance imaging (MRI) can also be used to determine fat content in the liver [205]. If these methods allow the diagnosis of fatty liver, they do not permit the distinction between simple fatty liver and NASH. The actual diagnosis of NASH requires liver biopsy and microscopic evaluation of the tissue. Different scoring systems are available to evaluate NASH. The SAF score assess the main histological lesions: the grade of steatosis (S), the grade of activity (A) and the stage of fibrosis (F) [206]. Elastography allows the indirect measure of tissue stiffness using the propagation of shear waves within the liver [207]. This can be coupled to ultrasonography or magnetic resonance.

Identifying NAFLD patients needing a screening for HCC is still an issue. Indeed, the heterogeneity among NAFLD patients, the poor knowledge of involved molecular pathways in hepatocarcinogenesis, and the coexistence of other risk factors for HCC development make the identification of predictive biomarkers to identify high-risk groups a real challenge and an unmet clinical need [208]. An approach to identify high-risk HCC patients can be based on the combination of biochemical, clinical (i.e. presence of diabetes and/or obesity), histological (severity of fibrosis) and genetic (mutations) features.

The European and American guidelines for the management of patients with HCC do not differ for patients with NAFLD-associated HCC from patients with HCC of other etiologies. But it is now recognized that NAFLD-associated HCC patients are more likely to possess features of metabolic syndrome, have a higher risk of cardiovascular comorbidities and are more likely to be older [93]. Current guidelines recommend the use of imaging rather than biopsy for the diagnosis of HCC. Although the lack of biopsy is an issue for understanding the pathology, biopsy-related risks are too high [209]. Indeed, the procedure is invasive and associated with anxiety and discomfort, plus there is a risk of hemorrhage and tumor seeding. Moreover, the likelihood of the biopsy being comprehensively representative of a large or multifocal tumor is low. The discovery of new biomarkers, such as circulating tumor cells might address the monitoring problem [210]. In patients with HCC, circulating tumor cells can indeed be detected in two-thirds of patients.

Because of the association with a number of comorbidities and mortality, patients need to be treated as soon as the diagnosis of NAFLD is made. Currently, there are no specific medications for the treatment of NAFLD. So the first step in the management of the disease is to lose weight and improve insulin resistance by implementing lifestyle modifications that focus on healthy eating habits and regular exercise [211]. Because the weight loss can be difficult to achieve and to sustain, medication or surgical intervention is also an option. Pharmacological treatments focus on coexisting conditions like diabetes, fat disorders, and obesity/weight lost in order to reduce insulin resistance and improve liver function.

HCC can be treated by surgical resection, liver transplantation, liver directed therapy or systemic therapy [212]. Better understanding of the pathogenesis led to the identification of potential therapeutic targets. For a number of years, sorafenib (a multi-kinase inhibitor) has been the only first-line medical therapy for patients with HCC [213]. But this drug only provides a modest median 10 weeks gain in overall survival. However, a number of encouraging new studies for medical therapy of HCC have emerged, such as lenvatinib (phase III trial) and regorafenib (phase III trial). Lenvatinib is another multi-kinase inhibitor and is an effective inhibitor of tumor angiogenesis that interferes with tumor angiogenesis-related molecules and

suppresses growth signals mediated by VEGFR and FGFR [214]. Regorafenib is a multi-kinase as well. It was shown to a 13 weeks median survival benefit over placebo in HCC patients [215].

2.6 Protein tyrosine phosphatases in NAFLD and HCC

Protein tyrosine phosphatases have been studied in different pathologies, including obesity, NAFLD and HCC.

2.6.1 Cys-based PTP, class I, subclass I

Some classical phosphatases from class I cys-based PTPs have been found to play a role in NASH or HCC. Oxidative stress accompanying obesity can inactivate PTPs in the liver [216]. Indeed, it was shown that oxidative stress activates signaling pathways that exacerbate disease progression. In obese mice, oxidative stress accompanying obesity inactivates hepatic T cell protein tyrosine phosphatase (TCPTP). This inactivation promotes lipogenesis, steatosis and insulin-STAT-5 signaling. Moreover, TCPTP depletion in hepatocytes promotes T cell recruitment and ensuing NASH and fibrosis, and HCC in obese mice via STAT-1 and STAT-3 signaling [217].

Protein tyrosine phosphatase 1B (PTP1B) is a negative regulator of the leptin [218] and insulin [219] signaling pathways. Mice with whole body deletion of PTP1B were protected against the development of obesity and diabetes [220]. Selective deletion of this PTP in the liver attenuates the HFD-induced ER stress [221], which could be a mechanism for the improvement of insulin sensitivity and the observed decreased levels of TG and cholesterol in the blood and in the liver. Moreover, it was recently shown that PTP1B plays a dual role in NASH progression and reversion. Using a methionine-choline deficient diet mouse model, Gonzalez *et al.* [222] demonstrated that during NASH progression, PTP1B restrains inflammation. On the other hand, the lack of the phosphatase accelerates the reversion of NASH when replacing MCD diet for normal diet. The proposed mechanism is that this PTP targets the proliferative responses mediated by Met signaling in hepatic progenitor cells (HPC, called oval cells in rodents). HPC represent a reserve compartment that is activated when mature epithelial cells of the liver are damaged or in case of severe cell loss.

2.6.2 DUSPs (cys-based PTPs, class I, subclass II)

Some MKP, A-DUSPs and other DUSPs such as PTEN have also been studied in obesity, NAFLD and HCC.

2.6.2.1 MKPs

MKP-1 (DUSP-1) has been suggested to be involved in obesity and diabetes. MKP-1 KO mice are resistant to diet-induced obesity due to enhanced energy expenditure [223]. MKP-1 deficient mice fed a HFD or leptin receptor-deficient mice lacking MKP-1 are protected from the development of hepatosteatosis [224]. In this model, loss of MKP-1 inhibited PPARγ function by increasing MAPK-dependent phosphorylation of PPARγ. Another group showed that liver-specific deletion of MKP-1 enhances gluconeogenesis and causes hepatic insulin resistance in normal diet fed mice, while conferring protection from hepatosteatosis in HFD fed mice [225]. These observations suggest that MKP-1 plays an important role in regulating liver metabolism. Tsujita *et al.* studied HCC tumors from 77 patients and observed a decreased in the expression of MKP-1 in 15% of HCCs [226]. Decreased MKP-1 expression significantly correlated with a larger tumor size. Moreover, the disease-free survival rates in MKP-1-negative and -positive patients were 0 and 31% at 5 years, respectively. However, this study did not discriminate the cause of HCC. This could explain why MKP-1 shows a negative role in hepatosteatosis development but shows a protective role in HCC development.

MKP-3, also called DUSP6, is a cytoplasmic phosphatase that can inactivate ERK and JNK. Its expression was studied in surgically resected HCC [227]. MKP3 is overexpressed in tumor tissue compared to adjacent tissue or normal liver tissue. In parallel, phosphorylation of ERK and JNK were up-regulated in tumor tissue compared to adjacent tissue, which have been implicated in tumor development. Moreover, its higher expression in tumor tissue was associated with recurrence after curative resection of HCC.

MKP-4, or DUSP9, has a protective effect against the development of insulin resistance through its ability to dephosphorylate and inactivate mediators, such as ERK and JNK [228]. MKP-4 is also a potential tumor suppressor in HCC. Indeed, it

was demonstrated that its expression was down-regulated in HCC tissues compared to adjacent tissues [229]. This was later supported by a study by Shen *et al.* that showed that MKP-4 interacts with ERK1/2 and negatively regulates its pathway [230]. Lower expression of MKP-4 was correlated with higher expression of ERK1/2 and p-ERK1/2 in HCC tissue. In 2019, Ye *et al.* [231] showed that expression of MKP-4 is down-regulated in hepatocytes in NAFLD and that MKP-4 prevents NAFLD and NASH progression in mice. They used a conditional liver-specific MKP-4 KO mouse and showed that MKP-4 is a key suppressor of HFD-induced hepatic steatosis and inflammatory responses. This DUSP exerts its effect by blocking apoptosis signal-regulating kinase 1 (AKS1) phosphorylation and the subsequent activation of p38 and JNK signaling.

MKP-7 or DUSP16, is a JNK-specific kinase that has been reported to negatively modulate the MAPKs signaling. Wu *et al.* identified that MKP-7 could directly interact with TAK-1 in human hepatocytes [232] and negatively regulate JNK signaling to reduce metabolic stress-induced hepatic steatosis.

MKPX, also called DUSP7, expression is reduced in liver samples from patients with hepatic steatosis or NASH, as well as in the liver of obese mice (from HFD or genetically obese *ob/ob*) [233]. In addition, DUSP7 knock-out in mice accelerated insulin resistance, glucose intolerance, liver dysfunction, fibrosis and hepatic steatosis. DUSP7 interacts with transforming growth factor β (TGF-β)-activated kinase 1 (TAK1). DUSP7 deletion promoted activation of TAK1 in mice fed HFD, contributing to lipid deposition, inflammatory response and ROS production.

2.6.2.2 A-DUSPs

Some A-DUSPs have studied in NAFLD and HCC. Indeed, DUSP12 expression was decreased in the liver of HFD fed mice [234]. Huang *et al.* showed that hepatocyte-specific DUSP12 KO mice under HFD exhibit an increase in hepatic steatosis, insulin resistance and inflammation compare to control littermates. Consistently, DUSP12 overexpression in hepatocyte reduced HFD-induced steatosis and improved insulin sensitivity. In the liver of DUSP12 KO mice, apoptosis signal-regulating kinase 1 (ASK1) was upregulated, activating the MAPK pathway and hepatic metabolism.

DUSP12 physically binds to ASK1, promotes its dephosphorylation and inhibits its action on ASK1-related proteins.

Similarly, DUSP26 is decreased in fatty liver of HFD fed mice [235]. Using liver-specific DUSP26 KO mice, Ye *et al.* demonstrated that DUSP26 deletion promotes steatosis, inflammatory response and insulin resistance. Accordingly, DUSP26 overexpression in the liver inhibits HFD-induced obesity and hepatic steatosis. At the molecular level, DUSP26 deficiency in hepatocytes activates p38/JNK pathway by interacting with transforming growth factor beta-activated kinase 1 (TAK1).

Finally, DUSP28 expression is significantly upregulated in human HCC tissues [236]. The overexpression of DUSP28 in vitro promotes HCC cells proliferation and colony formation and the knockdown of the phosphatase had the opposite effect. Investigation of the mechanism revealed that DUSP28 could activate the p38 MAPK signaling pathway [236].

2.6.2.3 Other DUSPs

Dysregulation of PTEN expression/activity in hepatocytes represents an important and recurrent molecular mechanism contributing to the development of liver disorders. PTEN expression in hepatocytes is downregulated in obese animals and humans displaying steatosis [124]. PTEN could also help differential diagnosis of NAFLD and alcoholic liver disease (ALD) because PTEN protein expression is downregulated in NAFLD, but not in ALD [237]. Genetic deletion of PTEN expression, specifically in the liver of rodents, triggers liver steatosis, hepatomegaly and HCC [238,239]. Liver-specific PTEN KO mice have improved systemic insulin sensitivity and glucose tolerance. Moreover, the association of SHP2 and PTEN was highlighted in NASH and HCC development [240]. SHP2 and PTEN deficiencies were detected in liver cancer patients with poor prognosis. Ablating both SHP2 and PTEN in hepatocytes induces early-onset NASH and promotes genesis of liver tumor-initiating cells. This could be due to increased c-Jun expression/activation and elevated ROS and inflammation in the liver.

Objectives

OBJECTIVES

DUSP3 is a ubiquitously expressed atypical dual specificity phosphatase. Although some *in vitro* and *in vivo* substrates have been identified, the physiological roles of this phosphatase remain unclear. DUSP3-KO mice were generated few years ago in the laboratory. While these mice are born healthy and have no spontaneous phenotype at young age, they become obese and develop NAFLD with aging if they are fed high fat diet. Therefore, the overall goal of this project was to investigate the role of DUSP3 in the development of obesity, associated insulin resistance, NAFLD and HCC.

The first part of this work focused on describing more in depth the obesity phenotype and related disorders such as NAFLD and subsequent complications such as the onset of diabetes and progression of NAFLD to NASH and HCC. To exacerbate the phenotype, we used a diet-induced obesity model and compared it to regular chow diet in WT and DUSP3-KO mice.

The second part of the work focused on understanding the mechanisms behind the development of obesity and NAFLD when DUSP3 was deleted. Insulin plays an important role in the setting of these two pathologies. Thus, we investigated the insulin and its signaling pathway. Non-biased liver mRNA sequencing method was also used to get better insights into the mechanisms behind NAFLD development.

In the third part of this work, we studied the kinetic and aggressiveness of hepatocellular carcinoma development in DUSP3-KO mice by using a chemically induced hepatocarcinogenesis model combined to HFD. Given the observed NAFLD and obesity in DUSP3-KO mice under HFD, we hypothesized that DUSP3 deletion may accelerate the progression to HCC. We also investigated whether DUSP3 could be a tumor suppressor in the liver.

Materials and methods

MATERIALS AND METHODS

Mice

DUSP3 full knockout (DUSP3-KO) mice were generated as previously described [20]. They were backcrossed to C57/BL/6 mice for at least ten generations. Genotyping was performed as described previously [20]. All mice were bred in a specific pathogen-free animal facility (SPF). C57BL/6 (WT) mice used as controls were purchased from Charles River Laboratories (France). Immunodeficient NOD/SCID mice were also used in specific experiments and were from Janvier Labs (France). Only male mice were used in all experiments. DUSP3-KO and WT mice were matched for age in all experiments. All mice were maintained in filter-topped cages on autoclaved water and chow diet (CD; composed of 12% fat, 27% protein, and 61% carbohydrates based on caloric content, RM3; from Special Diet Service) or high fat diet (HFD; composed of 42% fat, 15% protein, and 43% carbohydrates based on caloric content; from sniff®, TD.88137). Animals were maintained in a temperature and light (12 hours light/dark cycle) controlled SPF animal facility.

Experimental protocol was approved by the Animal Ethical Committee of the University of Liège (protocol number 1738) and carried out in accordance with the European Community Guidelines

Obesity model

Two-month-old WT and DUSP3 KO mice were fed HFD for 16 months. Weight of the animals was evaluated every week for all duration of the experiment. The food consumption was evaluated over a 27-weeks period. At dissection, mice were bled under anesthesia via retro-orbital plexus and sacrificed by cervical dislocation. All soft tissues were harvested and weighted. Subcutaneous, epididymal and brown fat were dissected, weighed and fixed in 4% paraformaldehyde for 24 hours for paraffin block preparation. Livers were weighted and pictured. One lobe was fixed in 4% paraformaldehyde for 24 hours for paraffin block preparation and a second lobe was snap frozen for proteins extraction.

MicroCT imaging

Mice underwent an *in vivo* X-ray computed tomography (CT) images to assess body composition in terms of volume. CT scans were acquired using an eXplore 120 micro-CT (Gamma Medica, USA/GE Healthcare) with a customized protocol (70 kV, 0.512 mAs, 360 views over 360°, continuous rotation) provided by the manufacturer. Performance characteristics of this scanner have been described previously [241]. During imaging session, mice were anesthetized with isoflurane and placed in prone position in a dedicated animal holder equipped with an air warming system (Equipement Minerve). Mice were continuously monitored for respiratory rate and temperature. All micro-CT images were reconstructed using Feldkamp's filtered back projection algorithm with a cutoff at Nyquist frequency to obtain a 3D volume with an isotropic voxel size of 100 µm. In order to assess the CT signal intensity of the adipose tissue, CT scans of different freshly harvested fat types (epididymal white fat, subcutaneous white fat, adrenal white fat and brown fat) were also acquired.

CT images were used to assess fat volume as well as lean volume. A semi-automated segmentation procedure was performed using PMOD 3.6 software (PMOD Technologies). Briefly, an intensity threshold range (-280 to -160 HU (Hounsfield unit)) for fat was obtained based on the images of the ex-vivo harvested fat types. In-vivo CT image of the whole mouse was first manually segmented to remove the bed and other extra signals (e.g. tubes of warming system). The resulting image was sent to the PMOD automated segmentation to extract the fat. Based on the mean signal intensity (threshold for bone: 250 HU), extracted on a spherical region of interest placed on the bone, binary mask of the bone was extracted using automated segmentation method implemented in PMOD. A total body mask was also generated using a range of signal intensities containing fat, bone, and muscle. Knowing the voxel size and the number of voxels in the obtained masks, the fat, bone and total body volumes were calculated.

The % of Fat mass was calculated as follow:

% Fat mass = Fat Volume *100/ Total Body Volume

% Lean mass= [Total Body Volume – Fat Volume] *100/ Total Body Volume

Glucose tolerance assay

For glucose tolerance assay, mice were starved for 6 hours. Blood was drawn from a tail nick before and at the indicated time points after *per os* injection of glucose (2 g/kg body weight). Blood glucose was instantly measured using a Contour XT glucometer (Ascencia Diabetes Care).

^{18}F-FDG biodistribution

Mice were anesthetized with isoflurane (4% induction, 1.5-2% for maintenance) and fluorodeoxyglucose F 18 (^{18}F-FDG) (12 ± 1 MBq) was administered via the caudal vein. Positron emission tomography (PET) data were recorded during 60 minutes using a Siemens FOCUS 120 microPET (Siemens). Immediately after PET acquisition, the anesthetized mice were transferred into the eXplore 120 micro-CT (Gamma Medica, USA/GE Healthcare), and a whole-body CT image was acquired using a customized protocol (70 kV, 0.512 mAs, 360 views over 360°, continuous rotation) provided by the manufacturer. All microCT images were reconstructed using the Feldkamp's filtered backprojection algorithm with a cutoff at the Nyquist frequency to obtain a 3D volume with an isotropic voxel size of 100 µm. Images were processed using PMOD 3.6 software (PMOD Technologies). PET images were converted into standardized uptake value (SUV) parameter by normalizing the tissue concentration to the injected dose and the body weight. For each animal, the structural CT image was manually co-registered with the corresponding PET images. CT images were segmented to extract the regions of interest (heart, liver, kidney, bladder, muscle). Time-activity curves expressed in SUV units were extracted for all segmented regions.

DEN-induced hepatocarcinogenesis mouse model

For chemical induction of hepatocarcinogenesis, mice were injected intraperitoneally with diethylnitrosamine (DEN) at 25 mg/kg (Sigma) at postnatal day 14, and then weaned at 5 weeks and maintained on regular CD (Figure M.1). Four weeks after DEN injection, mice were separated into two dietary groups and fed either CD or HFD until sacrifice. Weight of the animals was evaluated every week for all duration of the experiment. Animals were sacrificed by cervical dislocation at week 26, 30, 34 and

37 weeks after birth. At dissection, mice were bled under anesthesia via retro-orbital plexus and sacrificed by cervical dislocation. All soft tissues were harvested and weighted. Livers and tumors were pictured and livers were separated into individual lobes. Externally visible tumors (>1 mm) were counted and measured. Large lobes were fixed in 4% formalin for 24 hours for paraffin block preparation.

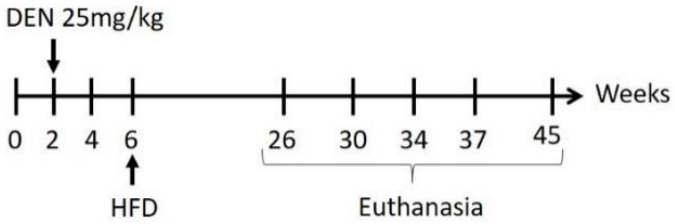

Figure M.1. *Chemical model of hepato-carcinogenesis in mice.* Week 0 represents birth day. 14-day-old WT and DUSP3-KO mice received a single injection of DEN (25mg/kg). 4 weeks later, mice diet was switched to HFD for half of the mice while the other half were kept under CD. Mice were euthanized at 26, 30, 34 and 37 weeks old. Mice under CD diet were also euhtanized at 45 weeks old.

shRNA lentiviral plasmids and HepG2 transduction

Silencing of human DUSP3 gene expression into HepG2 cells was achieved using short hairpin RNA (shRNAs) lentiviral plasmids (Sigma, TRCN0000314903, TRCN0000367555 and TRCN0000314904), and control shRNA anti-eGFP shRNA plasmid (Sigma, SHC005). Lentiviral vectors were generated by the GIGA Viral Vectors core-facility. Briefly Lenti-X 293T cells (Clontech®, 632180) were co-transfected with a pSPAX2 (Addgene®) and a VSV-G encoding vector. Viral supernatants were collected 48h, 72h and 96h post-transduction, filtered (0.2µM) and concentrated 100 x by ultracentrifugation. Lentiviral vectors were next titrated using qPCR Lentivirus Titration Kit following the manufacturer's instructions (ABM®, LV900).

HepG2 cells (American Type Culture Collection, Manassas, VA, USA) were cultured in DMEM complete media (Gibco) containing 4 mM L-glutamine, 0.1 mM minimum essential medium (MEM) and non-essential amino acids, supplemented with 10% fetal bovine serum (Sigma, F7524) in a humidified 37°C incubator containing 5% CO2. HepG2 cells with less than 10 passages were used for experiments. Cells were transduced with lentiviral vectors (30 TU/cell) and were selected with 3 µg/mL puromycine (Invivogen, ant-pr-1). The absence of RCL and mycoplasma in cell

supernatant was confirmed with qPCR Lentivirus Titration kit and MycoAlert™ PLUS Mycoplasma Detection Kit (Lonza, LT07-710) respectively.

Ectopic xenograft of HepG2 cells in NOD/SCID mice

Stably transfected HepG2 cells were collected by trypsin digestion. 8-week-old NOD/SCID mice were anesthetized with a mixture of ketamine and xylazine and shaved on both flanks. A suspension of 2.10^6 shRNA transduced cells was injected subcutaneously into the left flank and a suspension of control cells was injected into the right flank of the mice. Animals were weighted every other day and tumors were measured using a caliper once a week for 4 weeks. The tumor volume was calculated using the formula $V = l \times W^2 /2$; where l equals the length (greatest dimension) and W equal the width of tumors. Mice were sacrificed 4 weeks after the injection. The tumors were weighted and measured.

Adeno-associated virus production and *in vivo* reconstitution of DUSP3 expression in the liver of DUSP3-KO mice

AAV gene transfer plasmids were purchased at Vector Builder: pAAV TBG mDUSP3-IRES-Luc2 (VB180920-1068bft) allowing mouse DUSP3 CDS and Firefly humanized luciferase expression under the control of liver-specific TBG promoter and pAAV TBG Stuffer-IRES-Luc2 [VB180921-1101yqg]) (Figure M.2).

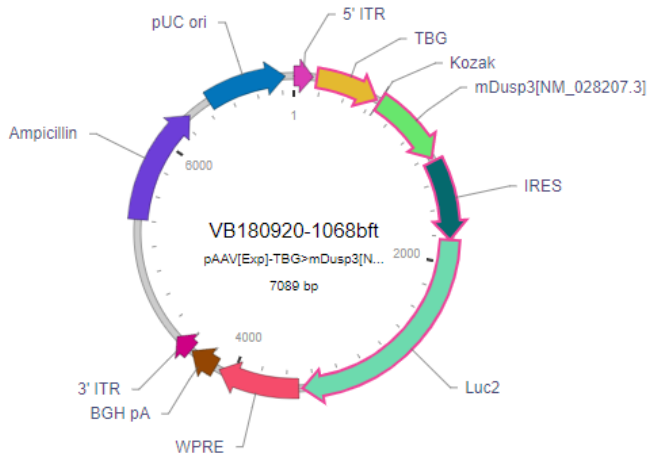

Figure M.2. *Plasmid used for AAV construction.* AAV gene transfer plasmids were purchased at Vector Builder: pAAV-TBG-mDUSP3-IRES-Luc2 and pAAV-TBG-Stuffer-IRES-Luc2. These plasmids allow mouse DUSP3 and Firefly humanized luciferase expression under the control of the liver-specific TBG promoter.

These plasmids were co-transfected into 293AAV Cell Line (Cell Biolabs, AAV-100) together with a helper plasmid (Part No. 340202 VPK-401 kit) and REP-Cap plasmid (pAR-(rh)8, a kind gift of Dr. Miguel Esteves (Gene Therapy Center, University of Massachusetts Medical School, 368 Plantation Street, ASC6-2055, Worcester, MA 01605). After 3 days, cells were lysed and rAAV were collected and clarified. rAAV vectors were then titrated (Table M.1) with qPCR Adeno-Associated Virus Titration Kit (ABMGood, G931) and used for in vivo injections.

Description	Titer
pAAV TBG mDUSP3-IRES-Luc2 (RC8)	6.98E+12
pAAV TBG mDUSP3-IRES-Luc2 (RC8)	2E+12
pAAV TBG mDUSP3-IRES-Luc2 (RC8)	2.67E+12
pAAV TBG Stuffer-IRES-Luc2 (RC8)	1.40E+13
pAAV TBG Stuffer-IRES-Luc2 (RC8)	2.85E+12

Table M.1. *rAAV vectors titration.*

20 DUSP3-KO mice were used: 10 mice received the AAV-control and 10 mice received the AAV-DUSP3. AAV were diluted in PBS to obtain 10^{11} particles in 100 µl. AAVs were injected intraperitoneally at postnatal day 10 and through the tail vein at postnatal day 50 (Figure M.3). Mice were injected intraperitoneally at postnatal day 14 with DEN (25 mg/kg). Four weeks later, the food was switched to HFD. To ensure that DUSP3 expression was maintained, we performed a second injection of AAV at week 7 after birth. Mice were monitored weekly for weight, three times for fasting insulin level in blood (week 8, 18 and 25 after birth) and once for glucose tolerance using OGTT assay (week 25 after birth).

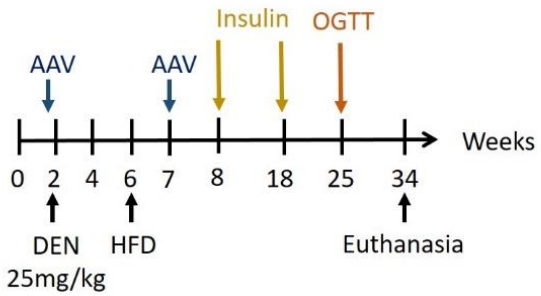

Figure M.3. *Illustration of the AAV protocol.* 10-day-old DUSP3-KO mice were injected intraperitoneally with 10^{11} particles of AAV. 10 mice received the AAV containing the stuffer sequence and 10 mice received the AAV expressing DUSP3. 4 days later, mice received a single injection of DEN (25mg/kg of body weight). 6 weeks after birth, food was replaced with HFD for all mice. At 7 weeks old, mice received a second injection of 10^{11} particles of AAV. Weight was monitored weekly, fasting insulin levels in blood was measured on 3 occasions and OGTT was performed once. Mice were euthanized at 34 weeks old.

Every two months, the expression of luciferase was monitored in 2 mice from each group using Imaging System Xenogen IVIS Lumina III (PerkinElmer, Waltham, MA, United States). 100 µl of luciferin potassium salt (30mg/ml) was intraperitoneally injected in mice. After 12 minutes, the photons emitted by the luciferase activity were detected. The bioluminescence was quantified using the Living Image Software (Caliper Life Sciences, Waltham, MA, United States). Mice were sacrificed at 34 weeks after birth. Overnight fasting animals were sacrificed by cervical dislocation and all soft tissues were harvested and weighted. Luciferase expression in soft tissue was monitored using the Xenogen IVIS Lumina III. Livers were pictured and separated into individual lobes. Externally visible tumors (>1 mm) were counted and measured. Large lobes were fixed in 4% formalin for 24 hours for paraffin block preparation and another lobe was snap-frozen for protein extraction.

Serological analysis

Blood was collected from the retro-orbital plexus using capillary at the termination time point. Serum was separated after clotting by centrifugation at 2300 g for 10 minutes. ALT, AST, CRP, TG, LDL, HDL and cholesterol levels in serum were measured using AU480 chemistry analyzer (Beckman Coulter). Plasma insulin concentration was measured by ELISA (Mercodia).

HOMA-IR

Insulin sensitivity was estimated using the Homeostatic Model Assessment of Insulin Resistance (HOMA-IR) method, calculated using the formula: basal insulin (mU/l) * basal glucose (mg/dl) / 405.

Proliferation assay

Proliferation assay was performed in 6 wells tissue culture plates. Control (eGFP) and DUSP3 shRNA transduced HepG2 cells were plated in duplicate (500.000 cells per well) in 2 ml complete DMEM and cultured at 37°C and 5% CO_2. Cells were harvested using trypsin after 24, 48, 72 and 96 hours. Cells were counted using TC20™ Automated Cell Counter (BioRad).

Adipocytes size assessment

Epididymal fat was fixed in 4% paraformaldehyde for 24 hours and embedded in paraffin, sectioned (5µm) and stained with hematoxylin and eosin (H&E) to evaluate morphology. Resulting slides were scanned using the NDP NanoZoomer Digital Pathology scanner (Hamamatsu). For adipocytes size quantification, 3 fields per section per mouse were analyzed with a macro in ImageJ software. The macro blurs the file with a Gaussian filter, then uses Hue Saturation Brightness model with the color threshold tool to detect the edge of the adipocytes. The macro counts and measures all adipocytes with a size bigger than 342.5µm^2 and circularity between 0.3 and 1.

Liver histology

Livers were fixed in 4% paraformaldehyde for 24 hours and embedded in paraffin, sectioned (5µm) and stained with H&E to evaluate morphology. Masson's trichrome (Merck) staining, which colors collagen in blue, was used to assess fibrosis. Reticulin or Foot staining, which colors reticulin fibers, was used to evaluate hepatic trabeculae architecture. Liver histology was visualized by light microscopy and sections were scanned using the NDP NanoZoomer Digital Pathology scanner (Hamamatsu). A blind analysis of liver histology was evaluated by two pathologists. For each specimen

a SAF (Steatosis, Activity, Fibrosis) score, summarizing the main histological lesions, was defined. This score was developed by the Fatty Liver Inhibition of Progression consortium and summarizes the main histological lesions [206]. The steatosis score (from 0-3) assesses the quantities of large or medium-sized lipid droplets. The activity score (from 0 to 4) is the addition of two factors: the evaluation of hepatocytes ballooning (from 0 to 2) and the presence of lobular inflammation (from 0 to 2). Ballooning is defined as cellular enlargement 1.5 to 2 times the normal hepatocyte diameter, with rarefied cytoplasm [242]. The fibrosis score (from 0 to 2) is given depending of the quantity of fibrosis found in the liver, according to the NASH Clinical Research Center. The total score is therefore between 0 and 9. The presence of dysplastic nodules and hepatocellular carcinoma was also assessed. This required the analyze of different parameters, including loss of architecture and modifications in the reticular fibers. Three different staining were needed to evaluate the SAF score and the presence of dysplasia (Figure M.4). H&E staining was used to assess steatosis, inflammation, ballooning and loss of architecture. Masson's trichrome is a staining that colors collagen fibers in blue, allowing to show presence of fibrosis in the liver. Foot staining shows the reticular fibers in the liver, which allow to see any modifications in the liver structure.

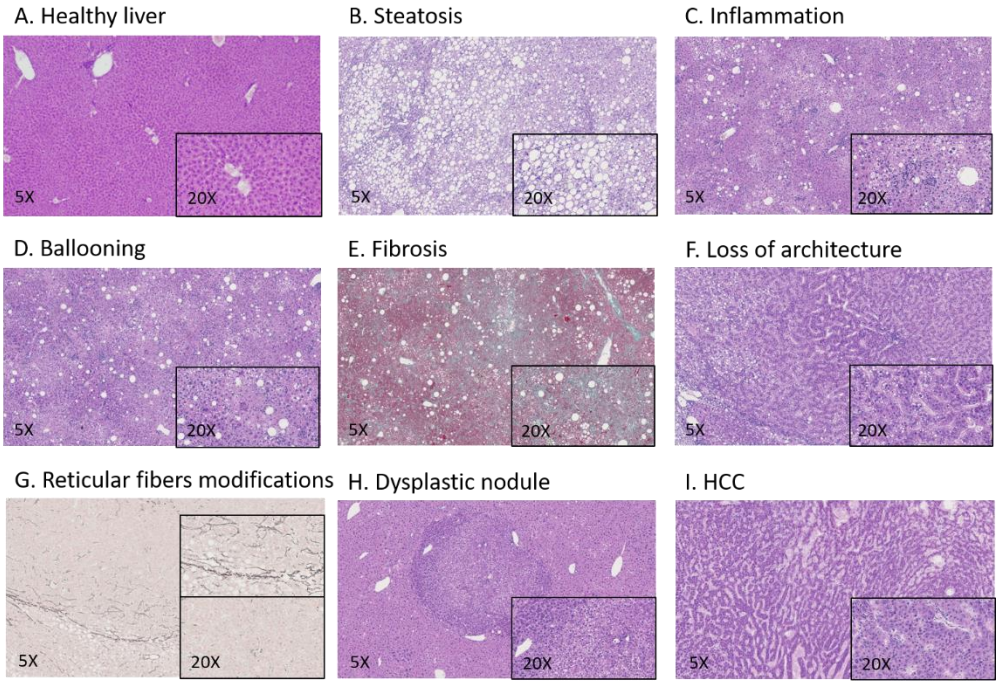

Figure M.4. *Representation of the criteria used for SAF scoring of NAFLD.* Representative images of the different criteria used in the SAF scoring and analyze of dysplasia. 5µm paraffin sections were used for staining. (A) H&E of a healthy liver. (B) H&E of a liver showing steatosis. (C) H&E showing immune cells infiltration in the liver. (D) H&E of the liver showing ballooning in hepatocytes. (E) Masson's trichrome staining showing collagen depot in blue. (F) H&E showing the loss of architecture in the liver. (G) Foot staining showing thickening and loss of the reticular fibers. (H) H&E of a dysplastic nodule. (I) H&E of hepatocellular carcinoma (HCC).

Immunohistochemistry

Paraffin-embedded liver tissues were used for immunostaining with primary antibody CD45 (Abcam, Ab10558) and revealed with DAB substrate. Sections were counterstained with hematoxylin. CD45 quantification was assessed using ImageJ software. One section per mouse, divided in 4 fields, was used for quantification. First, the image was split into 3 unmixed channels using the color deconvolution plugin from ImageJ (Hematoxylin, DAB and a third component not used here). A median filter (=2) was applied on the DAB channel and a threshold was applied to the image using Max Entropy algorithm. The total DAB area was measured. The total area of the tissue was detected using the Hue Saturation Brightness model with Color Threshold tool. DAB area is expressed as a percentage of the total area.

Immunofluorescence staining

5 µm sections from paraffin-embedded liver tissues were used for immunofluorescence staining with primary antibody anti-DUSP3 (Abcam, Ab125077). Immunoreactivity was revealed using anti-rabbit Alexa 488 secondary antibody. Nucleus were stained with DAPI. Fluorescence was visualized using the Leica TCS SP5 Confocal microscope (Leica).

Tissue homogenization and Western blot

Tissue were mechanically dissolved using a tissue lyser and cells were lysed using RIPA buffer (50 mM Tris-HCl (pH=8.0), 150 mM NaCl, 1% NP-40, 0.5% sodium deoxycholate, 0.1% SDS, 1 mM orthovanadate (Sigma-Aldrich), complete protease inhibitor cocktail tablets EDTA free (Roche), phosSTOP (Roche) and 1 mM phenylmethylsulfonyl fluoride (PMSF; Sigma-Aldrich)) on ice during 20 minutes. Lysates were clarified by centrifugation at 21.000g during 20 minutes at 4°C. The resulting supernatant was collected and protein concentration was measured using the colorimetric Bradford reagent (Bio-Rad). Samples were denatured at 95°C in Laemmli buffer. 40 µg of total lysates were run on SDS-PAGE gel and transferred to Hybond-nitrocellulose membranes. To block the non-specific binding sites, membranes were incubated for one hour in Tris-buffered saline-Tween 20 containing 5% of non-fat milk. The membranes were next immunoblotted with specific antibodies (Table M.2). Immunoreactivity was revealed using HRP conjugated secondary antibodies. The blots were developed by enhanced chemiluminescence (Thermo Scientific) according to manufacturer's instructions.

Target	Reference	Firm
DUSP3	8889	Santacruz
Phospho-p44/42 MAPK (ERK1/2) (Thr202/Tyr204)	9101	Cell Signaling
P44/42 MAPK (ERK1/2)	9102	Cell Signaling
Phospho-Akt (Ser473)	9271	Cell Signaling
Akt	9272	Cell Signaling
Phospho-IGF-1 Receptor β (Tyr1135/1136)/Insulin Receptor β (Tyr1150/1151)	3024	Cell Signaling
Insulin Receptor β (4B8)	3025	Cell Signaling
Phospho-GSK-3α/β (Ser21/9)	9331	Cell Signaling
GSK-3α/β	7291	Santacruz
Phospho-p38 MAPK (Thr180/Tyr182)	9215	Cell Signaling
P38 MAPK	9212	Cell Signaling

Table M.2. *Antibodies used for Western blot.*

RNA extraction

Total RNA was extracted from 20mg of frozen liver using Maxwell® 16 LEV simplyRNA Tissue Kit (Promega), according to manufacturer's instruction. RNA quantity was assessed using a spectrophotometer (NanoDrop Technologies). Total RNA integrity was evaluated by QIAxcel Advanced technology (Qiagen) and all the samples had a RNA Integrity Score (RIS) > 6.5.

RNA sequencing

RNA libraries were prepared with Truseq stranded mRNA sample prep kit from Illumina, based on polyA selection of mRNA. cDNAs fragments were sequenced using the Illumina NextSeq500. Biological triplicates were performed for all the conditions.

Differential gene expression analysis

Raw reads were quality controlled using FastQC (version 0.11.5) and aligned to the Ensembl mouse reference genome GRCm38 (release 97) using STAR (version 7.1a; Dobin *et al.*, 2013). Gene expression quantification was obtained with the --quantMode GeneCounts STAR option. Normalization and differential expression

analysis were performed using the DESeq2 R package [243], with the apeglm method for effect size shrinkage [244]. Genes with a q value below 0.05 and a fold change above 1.5 were considered differentially expressed. Heatmaps and fold change plots were done with the ggplot2 R package.

Gene Set Enrichment Analysis (GSEA) analysis

For GSEA analysis of RNA-sequencing data, GSEA software (version 4.0.3) available on the GSEA-Broad Institute website was used. Mouse Ensembl gene identifiers were converted to human orthologues. Normalized gene expression data set was run against a library of 50 curated gene sets for hallmark pathways (MSigDB v7.1). The statistical significance (False Discovery Rate (FDR) q-value) was estimated by running 1000 gene set permutations.

qRT-PCR

2µg of liver total RNA were reverse-transcribed to obtain cDNA (RevertAid H Minus First Strand cDNA Synthesis Kit, Thermo Scientific). Each cDNA was analyzed, in triplicate, with the ABsolute Blue QPCR Mix, SYBR Green, ROX (ThermoFisher Scientific) in the CFX384 Touch Real-Time PCR Detection System (BioRad) The results were normalized to Ribosomal Protein S9 (RPS9). The relative mRNA expression levels were calculated using the 2-ΔCt method. Used primers are presented in Table M.3.

Gene	FW	RV
DUSP3	GGGTGATGCCCAGTTTCT	GATCTCAACGACCTGCTCTC
DUSP4	CACGGACATCTGCCTGCTTAAA	GGCCAGGGCCTTGGTTT
DUSP9	AGAAGGCTACCCAGCATACTA	GCACTGGGCTAGACATTGAG
DUSP12	TCTCTTGTGAGCAAAGGCTATT	CTTCGCTGTTGACCCAACTA
DUSP26	TAACCATGCTGACGAAGTCTG	TTGAGCACGTGGGTGATG
FASN	TGGCTGTGTATTCCAGTTGTAG	CTCAAGATGAAGGTGGCAGAG
PNPLA3	TCTCACTCACCAGGGTGTC	GGGAATGAAGCAGGAACACA
SREBF1	CATGCCCTCCATAGACACATC	AGAAGCTCAAGCAGGAGAAC
IRS2	GTCCAGGCACTGGAGCTTT	GCTGGTAGCGCTTCACTCTT
LEPR	GACTTGCAGATGGTCACCCA	TGGGCTCAGACGTAGGATGA
GCK	CAACTGGACCAAGGGCTTCAA	TGTGGCCACCGTGTCATTC
RPS9	CACGGAGACCCTTCGAGA	GTAAACTTGACCCTCCAAACCT

Table M.3. *qRT-PCR primers.*

Statistical analysis

Statistical analysis and graphics were performed with GraphPad prism 7. The values plotted represent the mean of the biological replicates ± the standard deviation (SD). Mann-Whitney tests were employed when two groups were compared. P-value less than 0.05 was considered as significant. *$p<0.05$, **$p<0.01$, ***$p<0.001$. Relationships between variables were examined by Spearman correlation coefficient. Test was performed 2-sided and $p < 0.05$ was considered significant. For high throughput sequencing, the statistical significance is given as the adjusted p-value, q-value, representing the p-value corrected to the multiple testing. One-way ANOVA was used to compare means between groups, and Bonferroni test was applied to compare all pairs of groups.

Results

RESULTS

Full DUSP3-KO mice were generated few years ago in the laboratory. These mice are viable, fertile, develop normally and have no apparent or spontaneous phenotype or pathology, thus providing a good model to unravel DUSP3 function under different challenges. DUSP3 is expressed ubiquitously in mice tissues, though it is highly expressed in platelets, monocytes and macrophages [245]. Previous study from our lab shed light on the role of DUSP3 in platelets biology [30]. Indeed, DUSP3 seems to have a pro-thrombotic function in both mice and human platelets [30]. As a continuation of this work and given the role of platelets in atherosclerosis [246], we hypothesized that DUSP3-KO mice could be less susceptible to atherosclerosis. To investigate such hypothesis, wild-type (WT) and DUSP3-KO male mice were fed atherogenic high fat diet (HFD) for 10 weeks. Unfortunately, we did not observe any difference in term of atherosclerosis. However, and unexpectedly, we observed that DUSP3-KO mice, became obese and developed hepatosteatosis after 10 weeks under HFD. This phenotype was not observed in WT mice. We therefore decided to investigate DUSP3 role in obesity, NAFLD and hepatocellular carcinoma (HCC).

DUSP3-KO mice become obese while aging

In order to investigate the role of DUSP3 in obesity and NAFLD, 2-month-old WT and DUSP3-KO male mice were fed chow diet (CD) or HFD for 16 months. Their weight was monitored every week. We observed that DUSP3-KO mice gained significantly more weight than WT mice over time, under both CD and HFD (Figure R.1.A, R.1.B and R.1.C). Indeed, at 18 months of age, mutant mice gained 63% and 86% of their basal weight, while WT littermates gained 45% and 58% under CD and HFD, respectively (Figure R.1.D).

Obesity can result from an imbalance between caloric intake and expense. To evaluate if DUSP3-KO mice consume more food, mice were placed in individual clean cages and the food was weighted every week for 27 weeks. Interestingly, we observed that food consumption was similar between DUSP3-KO mice and WT mice, under both CD and HFD (Figure R.1.E). Moreover, the food consumption did not vary over time.

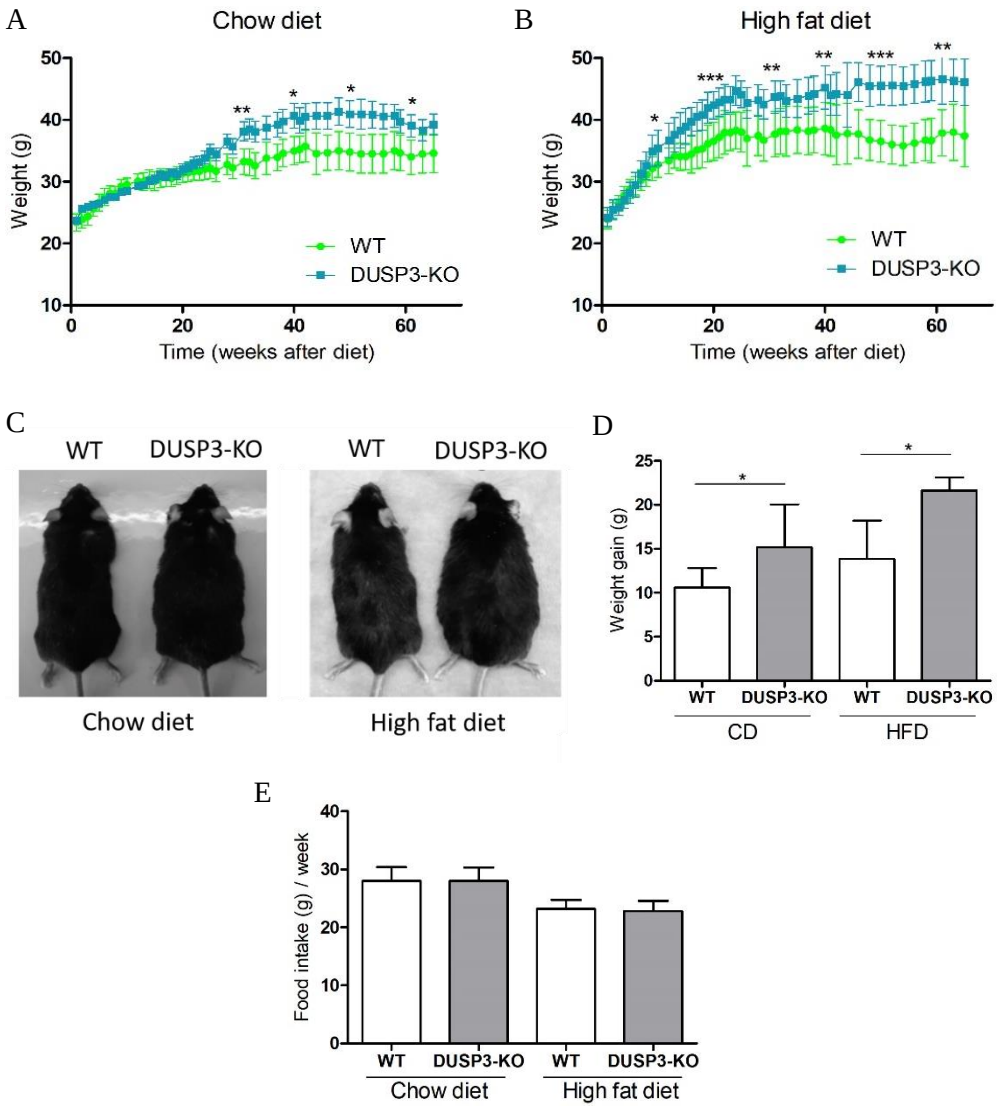

Figure R.1. *DUSP3 genetic deletion promotes obesity*. 2-month-old mice were given CD (A) or HFD (B) for 65 weeks and body weight was monitored every week. Data are expressed as mean ± SD (n=10 mice in each group). (C) Representative images of 18-month-old WT and DUSP3-KO mice fed CD (left) and 18-month-old WT and DUSP3-KO mice fed HFD (right). (D) Weight gain of WT and DUSP3-KO mice between the start and the end of the experiment, on CD and HFD. (n=5-10 mice in each group). (E) Food consumption was monitored every week for 27 weeks, for WT and DUSP3-KO mice, under CD and HFD (n=5 mice in each group). All data are expressed as mean ± SD (*, $p<0.05$; **, $p<0.01$).

DUSP3 deletion promotes fat accumulation in mice body

To investigate the origin of the observed body weight difference between DUSP3-KO and WT mice, we analyzed body composition using X-ray computed tomography (CT scan) on live mice. The scans were performed on mice at the age of 5 and 18 months old. The volume of the total body and the volume of the fat were calculated using PMOD 3.6 software (Figure R.2). We observed that at 5 months, DUSP3-KO mice tend to have slightly less fat than WT mice. When aging (18 months old), DUSP3-KO mice gain more fat compared to WT mice, regardless of the type of diet. Indeed, at 18 months of age, under CD, mutant mice had 153% more fat tissue than controls, whereas, under HFD mutant mice had only 23% more.

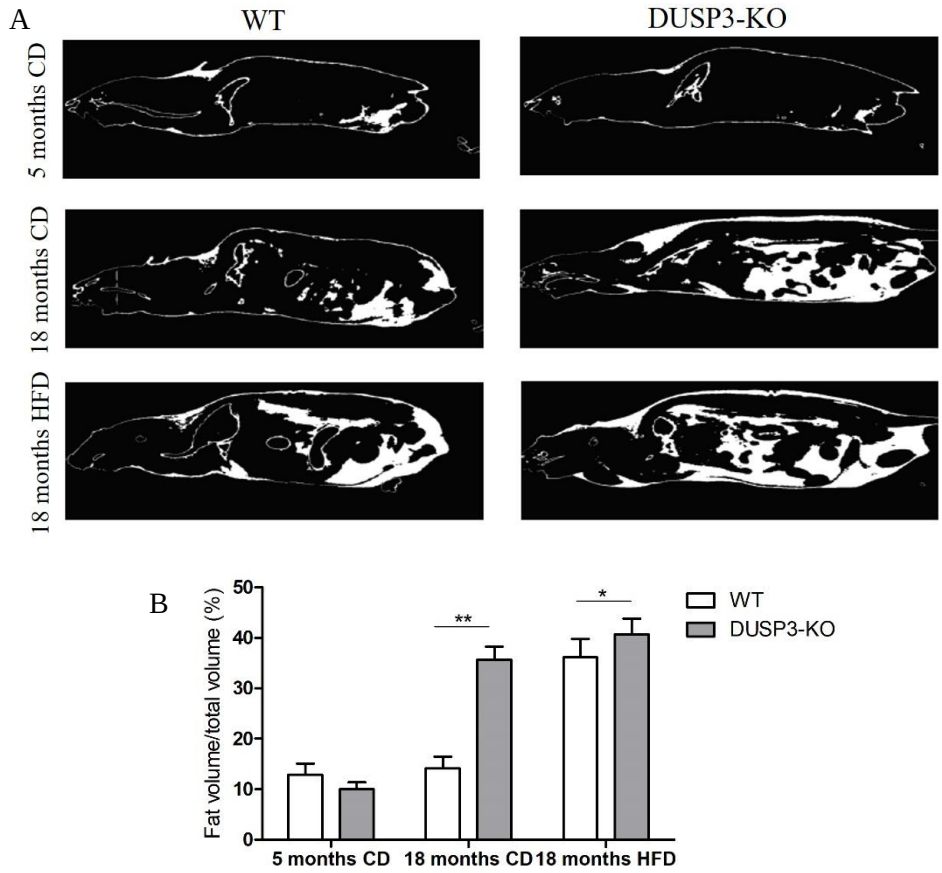

Figure R.2. *Body composition of WT and DUSP3-KO mice*. (A) Representative transversal CT scan images of 5 months WT and DUSP3-KO mice under CD diet, and 18 months old WT and DUSP3-KO mice under CD and HFD. White color represents fat and black represents lean mass. (B) Quantification of the fat mass in mice using PMOD 3.6 software, expressed as a percentage of the total body volume (n=3 mice in each group). Results are shown as mean ± SD (*, $p<0.05$; **, $p<0.01$).

These results were further confirmed at dissection by quantification of the different types of body fat. Mice were euthanized at 5 and 18 months old. Brown adipose tissue (BAT) and white adipose tissues (WAT) (composed of epididymal and sub-cutaneous fat) were collected and weighted (Figure R.3). We observed no difference in BAT between the different groups of mice. At 18 months old, under HFD, we could not detect any brown fat in mice. On the other hand, we observed that young DUSP3-KO have less WAT compared to WT mice. However, 18-month-old DUSP3-KO mice have significantly more epididymal and subcutaneous WAT compared to WT mice, independently of the type of food consumed.

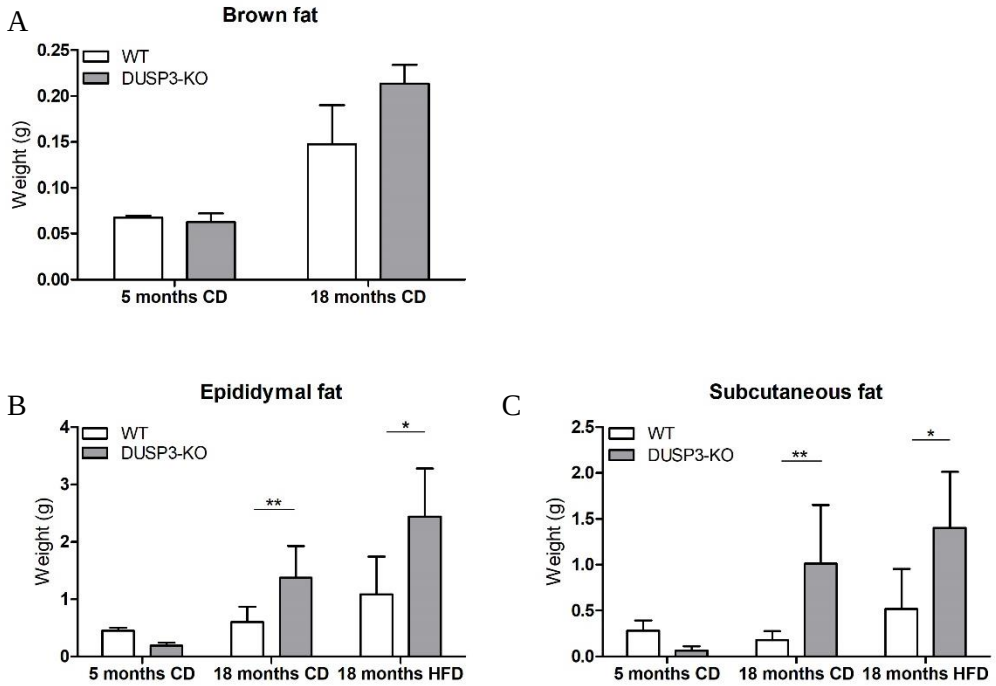

Figure R.3. *Body fat quantification of WT and DUSP3-KO mice at dissection.* Brown (A), epididymal (B) and subcutaneous (C) adipose tissues from 5- and 18-month-old mice under CD and HFD were dissected and weighted. Results are shown as mean ± SD (n=3-10 mice in each group). (*, $p<0.05$; **, $p<0.01$)

With the development of obesity, white adipose tissue undergoes remodeling where adipocytes increase in number (hyperplasia) and size (hypertrophy). Adipocytes hypertrophy results from an increase in lipid deposition versus lipolysis [247]. Excessive lipid accumulation in adipocytes triggers pathological changes to the adipose tissue. In order to analyze the size of the adipocytes, hematoxylin-eosin (H&E) staining of epididymal WAT was performed. Adipocyte area was calculated

using ImageJ software. As shown in Figure R.4, we observed that DUSP3-KO mice have significantly larger adipocytes compared to WT mice, at 18 months old, both under CD and HFD. In 5-month-old mice, we observed a slight but not significant increase of the size of the adipocytes.

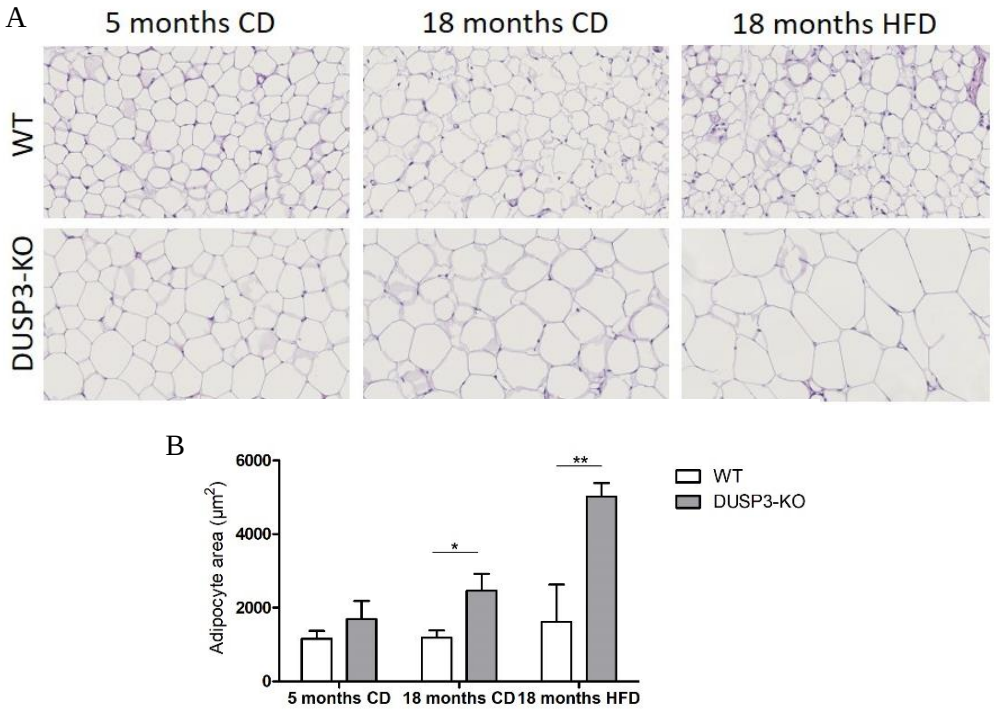

Figure R4. *Epididymal adipocytes size in WT and DUSP3-KO mice.* Hematoxylin-eosin staining was performed on 5µm sections of epididymal WAT. Area of the adipocytes was measured using ImageJ software (n=3 mice in each group). (A) Representative paraffin sections (20x magnification) of epididymal WAT from WT and DUSP3-KO mice under CD at 5 months old, and under CD and HFD at 18 months old. (B) Quantification of the average adipocytes area, in μm^2, obtained by measuring adipocytes area from 3 fields per mouse. Data are represented as mean ± SD (*, $p<0.05$; **, $p<0.01$).

DUSP3-KO mice show modifications in serum triglycerides, cholesterol and CRP concentrations

Obesity is frequently associated with metabolic syndrome. Characteristics of such syndrome include, among others, an increase of blood triglycerides (TG), reduced HDL cholesterol and elevated LDL cholesterol [44]. To investigate if the onset of obesity in DUSP3-KO mice is associated with metabolic syndrome, we quantified TG and cholesterol in mice serum using the AU480 chemistry analyzer (Figure R.5). At the age of 5 months, under CD, we observed that DUSP3-KO mice display lower

levels of TG than WT mice, while the level of cholesterol was similar in the two groups of animals. In older mice (18 months), DUSP3-KO mice displayed higher levels of TG under CD. The difference disappeared when mice were fed HFD. The levels of cholesterol were however significantly higher in mutant mice compared to 18-month-old WT mice under HFD. Both LDL and HDL were elevated, though LDL on HDL ratio was higher in DUSP3-KO mice compared to WT mice of the same age.

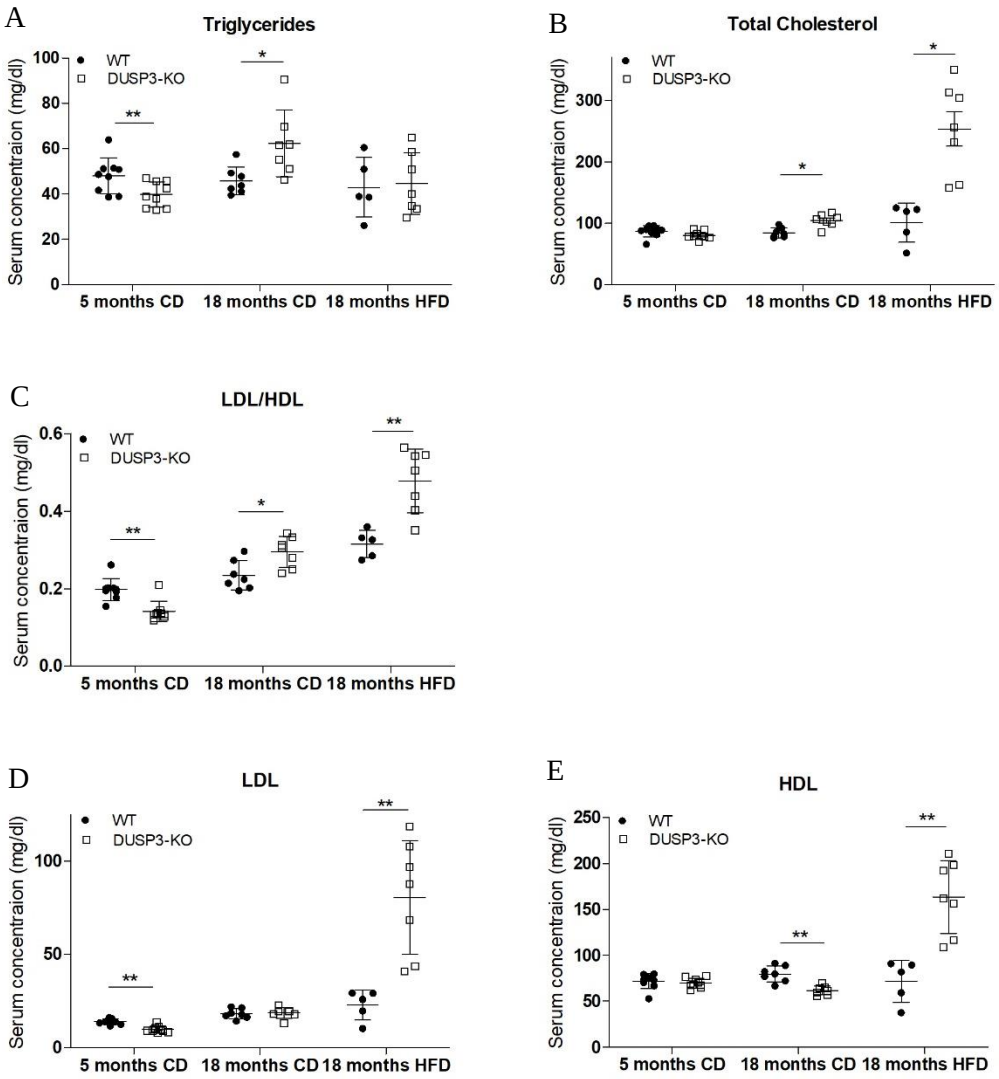

Figure R.5. *Serum levels of triglycerides and cholesterol in WT and DUSP3-KO mice*. Concentrations of triglycerides (A), total cholesterol (B), LDL/HDL ratio (C), LDL (D) and HDL (E) in serum were analyzed using the AU480 chemistry analyzer, from WT and DUSP3-KO mice under CD at 5 months old, and under CD and HFD at 18 months old. Each dot represents a mouse. (n=5-7 mice in each group). Data are showed as mean ± SD (*, $p<0.05$; **, $p<0.01$).

To investigate if the observed obesity was associated with inflammation, another hallmark of metabolic syndrome, we measured the levels of c-reactive protein (CRP) which is secreted by the liver during inflammation [248] (Figure R.6). We observed that CRP concentration was higher in the serum of DUSP3-KO mice than in the serum of WT mice under CD. Under HFD, CRP level was elevated in both groups of mice with slight but not significant increase in the mutant group over the WT.

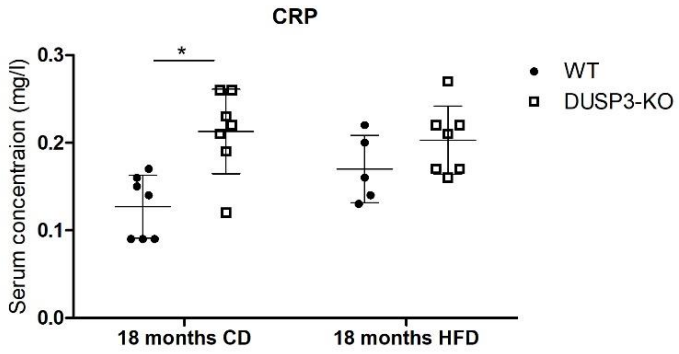

Figure R.6. *CRP in the plasma of WT and DUSP3-KO mice.* C-reactive protein was measured in the serum of mice using the AU480 chemistry analyzer, from WT and DUSP3-KO mice under CD and HFD at 18 months old. Each dot represents a mouse. (n=5-7 mice in each group group). Data are shown as mean ± SD (*, $p<0.05$; **, $p<0.01$).

DUSP3 deletion promotes NAFLD, NASH, fibrosis and HCC under HFD

Obesity is often associated with the development of NAFLD [82]. At the time of dissection (5- and 18-month-old mice), we carefully observed the livers. Livers were harvested, pictured and weighted. Macroscopically, we observed that livers from DUSP3-KO mice had a lighter color compared to WT mice, suggesting an accumulation of fat (Figure R.7.A). In addition to the significant increase of adipose mass tissue, we observed that at 18 months with HFD, DUSP3-KO have a significantly increased liver to body weight ratio compared to WT mice (Figure R.7.B). One lobe of the liver was embedded in paraffin and hematoxylin-eosin staining was used to observe microscopic constitution of the tissue. 18-month-old DUSP3-KO livers appeared to contain more lipids droplets (Figure R.7.C).

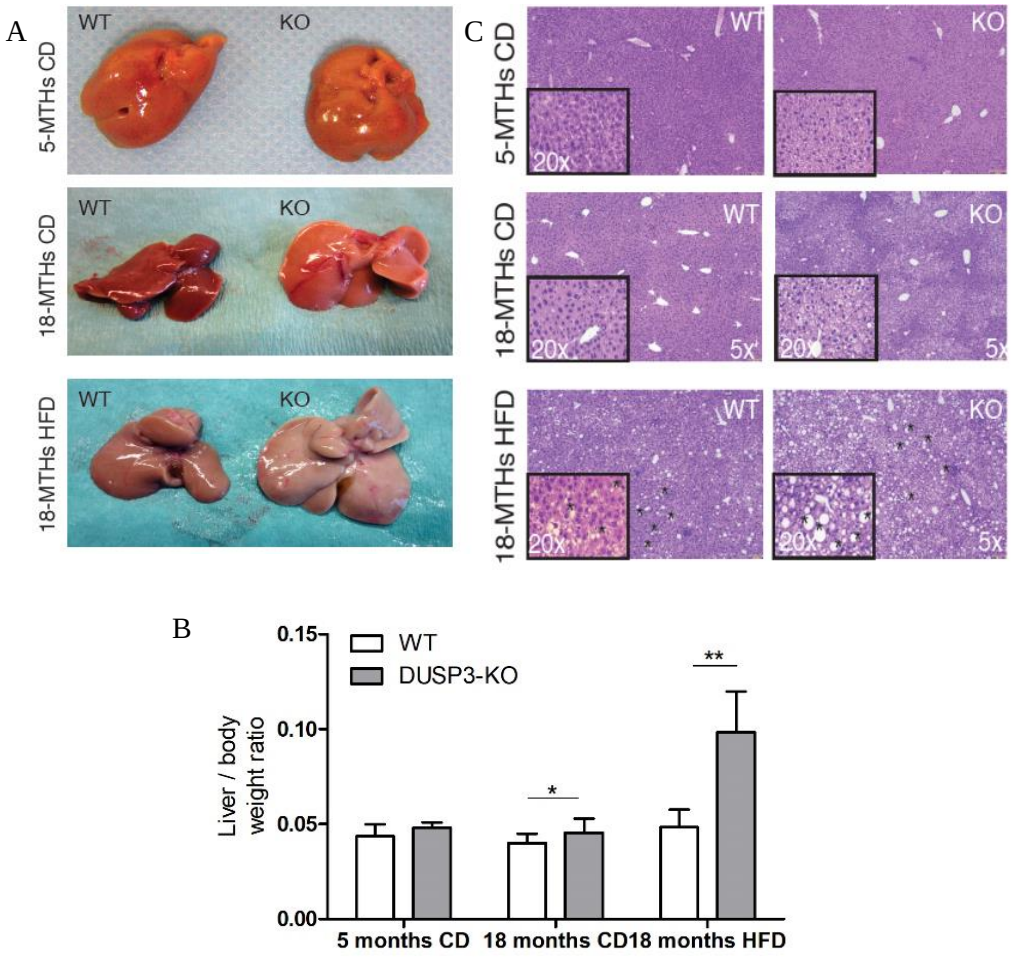

Figure R.7. *DUSP3 deletion promotes hepatosteatosis.* (A) Representative image of liver from 5- and 18-month-old WT and DUSP3-KO mice, under CD or HFD. (B) Quantification of liver weight to body weight ratio (n=3-7 mice in each group). Results are shown as mean ± SD (*, $p<0.05$; **, $p<0.01$). (C) Representative images of H&E staining of liver sections from WT and DUSP3-KO mice at 5 and 18 months old, under CD and HFD. 5x and 20x magnifications are shown. * indicate representative lipid droplet.

The presence of lipids in the liver is a characteristic of NAFLD. The accumulation of lipids seen in DUSP3-KO mice suggested that they might be more susceptible to NAFLD development. In order to evaluate the presence and degree of severity of the disease, two pathologists blindly analyzed stained sections of the livers and scored the lesions according to the SAF (Steatosis, Activity and Fibrosis) score.

Mice of 18 months old under CD and HFD were subjected to scoring. Under CD, we observed that DUSP3-KO mice have slightly higher scores for steatosis and activity compared to WT mice, leading to a slightly general higher SAF score (0.75 and 1 for

WT and DUSP3-KO mice, respectively (Figure R.8.A-D). Under HFD, the difference was more striking. Indeed, DUSP3-KO mice had higher scores for steatosis, activity and fibrosis, leading to a general SAF score significantly higher than WT mice (2.8 and 6.6 for WT and DUSP3-KO mice, respectively. $P<0.05$ *). Moreover, we observed that 40% of the analyzed DUSP3-KO mice under CD developed dysplastic nodules while none of the CD fed WT did (Figure R.8.E). Interestingly, we also observed that 80% of the analyzed HFD DUSP3-KO mice developed dysplastic nodules, of which 50% developed hepatocellular carcinoma. On the other hand, only 20% of the WT mice developed dysplastic nodules, and none of them developed HCC.

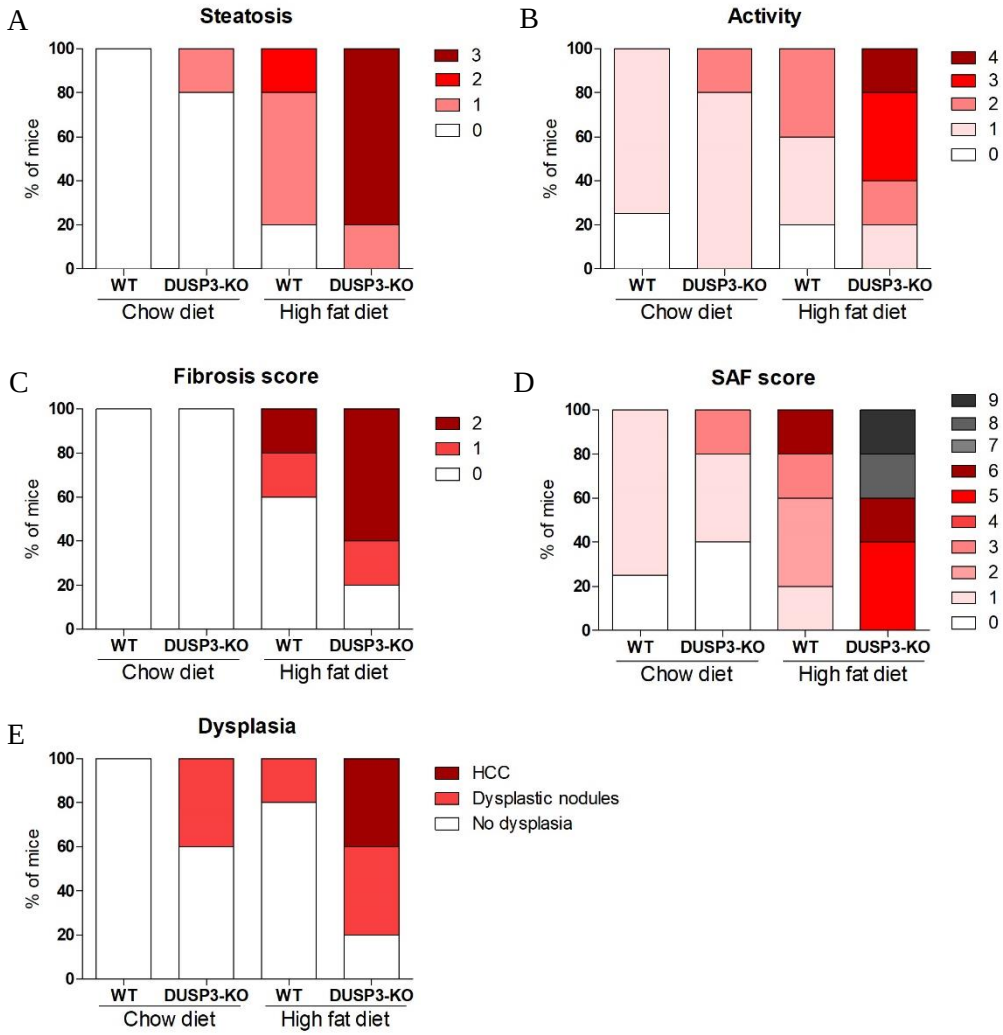

Figure R.8. *Evaluation of NAFLD and HCC in the liver of WT and DUSP3-KO mice.* 5µm paraffin sections of liver from 18-month-old mice under CD and HFD were stained with H&E, Masson's trichrome and Foot stains. These sections were analyzed by a pathologist to evaluate the SAF (Steatosis, Activity, Fibrosis) score and the presence of dysplastic nodules and hepatocellular carcinoma (HCC). (A) Steatosis score (from 0-3) evaluates the quantities of large or medium-sized lipid droplets. (B) Activity score (from 0 to 4) is the addition of two factors: the evaluation of ballooning of hepatocytes (from 0 to 2) and the presence of lobular inflammation (from 0 to 2). (C) Fibrosis score (from 0 to 2) is given depending of the quantity of fibrosis found in the liver. (D) SAF score (from 0 to9) is the addition of steatosis, activity and fibrosis scores. (E) Evaluation of the presence of dysplastic nodules and HCC in the liver. Data are expressed as a percentage of mice in each category (n=5 mice in each group).

Aspartate aminotransferase (AST) and alanine aminotransferase (ALT) are two hepatic proteins found in the serum in case of liver dysfunction. We measured these two enzymes in the serum of WT and mutant mice, at 5 and 18 months old under CD and HFD, using the AU480 chemistry analyzer. In accordance with the scoring, we observed that under HFD, 18-month-old DUSP3-KO mice presented higher levels of AST and ALT (Figure R.9).

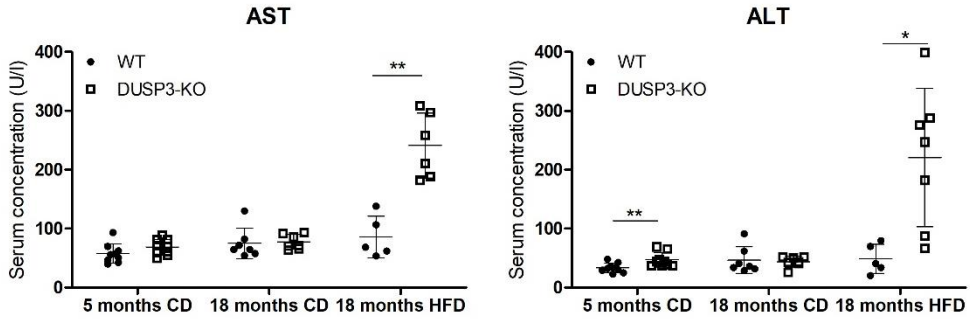

Figure R.9. *Serum analysis of AST and ALT.* Aspartate aminotransferase (AST) and alanine aminotransferase (ALT) were measured in the serum of WT and DUSP3-KO mice at 5 months old under CD and at 18 months old under CD and HFD, using the AU480 chemistry analyzer (n=5-7 in each group). Each dot represents one mouse. Results are shown as mean ± SD (*, $p<0.05$; **, $p<0.01$).

DUSP3 deletion promotes leukocytes infiltration in the liver under HFD

Leukocytes play an important role in the development of NAFLD and are considered a marker of advanced disease and inflammation [249–251]. To get insights into the extend of inflammation in fatty liver of the mice, we quantified leukocytes infiltration in the livers of 18-month-old mice using anti-CD45 antibody. We observed that DUSP3-KO mice have significantly more $CD45^+$ cells compared to WT mice when fed HFD (Figure R.10).

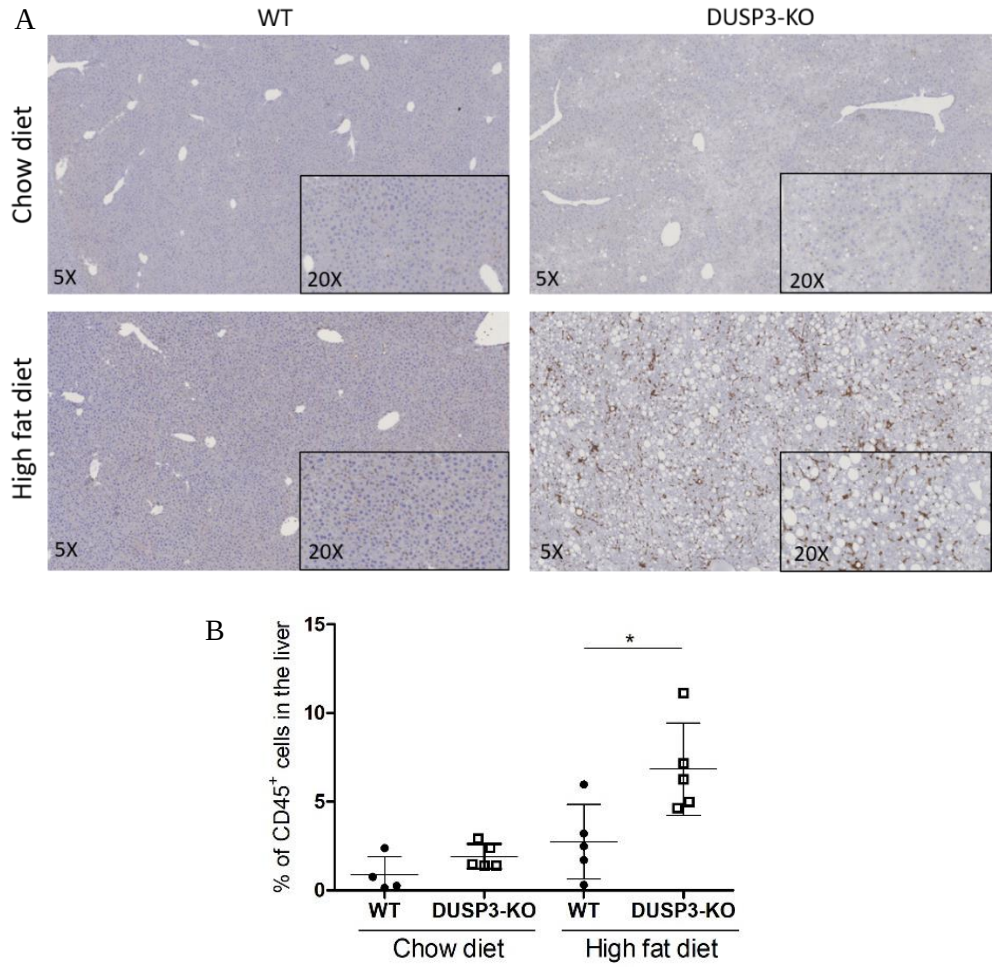

Figure R.10. *Leukocytes quantification in mice liver using anti-CD45 antibody.* Liver sections (5µm) were stained with anti-CD45 antibody (a pan marker for leukocytes) and secondary antibody coupled to HRP, and counter-stained with hematoxylin. Nuclei are colored in blue-purple and brown color indicates CD45 stained cells. (A) Representative images of stained liver from 18-month-old mice under CD and HFD. 5x and 20x magnification. (B) Quantification of the percentage of CD45+ cells in the liver. Total area and CD45 stained area of the section were calculated using ImageJ software. A whole section was used per mouse (n=4-5 mice in each group). Results are represented as mean ± SD (*, $p<0.05$; **, $p<0.01$).

DUSP3 deficiency exacerbates HFD-induced insulin resistance

Insulin resistance is considered one of the pathogenic features of obesity and NAFLD [252]. To investigate if this is also true for DUSP3-KO mice, 5-month and 18-month-old WT and mutant mice under CD or HFD were starved overnight. The next day, we collected blood and levels of fasting insulin in the serum was measured by ELISA. We observed that, at 18 months old, DUSP3-KO mice have significantly higher levels of insulin compared to WT mice (Figure R.11.A). Indeed, at 18 months, DUSP3-KO mice have 8.8 and 2.42 times more insulin than WT mice, under CD and HFD respectively. To further investigate the development of insulin resistance in DUSP3-KO mice and its influence on glucose tolerance, we monitored fasting insulin levels, fasting glucose levels and glucose tolerance in a new group of WT and mutant mice fed either CD or HFD, during 20 weeks. At each time point of the analysis, mice were starved for 6 hours and then blood was collected from the tail vein for both fasting insulin and glucose measurements. Mice were then submitted to oral glucose tolerance test (OGTT) to evaluate their glucose tolerance. Mice received a single dose of 2 g/kg of body weight of glucose *per os*. Glucose concentration in blood was measured at 15, 30, 60, 90 and 120 minutes after glucose injection. 4-month-old mice were tested to evaluate basal insulin and glucose levels (T0). After this first reference time point, half of the mice were put under HFD and the other half was kept under standard CD. T1 to T3 correspond to 4 weeks, 12 weeks and 20 weeks after the start of the HFD feeding, respectively. As expected, DUSP3 deletion was associated with an increase of plasma insulin levels at all time points analyzed (Figure R.11.B). Such increase was more pronounced under HFD in mutant mice compared to WT mice. Surprisingly, even with such high insulin levels, we did not observe any difference in fasting glucose levels between the different groups of mice, both under CD or HFD (Figure R.11.C). Fasting glucose and insulin levels allowed us to calculate the homeostatic model assessment for insulin resistance (HOMA-IR) score. HOMA-IR score is calculated as basal insulin (mU/l) * basal glucose (mg/dl) / 405 and is used to estimate insulin sensitivity. HOMA-IR score was higher in DUSP3-KO mice compared to WT mice, under both CD and HFD and at all time points analyzed (Figure R.11.D). This difference was significant under CD at T3, and under HFD at T1 and T3.

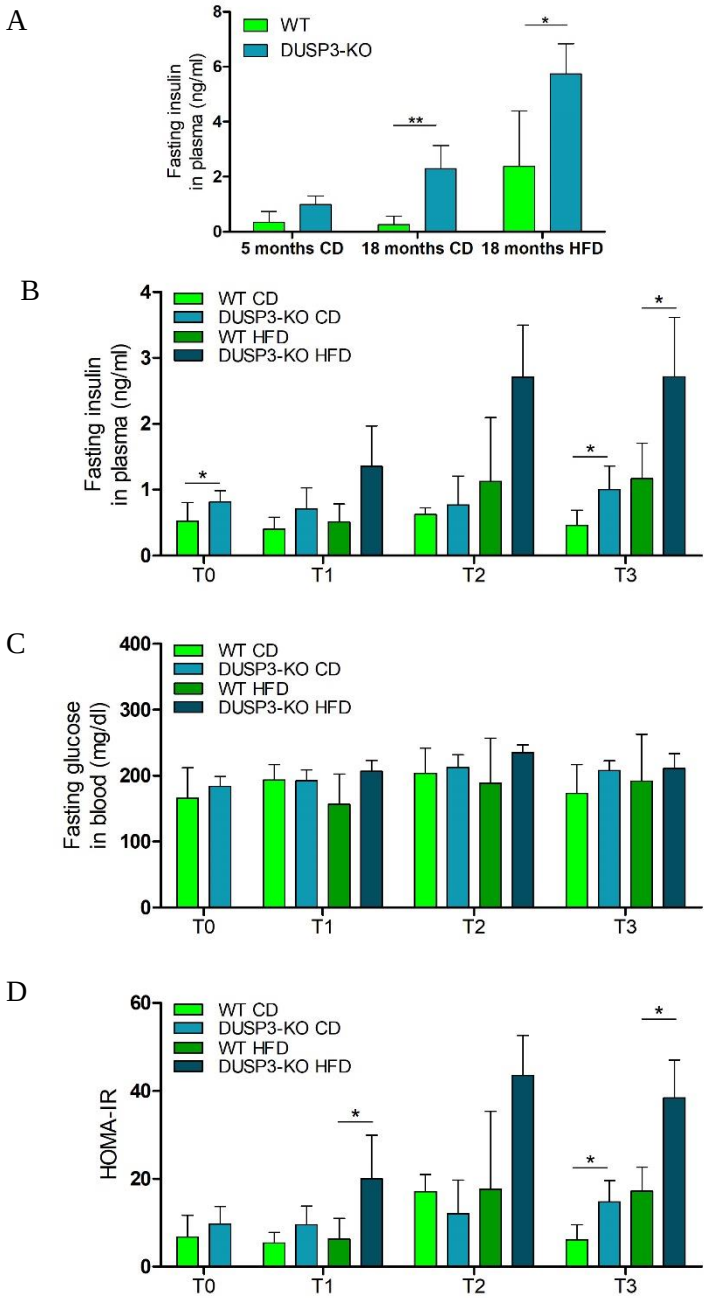

Figure R.11. *DUSP3 deletion exacerbate insulin resistance.* (A) Fasting blood insulin was measured by ELISA in 5-month-old WT and DUSP3-KO mice under CD, and in 18-month-old WT and DUSP3-KO mice under CD and HFD (n=4-8 mice in each group). Fasting blood insulin (B) and glucose (C) were measured at different time points in WT and DUSP3-KO mice (n=5-10 mice in each group). T0 represent the first reference time point (4-month-old mice). T1, T2 and T3 represent 4, 12 and 20 weeks after T0, respectively. At all time points, mice were starved for 6 hours and blood was collected from the tail vein. For the same mice, homeostatic model assessment of insulin resistance (HOMA-IR) score (D) was calculated using the formula basal insulin (mU/l) * basal glucose (mg/dl) / 405. Data are shown as mean ± SD (*, $p<0.05$; **, $p<0.01$).

Despite the evident insulin resistance in DUSP3-KO mice, glucose homeostasis was not altered by DUSP3 deletion as demonstrated by the OGTT assay (Figure R.12.A). Indeed, glucose tolerance was similar between WT and DUSP3-KO mice under CD and HFD at all time points analyzed, except at T1. Indeed, at this time point, level of glucose remained significantly higher in mutant mice under HFD. Though, at 120 minutes after injection, the level was back to normal, suggesting that metabolism was not altered in these mice. Moreover, in the following weeks, we did not observe any differences between the different groups of animals. However, even thought we did not observe any difference between the groups, when looking at the assay per group, we observed that DUSP3-KO under HFD display a slight modification in the glucose tolerance over time (Figure R.12.B).

A

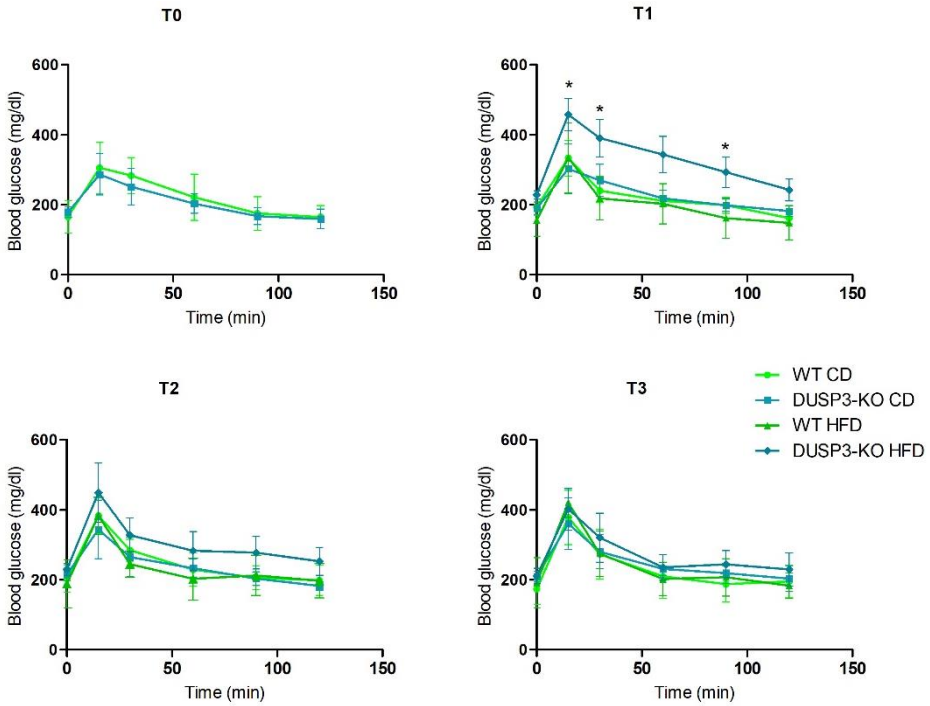
T0
T1
T2
T3
Blood glucose (mg/dl)
Time (min)
0
200
400
600
0
50
100
150
*
*
*
WT CD
DUSP3-KO CD
WT HFD
DUSP3-KO HFD

B

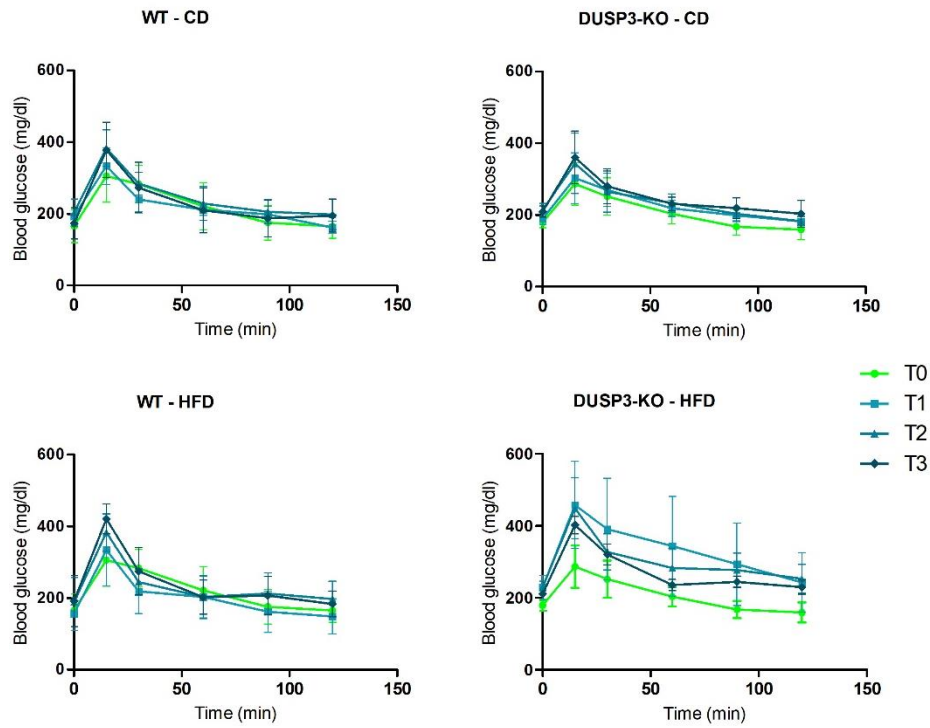
WT - CD
DUSP3-KO - CD
WT - HFD
DUSP3-KO - HFD
Blood glucose (mg/dl)
Time (min)
0
200
400
600
0
50
100
150
T0
T1
T2
T3

Figure R.12. *DUSP3 deletion does not alter glucose tolerance.* WT and DUSP3-KO mice were submitted to OGTT. Mice were starved for 6 hours. Blood glucose concentration was then measured in a drop of blood from the tail vein using a glucometer. Mice were then given a single dose of 2 g/kg of body weight of glucose *per os*. Glucose concentration in the blood was measured after 15, 30, 60, 90 and 120 minutes after injection. T0 represent the first day of the experiment (4-month-old mice). T1, T2 and T3 represent 4, 12 and 20 weeks after T0, respectively. Data are shown as mean ± SD (*, $p<0.05$; **, $p<0.01$). (A) Data are shown per time point. (B) Data are shown per gourp.

DUSP3 deletion does not modify glucose distribution

We showed that DUSP3 deletion does not modify glucose clearance in the blood after glucose ingestion. We then wanted to evaluate if the distribution of glucose in the different organs of the body was different between WT and DUSP3-KO mice. This was assessed by using ^{18}F-fluorodeoxyglucose (FDG) positron emission tomography (PET). This technique is used to monitor regional uptake of the glucose analog ^{18}F-FDG, a short-life radiotracer, in situ in a non-invasive way. 3 WT and 3 DUSP3-KO mice of 9 months and fed CD were used in this experiment. Mice were anesthetized and injected in the caudal vein with ^{18}F-FDG (12 ± 1 MBq). PET emission data were recorded during 60 minutes. After PET acquisition, a whole-body CT image was acquired using the eXplore 120 micro-CT. Structural CT image and corresponding PET image were superimposed to extract the dynamic PET data for the regions of interest. Glucose uptake was monitored in liver, heart, kidney, bladder and muscle. As showed in Figure R.13, we observe no significant difference between WT and DUSP3-KO mice in the distribution of glucose between the different organs.

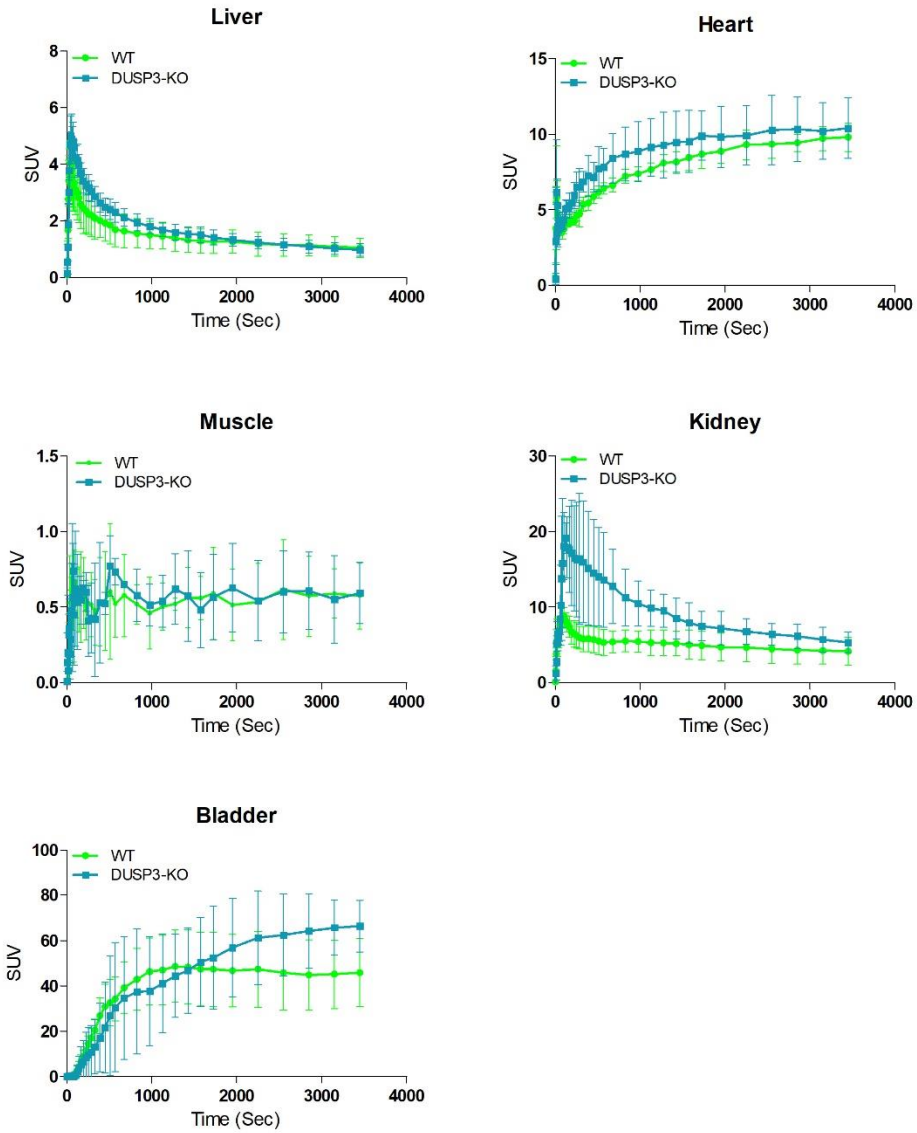

Figure R.13. *Glucose distribution in different organs of WT and DUSP3-KO mice.* ^{18}F-FDG bio-distribution was analyzed by ^{18}F-FDG PET imaging. 9-month-old WT and DUSP3-KO mice fed CD were injected with 12 ± 1 MBq of ^{18}F-FDG. PET emission was recorded for 60 minutes (n=3 mice in each group) and PET images were superimposed to CT scan images to obtain the dynamic glucose distribution in the regions of interest: liver, heart, kidney, bladder and muscle. Data are shown as mean ± SD (*, $p<0.05$; **, $p<0.01$).

DUSP3 expression is reduced under HFD and its genetic deletion enhances IR phosphorylation and signaling

To investigate DUSP3 function in NAFLD, we evaluated its expression in liver samples from 18-month-old WT mice under CD and HFD. Using Western blot analysis, we observed that DUSP3 expression is significantly decreased in the livers of HFD fed mice compared to CD fed mice (Figure R.14.A and R.14.B). DUSP3 mRNA level was also significantly reduced under HFD as demonstrate by RNA sequencing data (Figure R.14.C). Data from qRT-PCR analysis showed a slight but not significant decreased of DUSP3 mRNA expression in WT mice fed HFD (Figure R.14.D).

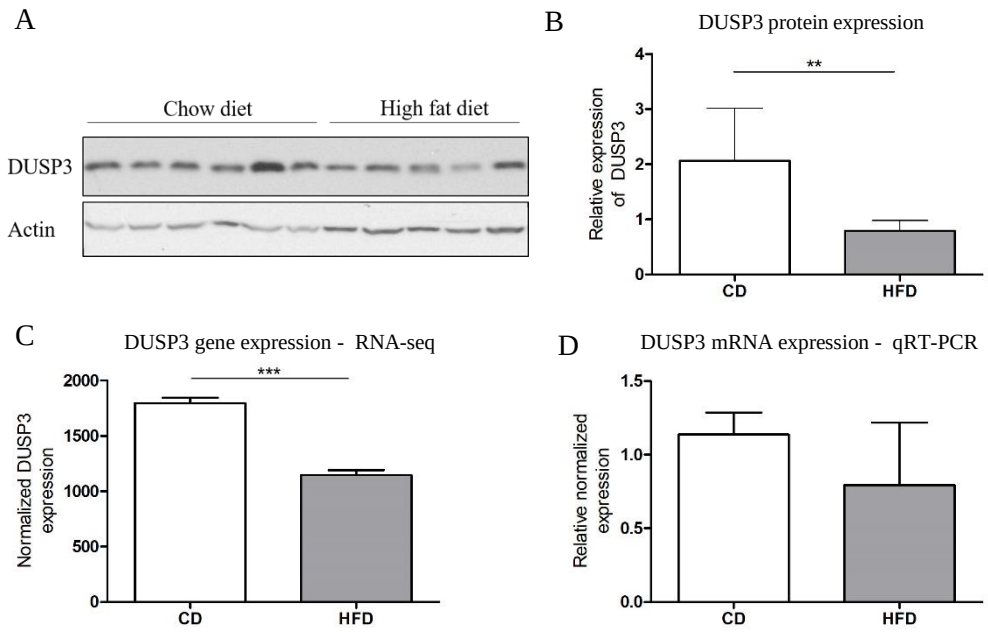

Figure R.14. *DUSP3 expression is reduced in the liver of WT mice fed HFD.* DUSP3 protein expression was evaluated in liver extracts from WT mice fed CD or HFD at 18 months old (n=5-6 mice in each group). Protein extracts from liver were prepared using RIPA buffer and resolved on SDS-PAGE. (A) Representative Western blot image of liver samples from 18-month-old WT mice fed CD or HFD. Anti-DUSP3 antibody was used and anti-actin antibody was used for normalization. (B) Densitometry quantifications of DUSP3 expression normalized on actin expression. (C) DUSP3 gene expression quantification from RNA sequencing data. Normalization was made on HPRT housekeeping gene (n=3 mice in each group). (D) DUSP3 mRNA expression quantification from qRT-PCR normalized on RPS9 housekeeping gene (n=3 mice in each group). Data are shown as mean ± SD (*, $p<0.05$; **, $p<0.01$).

Insulin resistance observed in DUSP3-KO mice suggests that this phosphatase could play a role in insulin receptor (IR) signaling pathway. Hyperinsulinemia that accompanies insulin resistance leads to constant hyper-activation of the insulin and IGF receptors, and downstream signaling pathways. Therefore, we analyzed the phosphorylation levels of the major axes of insulin receptor (IR) pathways that includes IR itself, Akt, MAPK ERK1/2, p38 and GSK3α/β. Liver extracts from CD and HFD fed 18-month-old mice were used for Western blot analysis. As shown in Figure R.15, under both CD and HFD, IR was highly phosphorylated on tyrosine 1150/1151 in the absence of DUSP3. Under CD, Akt, ERK1/2 and p38 were also highly phosphorylated on serine 473, threonine 202/tyrosine 204 and threonine 180/tyrosine 182 respectively in liver extract from DUSP3-KO mice over WT mice. Such difference was abolished under HFD. This is probably due to the exhaustion of the pathway under HFD. For GSK3α/β, we did not observe any difference between mutant and WT mice.

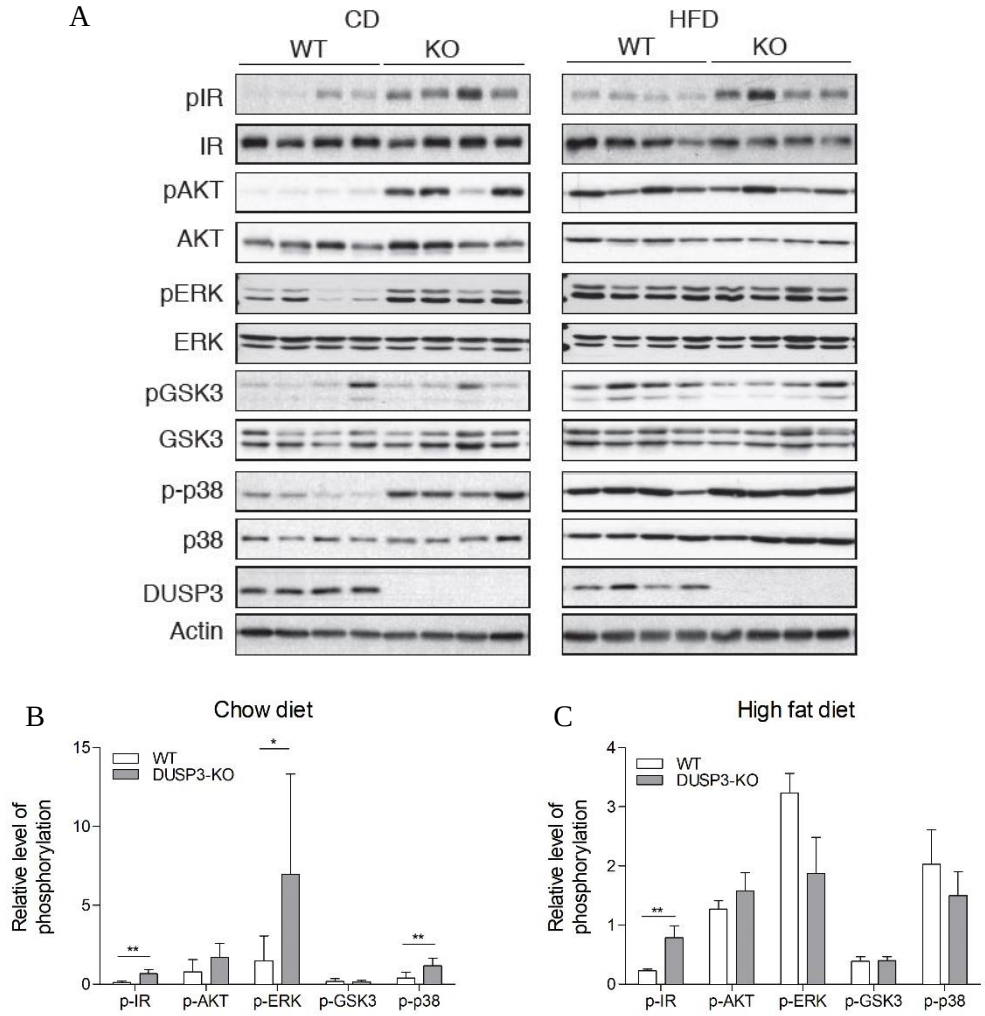

Figure R.15. *DUSP3 deletion affects insulin receptor signaling in the liver*. Protein extracts from liver of 18-month-old mice fed CD or HFD were prepared using RIPA buffer and resolved on SDS-PAGE. (A) Western blots were performed using anti-phospho-IR (Tyr1150/1151), anti-phospho-Akt (Ser473), anti-phospho-ERK1/2 (Thr202/Tyr204), anti-phospho-GSK3α/β (Ser21/9), anti-phospho-p38 (Thr180/Tyr182) and anti-IR, anti-Akt, anti-ERK, anti-GSK3 and anti-p38 as control. Anti-DUSP3 and anti-actine were also used. Densitometry ratios of the phosphorylated forms bands on the corresponding total proteins are shown as histograms for CD (B) and HFD (C) (n=6 mice in each group). Data are shown as mean ± SD (*, $p<0.05$; **, $p<0.01$).

Analysis of differential gene expression by RNA sequencing

Collectively, our data demonstrate that DUSP3 deletion promotes obesity and liver damages. To get an insight of the mechanisms behind the development of NALFD, we performed Next Generation Sequencing (NGS) analysis with RNA libraries prepared from liver samples of WT and DUSP3-KO mice, both under CD and HFD, of 18 months old. Three mice of each group were randomly selected from the experiment described in Figure 1. In the following results, each sample represents one mouse. Principal component analysis (PCA) on genes expression showed that the first principal component (PC1) accounts for 42% of the variance, PC2 for 16%, and PC3 for 13%. As shown in Figure R.16, samples were well discriminated between the two types of diet. PC3 even distinguished between WT and DUSP3-KO mice under CD. However, WT and DUSP3-KO mice under HFD were not discriminated by the PCA. Interestingly, the WT mouse under HFD that is closer to the DUSP3-KO mice under HFD (number 1) is the only WT mouse under HFD that presented dysplasia. All the DUSP3-KO mice under HFD also presented dysplasia. This result suggest that the severity of the disease might influence the discrimination in the PCA.

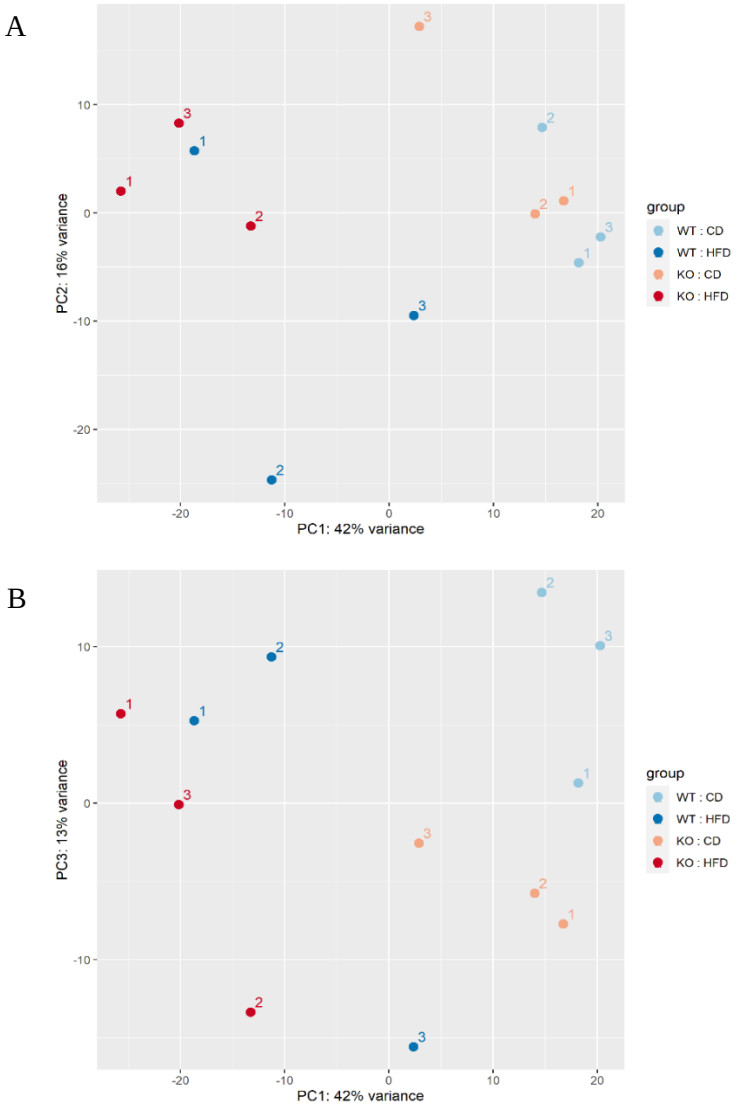

Figure R.16. *Principal component analysis.* Distribution of the liver samples from WT and DUSP3-KO mice of 18 months, under CD and HFD. PCA was performed using normalized RNA-Seq data of all the genes obtained from the different liver samples. Each dot represents one mouse. (A) PC1 and PC2. (B) PC1 and PC3.

A differential expression analysis showed that 341 genes were differentially expressed between the WT and DUSP3-KO mice under CD, of which 207 were downregulated and 134 were upregulated in DUSP3-KO mice compared to WT mice. The difference between WT and DUSP3-KO mice under HFD was lower, as expected from the PCA. Only 103 genes were differentially expressed between the two groups, of which 42 were downregulated and 61 were upregulated in DUSP3-KO mice compared to WT mice. The effect of the diet was more striking. 1428 genes were differentially

expressed between WT under CD and HFD and 1922 genes were differentially expressed between DUSP3-KO mice under CD and HFD.

The type of diet clearly separates the mice. To investigate the effect of HFD in the two different genotypes, we generated a Fold Change (FC) plot (Figure R.17). This graph compares the genes upregulated and downregulated in WT or in DUSP3-KO mice when fed HFD compared to when they are fed CD. Genes with adjusted p-value < 0.05 and fold change > 1.5 in at least one genotype were plotted. Each blue dot represents a gene differentially expressed in WT mice fed HFD compared to WT mice fed CD. On the left axis, there are the downregulated genes and on the right axis, the upregulated genes. Each green dot represents a gene differentially expressed in DUSP3-KO mice fed HFD compared to DUSP3-KO mice fed CD. The genes on the upper axe are upregulated, and the ones on the lower axe are downregulated. The red dots represent the genes differentially expressed in WT and DUSP3-KO mice when fed HFD compared to the mice of the same genotype fed CD. These results show that, when fed HFD, WT and DUSP3-KO mice partially regulate different genes.

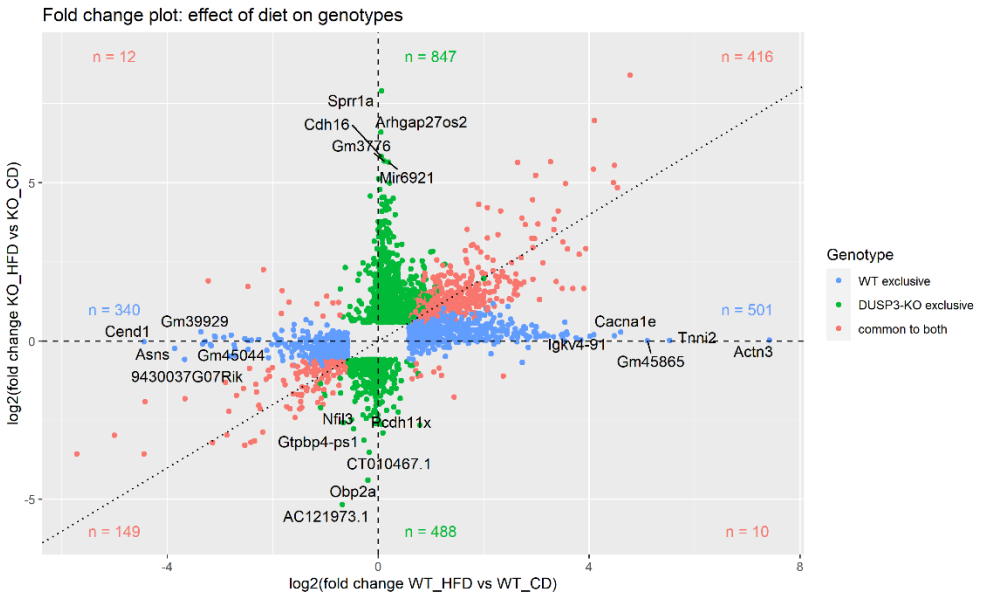

Figure R.17. *Fold change plot showing the effect of diet according to the genotype.* Comparison of the fold change difference between CD and HFD for WT and DUSP3-KO mice. Genes with adjusted p-value < 0.05 and fold change > 1.5 in at least one genotype were plotted. The genes exclusive to WT mice are colored in blue, the ones exclusive to DUSP3-KO mice are colored in green and the genes common to both genotypes are colored in red. Gene names of the 5 highest or lowest fold changes are labeled. Colored numbers represent the number of genes present on each axis, for the corresponding color.

Another FC plot was generated to visualize the effect of the genotype, either under CD or HFD (Figure R.18). This graphic shows the genes upregulated and downregulated in DUSP3-KO mice compared to WT mice, in both CD and HFD. Genes with adjusted p-value < 0.05 and fold change > 1.5 in at least one diet were plotted. Each blue dot represents a gene differentially expressed in DUSP3-KO mice fed CD compared to WT mice fed CD. On the left axis, there are the downregulated genes and on the right axis, the genes upregulated. Each green dot represents a gene differentially expressed in DUSP3-KO mice fed HFD compared to WT mice fed HFD. On the upper axis, there are the upregulated genes and on the lower axis, the downregulated genes. The red dots represent the genes differentially expressed in KO mice compared to WT mice, regardless of the type of diet. These data show that some genes are differentially expressed between DUSP3-KO and WT mice, under HFD or CD.

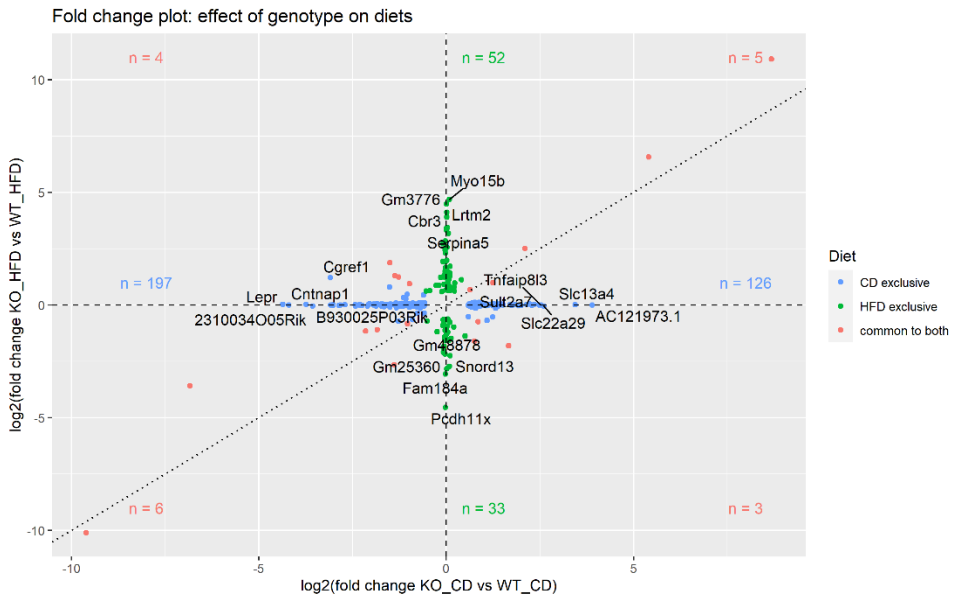

Figure R.18. *Fold change plot showing the effect of the genotype according to the diet.* Comparison of the fold change difference between WT and DUSP3-KO genotypes for CD and HFD. Genes with adjusted p-value < 0.05 and fold change > 1.5 in at least one diet were plotted. The genes exclusive to the normal diet are colored in blue, the ones exclusive to the high-fat diet are colored in green and the ones common to both are colored in red. Genes with the 5 highest or lowest fold changes in each diet are labeled. Colored numbers represent the number of genes present on each axis, for the corresponding color.

In order to understand the different mechanisms and pathways involved in the liver of WT and DUSP3-KO mice leading to the development of NAFLD, we performed a gene set enrichment analysis (GSEA). GSEA compares our gene sets with other curated gene sets known to be differentially expressed when some pathways are activated. First, we compared the pathways that are differently regulated between WT and DUSP3-KO fed CD (Figure R.19). It is interesting to note that the fatty acid metabolism involved genes are downregulated in DUSP3-KO mice compared to WT mice. Genes significantly differentially expressed between the two conditions are illustrated in a heatmap in Figure R.20 and can be found in Supplemental Table S.1.

A

HALLMARK	NES	p-value	FDR q-value
G2M checkpoint	1,71	0	0,013
E2F targets	1,48	0,005	0,074
Mitotic spindle	1,46	0	0,062

B

HALLMARK	NES	p-value	FDR q-value
Fatty acid metabolism	-1,78	0	0,005
Hypoxia	-0,58	0	0,037
Myc targets	-1,52	0	0,05
Adipogenesis	-1,49	0,005	0,047
Peroxisome	-1,4	0,023	0,103

Figure R.19. *GSEA analysis of the pathways regulated in DUSP3-KO compared to WT mice fed CD.* Pathways with FDR q-value < 0.1 are showed. Pathways significantly upregulated (A) and downregulated (B) in DUSP3-KO compared to WT mice fed CD. NES, normalized enrichment score; FDR, False Discovery Rate.

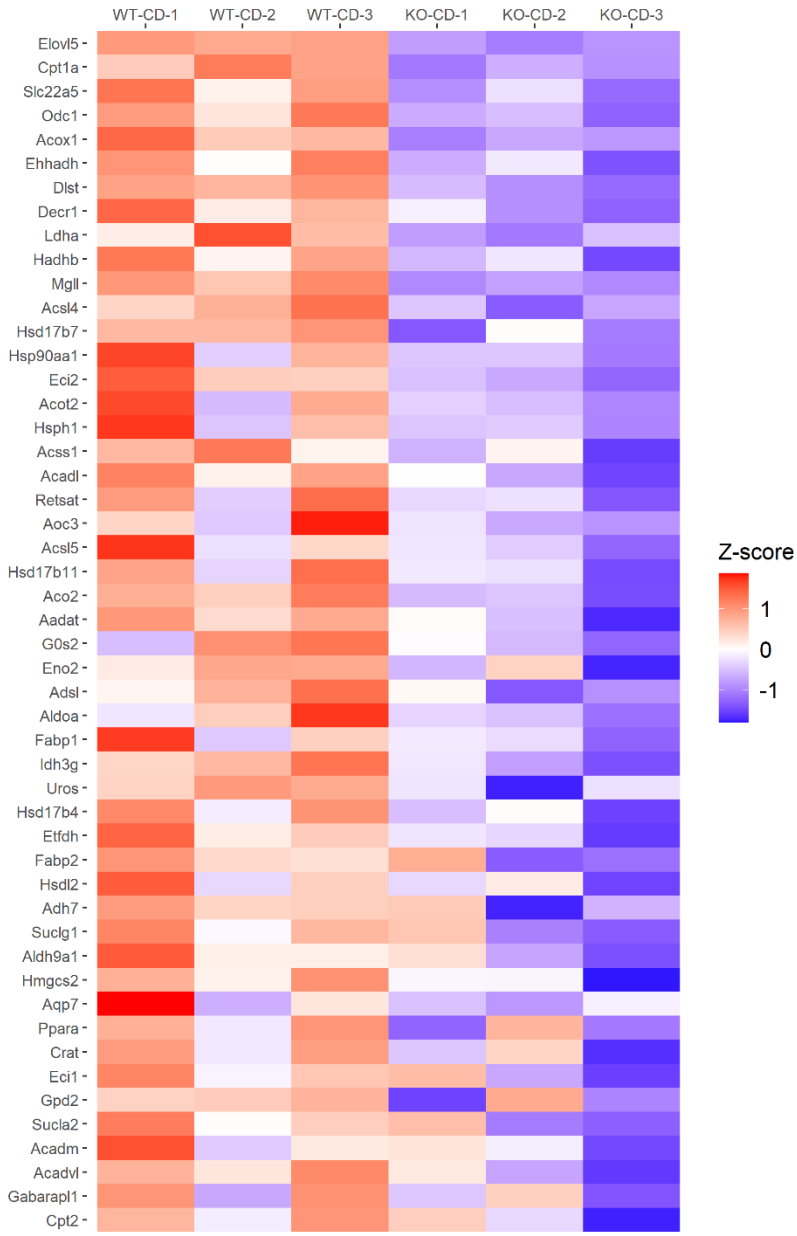

Figure R.20. *Fatty acid metabolism genes are downregulated in DUSP3-KO mice fed CD.* Heatmap representation of the significant differentially expressed genes (q value < 0.05) implicated in the fatty acid metabolism pathway in WT and DUSP3-KO mice fed CD.

We performed the same test for DUSP3-KO mice fed HFD compared to WT mice fed HFD (Figure R.21). In this case, we found that bile acid metabolism, unfolded protein response and DNA repair pathways are significantly downregulated in DUSP3-KO compared to WT mice. As discussed in the introduction, these processes are known to be involved in the pathogenesis of NAFLD. Genes from the bile acide metabolism and the DNA repair pathways which are significantly differentially expressed between the two conditions are illustrated in a heatmap in Figure R.22 and can be found in Supplemental Table S.2 and S.3.

A

HALLMARK	NES	p-value	FDR q-value
Apical surface	1,58	0,007	0,09
Estrogen response early	1,53	0,001	0,072
Apical junction	1,5	0,001	0,066
Angiogenesis	1,45	0,041	0,081
Mitotic spindle	1,44	0,001	0,073
UV response DN	1,42	0,007	0,078
KRAS signaling	1,42	0,006	0,071

B

HALLMARK	NES	p-value	FDR q-value
Oxidative phosphorylation	-2,03	0	0
Myc targets	-1,78	0	0,004
Bile acid metabolism	-1,52	0,003	0,051
Coagulation	-1,48	0	0,052
Unfolded protein response	-1,46	0,008	0,048
DNA repair	-1,31	0,036	0,103

Figure R.21. *GSEA analysis of the pathways regulated DUSP3-KO mice fed compared to WT mice fed HFD.* Pathways with a FDR q-value < 0.1 are showed. Pathways significantly upregulated (A) and downregulated (B) in DUSP3-KO compared to WT mice fed HFD. NES, normalized enrichment score; FDR, False Discovery Rate.

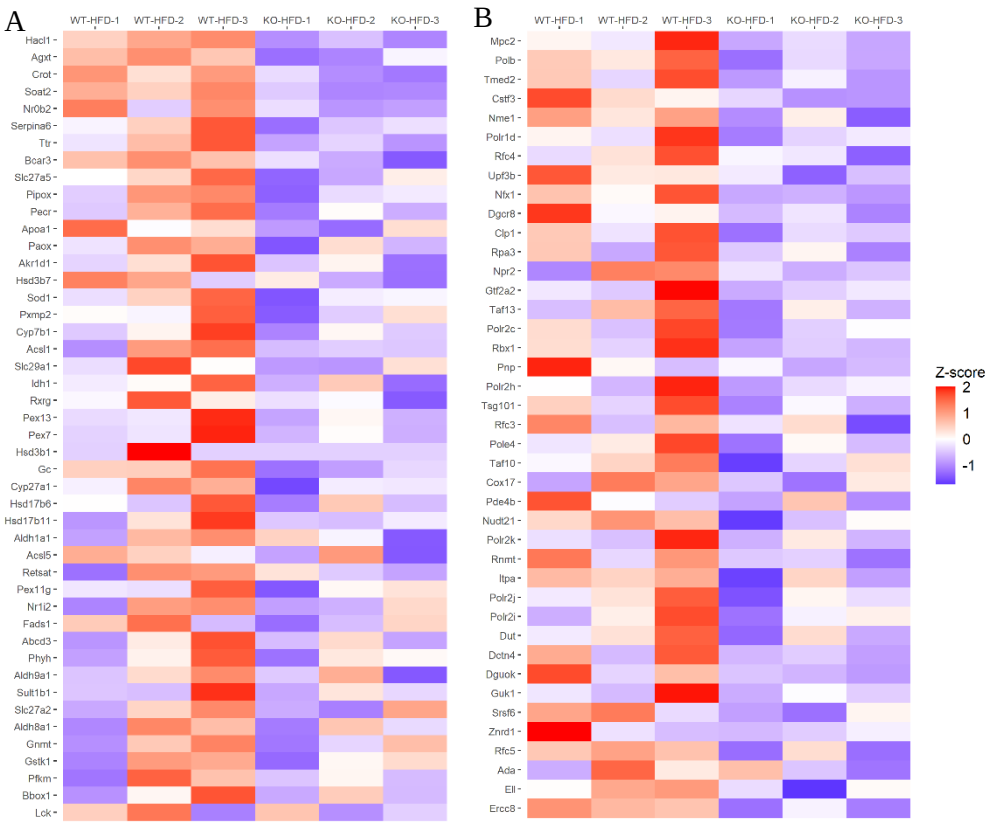

Figure R.22. *Bile acid metabolism and DNA repair pathways genes are downregulated in DUSP3-KO mice fed HFD.* Heatmap representation of the differentially expressed genes implicated in the bile acid metabolism (A) and DNA repair (B) pathways in WT and DUSP3-KO mice fed HFD.

Regulated pathways between WT mice fed CD and HFD, as well as regulated pathways between DUSP3-KO mice fed CD and HFD are showed in Figure R.23 and R.24. We observed that the pathways downregulated by the HFD are the same in WT and DUSP3-KO mice. Moreover, in term of up-regulated pathways, HFD has nearly the same effect in WT and DUSP3-KO mice with the exception of few pathways. Indeed, MTORC1 signaling pathway is upregulated in WT mice under HFD, but not in DUSP3-KO mice (Figure R.25), while IL6-JAK-STAT3 pathway is upregulated in DUSP3-KO mice when fed HFD, but not in WT mice (Figure R.26). Differentially expressed genes in these two pathways are illustrated in a heatmap in Figure R.25 and R.26 and the gene list can be found in Supplemental Table S.4 to S.7.

A

HALLMARK	NES	p-value	FDR q-value
Allograft rejection	2,38	0	0
Interferon gamma response	2,26	0	0
Interferon alpha response	2,25	0	0
E2F targets	2,17	0	0
G2M checkpoint	2,05	0	0
Inflammatory response	1,91	0	0
Pancreas Beta Cells	1,69	0	0,003
IL2 STAT5 signaling	1,65	0	0,003
TNFA signaling via NFKB	1,61	0	0,006
Myogenesis	1,55	0,001	0,01
Epithelial mesenchymal transition	1,54	0,001	0,01
Mitotic spindle	1,48	0,003	0,022
MTORC1 signaling	1,43	0,004	0,036
Angiogenesis	1,42	0,049	0,037
Complement	1,41	0,01	0,04
Cholesterol homeostasis	1,39	0,034	0,046
Apoptosis	1,36	0,025	0,06

B

HALLMARK	NES	p-value	FDR q-value
Oxidative phosphorylation	-2,57	0	0
Bile acid metabolism	-2,07	0	0
Fatty acid metabolism	-1,93	0	0,001
Xenobiotic metabolism	-1,85	0	0,001
Myc targets	-1,79	0	0,001
Peroxisome	-1,78	0	0,001
Adipogenesis	-1,78	0	0,001

Figure R.23. *GSEA analysis of the pathways regulated WT mice fed HFD compared to WT mice fed CD.* Pathways with a p-value < 0.05 and a FDR q-value < 0.1 are showed. (A) Pathways significantly upregulated in WT mice fed HFD, compared to WT mice fed CD. (B) Pathways significantly downregulated in WT mice fed HFD, compared to WT mice fed CD. In blue, pathways specific to WT mice compared to DUSP3-KO mice. NES, normalized enrichment score; FDR, False Discovery Rate.

A

HALLMARK	NES	p-value	FDR q-value
Allograft rejection	2,08	0	0
Inflammatory response	1,89	0	0
Angiogenesis	1,79	0	0,001
KRAS signaling	1,75	0	0,001
IL2 STAT5 signaling	1,73	0	0,001
IL6 JAK STAT3	1,73	0,001	0,001
Interferon gamma response	1,71	0	0,001
Apoptosis	1,69	0,001	0,012
Apical junction	1,69	0	0,001
Interferon alpha response	1,68	0	0,001
Cholesterol homeostasis	1,65	0,001	0,002
Apical surface	1,64	0,002	0,002
TNFa signaling via NFKB	1,6	0	0,003
Epithelial mesenchymal transition	1,57	0,001	0,005
UV response DN	1,53	0,001	0,008
Hypoxia	1,48	0,002	0,015
Pancreas beta cells	1,48	0,033	0,014
Complement	1,46	0,001	0,016
G2M checkpoint	1,45	0	0,018
Estrogen response early	1,43	0,003	0,021
Myogenesis	1,42	0,003	0,022
E2F targets	1,41	0,005	0,024

B

HALLMARK	NES	p-value	FDR q-value
Oxidative phosphorylation	-2,47	0	0
Bile acid metabolism	-1,98	0	0,002
Fatty acid metabolism	-1,88	0	0,001
Xenobiotic metabolism	-1,73	0	0,004
Myc targets	-1,59	0	0,013
Peroxisome	-1,54	0	0,014
Adipogenesis	-1,14	0	0,228

Figure R.24. *GSEA analysis of the pathways regulated DUSP3-KO mice fed HFD compared to DUSP3-KO mice fed CD.* Pathways with a p-value < 0.05 and a FDR q-value < 0.1 are showed. (A) Pathways significantly upregulated in DUSP3-KO mice fed HFD, compared to DUSP3-KO mice fed CD. (B) Pathways significantly downregulated in DUSP3-KO mice fed HFD, compared to DUSP3-KO mice fed CD. In blue, pathways specific to WT mice compared to DUSP3-KO mice. NES, normalized enrichment score; FDR, False Discovery Rate.

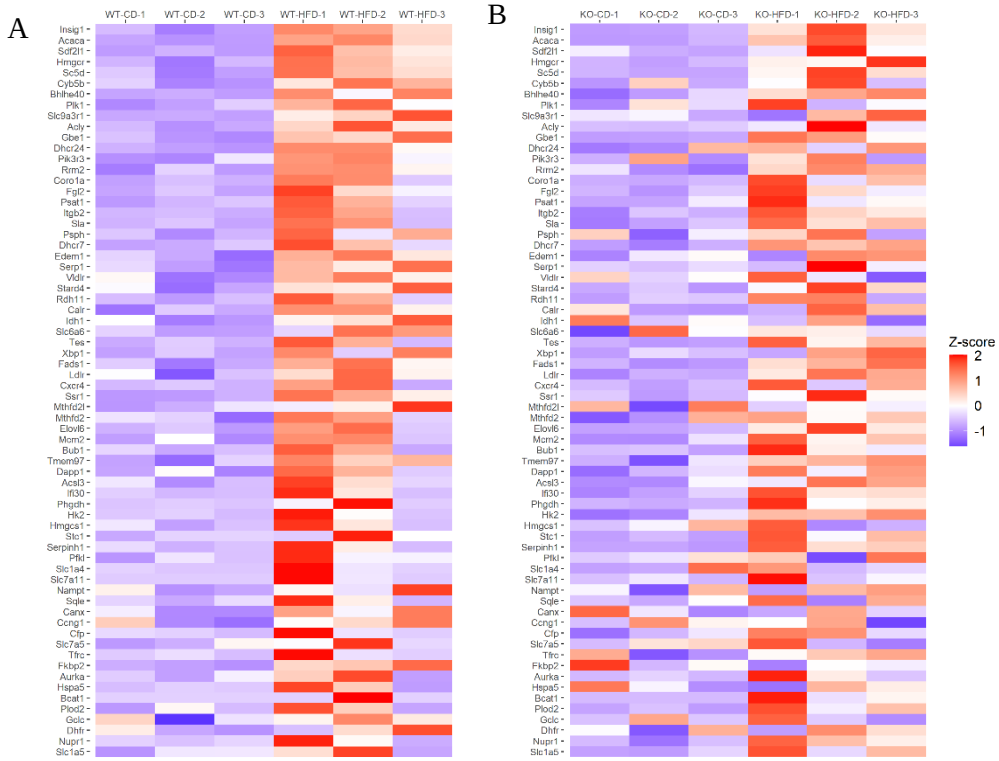

Figure R.25. *MTORC1 signaling pathway is upregulated in WT mice fed HFD compared to WT mice fed CD.* Representation of the differentially expressed genes implicated in MTORC1 signaling in WT (A) and DUSP3-KO (B) mice.

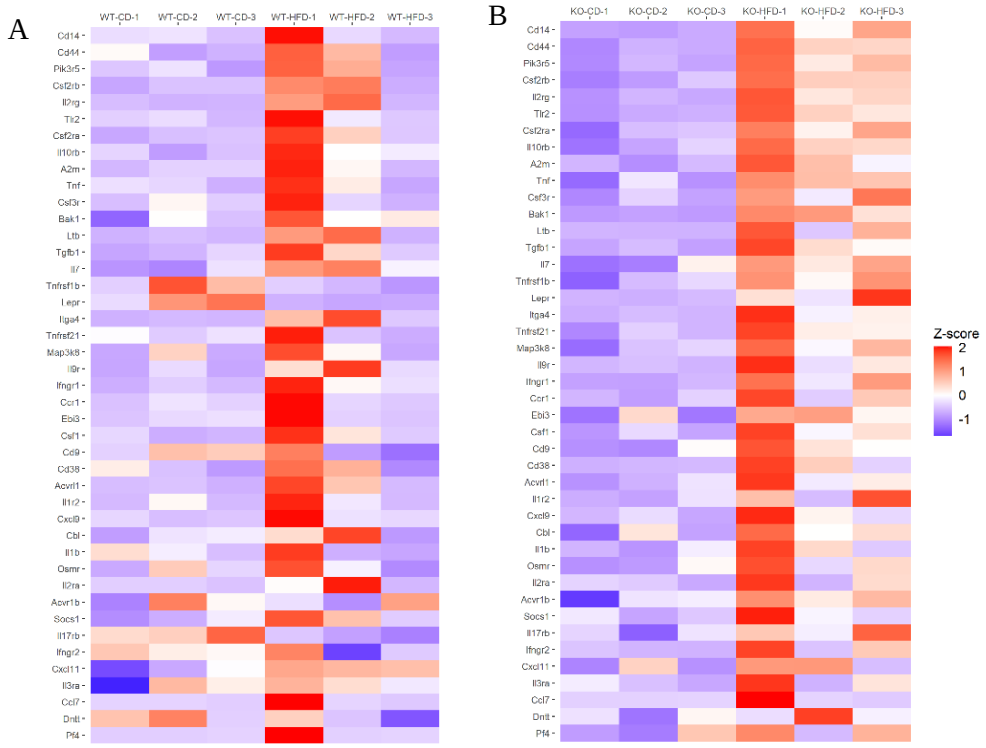

Figure R.26. *IL6-JAK-STAT5 signaling pathway is upregulated in DUSP3-KO mice fed HFD compared to DUSP3-KO mice fed CD.* Representation of the differentially expressed genes implicated in IL6-JAK-STAT5 signaling in WT (A) and DUSP3-KO (B) mice.

As discussed in the introduction, different studies highlighted the roles of some DUSPs in the development of obesity and NAFLD with some being upregulated and others being downregulated. We analyzed the gene expression of the main DUSPs in the liver of the mice from the different groups (Figure R.27). As already discussed (Figure R.14), DUSP3 RNA expression is significantly downregulated ($p<0.0001$) in the liver of WT mice under HFD compared to WT mice fed CD. However, we observed no difference for the other DUSPs in term of gene expression. In the absence of DUSP3 (DUSP3-KO mice), we did not observe any upregulation of any other DUSP, suggesting that there was no redundancy of other DUSPs to compensate for DUSP3 deletion.

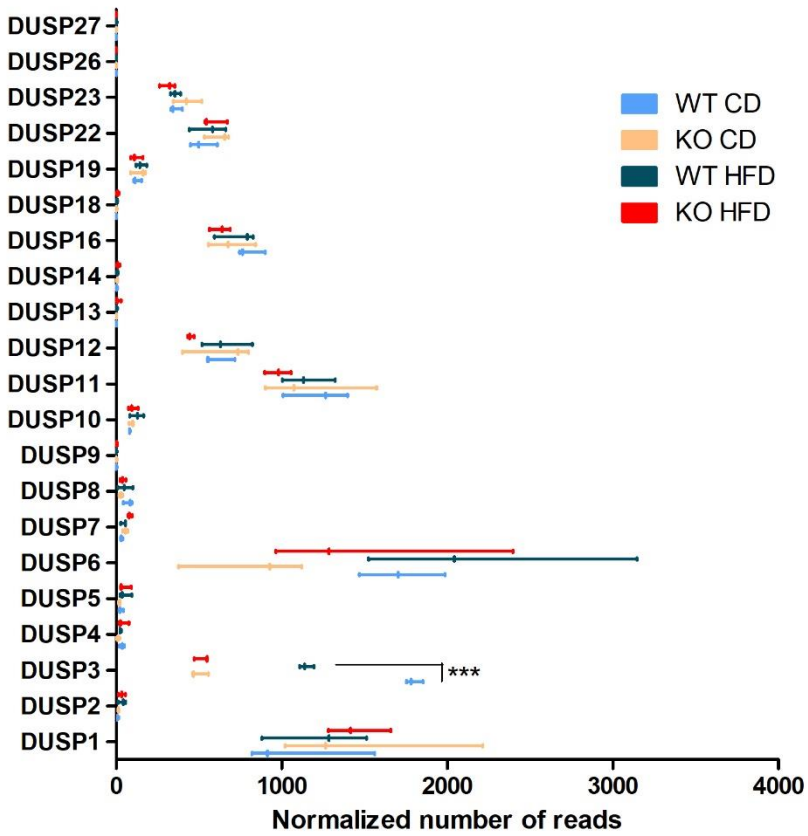

Figure R.27. *Expression of DUSPs in mice liver.* Normalized number of reads for DUSPs are shown as box-and-whisker plots (from minimum to maximum) for the mice from the different groups. (***, $p<0.0001$)

In order to validate the RNA sequencing data, RNA samples used for RNAseq were submitted to quantitative real-time polymerase chain reaction (qRT PCR) (Figure R.28). We chose to evaluate genes expressing DUSPs which have been shown to be regulated in NAFLD and HCC, and genes implicated in lipid metabolism in the liver and for which the expression was up- or down-regulated between the different conditions. Results were similar to the one from RNAseq data (Figure S.1).

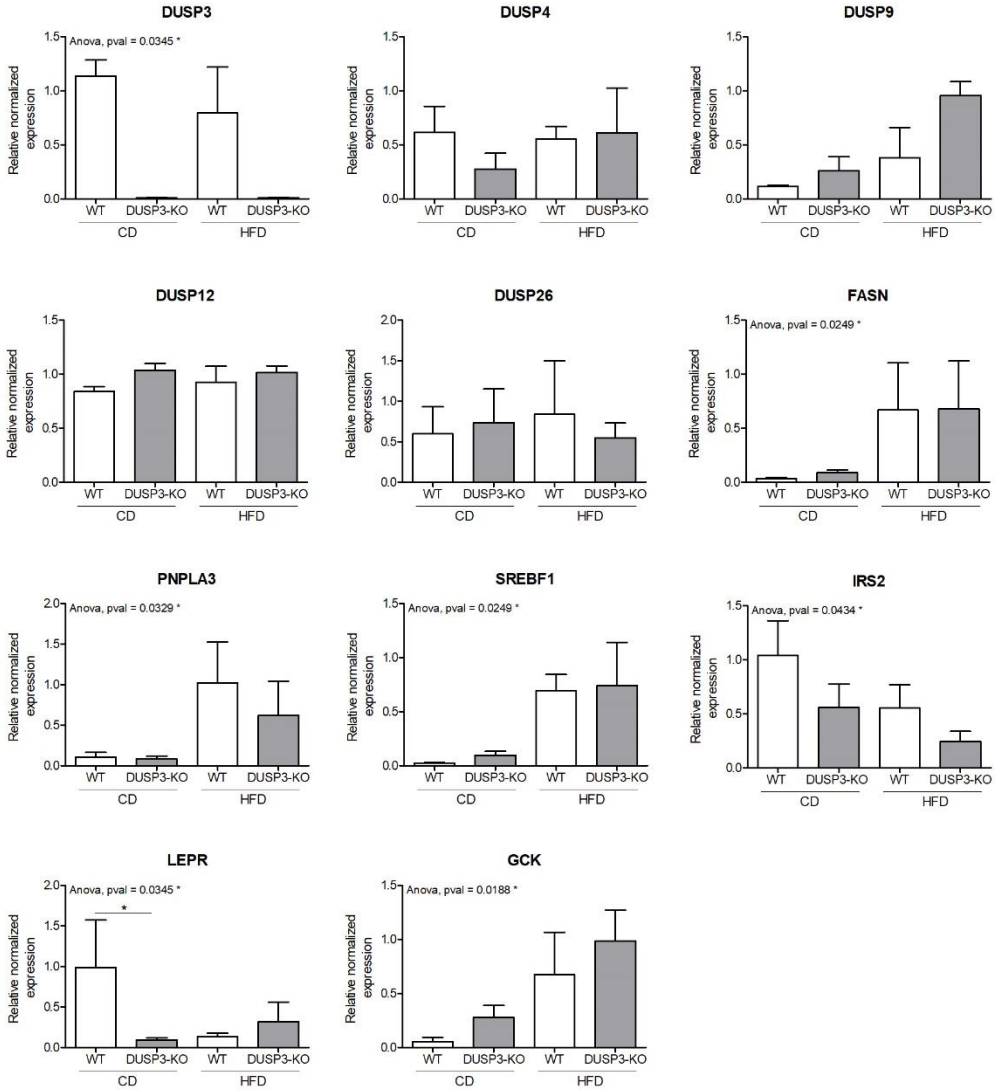

Figure R.28. *Validation of RNAseq data set.* qRT-PCR of few DUSPs and proteins of interest encoding genes. Total RNA was extracted from liver of WT and DUSP3-KO mice, under CD and HFD, at 18 months old (n=3 mice in each group). Quantitative RT-PCR was performed. Data are normalized according to RSP9 mRNA levels. Statistical significance was tested by one-way ANOVA with Dunn's post-tests. Data are shown as mean ± SD (*, $p<0.05$; **, $p<0.01$). FASN, fatty acid synthase; LEPR, leptin receptor; GCK, glucokinase.

DUSP3 deletion promotes HCC development in an *in vivo* model of carcinogenesis

Collectively, our data demonstrate that DUSP3 genetic deletion leads to obesity and associated metabolic disorders including insulin resistance, NAFLD and associated liver damages and the development of HCC in some mice. Such phenotypes developed with aging and were exacerbated by HFD. As discussed in the introduction, obesity and NAFLD can lead to HCC, among other disorders. In WT mice, it has been demonstrated that HFD alone is not sufficient to induce HCC [98]. Administration of diethylnitrosamine (DEN) genotoxic drug is required to induce liver cancer in mice [253]. DEN undergoes metabolic activation in hepatocytes by enzymes of the cytochrome P450 family [254]. It acts as a complete carcinogen when injected into mice younger than 2 weeks, when hepatocytes are still actively proliferating. DEN is a DNA alkylating agent leading to the formation of mutagenic adducts. In addition, DEN bio-activation by cytochrome P450 can generate reactive oxygen species (ROS), which damage DNA, proteins and lipids, and lead to hepatocyte death. In our model, both WT and DUSP3-KO mice received a single intra-peritoneal injection of DEN (25mg/kg) at day 14 after birth. 4 weeks later, mice diet was switched to HFD for half of the mice while the other half was kept under CD. Development of tumors in this model takes between 35 to 45 weeks after DEN injection under CD. The process is accelerated with HFD. Park *et al.* showed that 36 weeks after DEN injection the number of tumors was increased in HFD fed mice compared to CD fed mice [98]. Because we hypothesized that DUSP3 deletion would accelerate tumor development, we chose to euthanized mice at earlier time points: 24, 28, 32 and 35 weeks post-DEN injection. WT and mutant mice under CD were also euthanized at 43 weeks after DEN injection.

All mice were monitored for weight every week. As expected and reported above (Figure R.1), DUSP3-KO mice gained more weight than WT mice, especially under HFD (Figure R.29). However, 30 weeks after injection, DUSP3-KO mice fed HFD started losing weight, suggesting a more severe evolution of the disease in the mutant mice compared to WT mice.

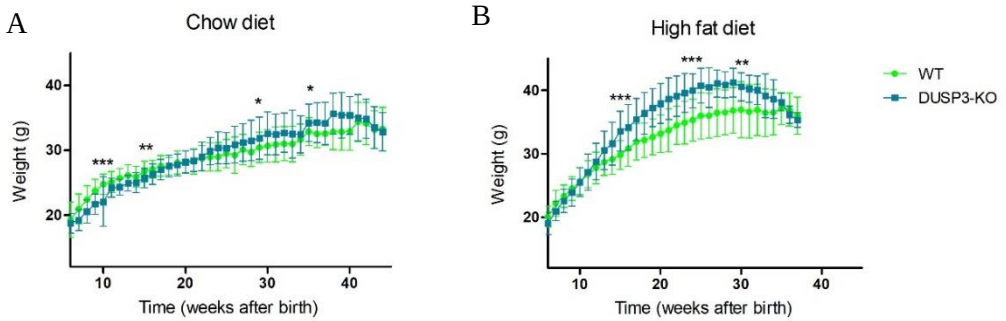

Figure R.29. *WT and DUSP3-KO mice weight in DEN model of carcinogenesis.* 14-day-old WT and DUSP3-KO mice were injected with DEN. 4 weeks later, half the mice were given HFD. From that day, weight was monitored every week (n=10 mice in each group). Data are shown as mean ± SD (*, $p<0.05$; **, $p<0.01$; ***, $p<0.0001$).

Mice were euthanized at different time points. For clarity, results from 24 and 32 weeks post-DEN injection are presented, as representative evolution of the disease in WT and DUSP3-KO mice. At the time of euthanasia, serum was collected as well as all soft tissues for further analysis. Livers were weighted, pictured and all visible tumors (>1mm) were measured and counted. As expected, under HFD, DUSP3-KO mice exhibited a higher liver to body weight ratio compared to WT mice (Figure R.30.A). We also observed that with HFD, DUSP3-KO mice develop more tumors per liver (Figure R.30.B) compared to WT mice at both time points. Tumor size was also increased under HFD at 32 weeks post-DEN injection in mutant mice compared to WT mice (Figure R.30.C).

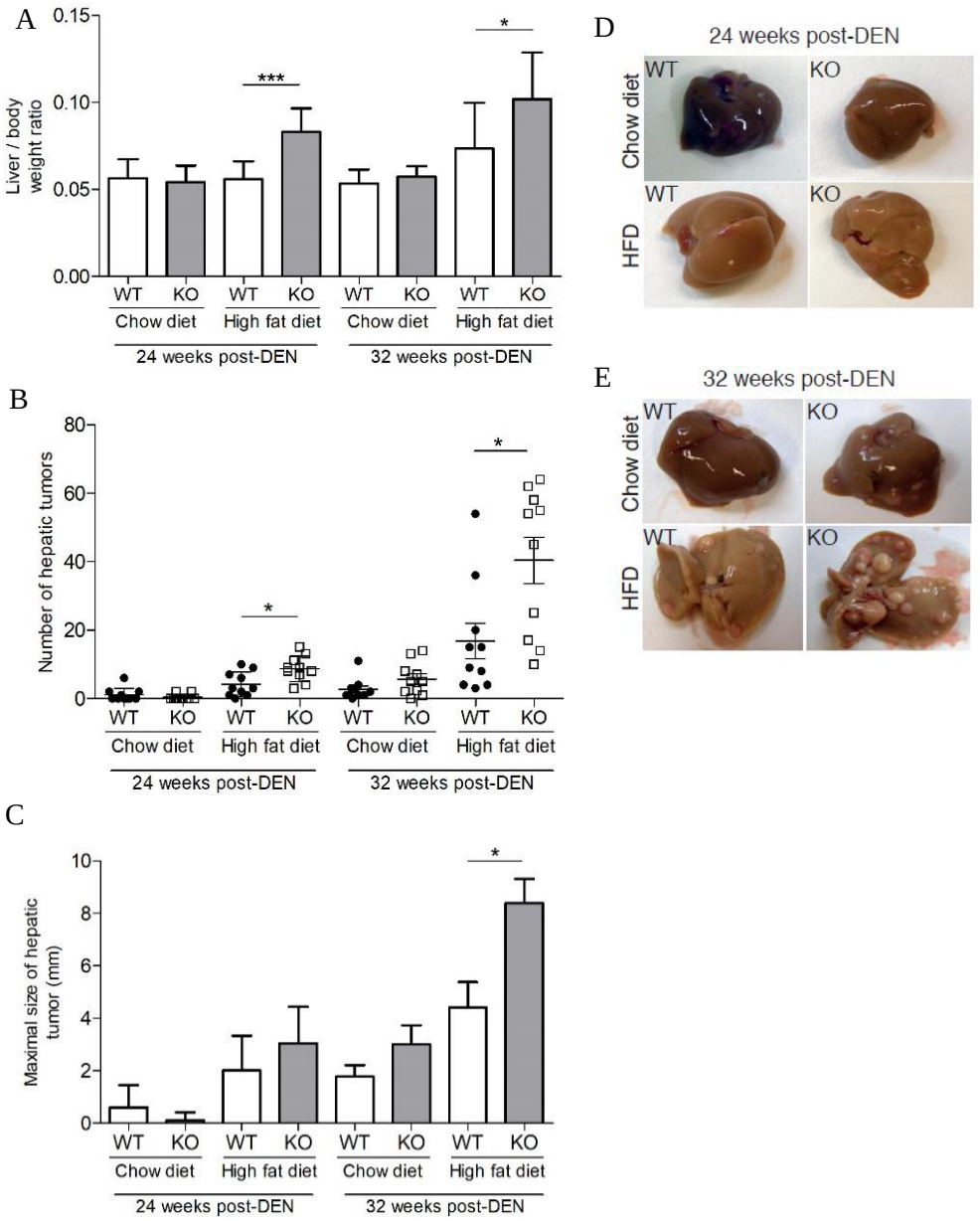

Figure R30. *DUSP3 deletion associated with HFD promote DEN-induced hepatocarcinogenesis.* Mice were euthanized 24 and 32 weeks after DEN injection. (A) Liver weight to body weight ratio of WT and DUSP3-KO mice, under CD and HFD at both time points. Tumor multiplicity (B) and maximal size of tumors (C) in livers of DEN-injected WT and DUSP3-KO mice. Data are shown as mean ± SD (n=10 mice in each group) (*, $p<0.05$; **, $p<0.01$). Representative pictures of liver of WT and DUSP3-KO mice at 24 (D) and 32 (E) weeks after DEN injection.

SAF score was used to quantify the extent of liver damage in mice at 24 and 32 weeks after DEN injection. As shown in Figure R.31.A, at 24 weeks post-DEN injection, under HFD, DUSP3-KO mice have a higher general SAF score than WT mice (4.6 and 5.2 for WT and DUSP3-KO mice, respectively). Consistently, at 32 weeks post-DEN injection, under HFD, DUSP3-KO mice have a higher general SAF score than WT mice (4.6 and 5.4 for WT and DUSP3-KO mice, respectively). Moreover, at 24 weeks post-DEN injection, all mice display dysplasia, with no difference between the different groups. However, at 32 weeks post-DEN injection, 40% of DUSP3-KO under CD and 60% of DUSP3-KO mice under HFD display HCC, and only 20% of WT mice under HFD displayed HCC (Figure R.31.B). Consistently, levels of serum AST and ALT were higher in DUSP3-KO mice fed HFD compared to WT mice (Figure R.31.E and R.31.F).

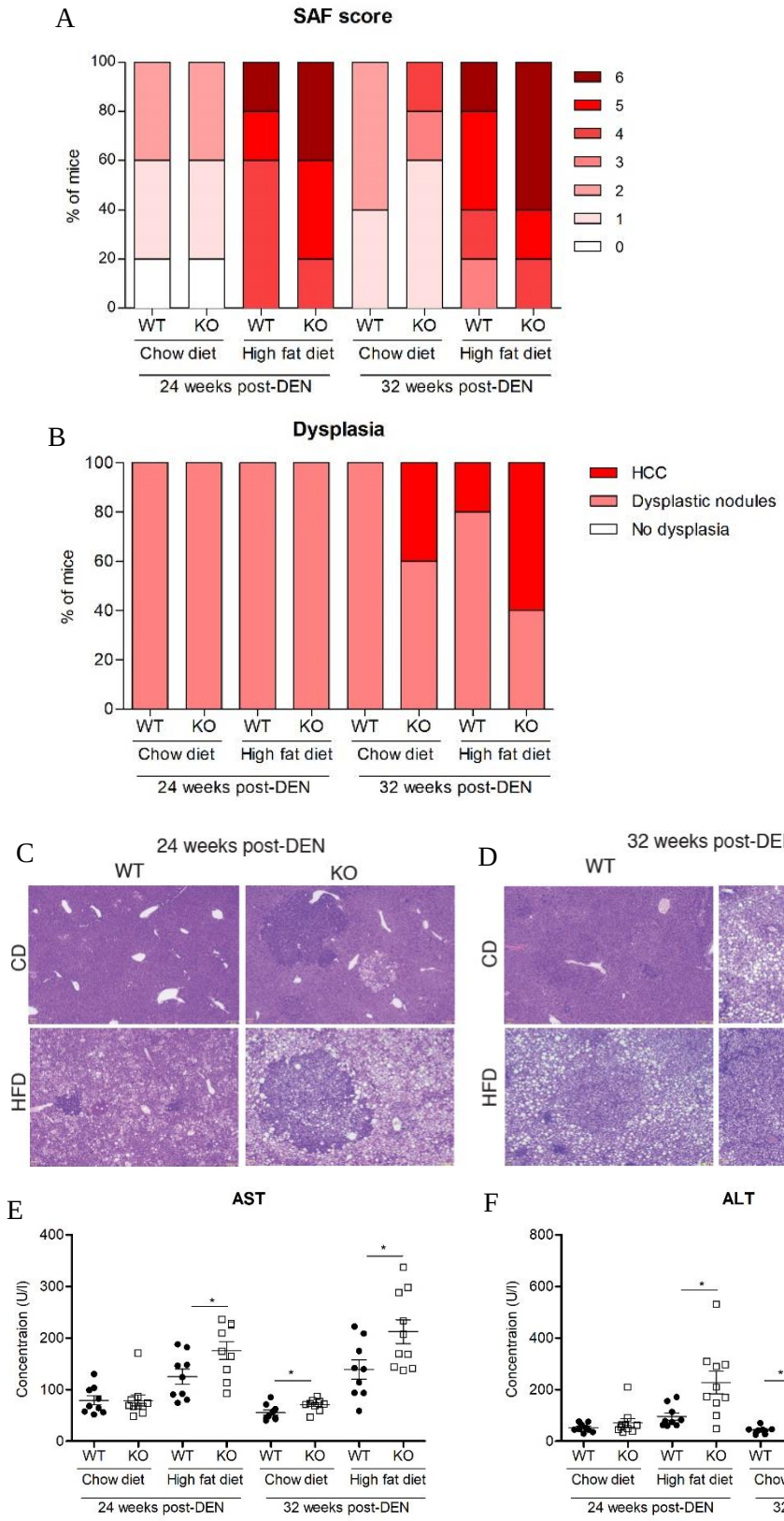
A
SAF score
% of mice
100
80
60
40
20
0
6
5
4
3
2
1
0
WT KO WT KO WT KO WT KO
Chow diet
High fat diet
Chow diet
High fat diet
24 weeks post-DEN
32 weeks post-DEN
B
Dysplasia
% of mice
HCC
Dysplastic nodules
No dysplasia
C
24 weeks post-DEN
D
32 weeks post-DEN
WT
KO
CD
HFD
E
AST
Concentraion (U/l)
F
ALT
Concentraion (U/l)

Figure R.31. *Evaluation of NAFLD and HCC in the liver of WT and DUSP3-KO mice in DEN induced hepatocarcinogenesis model.* 5µm sections of liver from mice under CD and HFD at 24 and 32 weeks after DEN injection were stained with H&E, Masson's trichrome and Foot stains. These sections were analyzed by a pathologist to evaluate the SAF (Steatosis, Activity, Fibrosis) score and the presence of dysplastic nodules and hepatocellular carcinoma (HCC). (A) SAF score (from 0 to 9) of the different groups of mice. (B) Evaluation of the presence of dysplastic nodules and HCC in the liver. (A-B) Data are expressed as a percentage of mice in each category (n=5 mice in each group). Representative images of liver of WT and DUSP3-KO mice under CD or HFD at 24 (C) or 32 (D) weeks after DEN injection. AST (E) and ALT (F) in the serum of mice were measured using the AU480 chemistry analyzer. Each dot represents one mouse (n=10 mice in each group). Results are shown as mean ± SD (*, $p<0.05$; **, $p<0.01$).

At 35 weeks post-DEN injection, we observed no difference between WT and DUSP3-KO mice under CD in term of tumor number and size. We decided to wait until week 43 after DEN injection to evaluate if, with time, we would observe a difference. Under CD, at 43 weeks post-DEN injection, livers of DUSP3-KO mice were significantly bigger. However, we observed no difference in the number of hepatic tumors, or their size. SAF score was slightly higher in DUSP3-KO mice (3.5) compared to WT mice (1).

DUSP3 deletion alters cholesterol but not triglycerides metabolism under HFD

We measured TG and cholesterol in the serum of mice at 24 and 32 weeks after DEN injection. We observed no difference in TG between the different groups (Figure R.32.A). However, total cholesterol, LDL and HDL levels were slightly higher in DUSP3-KO mice under HFD compared to WT mice (Figure R.32.B-D). LDL/HDL ratio was higher in DUSP3-KO mice fed HFD compared to WT mice (Figure R.32.E).

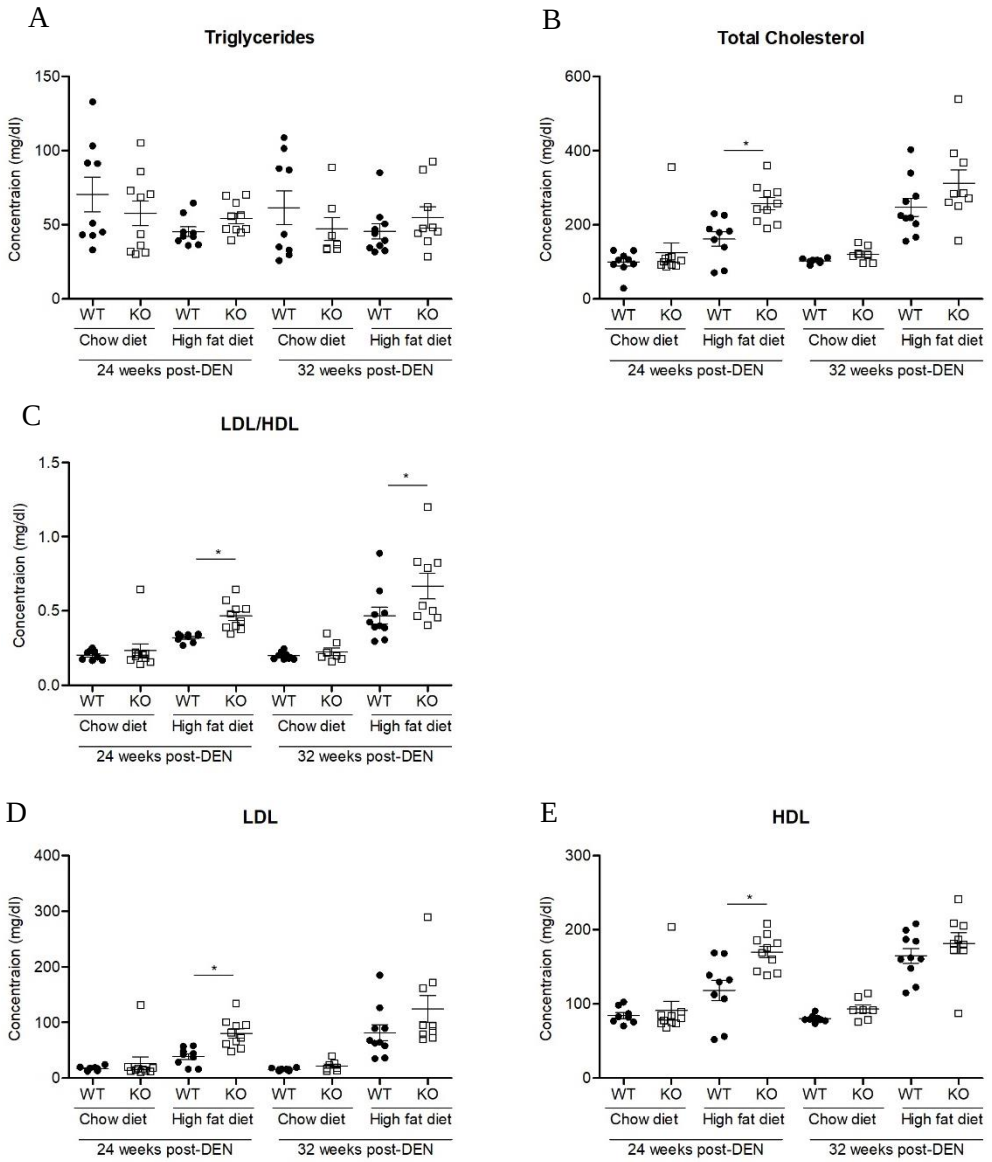

Figure R.32. *Serum levels of triglycerides and cholesterol in WT and DUSP3-KO mice in DEN-induced hepatocarcinogenesis model*. Concentrations of triglycerides (A), total cholesterol (B), LDL (C), HDL (D) and LDL/HDL ratio (E) in serum were analyzed using the AU480 chemistry analyzer, from WT and DUSP3-KO mice under CD and HFD at 24 and 32 weeks post-DEN injection. Each dot represents a mouse. (n=7-10 mice in each group). Data are shown as mean ± SD (*, $p<0.05$; **, $p<0.01$).

DUSP3 deletion promotes insulin resistance in DEN-induced hepatocarcinogenesis

To investigate if the rapid liver damages observed in DEN-injected mice were associated with insulin resistance as it was the case in older mice under CD and HFD (Figure R.11), we measured fasting insulin levels in the serum of mice at 24 and 32 weeks after DEN injection (Figure R.33). Similar to the condition with no DEN, DEN-injected mice had higher insulin levels than control mice, regardless of the type of diet. These results indicate that DEN-induced carcinogenesis was associated with insulin resistance.

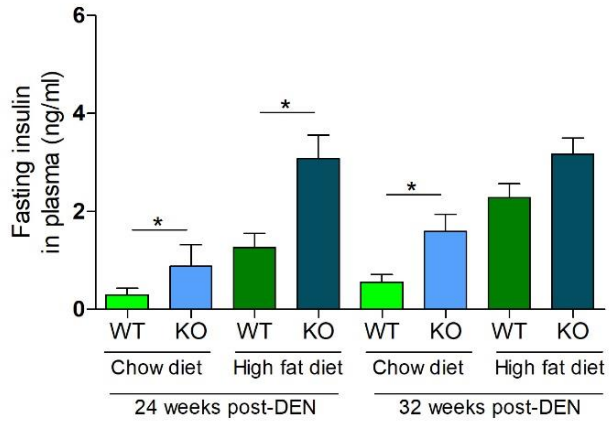

Figure R.33. *DUSP3 deletion promotes insulin resistance in DEN-induced hepatocarcinogenesis model.* Fasting insulin concentration was measured by ELISA in the serum of mice at 24 and 32 weeks after DEN-injection, both under CD and HFD (n=7-10 mice in each group). Data are shown as mean ± SD (*, $p<0.05$; **, $p<0.01$).

DUSP3 deletion does not affect HepG2 cells growth

Altogether, the above results suggest that DUSP3 could play a role as a tumor suppressor in the liver. To investigate such hypothesis, we downregulated DUSP3 expression in HepG2 cells using short hairpin RNA (shRNA) lentiviral plasmid. HepG2 is an immortalized cell line consisting of human liver carcinoma cells. HepG2 cells were cultured in DMEM complete media and transduced with 3 different shRNA anti-DUSP3 (shDUSP3-1 to 3) or anti-eGFP lentiviral vectors (30 TU/cell) and were selected with puromycin. The efficacy of the three different shRNA was demonstrated

by the significant decrease of DUSP3 protein level with all used shDUSP3 constructs compared to control (Figure R.34).

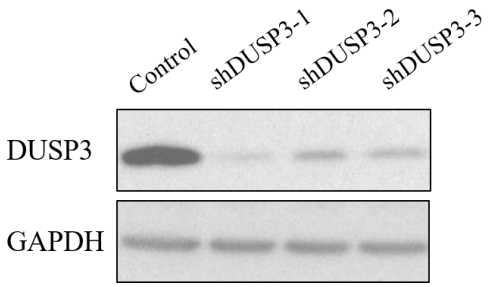

Figure R.34. *shRNA-mediated DUSP3 knockdown in HepG2 cells.* HepG2 cells were transduced with eGFP-targeting shRNA (control) of with DUSP3-targeting shRNA (shDUSP3-1 to 3). Efficiency of DUSP3 downregulation was measured at protein level using Western blot analysis. Equal amounts of total cell lysates were resolved by SDS-PAGE and immunoblotted with anti-DUSP3 antibody. Anti-GAPDH antibody was used for normalization.

To investigate the role of DUSP3 in cells proliferation, $5x10^5$ shDUSP3-transduced HepG2 cells were seeded in a 6-well plate. Cells were collected and counted after 24, 48, 72 and 96 hours. As shown in Figure R.35, we did not observe any difference in term of cell numbers at any time point analyzed in any of the condition. These data suggest that in this cellular model, DUSP3 is dispensable for cell proliferation.

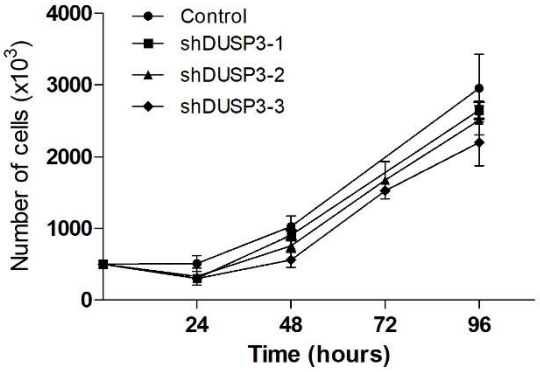

Figure R.35. *DUSP3 deletion is dispensable for cell proliferation in DUSP3-knockdown HepG2 cells.* shDUSP3-transduced and sh-eGFP-transduced HepG2 cells were seeded in 6-well plate and collected and counted after 24, 48, 72 and 96 hours. The graph represents two different experiments, with 3 biological replicates. Data are shown as mean ± SD.

To investigate if the observed result *in vitro* could be due to artificial cell culture conditions, we used an *in vivo* ectopic xenograft model using the shDUSP3-transduced HepG2 cells (shDUSP3-1 and shDUSP3-2). 6-week-old immunodeficient NOD/SCID mice were injected subcutaneously with $2x10^6$ control (eGFP-transduced)

HepG2 cells on the right flank. In the same mice, $2x10^6$ DUSP3-knockdown HepG2 cells were injected in the left flank. Tumor size was measured every 2 days with a caliper. Tumor volume was measured as length x width^2 x 0.5. We observed no difference in the tumor growth in the different groups (Figure R.36.A). These data were further confirmed at the time of mice sacrifice, 4 weeks after cells injection. Indeed, we did not observe any difference in tumor size or weights between the controls and shDUSP3-transduced cells (Figure R.36.B and R.36.C).

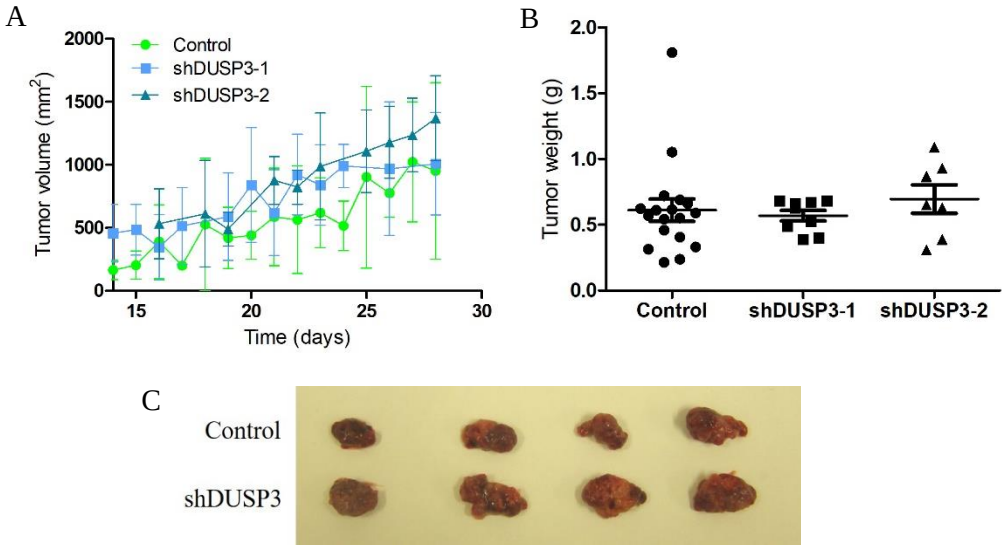

Figure R.36. *DUSP3 deletion in HepG2 cells does not alter tumor growth in an ectopic xenograft model.* Immunodeficient NOD/SCID mice were injected subcutaneously with $5x10^6$ control (eGFP-transduced) HepG2 cells in the right flank and with $5x10^6$ DUSP3-knockdown HepG2 cells (shDUSP3-1 or shDUSP3-2) in the left flank. Tumors were measured every two days with a caliper. Mice were euthanized after 4 weeks and tumors were measured and weighted. (A) Tumor volume over time measured as length x width^2 x 0.5. (B) Tumor weight at dissection. Each dot represents a mouse. (C) Representative picture of tumors harvested at dissection. Data are shown as mean ± SD (n=7-8 mice in each group) (*, $p<0.05$; **, $p<0.01$).

Again, these data suggest that DUSP3, in this model, is not involved in cell proliferation.

Liver-specific DUSP3 expression in DUSP3-KO mice

Because DUSP3-KO mouse is a full knock-out, it is difficult to exclude the contribution of other cell types or organs to the observed phenotype. To understand if liver damages observed in DEN-induced carcinogenesis are due to DUSP3 deletion in hepatocytes, we sought to reconstitute DUSP3 expression *in vivo* in hepatocytes of

DUSP3-KO mice, using adeno-associated virus vectors serotype 8 (AAV8) and thyroid-binding globulin (TBG) promoter. AAV8 has a high affinity to mouse hepatocytes [255], but to ensure hepatocyte specificity, we used the liver-specific TBG promoter [256]. AAV8-TBG containing DUSP3 sequence (AAV-DUSP3) or a stuffer sequence (AAV-control) were used. The plasmid also contained the sequence for Luciferase, allowing monitoring of the expression of the phosphatase by bioluminescence after injection of Luciferin to the mice. The amount of photons emitted by the organ is then proportional to the number of cells expressing the Luciferase gene. Targeted expression of DUSP3 using the AAV vector was evaluated 4 weeks after injection of 10^{11} viral particles in the tail vein of DUSP3-KO mice. Different organs were collected and subjected to anti-DUSP3 immunoblotting. As shown in Figure R.37.A, the expression of DUSP3 was only visible in the liver of the mice, while all the other organs remain free of DUSP3 expression. These data clearly demonstrate the efficacy of the AAV vector in targeting the expression to the liver, though the expression was 53% lower than in WT mice liver (Figure R.37.B).

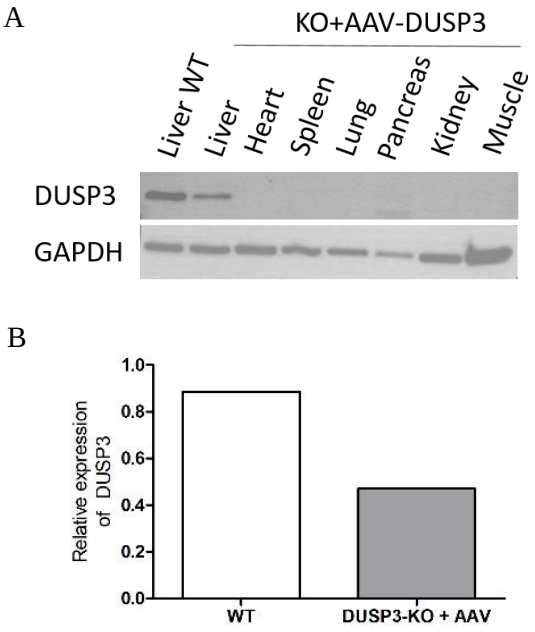

Figure R.37. *DUSP3 expression in different organs after DUSP3-AAV injection.* One DUSP3-KO mice was injected with 10^{11} particles of DUSP3-AAV in the tail vein. After 4 weeks, organs were harvested and DUSP3 protein expression was measured by Western blot analysis in different organs. The expression of DUSP3 in the liver of the DUSP3-KO mice was compared to DUSP3 expression in the liver of a WT mice of the same age. (A) Anti-DUSP3 and anti-GAPDH immunoblot in the liver of WT mice and in different organs of DUSP3-KO mice. (B) Quantification of DUSP3 expression in the liver of DUSP3-KO mice injected with AAV-DUSP3 and WT mice by densitometry analysis.

Having such data in hand, we combined the DEN-induced hepatocarcinogenesis model with injection of AAV. We injected intraperitoneally (i.p.) 10-day-old DUSP3-KO mice with 10^{11} particles of AAV-DUSP3 or AAV-control. Four days later, mice received a single i.p. injection of DEN carcinogen (25mg/kg of body weight). Four weeks later, the food was switched to HFD. To ensure that DUSP3 expression was maintained, we performed a second injection of AAV at week 7 after birth. Mice were monitored weekly for weight, three times for fasting insulin level in blood (week 8, 18 and 25 after birth) and once for glucose tolerance using OGTT assay (week 25 after birth). 10 mice received the AAV-control containing the stuffer sequence and 10 mice received the AAV expressing DUSP3. Mice were euthanized at 32 weeks after DEN injection.

As shown in Figure R.38, we did not observe any difference between the experimental groups for the weight of the animal.

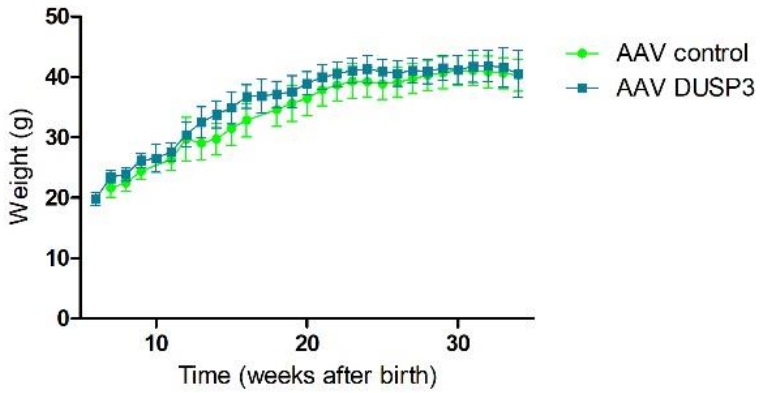

Figure R.38. *DUSP3 expression reconstitution in the liver does not affect weight of the mice.* Weight of DUSP3-KO mice injected with AAV-control or with AAV-DUSP3 was monitored every week from week 6 to week 34 after birth. Data are shown as mean ± SD.

DUSP3 expression was also monitored every other week by bioluminescence emitted by Luciferin in the Xenogen Lumina III. This allowed us to ensure that DUSP3 was expressed in the liver of the mice over time (Figure R.39). We observed that the control AAV was not really performant. This could have been due to an interference between the Luciferase gene and the stuffer sequence.

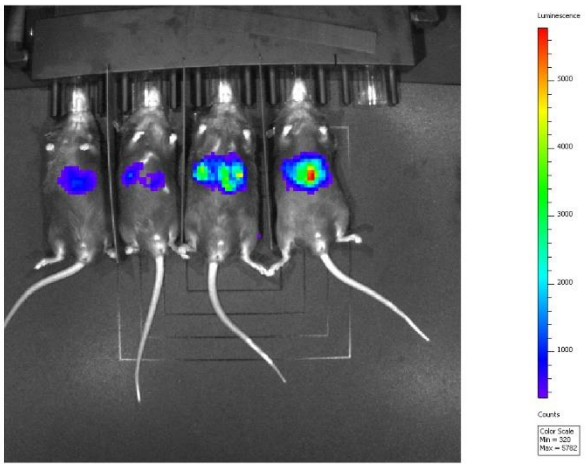

Figure R.39. *Luciferase expression in the liver of DUSP3-KO mice.* Luciferase expression was monitored in two mice injected with AAV-control and in two mice injected with AAV-DUSP3 three months after birth, using the Xenogen Lumina III.

DUSP3 reconstitution in the liver does not alter triglycerides or cholesterol metabolism

We measured TG and cholesterols in the serum of the mice at 34 weeks (Figure R.40). We observed more TG in the DUSP3-AAV mice than in the control mice, but no difference in cholesterol. We also measured AST and ALT and found no difference between the groups.

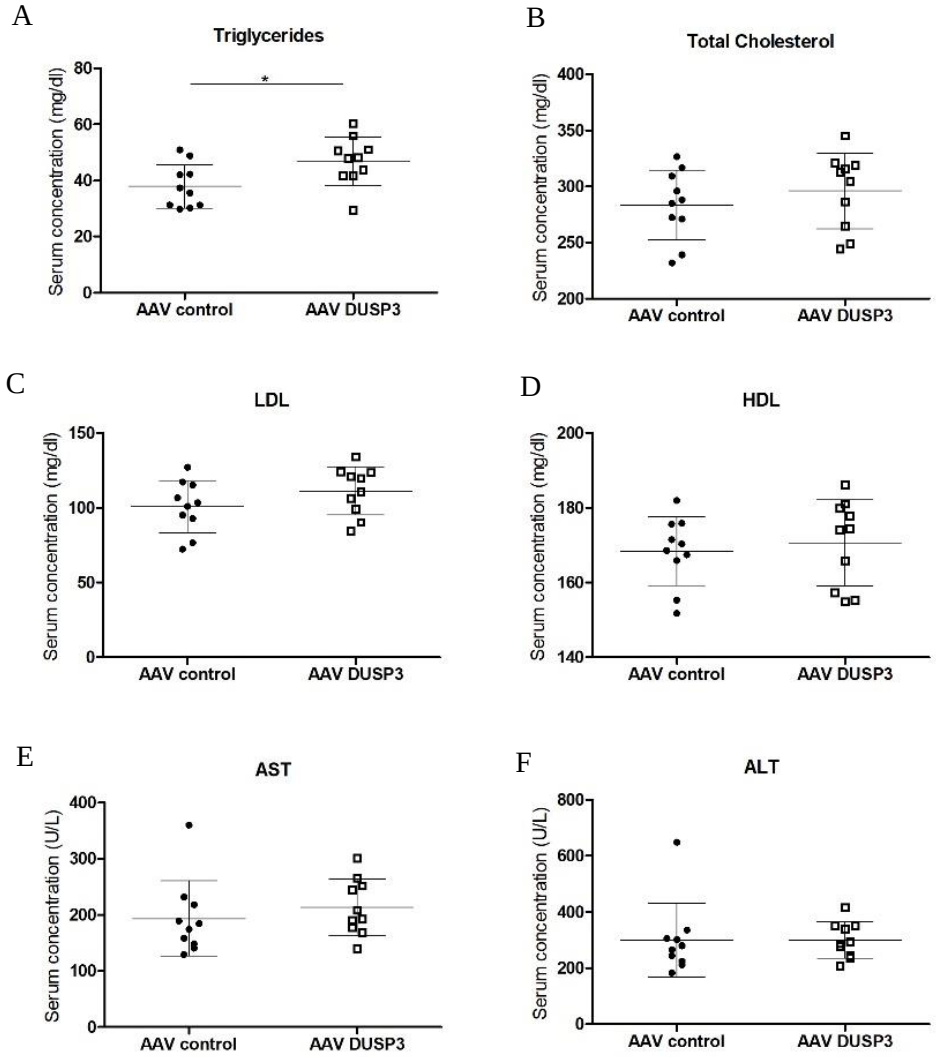

Figure R.40. *Triglycerides, cholesterol, AST and ALT concentrations in the serum of AAV mice at 34 weeks old*. Concentrations of triglycerides (A), total cholesterol (B), LDL (C), HDL (D) AST (E) and ALT (F) in serum were analyzed using the AU480 chemistry analyzer, from mice injected with AAV-DUSP3 and AAV-control. Each dot represents a mouse. (n=7-10 mice in each group). Data are shown as mean ± SD (*, $p<0.05$; **, $p<0.01$).

DUSP3 reconstitution in the liver increased fasting insulin concentration

Surprisingly and unexpectedly, the levels of fasting insulin were higher in the plasma of the AAV-DUSP3 injected mice compared to the AAV-control injected mice at 18 and 25 weeks of age (Figure R.41). However, the glucose tolerance measured at 25 weeks after birth was the same for the two groups of mice.

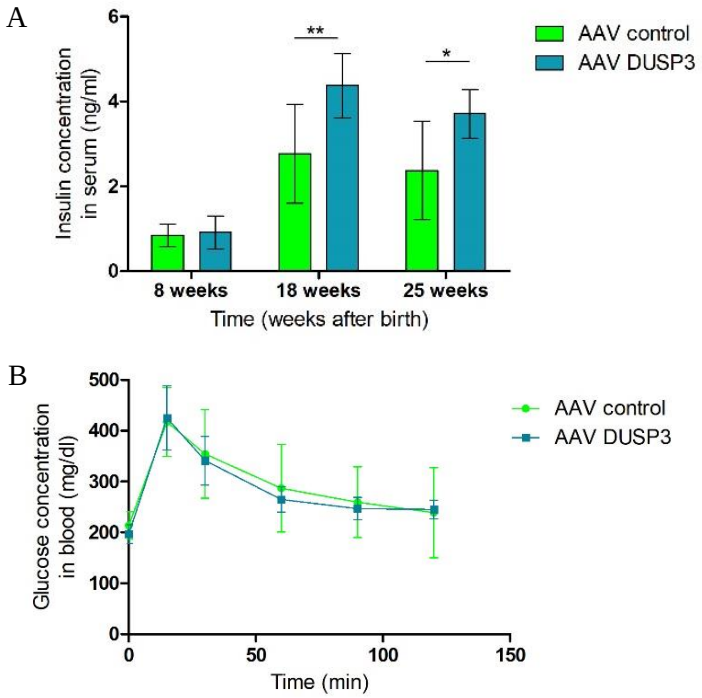

Figure R.41. *Fasting plasma insulin and OGTT in AAV mice.* (A) Insulin was measured by ELISA in serum of AAV-DUSP3 and AAV-control mice at 8, 18 and 25 weeks after birth. (B) OGTT was performed on 25-week-old AAV-DUSP3 and AAV-control mice. Data are shown as mean ± SD (*, $p<0.05$; **, $p<0.01$).

DUSP3 expression reconstitution in the liver does not affect the number of tumors in DEN-induced hepatocarcinogenesis model

Mice were euthanized at 34 weeks old. Before dissection, mice were injected with Luciferin and monitored using the Xenogen Lumina III to evaluate Luciferase expression in the body. At dissection, al soft tissues were harvested and placed in the Xenogen (Figure R.42). We observed that only the liver expressed Luciferase, showing the specificity of the AAV.

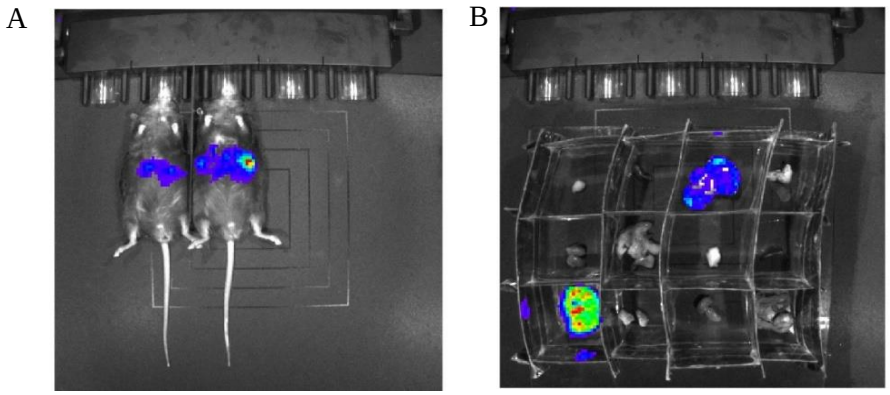

Figure R.42. *Luciferase expression is specific to the liver in AAV-injected mice.* AAV-control and AAV-DUSP3 mice were euthanized 32 weeks post-DEN injection. Before dissection, mice were injected with Luciferin and monitored using the Xenogen Lumina III to evaluate Luciferase expression. (A) Representative image of AAV-control mice (left) and AAV-DUSP3 mice (right) in the Xenogen. (B) Organs from the mice in (A) in the Xenogen. From left to right, top to bottom: heart, spleen, liver, lungs, kidney, intestines from the AAV-control mice; heart, spleen, liver, lungs, kidney, intestines from AAV-DUSP3 mice.

Livers were harvested and weighted. Tumors (>1mm) were counted. We did not observe any difference in the liver weight, nor the number or size of tumors between the two groups (Figure R.43).

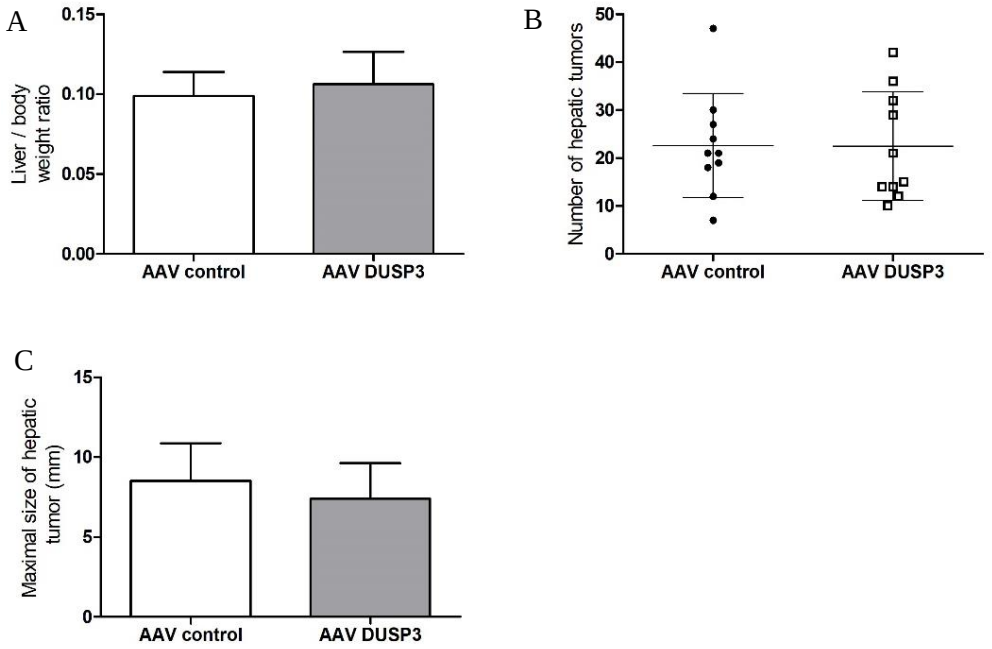

Figure R.43. *Liver-specific DUSP3 expression does not decrease the size of the liver or reduce tumor multiplicity in the liver of DUSP3-KO mice.* AAV-control and AAV-DUSP3 injected mice were euthanized at 32 weeks post-DEN injection. (A) Liver weight to body weight ratio. (B) Number of hepatic tumors per mouse. Each dot represents one mouse. (C) Maximal size of hepatic tumor. Data are shown as mean ± SD (*, $p<0.05$; **, $p<0.01$).

Although Luciferase expression was present in the liver when monitored using luminescence, it could be dissociated from DUSP3 expression for some reason. To investigate this hypothesis, we performed Western blot analysis on liver extracts and evaluated the expression level of DUSP3. As shown in Figure R.44, the expression of DUSP3 protein was extremely variable between mice.

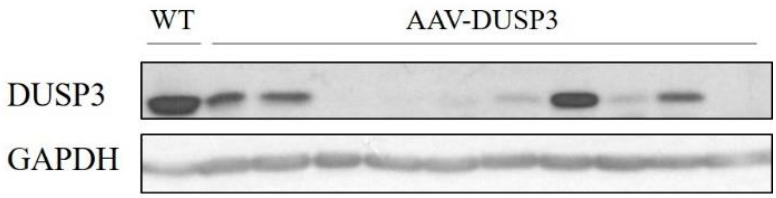

Figure R.44. *DUSP3 expression in the liver of AAV-DUSP3 mice.* DUSP3 protein expression was measured by Western blot analysis in the liver of AAV-DUSP3 mice and compared to DUSP3 expression in the liver of a WT mouse. Anti-DUSP3 and anti-GAPDH antibody were used.

To investigate the expression of DUSP3 within the liver, immune-fluorescence staining on 5 µm paraffin sections was performed (Figure R.45). We observed that DUSP3 expression was highly variable between mice, but also within cells in the same liver of mice.

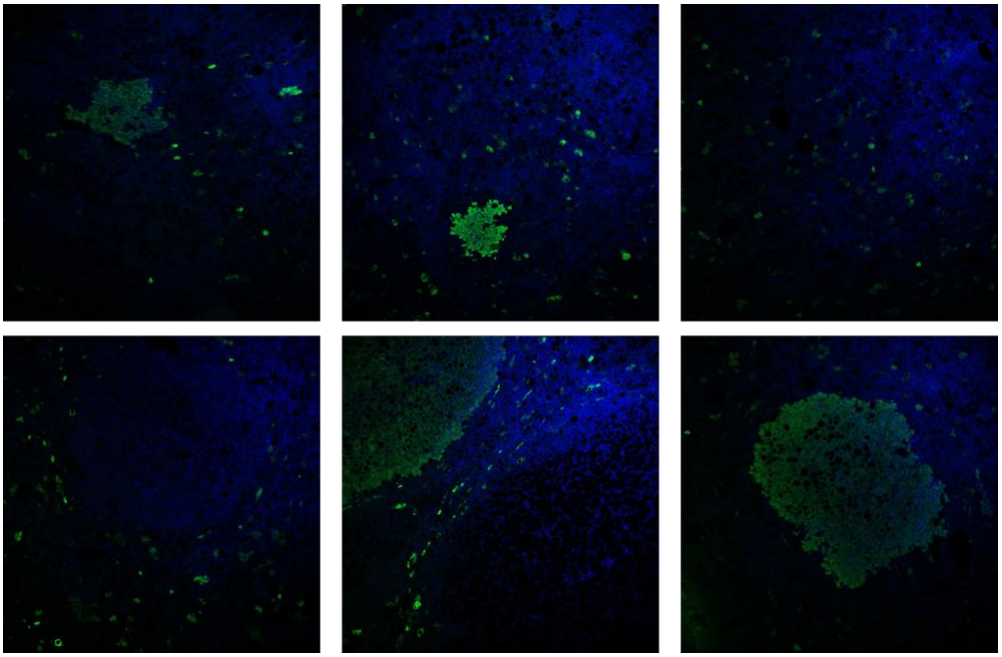

Figure R.45. *DUSP3 expression in AAV-DUSP3 mice is highly variable between mice and within the liver.* 5µm paraffin liver sections were subjected to anti-DUSP3 (green) and DAPI (blue) staining and visualized using fluorescent microscope. Representative images (10x magnification) of DUSP3 expression in the liver of AAV-DUSP3 mice.

Given the high variability of DUSP3 expression within the liver of the mice injected with AAV, we performed a correlation test between DUSP3 expression in the liver (obtained by quantification of Western blot analysis) and the number of hepatic tumors. Unfortunately, we found no significant correlation (Figure R.46) between the two parameters.

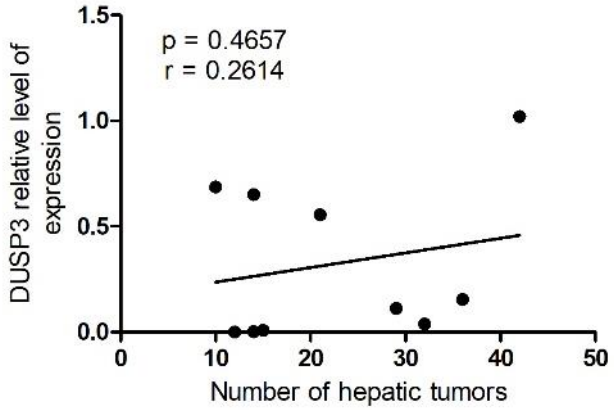

Figure R.46. *Correlation between DUSP3 expression in the liver and the number of hepatic tumors.* Spearmans's correlation test was performed.

The low and extreme variable expression of DUSP3 in this model does not allow us to conclude if DUSP3 plays a role in the hepatocytes in the development of NAFLD and HCC.

Discussion and perspectives

DISCUSSION AND PERSPECTIVES

Obesity, NAFLD and HCC are multifactorial pathologies that are closely linked. A number of signaling molecules, including DUSPs, have been studied in both diseases. In the present work, we investigated the role of DUSP3 in the development of obesity, insulin resistance, NAFLD and DEN-induced HCC.

While DUSP3-KO mice are born healthy and have no spontaneous phenotype at young age, they become obese and develop NAFLD and even HCC in some cases when old and under HFD. However, DUSP3 deletion was not associated with hyperphagia since food consumption was similar between WT and DUSP3-KO mice under both CD and HFD and thus, excluding the fact that the weight gain observed is a result of increased appetite in DUSP3-KO mice.

Obesity occurs when an imbalance between energy intake and energy expenditure leads to an increase in body weight. Thus, in the case of DUSP3-KO mice, energy expenditure may be reduced and could explain the observed gain of weight while aging. Unfortunately, for technical reasons, we were not able to investigate if DUSP3-KO mice expand less energy than WT mice. Genetic factors can also be excluded since mutations in DUSP3 gene have never been identified in GWAS in obesity or related disorders such as NAFLD.

Weight gain in DUSP3-KO mice over WT mice was at least partially due to an increase of WAT accumulation, as demonstrated by CT scan and WAT dissection and quantification. This increase of WAT mass was in part due to adipocytes hypertrophy. In obesity, hypertrophy of WAT adipocytes has been associated with increased glucose intolerance, hyperinsulinemia, type 2 diabetes and cardio-metabolic complications [257,258]. Moreover, obesity is characterized by a state of chronic, low-grade inflammation [259]. Adipose tissue is known to secrete a large number of adipokines, including inflammatory cytokines. In obesity, inflammation of the adipose tissue also triggers the secretion of IL-6 and TNFα, which leads to local and generalized inflammation [260]. Preliminary results showed that both cytokines are increased in DUSP3-KO mice under HFD, but not under CD, compared to WT mice, both with or without DEN. Though this result was not statistically significant because

of the small number of biological replicates (Figure S.2). However, the increased body weight and WAT in DUSP3-KO mice seems to be associated with inflammation. Indeed, CRP levels were significantly higher in DUSP3-KO mice under CD, and slightly increased in DUSP3-KO mice under HFD, compared to WT mice.

The difference of weight in old mice (18 months) was not only due to a difference in WAT weight, but was also attributable to an increase in liver weight in DUSP3-KO mice. Indeed, we observed that the livers of the DUSP3-KO mice were larger (under both CD and HFD) and contained more fat than the livers of WT mice, under HFD. Under HFD, this was associated with a higher SAF score for the DUSP3-KO mice. Some DUSP3-KO mice under HFD even developed HCC. Accordingly, serum levels of ALT and AST were higher in DUSP3-KO mice. Moreover, this phenotype was associated with leukocytes infiltration. Indeed, we observed more leukocytes in DUSP3-KO mice liver under HFD, compared to WT mice.

The increased accumulation of fat in WAT and liver in 18-month-old DUSP3-KO mice was accompanied by an elevation of the blood cholesterol. LDL and HDL were both elevated in DUSP3-KO mice under HFD. The LDL/HDL ratio was significantly increased in DUSP3-KO mice compared to WT mice, under both CD and HFD. A possible explanation could be a dysregulation in cholesterol metabolism in the liver of DUSP3-KO mice. Master regulators of cholesterol synthesis in the liver include SREBF1 and 2, HMG-CoA reductase and ChREBP. Their expression has been shown to be upregulated in NAFLD liver. Moreover, their expression is also increased by insulin [261]. Data from the RNA sequencing analysis confirmed the increased expression of these genes in 18-month-old mice fed HFD. However, we observed no difference between WT and DUSP3-KO mice. SREBF1 is a predominant transcription factor controlling the synthesis of cholesterol in the liver and can be phosphorylated and activated by the MAPKs ERK [262], p38 and JNK [263], reported substrates of DUSP3 [22]. Kotzka *et al.* showed that transgenic mice expressing a SREBF1 variant lacking MAPK phosphorylation sites were immune to the development of hepatosteatosis [263]. As we did not observe any difference SREBF1 expression between WT and DUSP3-KO mice, it would be interesting to study the phosphorylation of SREBF1 in DUSP3-KO mice to determine if, in absence of the

phosphatase, SREBF1 is more active. Levels of triglycerides were also higher in DUSP3-KO mice under CD compared to WT mice, but the difference was lost when mice were fed HFD. This could be due to the time point at which the measures were performed. It would be interesting to monitor the evolution of TG and cholesterol over weeks after switching to HFD.

At a younger age, DUSP3-KO mice tend to be leaner, as shown by the weight curves (Figure 1). At 5 months old, DUSP3-KO mice presented a slight, but not significant, decrease in WAT weight compared to WT mice. Though, the size of the adipocytes was slightly, but not significantly, increased in DUSP3-KO mice. Triglycerides levels and cholesterol levels were also lower in young DUSP3-KO mice. These results suggest that the process leading to fat accumulation does not start from birth, but seems to appear while aging. Interestingly, increased levels of insulin were observed in DUSP3-KO mice from a young age, as early as 14 weeks old. Constant increased insulin levels in DUSP3-KO mice could cause the increased accumulation of fat by stimulating the insulin signaling pathway in adipose tissue. Indeed, studies have shown that insulin plays a key role in regulating white adipose lipid accumulation [264]. Increased fasting levels of insulin in DUSP3-KO mice were increased with age and HFD. Initial increased of insulin in DUSP3-KO mice may lead to the development of obesity and insulin resistance, which promote the development of NAFLD. Indeed, as discussed in the introduction, insulin resistance is a major mechanism in the development and progression of NAFLD. In parallel, fat accumulation in the liver promotes insulin resistance. Studies have shown that liver fat content is an independent predictor of reduced peripheral and hepatic insulin action [265].

A possible explanation for the increased insulin levels is that DUSP3 regulates insulin production or secretion in the pancreas. Using immunofluorescence staining, we found that DUSP3 is expressed ubiquitously in the pancreas of WT mice, but its expression is higher in Langerhans islet, co-localizing with insulin. This co-localization suggests that DUSP3 could play a role in insulin production or secretion. To further investigate this possibility, DUSP3 knock-down Min6 cells (cell line derived from a mouse insulinoma) that display characteristics of pancreatic β-cells – were generated using two shRNA targeting DUSP3. Min6 cells were stimulated with

glucose and insulin production was measured by ELISA. Unfortunately, results from the two knock-down gave opposite results suggesting lack of specificity or an off-target effect of one of the shRNA. Additional shRNA should be tested to further investigate this hypothesis.

Despite the increased levels of insulin, we did not observe any difference in fasting glucose levels. However, the HOMA-IR index that was significantly higher in mutant compared to WT mice clearly suggest that DUSP3-KO mice developed severe insulin resistance. Steady fasting glucose levels suggested that glucose tolerance was not impaired. This was confirmed by the OGTT. Indeed, OGTT highlighted that, even under HFD, no group of mice developed glucose intolerance. These results indicate that, despite the variation in insulin levels between WT and DUSP3-KO mice, no difference in glucose tolerance was found between the different groups. Furthermore, the ^{18}F-FDG PET analysis showed that glucose clearance did not differ between the two groups of animals. These results suggest that, even if mutant mice are developing insulin resistance, they still produce enough insulin to compensate the resistance developing in certain tissues. This phenomenon is frequently observed in human. Indeed, most obese, insulin-resistant individuals do not develop hyperglycemia. Under normal conditions, the pancreatic islet β-cells increase insulin release sufficiently to overcome the reduced efficiency of insulin action [79]. Type 2 diabetes appears when β-cells are unable to compensate fully the decrease in insulin sensitivity.

Insulin resistance observed in DUSP3-KO mice suggests that this phosphatase could play a role in the insulin receptor (IR) signaling pathway. Indeed, we observed that IR is hyper-phosphorylated in DUSP3-KO mice compared to WT mice, both under CD and HFD. This correlates with the increase of insulin levels in the blood. To my knowledge, there is no study linking hyper-phosphorylation of IR to insulin resistance. However, IR activation seems to play a crucial role in the establishment of liver steatosis during insulin-resistant states. Indeed, mice with specific deletion of IR exhibit marked insulin resistance but lack hepatic steatosis under HFD [266]. Moreover, hepatic knockdown of IR with antisense oligonucleotides blocks the development of liver steatosis in genetically obese mice [267]. Similarly, human patients with inactivating mutation in the IR are insulin resistant but do not display

increased levels of DNL and do not develop hepatic steatosis [268]. So, the observed activation of IR could partially explain the development of hepatosteatosis in our model. We also observed a slight, but not significant increase in Akt phosphorylation in DUSP3-KO mice compared to WT mice, both under CD and HFD. Under CD, we observed an increase in ERK1/2 and p38 phosphorylation. This difference is lost in HFD fed mice. This may be due to an exhaustion of the pathway. Moreover, insulin is not the only molecule capable of activating these molecular pathways. Indeed, Akt/PI3K pathway can also be activated by TNFα [269] and by IGF1 [270] in the liver. Hepatocyte growth factor (HGF) by binding to its receptor cMet can activate the MAPK pathway, including ERK and p38 [271].

The observed and very consistent phosphorylation of IR in DUSP3-KO mice suggests that IR may be a substrate for DUSP3. This is indeed the first time we observe a hyper-phosphorylation, at basal level, of a protein in DUSP3-KO mice. In the very first studies on DUSP3, Ishibashi *et al*. reported that insulin receptor is a substrate for this phosphatase [9]. The study was however based on *in vitro* assays, using recombinant proteins. Our study is therefore the first to confirm *in vivo* that IR could indeed be a substrate for DUSP3. To further confirm this, it will be interesting to immune-precipitate phosphorylated IR from mutant mice and perform a DUSP3 phosphatase assay using WT and phosphatase dead mutant.

To get better insights into the mechanisms behind NAFLD development in both WT and DUSP3-KO mice, we performed RNA sequencing analysis using RNA from WT and DUSP3-KO mice livers. As expected, PCA demonstrated a strong effect of the diet in the discrimination of the samples. On the other hand, WT and DUSP3-KO samples were poorly discriminated by the PCA. One possible explanation is that the variability between the samples was too high. This is especially true for mice fed HFD. Indeed, these mice under HFD were at different stages of the disease. In Figure 17.A, we can clearly see that DUSP3-KO mice clustered with one WT mice (number 1) that was in an advanced disease stage. These mice presented all dysplasia except the two WT mice (number 2 and 3) that were clustered separately from all the other WT and DUSP3-KO mice. Mice fed CD were better discriminated by the PC1 and PC3. This

could be explained by the fact that the SAF scores of these mice were more similar, making the groups more homogeneous.

A differential expression analysis showed that a large number of genes were differential expressed between mice fed CD or HFD, regardless of the genotype. 416 genes were upregulated, both in WT and DUSP3-KO mice, when fed HFD, and 149 were upregulated. Among these genes, we observed a decrease of IRS2 expression in HFD fed mice compare to CD fed mice. IRS2 expression was also decreased in DUSP3-KO mice compared to WT mice. Shimomura *et al.* showed that chronic hyperinsulinemia downregulates mRNA for IRS-2, leading to insulin resistance [70]. But, despite the reduction of IRS2, insulin continues to increase SREBF1 expression, a transcription factor that activates fatty acid synthesis. Eventually, the combination of insulin resistance, leading to glucose overproduction, with partial insulin sensitivity, enhancing fatty acid synthesis, may further increase insulin secretion and resistance by creating a vicious cycle. This was confirmed in our model where SREBF1 expression is increased as demonstrated by RNA sequencing and qRT-PCR in HFD fed mice.

The differential expression analysis also showed that a large number of genes are down- and up-regulated specifically in WT or in DUSP3-KO mice when fed HFD. In WT mice, 501 genes were upregulated with HFD and 340 genes were downregulated. In DUSP3-KO mice, 847 genes were upregulated and 488 were downregulated. By running a GSEA analysis, we observed that some pathways were specifically regulated in WT or DUSP3-KO mice. In WT mice fed HFD compared to WT mice fed CD, we observed an upregulation of the mTORC1 signaling pathway, which is an important pathway in the development of insulin resistance and NAFLD [272]. It is surprising that this pathway is upregulated in WT mice and not in DUSP3-KO mice, given the fact that DUSP3-KO develop more severe NAFLD and HCC. This could indicate that in DUSP3-KO mice, the development of NALFD is not dependent of mTORC1 pathway regulation. In DUSP3-KO mice fed HFD, KRAS signaling pathway was upregulated. KRAS is part of the RAS/MAPK pathway. In the liver, this pathway is activated by insulin and controls mainly cellular proliferation. Interestingly, aberrant activation of the RAS cascade occurs in HCC. Xu *et al.*

reported that consumption of HFD in mice increased the levels of Ras activity and that the liver tissues with more HCC displayed more extensive Ras activity than those with fewer HCC [273]. The IL6-JAK-STAT3 was also upregulated in DUSP3-KO mice fed HFD compared to DUSP3-KO mice under CD, but not in WT mice. Activation of this pathway has been linked to the development of HCC [274]. STAT3 is activated in human HCC and STAT3-positive tumors are more aggressive. Moreover, He *et al.* reported that STAT3 plays a critical role during tumor progression in mice injected with DEN [275]. Park *et al.* also demonstrated the importance of the IL-6 and STAT3 activation in the development of obesity-induced HCC [98]. The activation of the IL-6 pathway is coherent with our preliminary results showing that DUSP3-KO mice have higher levels of IL6 in the serum.

According to the poor discrimination of WT and DUSP3-KO mice seen with the PCA, the differential expression analysis showed that a small number of genes were differentially expressed between WT and DUSP3-KO, under CD or HFD. Under CD, 126 genes were upregulated and 197 were downregulated, compared to WT mice. Under HFD, only 52 genes were upregulated in DUSP3-KO mice and 33 were downregulated, compared to WT mice. GSEA showed the pathways in which these genes were involved. Under CD, we observed that fatty acid metabolism in DUSP3-KO mice was downregulated. This could explain the fat accumulation in the liver of the mutant mice. G2/M checkpoint pathway was upregulated in DUSP3-KO mice compared to WT mice. G2/M checkpoint prevents cells with damaged DNA from entering the M phase so that DNA can be repaired. It was previously shown that G2/M checkpoint pathway is upregulated in the early stage of HCC development [276].

Under HFD, we observed that in DUSP3-KO mice, unfolded protein response (UPR) and DNA repair pathways were downregulated, compared to WT mice. UPR is an adaptive pathway used to restore normal ER function in the presence of ER stress. When UPR fails to restore the ER functions, apoptosis is stimulated [277]. However, insulin resistance and obesity are associated with an increased activation of UPR pathway. Bile acids have recently emerged as relevant signaling molecules that regulate lipid and carbohydrate metabolic pathways. Modulation of bile acid metabolism pathway appears to affect both insulin sensitivity and NAFLD

pathogenesis [278]. Downregulation of DNA repair pathway may suggest an increased in DNA damages in DUSP3-KO mice, leading to tumor development.

Recent studies showed that the expression of some DUSPs is downregulated in the liver of mice fed HFD. Ye *et al.* reported that the expressions of DUSP9 and DUSP26 were decreased in the liver of mice fed HFD for up to 24 weeks and in the liver of genetically obese mice (ob/ob) [231,235]. In the same way, Huang *et al.* showed that the expression of DUSP12 was decreased in liver with hepatic steatosis. Our RNA sequencing data showed no difference in term of expression of these DUSPs between CD and HFD, neither in WT nor in mutant mice. On the contrary, the expression of these three phosphatases slightly, but not significantly, increased with HFD. These discrepancies could be due to the different models used and to the duration of HFD feeding. In our model, mice were fed HFD for 60 weeks, compared to 12 to 24 weeks in the other models.

One drawback of our experimental design for RNA sequencing was the fact that we performed the experiment on whole liver extracts. It would have been interesting to separate hepatocytes from other cells. Moreover, given the previous findings from our lab on the importance of DUSP3 in macrophages function, it would be interesting to investigate the role of Kupffer cells in the observed phenotype. Another issue is the fact that the experiment was performed on a small piece a liver. This could clearly explain the heterogeneity observed, since it is possible that we captured the signature of small tumors in part of the mice but not in others. As already discussed above, the number of mice used is also critical, but the cost of such experiments required further funding to be performed.

The second part of this work focused on the development of HCC. As discussed in the introduction, NAFLD can lead to the development of HCC. Interestingly, some DUSP3-KO mice fed HFD spontaneously developed HCC while aging. We investigated HCC development by using the DEN-induced hepatocarcinogenesis model. In this model, we also observed a significant increase in the weight of the DUSP3-KO mice over time, compared to WT mice. As expected, DUSP3-KO mice developed more hepatic tumors under HFD. This was associated with a higher SAF score and higher levels of AST and ALT in the serum. However, we did not observe

any difference between WT and DUSP3-KO mice when fed CD. The fact that the number of tumors is increased in DUSP3-KO mice only with HFD suggests that DUSP3 could play a role in the metabolism of lipid in the liver. In this model, we also observed a higher level of insulin in the DUSP3-KO mice compared to WT mice, both under CD and HFD.

To investigate the role of DUSP3 as a potential tumor suppressor, we used DUSP3 knock-down HepG2 cells. In these cells, we observed no difference in proliferation with the control cells, suggesting that DUSP3 is not involved in tumor cells proliferation in this cellular model. We confirmed this result *in vivo*, using an ectopic xenograft model. In this cellular model, DUSP3 does not seems to play a role in cell proliferation.

Full knock-out mice do not allow to distinguish whether the observed phenotype is due to the loss of DUSP3 in the liver, or in another organ or cell type. To better understand the role of DUSP3 in the liver, we sought to reconstitute DUSP3 *in vivo* in the hepatocytes of DUSP3-KO mice using AAV. However, DUSP3 expression in the liver was highly variable between mice and within the liver, which does not allow us to conclude on the role of DUSP3 in the DEN-induced HCC model. The difference of expression could be due to the fact that we injected the AAV early in the protocol. The liver expands and regenerates over time. The concentration of AAV that we used could also have been too low. Further studies using targeted cell types and tissues DUSP3 deletion are required to better understand the contribution of each cell type to the observed phenotype.

To further investigate the role of DUSP3 in the hepatocytes, *in vitro* experiments on KD HepG2 cells might be useful. Preliminary results were obtained on HepG2 cells after insulin stimulation, to study the activation of the insulin pathway after insulin stimulation. However, the results were highly variable between the different shRNAs. *In vivo* insulin stimulation is frequently used in mice model, to evaluate the responsiveness of the insulin pathway in the liver. However, in our model, this experiment is skewed by the fact that DUSP3-KO mice have a higher basal insulin level.

We did not investigate any further the macrophage populations present in the liver of the mice, yet DUSP3 expression is important in these cells. Indeed, previous work in the laboratory highlighted the role of DUSP3 in macrophages recruitment and function in sepsis and LLC experimental metastasis model [33,37]. Given the important role of macrophages in NAFLD development and the potential role of DUSP3 in macrophages recruitment and polarization, it would be interesting to evaluate the different populations of macrophages in the livers of WT and DUSP3-KO mice. Moreover, macrophages interaction with adipocytes play an important role in the development of the chronic, low grade inflammation observed in obesity. As a preliminary experiment, we created chimeric mice by adoptive transfer of bone marrow cells from WT or DUSP3-KO mice in lethally irradiated WT mice. The resulting recipient WT mice had hematopoietic cells from either WT or DUSP3-KO mice. These mice were kept under HFD for 18 weeks and weighted every week. We observed no difference between the two groups of mice in weight gain suggesting that the hematopoietic compartment does not contribute to the observed phenotype. We cannot exclude however that Kupffer cells were not affected by the total body irradiation and thus, the adoptive transfer did not target the liver.

Collectively, our data highlight a new role of DUSP3 in the development of obesity, insulin resistance and NAFLD. AT the molecular level, our results suggest that DUSP3 could potentially targets IR, Akt or ERK. DUSP3 could also modulate insulin concentration in the blood (Figure D.1).

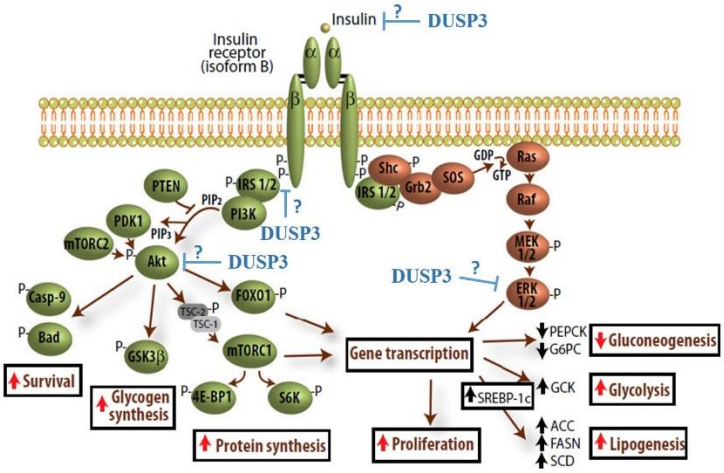

Figure D.1. *Potential targets of DUSP3 in insulin resistance development***.** Adapted from [63].

However, further investigations are needed to unravel the exact role of this phosphatase. Indeed, DUSP3 could play a role in various mechanisms of the pathogenesis (Figure D.2). The first phenotype observed was the development of obesity and the accumulation of WAT in DUSP3-KO mice. DUSP3 could play a role in lipogenesis in the adipose tissue. Excessive fat accumulation in WAT leads to dysregulation and inflammation of this tissue. DUSP3 is highly expressed in macrophages and could play a role in the setting of inflammation in WAT, leading to high levels of TNFα and IL-6. We observed that DUSP3-KO mice do not eat more than WT mice. However, for technical reasons, we were not able to measure DUSP3-KO mice energy expenditure compared to WT mice. Therefore, we cannot exclude that, while DUSP3-KO mice are not hyperphagic, they expend less energy which may explain the observed gain of weight. Insulin resistance is not only present in liver, but also in muscle. It is a possibility that DUSP3 exerts also an effect in development of insulin resistance in muscle. In DUSP3-KO mice, we observed an increased in insulin levels in the blood. DUSP3 could play a role in insulin production or release in the pancreas. However, the most striking effect observed in DUSP3-KO mice under HFD is the development of NAFLD, a complex disease where various molecular pathways are involved. DUSP3 could play a role in lipid metabolism, by regulating their synthesis. We observed a hyper-phosphorylation of IR, suggesting that IR could be a target of DUSP3 and thus being a key player in insulin signaling regulation. Inflammation also plays an important role in the setting of the disease. Given the already observed crucial role of DUSP3 in macrophages, it is possible that it also plays a role in Kupffer cells.

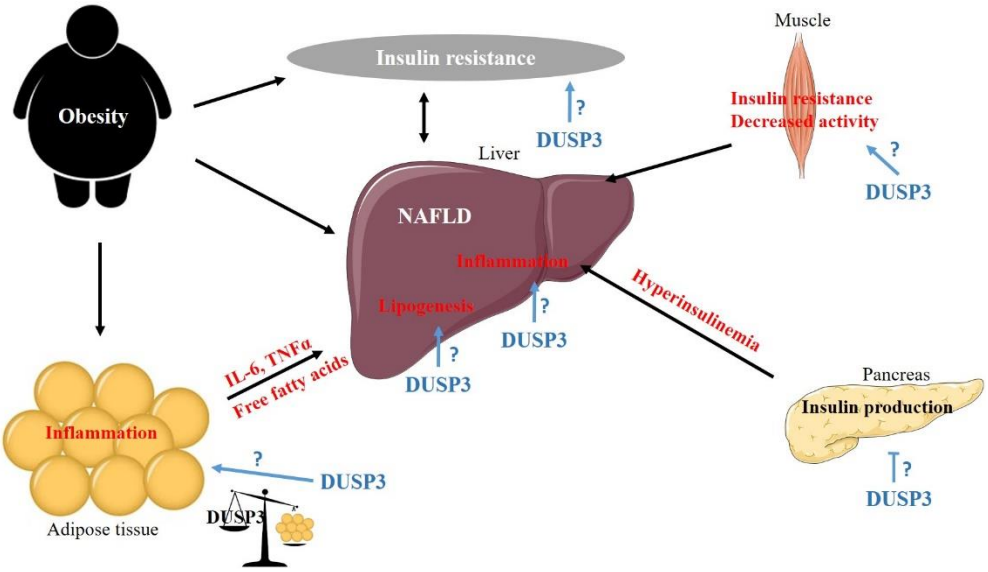

Figure D.2. *Potential roles of DUSP3 in the development of NAFLD and insulin resistance.*

To conclude, this work highlights the role of DUSP3 in the development of obesity, insulin resistance and NAFLD.

A large number of questions remain unanswered regarding the role of DUSP3 in the molecular mechanisms leading to this phenotype, as well as regarding its role in the different cells and organs. Further studies using targeted deletion of DUSP3 are indeed required. Some important experiments have already been discussed above. However, because development of NAFLD and HCC was the main phenotype in DUSP3-KO mice under HFD, the most important experiment is the development of the conditional knock-out mouse. This experiment would allow us to determine the role of DUSP3. Following experiments would dependent on the results from the conditional KO. If DUSP3 KO in the liver leads to NAFLD and insulin resistance, it would be interesting to over-express DUSP3 in the liver of WT mice in order to determine if DUSP3 could prevent NAFLD and insulin resistance in the liver in appropriate models.

Supplementary data

SUPPLEMENTARY DATA

1. Supplementary figures

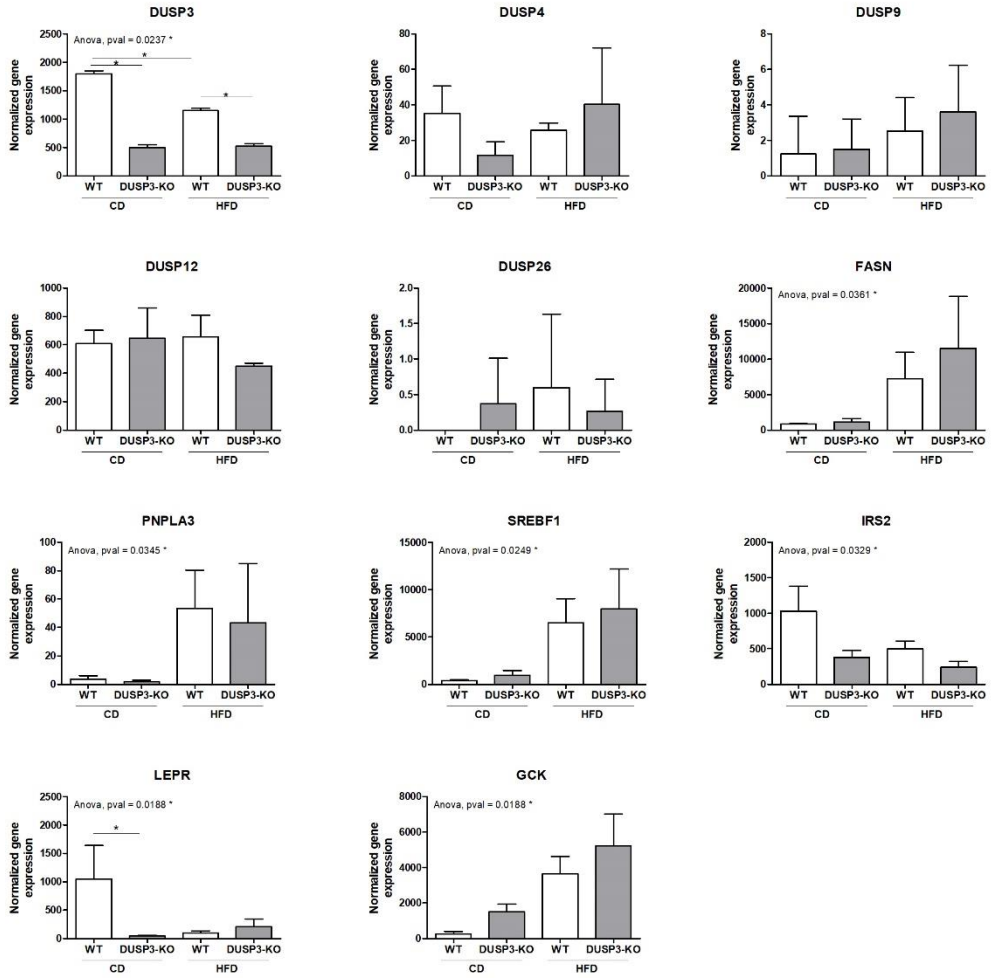

Figure S.1. *Normalized gene expression from RNAseq data.* Total RNA was extracted from liver of WT and DUSP3-KO mice, under CD and HFD, at 18 months old (n=3 mice in each group). RNA sequencing was performed using the Illumina NextSeq500. Genes are normalized on. Statistical significance was tested by one-way ANOVA with Dunns post-tests. Data are expressed as normalized number of reads and shown as mean ± SD (*, $p<0.05$). FASN, fatty acid synthase; LEPR, leptin receptor; GCK, glucokinase.

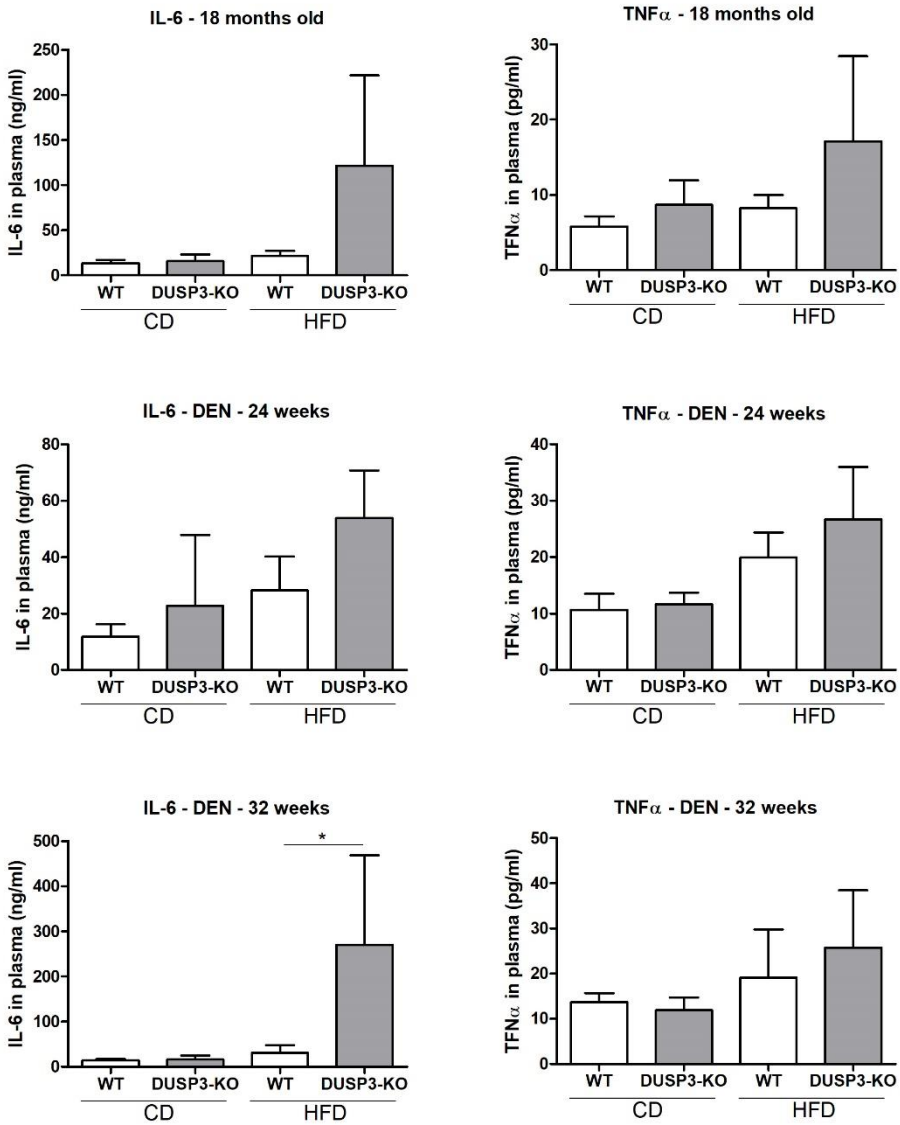

Figure S.2. *IL-6 and TNFα levels in plasma of mice.* IL-6 and TNFα levels were measured in mice plasma using V-PLEX assay from Meso Scale Discovery. IL-6 (A) and TNFα (B) in plasma of 18-month-old WT and DUSP3-KO under CD and HFD (n=3 mice in each group). IL-6 (C) and TNFα (D) in plasma of WT and DUSP3-KO mice 24 weeks post-DEN injection, under CD and HFD (n=4-5 mice in each group). IL-6 (E) and TNFα (F) in plasma of WT and DUSP3-KO mice 32 weeks post-DEN injection, under CD and HFD (n=4-5 mice in each group). Results are shown as mean ± SD (*, $p<0.05$).

2. Supplementary tables

Gene	WT-CD-1	WT-CD-2	WT-CD-3	KO-CD-1	KO-CD-2	KO-CD-3
Elovl5	29071,8203	27904,0397	28548,391	13617,396	11283,649	12945,856
Cpt1a	18187,185	22975,1403	20693,7717	7998,6079	10804,487	9261,172
Slc22a5	2308,55521	1553,99443	2076,32816	879,95088	1310,9379	683,58386
Odc1	1427,65914	1179,63333	1537,06582	853,94761	903,03592	644,68072
Acox1	106506,297	86017,0978	90173,4071	51189,01	58551,129	55651,507
Ehhadh	68540,0142	42978,0119	73412,5508	25753,645	38201,491	7324,9068
Dlst	7646,80789	7374,12204	7875,92079	5409,7217	4845,6785	4378,2713
Decr1	15532,1215	11504,5352	13253,9695	10486,601	7928,2868	6725,7983
Ldha	49597,9362	67828,3507	55861,2995	37155,562	33333,697	40824,962
Hadhb	6121,2714	4519,47725	5591,06292	3578,0509	4094,9915	2325,2967
Mgll	10705,756	9823,86871	10923,1454	6803,4973	7187,4288	6791,3779
Acsl4	955,147844	1029,21028	1148,03458	772,81738	592,19499	719,15246
Hsd17b7	1314,03143	1316,48436	1419,34743	686,48651	1109,4441	776,95142
Hsp90aa1	4118,72351	1715,72747	3034,89218	1630,9255	1627,9219	883,65719
Eci2	10227,6196	8482,50234	8439,84793	6735,8888	6413,398	5434,2138
Acot2	909,021741	277,095077	674,918764	328,68142	286,26853	151,16651
Hsph1	3008,32195	950,040262	1987,75908	951,71993	1002,5542	451,2765
Acss1	14,6253498	16,9650047	12,3324027	9,3611796	12,286203	5,5575924
Acadl	12036,6629	9673,44567	11415,3204	9318,5342	7728,0217	5918,8359
Retsat	53298,1497	28962,656	60291,9955	30499,763	31753,692	11644,268
Aoc3	11,2502691	4,52400125	22,4225503	6,2407864	2,4572406	1,1115185
Acsl5	13298,9431	8122,84424	9788,56433	8259,6808	7710,821	5520,9123
Hsd17b11	11235,6437	7049,52495	12831,3044	7593,9969	7380,3222	3221,1806
Aco2	4933,24299	4675,55529	5299,56976	3845,3646	3919,2988	3118,9209
Aadat	3336,82981	2911,1948	3218,75709	2712,6618	2350,3506	1573,9102
G0s2	4356,10418	6546,22981	6856,81588	5050,8765	4306,3142	3354,5628
Eno2	4,50010763	5,65500156	5,60563757	3,1203932	4,9144812	1,1115185
Adsl	376,884014	422,994117	466,389046	374,44718	271,52509	304,55606
Aldoa	2746,19068	3150,96687	3892,55473	2660,6553	2567,8164	2163,015
Fabp1	205783,172	99402,4864	143891,111	112779,33	106645,47	57734,493
Idh3g	1517,6613	1585,66244	1735,50539	1374,0131	1233,5348	1075,9499
Uros	666,015929	728,364201	710,794844	594,95497	420,18814	590,21631
Hsd17b4	17413,1665	13844,5748	17133,0707	12781,131	14331,856	9955,871
Etfdh	14786,2286	12135,6334	12826,8199	11307,265	11064,954	8403,0797
Fabp2	8725,70869	7170,54198	7003,68358	8182,7111	3101,0376	3494,6141
Hsdl2	6203,39836	3999,2171	4953,14136	3998,2638	4620,841	2539,8197
Adh7	276,756619	245,427068	248,890308	251,71172	120,40479	185,62359

Suclg1	7686,18383	5954,71664	7027,22726	6827,4203	4574,1534	4143,7409
Aldh9a1	8648,08183	6864,0409	6857,93701	7077,0518	5697,1124	4778,4179
Hmgcs2	145741,611	130397,55	152461,01	125115,29	124982,63	82862,591
Aqp7	16,8754036	1,13100031	6,72676509	2,0802621	0	4,4460739
Ppara	1705,54079	1321,00836	1808,37868	882,03115	1685,6671	952,57134
Crat	4489,98239	3620,332	4469,9354	3415,7904	4072,8763	2507,5857
Eci1	5265,12592	4081,78013	4686,31301	4780,4424	3497,882	2710,9936
Gpd2	771,768458	781,521216	820,665341	459,73793	834,23319	543,53254
Sucla2	5112,12226	4276,31218	4589,89605	4699,3122	3524,9117	3360,1204
Acadm	21489,1389	13958,8059	16348,2814	16555,766	15043,227	9941,4213
Acadvl	17653,9222	16606,4776	18453,7589	16554,726	14551,779	12755,786
Gabarapl1	14234,9655	10223,1118	14312,3139	10823,604	12945,972	8625,3834
Cpt2	6951,54126	6013,52866	7290,69223	6695,3237	5835,9464	4266,0079

Table S.1. *Fatty acid metabolism pathway genes are downregulated in DUSP3-KO mice fed CD compared to WT mice fed CD.* Normalized number of reads.

Gene	WT-HFD-1	WT-HFD-2	WT-HFD-3	KO-HFD-1	KO-HFD-2	KO-HFD-3
Hacl1	756,52	872,01	941,39	372,96	489,48	351,54
Agxt	4813,02	5477,85	4676,54	2064,94	2328,77	3706,24
Crot	17603,96	14893,19	17410,04	12631,23	10208,65	9558,83
Soat2	1399,37	1298,14	1507,80	1029,73	857,97	866,31
Nr0b2	1175,77	648,62	1126,06	690,40	498,18	525,14
Serpina6	3604,64	4321,46	5721,52	2180,66	3125,86	3389,25
Ttr	91896,51	118671,84	146287,83	75471,49	87931,21	71694,24
Bcar3	1077,95	1180,62	1075,39	887,43	792,34	646,93
Slc27a5	20966,37	23468,82	29787,72	13067,52	16491,20	22030,13
Pipox	3949,36	5707,52	5849,89	2846,03	4089,00	4235,70
Pecr	2672,97	3882,76	4492,99	2025,06	3142,46	2440,88
Apoa1	276434,86	173081,63	199600,11	114756,91	85857,06	199086,56
Paox	583,23	890,85	825,40	309,62	714,84	494,05
Akr1d1	2666,45	3348,07	4629,24	2534,06	3132,18	1827,64
Hsd3b7	247,83	234,15	182,42	206,42	170,80	151,15
Sod1	14789,38	17162,02	20453,79	11065,13	15211,76	15409,69
Pxmp2	2875,14	2780,19	4024,55	1785,81	2520,14	3099,90
Cyp7b1	2418,62	3524,81	6755,25	1259,60	3469,83	2440,02
Acsl1	9185,36	17633,01	19359,26	10860,28	11490,47	11264,68
Slc29a1	3153,71	4613,02	3381,56	2731,88	2702,01	3597,41
Idh1	10928,53	11511,02	15532,90	9532,65	12864,80	7940,21
Rxrg	163,04	210,82	170,04	157,16	163,69	124,38
Pex13	1371,42	1419,25	2309,55	1170,47	1541,18	1217,85
Pex7	1896,89	1991,62	3320,76	1738,90	2153,23	1706,72
Hsd3b1	0,00	0,90	0,00	0,00	0,00	0,00
Gc	118688,63	118901,50	129279,79	98733,12	103338,28	109013,14
Cyp27a1	8283,51	9738,30	9300,15	6732,75	8240,46	8202,78
Hsd17b6	1281,05	949,16	2343,33	535,59	1650,31	895,68
Hsd17b11	4128,24	5375,58	6968,07	4572,42	4485,96	4899,04
Aldh1a1	23489,34	38855,43	43065,11	36228,28	30599,07	17242,51
Acsl5	11176,35	10429,99	9183,04	7864,90	11560,05	6560,84
Retsat	4668,61	10847,15	10555,70	8619,42	6676,35	5807,68
Pex11g	1291,30	1275,71	1716,12	995,33	1360,10	1410,46
Nr1i2	1387,26	2013,15	2056,19	1458,20	1504,81	1829,37
Fads1	14431,62	16077,40	12346,14	11091,71	12380,86	14241,07
Abcd3	11192,19	14967,65	19891,88	12348,97	15564,44	11601,54
Phyh	27018,52	36239,41	50420,55	23041,92	37263,56	35505,09
Aldh9a1	4601,53	5340,59	6015,42	4639,66	5729,81	3814,20

Sult1b1	529,19	504,18	1486,40	422,21	838,20	590,79
Slc27a2	22139,35	30438,59	35737,83	22321,81	19647,90	33878,69
Aldh8a1	3671,72	6044,84	5469,28	3555,20	5384,25	4424,86
Gnmt	18879,42	29485,84	34317,86	17413,97	23102,71	30281,28
Gstk1	2482,91	3968,89	3865,77	2320,61	3300,61	3510,17
Pfkm	322,36	507,77	445,92	369,05	409,61	363,63
Bbox1	2820,17	3715,00	5062,77	3000,06	4097,69	3126,68
Lck	118,32	165,97	30,40	124,32	37,96	68,23

Table S.2. *Bile acid metabolism pathway genes are downregulated in DUSP3-KO mice fed HFD compared to WT mice fed HFD.* Normalized number of reads.

Gene	WT-HFD-1	WT-HFD-2	WT-HFD-3	KO-HFD-1	KO-HFD-2	KO-HFD-3
Mpc2	4295,01	3658,48	8108,77	2468,39	3412,11	2438,29
Polb	482,61	452,15	576,54	310,41	398,54	356,72
Tmed2	1277,32	976,97	1654,18	799,08	1052,50	787,72
Cstf3	406,21	325,66	309,67	281,48	245,13	247,02
Nme1	1099,37	976,07	1094,53	766,24	961,56	697,02
Polr1d	896,27	799,34	1341,14	577,03	772,57	821,40
Rfc4	87,58	102,27	135,13	93,04	90,15	62,19
Upf3b	449,07	359,75	361,47	334,64	259,37	310,94
Nfx1	1327,63	1218,30	1523,56	1064,13	1077,01	1034,74
Dgcr8	312,11	230,56	238,73	207,98	223,78	187,43
Clp1	350,31	306,82	411,01	252,55	302,86	294,53
Rpa3	286,96	173,15	378,36	197,81	246,72	144,24
Npr2	666,15	1544,85	1513,43	969,53	792,34	872,36
Gtf2a2	940,06	806,52	2078,71	666,94	830,29	942,32
Taf13	260,87	326,55	369,35	229,09	298,91	254,80
Polr2c	435,09	367,82	539,38	320,57	376,40	405,95
Rbx1	1038,82	924,04	1275,83	860,85	917,28	886,18
Pnp	1104,03	776,01	661,00	749,04	626,28	656,43
Polr2h	344,72	278,11	554,02	250,98	311,56	333,40
Tsg101	794,72	698,86	930,13	620,03	733,03	663,34
Rfc3	245,03	176,73	226,34	188,43	211,92	138,20
Pole4	515,22	549,94	673,39	435,51	538,50	486,28
Taf10	945,65	1020,93	1148,58	713,07	901,46	1002,78
Cox17	139,75	196,47	185,80	147,77	128,10	166,70
Pde4b	765,84	451,25	374,98	305,71	568,55	268,62
Nudt21	155,59	166,87	159,90	121,19	139,96	149,42
Polr2k	157,45	138,16	314,17	128,23	192,94	131,29
Rnmt	423,91	353,47	412,14	347,94	351,10	316,99
Itpa	500,31	486,24	506,73	373,74	485,52	417,18
Polr2j	501,24	534,69	624,96	409,70	521,11	493,19
Polr2i	467,70	570,57	752,21	406,58	536,13	568,33
Dut	189,13	201,85	234,22	159,50	203,22	174,47
Dctn4	805,90	678,23	870,45	675,54	691,91	657,29
Dguok	406,21	328,35	367,10	322,92	317,88	309,21
Guk1	1136,64	1023,62	1794,94	985,95	1194,83	1074,47
Srsf6	2952,47	3070,86	2589,94	2439,46	2320,08	2712,09
Znrd1	392,23	259,27	240,98	238,47	248,30	266,03
Rfc5	210,56	218,00	211,70	175,14	206,39	175,34
Ada	23,29	53,83	36,03	42,22	26,09	16,41

Ell	701,55	762,56	772,48	679,45	580,41	703,93
Ercc8	87,58	85,23	84,45	72,71	79,87	73,42

Table S.3. *DNA repair pathway genes are downregulated in DUSP3-KO mice fed HFD compared to WT mice fed HFD.* Normalized number of reads..

Gene	WT-CD-1	WT-CD-2	WT-CD-3	WT-HFD-1	WT-HFD-2	WT-HFD-3
Insig1	2558,31	740,81	1698,51	8512,70	7673,12	5759,81
Acaca	533,26	468,23	502,27	1265,21	1381,57	1035,98
Sdf2l1	118,13	209,24	112,11	1217,70	810,10	599,06
Hmgcr	849,40	525,92	867,75	2090,67	1668,65	1405,33
Sc5d	6763,66	3810,34	5170,64	14784,72	11663,54	10270,81
Cyb5b	5591,38	3342,11	3784,93	7731,02	11458,09	9443,16
Bhlhe40	1885,55	1992,82	1788,20	4643,46	2890,54	4782,39
Plk1	1,13	2,26	4,48	11,18	15,25	6,76
Slc9a3r1	1577,29	1603,76	1513,52	2527,63	2803,52	4009,91
Acly	1980,05	1576,61	1817,35	3130,42	4508,06	2895,11
Gbe1	1676,29	1409,23	1336,38	2444,71	2302,03	2999,83
Dhcr24	10034,11	9347,72	8974,63	17726,01	17732,59	13082,59
Pik3r3	19,13	18,10	28,03	42,86	44,86	29,28
Rrm2	70,88	96,14	79,60	146,27	148,03	112,61
Coro1a	100,13	190,01	147,99	810,56	758,07	219,58
Fgl2	79,88	119,89	77,36	417,39	234,15	167,78
Psat1	11,25	16,97	20,18	68,94	50,24	22,52
Itgb2	83,25	93,87	66,15	502,17	383,97	96,84
Sla	41,63	61,07	28,03	280,43	244,02	51,80
Psph	115,88	91,61	108,75	206,83	127,39	176,79
Dhcr7	479,26	512,34	614,38	1485,09	1063,09	671,13
Edem1	2783,32	2485,94	2058,39	3736,94	4136,65	3281,34
Serp1	5721,89	4864,43	4299,52	7430,09	6604,64	8592,98
Vldlr	86,63	49,76	54,94	105,28	122,01	88,96
Stard4	1986,80	601,69	1160,37	2386,01	2269,73	3817,35
Rdh11	511,89	417,34	516,84	1203,72	951,85	560,78
Calr	9076,72	11510,19	10566,63	16582,85	16557,36	13395,63
Idh1	10522,38	6936,42	7664,03	10928,53	11511,02	15532,90
Slc6a6	1089,03	909,32	914,84	1092,85	1764,65	1624,91
Tes	24,75	35,06	26,91	105,28	78,05	29,28
Xbp1	3691,21	4220,89	3706,45	6614,88	4255,07	6756,37
Fads1	10858,76	8785,61	9991,49	14431,62	16077,40	12346,14
Ldlr	2342,31	1074,45	1891,34	2679,49	3670,14	2464,95
Cxcr4	55,13	67,86	49,33	205,90	255,68	42,79
Ssr1	1730,29	1740,61	1831,92	2779,18	2546,04	2216,09
Mthfd2l	38,25	45,24	61,66	64,29	75,36	134,00
Mthfd2	43,88	39,59	14,57	88,51	78,05	39,41
Elovl6	1058,65	1131,00	983,23	1652,79	1811,30	1133,94
Mcm2	54,00	73,52	49,33	100,62	102,27	61,93

Bub1	2,25	0,00	1,12	13,04	8,97	0,00
Tmem97	1004,65	893,49	1099,83	1467,39	1296,35	1359,16
Dapp1	20,25	41,85	12,33	80,12	61,90	29,28
Acsl3	534,39	237,51	403,61	1269,87	741,03	472,95
Ifi30	290,26	245,43	256,74	819,87	444,08	260,12
Phgdh	2,25	4,52	2,24	14,91	81,64	4,50
Hk2	18,00	22,62	11,21	163,04	48,44	15,76
Hmgcs1	2773,19	1411,49	2056,15	7240,96	3783,18	2019,03
Stc1	0,00	1,13	1,12	0,93	8,07	2,25
Serpinh1	200,25	144,77	168,17	529,19	274,52	158,77
Pfkl	546,76	721,58	645,77	1262,42	750,89	749,96
Slc1a4	69,75	39,59	40,36	766,77	118,42	66,44
Slc7a11	0,00	0,00	0,00	9,32	0,90	0,00
Nampt	1735,92	956,83	1081,89	1690,99	1447,06	2899,61
Sqle	308,26	174,17	332,97	1136,64	508,67	215,08
Canx	7213,67	6141,33	6151,63	8599,34	7283,77	9028,76
Ccng1	1017,02	694,43	649,13	914,90	991,32	1181,24
Cfp	389,26	346,09	243,28	1686,33	435,11	331,06
Slc7a5	29,25	35,06	59,42	55,90	113,94	46,17
Tfrc	591,76	753,25	482,08	2980,42	767,94	628,34
Fkbp2	1234,15	1210,17	1186,15	1449,68	1483,85	1653,06
Aurka	9,00	4,52	12,33	19,57	33,19	4,50
Hspa5	11561,90	12559,76	12262,89	27084,67	18890,78	9591,80
Bcat1	0,00	0,00	0,00	0,00	7,18	0,00
Plod2	15,75	26,01	19,06	42,86	30,50	16,89
Gclc	6071,77	2740,41	4996,87	5558,36	7230,84	5736,16
Dhfr	1087,90	858,43	816,18	910,24	1131,28	1451,49
Nupr1	51,75	46,37	52,69	139,75	69,08	39,41
Slc1a5	57,38	144,77	145,75	210,56	383,97	76,57

Table S.4. *MTORC1 genes are upregulated in WT mice fed HFD compared to WT mice fed CD.* Normalized number of reads.

Gene	KO-CD-1	KO-CD-2	KO-CD-3	KO-HFD-1	KO-HFD-2	KO-HFD-3
Insig1	1570,60	1645,12	2140,78	4341,76	7674,28	4283,21
Acaca	447,26	460,73	602,44	1436,31	2086,80	1135,80
Sdf2l1	232,99	162,18	152,28	221,27	491,85	248,75
Hmgcr	722,89	579,91	761,39	1344,05	1292,89	2674,09
Sc5d	6251,19	5960,04	5976,63	7788,28	11276,96	8346,16
Cyb5b	5786,25	8386,56	6106,68	7450,51	10694,97	6441,65
Bhlhe40	927,80	1658,64	2578,72	3783,50	4795,14	5310,17
Plk1	2,08	8,60	5,56	15,64	3,95	6,91
Slc9a3r1	1851,43	1909,28	1615,04	1410,51	2280,54	2649,04
Acly	1680,85	1616,86	1951,83	2545,01	7852,99	2544,53
Gbe1	1883,68	1919,10	2026,30	5138,50	4625,92	3188,00
Dhcr24	11717,08	12205,11	20094,03	20407,00	15111,34	21624,18
Pik3r3	29,12	41,77	26,68	36,75	44,28	27,64
Rrm2	131,06	81,09	66,69	172,79	223,78	202,11
Coro1a	208,03	189,21	236,75	992,20	335,28	650,38
Fgl2	83,21	52,83	103,37	340,12	192,94	133,88
Psat1	7,28	7,37	22,23	71,15	21,35	27,64
Itgb2	72,81	206,41	165,62	659,90	408,82	361,04
Sla	24,96	56,52	86,70	271,31	163,69	196,93
Psph	127,94	108,12	121,16	127,45	137,59	114,01
Dhcr7	483,66	374,73	545,76	1244,75	1060,40	1190,21
Edem1	2502,56	2723,85	2786,58	2507,48	3075,25	3049,81
Serp1	5215,22	4974,68	5373,08	4896,12	9304,82	5638,39
Vldlr	121,70	88,46	104,48	164,98	94,89	47,50
Stard4	929,88	1181,93	791,40	1557,50	3225,49	1985,70
Rdh11	536,71	598,34	589,10	838,95	842,95	550,19
Calr	11685,87	9193,77	9082,22	9603,02	14504,04	12598,27
Idh1	13656,92	9638,53	10826,19	9532,65	12864,80	7940,21
Slc6a6	838,35	1960,88	1410,52	1506,68	1475,55	1301,63
Tes	20,80	11,06	14,45	128,23	59,31	88,96
Xbp1	3338,82	3866,47	3635,78	3426,97	5114,61	5663,44
Fads1	8101,58	7081,77	7397,16	11091,71	12380,86	14241,07
Ldlr	1723,50	2112,00	2045,19	3037,59	4198,12	3701,06
Cxcr4	56,17	38,09	57,80	216,58	64,05	161,52
Ssr1	1760,94	1609,49	1710,63	1921,85	2627,68	1949,42
Mthfd2l	83,21	28,26	96,70	55,51	66,42	62,19
Mthfd2	28,08	35,63	63,36	65,68	51,40	59,60
Elovl6	347,40	387,02	629,12	1742,80	3854,93	1771,50
Mcm2	45,77	45,46	77,81	154,81	93,31	114,01

Bub1	1,04	1,23	0,00	10,95	3,95	2,59
Tmem97	1180,55	904,26	1343,83	1595,03	1688,26	1806,05
Dapp1	11,44	27,03	35,57	75,06	38,75	67,37
Acsl3	314,12	310,84	453,50	433,16	673,72	607,20
Ifi30	248,59	325,58	454,61	1080,55	650,79	682,34
Phgdh	1,04	0,00	1,11	37,53	10,28	12,96
Hk2	18,72	34,40	121,16	218,14	213,50	264,30
Hmgcs1	3653,98	4263,31	5492,01	6676,45	2948,73	3445,39
Stc1	0,00	1,23	0,00	12,51	3,95	7,77
Serpinh1	136,26	137,61	121,16	500,40	310,77	335,99
Pfkl	931,96	960,78	1040,38	1071,95	780,48	1188,48
Slc1a4	92,57	103,20	393,48	342,46	121,78	154,61
Slc7a11	4,16	11,06	2,22	57,08	4,74	13,82
Nampt	1900,32	1464,52	2155,23	1662,27	2157,18	2243,95
Sqle	247,55	181,84	384,59	767,02	90,15	606,33
Canx	8191,03	6721,78	5998,87	6250,33	7679,82	6572,94
Ccng1	1075,50	1277,77	1155,98	1143,10	1254,14	947,50
Cfp	301,64	498,82	625,78	1094,63	1043,80	589,06
Slc7a5	49,93	66,35	68,91	91,48	49,03	39,73
Tfrc	965,24	540,59	632,45	815,50	909,37	971,69
Fkbp2	1833,75	1218,79	1390,51	1096,97	1378,29	1337,91
Aurka	13,52	15,97	13,34	40,66	22,14	14,68
Hspa5	13689,17	10934,72	9257,84	8803,94	12561,15	11473,70
Bcat1	0,00	0,00	0,00	6,26	0,79	1,73
Plod2	16,64	20,89	15,56	56,30	26,89	39,73
Gclc	5032,15	12235,83	5255,26	15353,72	5484,68	2743,19
Dhfr	1046,37	885,84	1143,75	953,89	1182,97	1090,02
Nupr1	47,85	33,17	48,91	97,73	77,49	65,64
Slc1a5	63,45	60,20	93,37	228,31	95,68	164,97

Table S.5. *MTORC1 genes in DUSP3-KO mice fed HFD compared to DUSP3-KO mice fed CD.* Normalized number of reads.

Gene	WT-CD-1	WT-CD-2	WT-CD-3	WT-HFD-1	WT-HFD-2	WT-HFD-3
Cd14	68,63	72,38	49,33	250,62	65,49	43,92
Cd44	281,26	151,55	176,02	502,17	379,48	149,77
Pik3r5	29,25	37,32	15,70	97,83	74,46	19,14
Csf2rb	108,00	136,85	136,78	340,99	357,06	115,98
Il2rg	33,75	27,14	28,03	148,14	181,22	29,28
Tlr2	52,88	61,07	38,12	226,40	69,08	48,42
Csf2ra	25,88	35,06	37,00	137,89	80,74	38,29
Il10rb	182,25	140,24	168,17	377,33	214,41	199,31
A2m	0,00	1,13	1,12	13,04	3,59	0,00
Tnf	7,88	6,79	2,24	37,27	14,35	1,13
Csf3r	43,88	82,56	51,57	190,99	55,62	37,16
Bak1	122,63	206,97	172,65	308,38	206,34	219,58
Ltb	19,13	26,01	21,30	118,32	143,54	19,14
Tgfb1	69,75	78,04	96,42	232,92	145,33	90,08
Il7	6,75	5,66	12,33	23,29	25,12	13,51
Tnfrsf1b	761,64	1394,52	1099,83	758,38	697,07	609,20
Lepr	374,63	1282,55	1483,25	138,82	71,77	90,08
Itga4	16,88	23,75	20,18	153,73	260,17	37,16
Tnfrsf21	144,00	116,49	128,93	272,05	112,14	99,09
Map3k8	47,25	93,87	48,21	140,68	78,95	47,29
Il9r	0,00	5,66	0,00	13,98	32,30	5,63
Ifngr1	374,63	441,09	398,00	1038,82	568,78	480,83
Ccr1	4,50	21,49	12,33	150,93	14,35	7,88
Ebi3	7,88	11,31	12,33	55,90	9,87	7,88
Csf1	190,13	168,52	172,65	321,43	226,97	183,55
Cd9	895,52	1128,74	1099,83	1268,01	793,96	708,29
Cd38	394,88	329,12	298,22	508,69	452,15	284,89
Acvrl1	48,38	50,90	43,72	150,00	99,58	47,29
Il1r2	1,13	6,79	1,12	22,36	4,49	1,13
Cxcl9	139,50	74,65	94,17	858,07	165,97	141,88
Cbl	165,38	216,02	221,98	266,46	382,18	162,15
Il1b	221,63	169,65	127,81	370,81	114,83	105,85
Osmr	95,63	174,17	118,84	244,10	133,67	78,82
Il2ra	2,25	2,26	1,12	7,45	29,61	0,00
Acvr1b	182,25	285,01	232,07	217,08	186,60	271,38
Socs1	4,50	6,79	11,21	26,09	17,94	9,01
Il17rb	410,63	432,04	605,41	264,60	208,13	159,90
Ifngr2	705,39	659,37	646,89	781,67	452,15	586,68
Cxcl11	83,25	98,40	112,11	129,50	126,49	124,99

Il3ra	14,63	53,16	44,85	54,04	47,55	39,41
Ccl7	7,88	7,92	6,73	62,42	8,07	5,63
Dntt	193,50	214,89	159,20	189,13	156,10	123,87
Pf4	11,25	12,44	21,30	572,98	16,15	22,52

Table S.6. *IL6-JAK-STAT5 genes in WT mice fed HFD compared to WT mice fed CD.* Normalized number of reads.

Gene	KO-CD-1	KO-CD-2	KO-CD-3	KO-HFD-1	KO-HFD-2	KO-HFD-3
Cd14	56,17	50,37	64,47	286,17	143,92	235,80
Cd44	175,78	255,55	241,20	727,93	499,76	489,73
Pik3r5	20,80	39,32	31,12	136,05	77,49	100,19
Csf2rb	44,73	79,86	133,38	395,63	267,28	265,16
Il2rg	34,32	50,37	44,46	168,10	96,47	106,24
Tlr2	82,17	95,83	98,93	236,13	168,43	154,61
Csf2ra	22,88	67,57	72,25	182,18	110,71	159,79
Il10rb	130,02	173,24	213,41	399,54	298,91	291,94
A2m	3,12	1,23	3,33	15,64	10,28	6,05
Tnf	6,24	11,06	7,78	17,20	15,02	14,68
Csf3r	46,81	81,09	58,91	154,81	91,73	172,74
Bak1	205,95	211,32	206,74	366,70	355,05	297,98
Ltb	15,60	14,74	14,45	128,23	23,72	87,24
Tgfb1	121,70	136,38	118,93	304,93	204,81	182,25
Il7	5,20	6,14	16,67	24,24	17,40	23,32
Tnfrsf1b	445,18	619,22	674,69	995,33	763,87	994,15
Lepr	45,77	40,54	53,35	168,10	97,26	360,17
Itga4	32,24	44,23	37,79	279,13	87,77	114,88
Tnfrsf21	105,05	149,89	133,38	305,71	192,15	189,16
Map3k8	44,73	60,20	63,36	101,64	69,59	86,37
Il9r	1,04	3,69	0,00	88,35	12,65	31,09
Ifngr1	458,70	457,05	486,85	787,35	547,99	730,71
Ccr1	6,24	1,23	12,23	64,11	11,07	35,41
Ebi3	5,20	22,12	5,56	27,37	28,47	19,00
Csf1	198,67	251,87	210,08	440,98	274,39	310,08
Cd9	548,15	523,39	900,33	1478,53	995,56	894,82
Cd38	290,20	299,78	304,56	722,45	500,55	341,17
Acvrl1	38,48	51,60	72,25	171,23	75,12	92,42
Il1r2	1,04	0,00	5,56	14,86	2,37	25,05
Cxcl9	96,73	152,35	72,25	534,02	225,37	146,83
Cbl	158,10	296,10	203,41	400,32	272,81	304,03
Il1b	84,25	62,66	122,27	272,09	165,27	98,46
Osmr	71,77	77,40	137,83	243,16	112,29	159,79
Il2ra	3,12	2,46	0,00	21,89	0,79	9,50
Acvr1b	209,07	296,10	301,22	379,21	323,42	354,13
Socs1	7,28	3,69	5,56	20,33	7,91	6,05
Il17rb	221,55	178,15	226,75	261,93	230,90	303,17
Ifngr2	591,83	573,77	572,43	888,21	590,69	730,71
Cxcl11	48,89	78,63	51,13	89,92	90,15	58,73

Il3ra	48,89	41,77	37,79	86,01	39,54	57,01
Ccl7	7,28	7,37	7,78	63,33	7,91	6,05
Dntt	93,61	22,12	120,04	91,48	248,30	103,65
Pf4	14,56	9,83	38,90	49,26	18,98	42,32

Table S.7. *IL6-JAK-STAT5 genes are upregulated in DUSP3-KO mice fed HFD compared to DUSP3-KO mice fed CD.* Normalized number of reads.

References

REFERENCES

[1] Li X, Wilmanns M, Thornton J, Kohn M. Elucidating human phosphatase-substrate networks. Sci Signal 2013;6:rs10. https://doi.org/10.1126/scisignal.2003203.

[2] Alonso A, Pulido R. The extended human PTPome: A growing tyrosine phosphatase family. FEBS J 2016;283:1404–29. https://doi.org/10.1111/febs.13600.

[3] Alonso A, Sasin J, Bottini N, Friedberg I, Friedberg I, Osterman A, et al. Protein tyrosine phosphatases in the human genome. Cell 2004;117:699–711. https://doi.org/10.1016/j.cell.2004.05.018.

[4] Denu JM, Dixon JE. Protein tyrosine phosphatases: mechanisms of catalysis and regulation. Curr Opin Chem Biol 1998;2:633–41. https://doi.org/10.1016/s1367-5931(98)80095-1.

[5] Maehama T, Taylor GS, Dixon JE. PTEN and myotubularin: novel phosphoinositide phosphatases. Annu Rev Biochem 2001;70:247–79. https://doi.org/10.1146/annurev.biochem.70.1.247.

[6] Deshpande T, Takagi T, Hao L, Buratowski S, Charbonneau H. Human PIR1 of the protein-tyrosine phosphatase superfamily has RNA 5'-triphosphatase and diphosphatase activities. J Biol Chem 1999;274:16590–4. https://doi.org/10.1074/jbc.274.23.16590.

[7] Tagliabracci VS, Turnbull J, Wang W, Girard J-M, Zhao X, Skurat A V, et al. Laforin is a glycogen phosphatase, deficiency of which leads to elevated phosphorylation of glycogen in vivo. Proc Natl Acad Sci U S A 2007;104:19262–6. https://doi.org/10.1073/pnas.0707952104.

[8] Camps M, Nichols A, Arkinstall S. Dual specificity phosphatases: a gene family for control of MAP kinase function. FASEB J Off Publ Fed Am Soc Exp Biol 2000;14:6–16.

[9] Ishibashi T, Bottaro DP, Chan A, Miki T, Aaronson SA. Expression cloning of a human dual-specificity phosphatase. Proc Natl Acad Sci U S A 1992;89:12170–4. https://doi.org/10.1073/pnas.89.24.12170.

[10] Singh P, Dejager L, Amand M, Theatre E, Vandereyken M, Zurashvili T, et al. DUSP3 Genetic Deletion Confers M2-like Macrophage-Dependent Tolerance to Septic Shock. J Immunol 2015;194:4951–62. https://doi.org/10.4049/jimmunol.1402431.

[11] Denu JM, Zhou G, Wu L, Zhao R, Yuvaniyama J, Saper MA, et al. The purification and characterization of a human dual-specific protein tyrosine phosphatase. J Biol Chem 1995;270:3796–803. https://doi.org/10.1074/jbc.270.8.3796.

[12] Todd JL, Tanner KG, Denu JM. Extracellular regulated kinases (ERK) 1 and ERK2 are authentic substrates for the dual-specificity protein-tyrosine

phosphatase VHR. A novel role in down-regulating the ERK pathway. J Biol Chem 1999;274:13271–80. https://doi.org/10.1074/jbc.274.19.13271.

[13] Alonso A, Saxena M, Williams S, Mustelin T. Inhibitory role for dual specificity phosphatase VHR in T cell antigen receptor and CD28-induced Erk and Jnk activation. J Biol Chem 2001;276:4766–71. https://doi.org/10.1074/jbc.M006497200.

[14] Wagner KW, Alam H, Dhar SS, Giri U, Li N, Wei Y, et al. KDM2A promotes lung tumorigenesis by epigenetically enhancing ERK1/2 signaling. J Clin Invest 2013;123:5231–46. https://doi.org/10.1172/JCI68642.

[15] Todd JL, Rigas JD, Rafty LA, Denu JM. Dual-specificity protein tyrosine phosphatase VHR down-regulates c-Jun N-terminal kinase (JNK). Oncogene 2002;21:2573–83. https://doi.org/10.1038/sj.onc.1205344.

[16] Schumacher MA, Todd JL, Rice AE, Tanner KG, Denu JM. Structural basis for the recognition of a bisphosphorylated MAP kinase peptide by human VHR protein Phosphatase. Biochemistry 2002;41:3009–17. https://doi.org/10.1021/bi015799l.

[17] Hoyt R, Zhu W, Cerignoli F, Alonso A, Mustelin T, David M. Cutting edge: selective tyrosine dephosphorylation of interferon-activated nuclear STAT5 by the VHR phosphatase. J Immunol 2007;179:3402–6. https://doi.org/10.4049/jimmunol.179.6.3402.

[18] Huang CF, Liu H, Huang S, Chen Y. Vaccinia H1-related Phosphatase Is a Phosphatase of ErbB Receptors and Is Down-regulated in Non-small Cell Lung 2011;286:10177–84. https://doi.org/10.1074/jbc.M110.163295.

[19] Panico K, Forti FL. Proteomic, cellular, and network analyses reveal new DUSP3 interactions with nucleolar proteins in HeLa cells. J Proteome Res 2013;12:5851–66. https://doi.org/10.1021/pr400867j.

[20] Amand M, Erpicum C, Bajou K, Cerignoli F, Blacher S, Martin M, et al. DUSP3/VHR is a pro-angiogenic atypical dual-specificity phosphatase. Mol Cancer 2014;13:108. https://doi.org/10.1186/1476-4598-13-108.

[21] Chen Y-R, Chou H-C, Yang C-H, Chen H-Y, Liu Y-W, Lin T-Y, et al. Deficiency in VHR/DUSP3, a suppressor of focal adhesion kinase, reveals its role in regulating cell adhesion and migration. Oncogene 2017;36:6509–17. https://doi.org/10.1038/onc.2017.255.

[22] Pavic K, Duan G, Köhn M. VHR/DUSP3 phosphatase: Structure, function and regulation. FEBS J 2015;282:1871–90. https://doi.org/10.1111/febs.13263.

[23] Denu JM, Tanner KG. Specific and reversible inactivation of protein tyrosine phosphatases by hydrogen peroxide: evidence for a sulfenic acid intermediate and implications for redox regulation. Biochemistry 1998;37:5633–42. https://doi.org/10.1021/bi973035t.

[24] Wentworth CC, Alam A, Jones RM, Nusrat A, Neish AS. Enteric commensal bacteria induce extracellular signal-regulated kinase pathway signaling via

formyl peptide receptor-dependent redox modulation of dual specific phosphatase 3. J Biol Chem 2011;286:38448–55. https://doi.org/10.1074/jbc.M111.268938.

[25] Pavic K, Rios P, Dzeyk K, Koehler C, Lemke EA, Kohn M. Unnatural amino acid mutagenesis reveals dimerization as a negative regulatory mechanism of VHR's phosphatase activity. ACS Chem Biol 2014;9:1451–9. https://doi.org/10.1021/cb500240n.

[26] Alonso A, Rahmouni S, Williams S, van Stipdonk M, Jaroszewski L, Godzik A, et al. Tyrosine phosphorylation of VHR phosphatase by ZAP-70. Nat Immunol 2003;4:44–8. https://doi.org/10.1038/ni856.

[27] Kang T-H, Kim K-T. Negative regulation of ERK activity by VRK3-mediated activation of VHR phosphatase. Nat Cell Biol 2006;8:863–9. https://doi.org/10.1038/ncb1447.

[28] Rahmouni S, Cerignoli F, Alonso A, Tsutji T, Henkens R, Zhu C, et al. Loss of the VHR dual-specific phosphatase causescell-cycle arrest and senescence. Nat Cell Biol 2006;8:524–31. https://doi.org/10.1038/ncb1398.

[29] Tambe MB, Narvi E, Kallio M. Reduced levels of Dusp3/Vhr phosphatase impair normal spindle bipolarity in an Erk1/2 activity-dependent manner. FEBS Lett 2016;590:2757–67. https://doi.org/10.1002/1873-3468.12310.

[30] Musumeci L, Kuijpers MJ, Gilio K, Hego A, Théâtre E, Maurissen L, et al. DUSP3 Phosphatase Deficiency or Inhibition Limit Platelet Activation and Arterial Thrombosis. Circulation 2015:656–68. https://doi.org/10.1161/CIRCULATIONAHA.114.010186.

[31] Torres TEP, Russo LC, Santos A, Marques GR, Magalhaes YT, Tabassum S, et al. Loss of DUSP3 activity radiosensitizes human tumor cell lines via attenuation of DNA repair pathways. Biochim Biophys Acta Gen Subj 2017;1861:1879–94. https://doi.org/10.1016/j.bbagen.2017.04.004.

[32] Hao L, ElShamy WM. BRCA1-IRIS activates cyclin D1 expression in breast cancer cells by downregulating the JNK phosphatase DUSP3/VHR. Int J Cancer 2007;121:39–46. https://doi.org/10.1002/ijc.22597.

[33] Vandereyken M, Jacques S, Van Overmeire E, Amand M, Rocks N, Delierneux C, et al. Dusp3 deletion in mice promotes experimental lung tumour metastasis in a macrophage dependent manner. PLoS One 2017;12:e0185786. https://doi.org/10.1371/journal.pone.0185786.

[34] Arnoldussen YJ, Lorenzo PI, Pretorius ME, Waehre H, Risberg B, Maelandsmo GM, et al. The mitogen-activated protein kinase phosphatase vaccinia H1-related protein inhibits apoptosis in prostate cancer cells and is overexpressed in prostate cancer. Cancer Res 2008;68:9255–64. https://doi.org/10.1158/0008-5472.CAN-08-1224.

[35] Henkens R, Delvenne P, Arafa M, Moutschen M, Zeddou M, Tautz L, et al. Cervix carcinoma is associated with an up-regulation and nuclear localization

of the dual-specificity protein phosphatase VHR. BMC Cancer 2008;8:147. https://doi.org/10.1186/1471-2407-8-147.

[36] Li S, Hsu DD, Wang H, Feng G-S. Dual faces of SH2-containing protein-tyrosine phosphatase Shp2/PTPN11 in tumorigenesis. Front Med 2012;6:275–9. https://doi.org/10.1007/s11684-012-0216-4.

[37] Vandereyken MM, Singh P, Wathieu CP, Jacques S, Zurashvilli T, Dejager L, et al. Dual-Specificity Phosphatase 3 Deletion Protects Female, but Not Male, Mice from Endotoxemia-Induced and Polymicrobial-Induced Septic Shock. J Immunol 2017;199:2515–27. https://doi.org/10.4049/jimmunol.1602092.

[38] Smith KB, Smith MS. Obesity Statistics. Prim Care - Clin Off Pract 2016;43:121–35. https://doi.org/10.1016/j.pop.2015.10.001.

[39] Global, regional, and national incidence, prevalence, and years lived with disability for 328 diseases and injuries for 195 countries, 1990-2016: a systematic analysis for the Global Burden of Disease Study 2016. Lancet (London, England) 2017;390:1211–59. https://doi.org/10.1016/S0140-6736(17)32154-2.

[40] WHO. Obesity and overweight. World Heal Organ - Obes Overweight Fact Sheet 2016. https://www.who.int/en/news-room/fact-sheets/detail/obesity-and-overweight (accessed July 14, 2020).

[41] Whitlock G, Lewington S, Sherliker P, Clarke R, Emberson J, Halsey J, et al. Body-mass index and cause-specific mortality in 900 000 adults: collaborative analyses of 57 prospective studies. Lancet (London, England) 2009;373:1083–96. https://doi.org/10.1016/S0140-6736(09)60318-4.

[42] Calle EE, Rodriguez C, Walker-Thurmond K, Thun MJ. Overweight, obesity, and mortality from cancer in a prospectively studied cohort of U.S. adults. N Engl J Med 2003;348:1625–38. https://doi.org/10.1056/NEJMoa021423.

[43] Kaur J. A comprehensive review on metabolic syndrome. Cardiol Res Pract 2014;2014:943162. https://doi.org/10.1155/2014/943162.

[44] Alberti KGMM, Eckel RH, Grundy SM, Zimmet PZ, Cleeman JI, Donato KA, et al. Harmonizing the metabolic syndrome: a joint interim statement of the International Diabetes Federation Task Force on Epidemiology and Prevention; National Heart, Lung, and Blood Institute; American Heart Association; World Heart Federation; International . Circulation 2009;120:1640–5. https://doi.org/10.1161/CIRCULATIONAHA.109.192644.

[45] Engin A. The Definition and Prevalence of Obesity and Metabolic Syndrome. Adv Exp Med Biol 2017;960:1–17. https://doi.org/10.1007/978-3-319-48382-5_1.

[46] Saklayen MG. The Global Epidemic of the Metabolic Syndrome. Curr Hypertens Rep 2018;20:12. https://doi.org/10.1007/s11906-018-0812-z.

[47] Esposito K, Chiodini P, Colao A, Lenzi A, Giugliano D. Metabolic syndrome

and risk of cancer: a systematic review and meta-analysis. Diabetes Care 2012;35:2402–11. https://doi.org/10.2337/dc12-0336.

[48] Castro-Martínez MG, Banderas-Lares DZ, Ramírez-Martínez JC, Escobedo-de la Peña J. Prevalence of nonalcoholic fatty liver disease in subjects with metabolic syndrome. Cir Cir 2012;80:128–33.

[49] McCracken E, Monaghan M, Sreenivasan S. Pathophysiology of the metabolic syndrome. Clin Dermatol 2018;36:14–20. https://doi.org/10.1016/j.clindermatol.2017.09.004.

[50] Yaribeygi H, Farrokhi FR, Butler AE, Sahebkar A. Insulin resistance: Review of the underlying molecular mechanisms. J Cell Physiol 2019;234:8152–61. https://doi.org/10.1002/jcp.27603.

[51] Poloz Y, Stambolic V. Obesity and cancer, a case for insulin signaling. Cell Death Dis 2015;6:e2037. https://doi.org/10.1038/cddis.2015.381.

[52] Vigneri R, Goldfine ID, Frittitta L. Insulin, insulin receptors, and cancer. J Endocrinol Invest 2016;39:1365–76. https://doi.org/10.1007/s40618-016-0508-7.

[53] Arcidiacono B, Iiritano S, Nocera A, Possidente K, Nevolo MT, Ventura V, et al. Insulin resistance and cancer risk: an overview of the pathogenetic mechanisms. Exp Diabetes Res 2012;2012:789174. https://doi.org/10.1155/2012/789174.

[54] Leavens KF, Birnbaum MJ. Insulin signaling to hepatic lipid metabolism in health and disease. Crit Rev Biochem Mol Biol 2011;46:200–15. https://doi.org/10.3109/10409238.2011.562481.

[55] Wilcox G. Insulin and insulin resistance. Clin Biochem Rev 2005;26:19–39.

[56] Celton-Morizur S, Merlen G, Couton D, Margall-Ducos G, Desdouets C. The insulin/Akt pathway controls a specific cell division program that leads to generation of binucleated tetraploid liver cells in rodents. J Clin Invest 2009;119:1880–7. https://doi.org/10.1172/jci38677.

[57] Avruch J. Insulin signal transduction through protein kinase cascades. Mol Cell Biochem 1998;182:31–48.

[58] Taniguchi CM, Emanuelli B, Kahn CR. Critical nodes in signalling pathways: insights into insulin action. Nat Rev Mol Cell Biol 2006;7:85–96. https://doi.org/10.1038/nrm1837.

[59] Cross DA, Alessi DR, Cohen P, Andjelkovich M, Hemmings BA. Inhibition of glycogen synthase kinase-3 by insulin mediated by protein kinase B. Nature 1995;378:785–9. https://doi.org/10.1038/378785a0.

[60] Porstmann T, Santos CR, Griffiths B, Cully M, Wu M, Leevers S, et al. SREBP activity is regulated by mTORC1 and contributes to Akt-dependent cell growth. Cell Metab 2008;8:224–36. https://doi.org/10.1016/j.cmet.2008.07.007.

[61] Price DJ, Grove JR, Calvo V, Avruch J, Bierer BE. Rapamycin-induced inhibition of the 70-kilodalton S6 protein kinase. Science 1992;257:973–7. https://doi.org/10.1126/science.1380182.

[62] Skolnik EY, Batzer A, Li N, Lee CH, Lowenstein E, Mohammadi M, et al. The function of GRB2 in linking the insulin receptor to Ras signaling pathways. Science 1993;260:1953–5. https://doi.org/10.1126/science.8316835.

[63] Chettouh H, Lequoy M, Fartoux L, Vigouroux C, Desbois-Mouthon C. Hyperinsulinaemia and insulin signalling in the pathogenesis and the clinical course of hepatocellular carcinoma. Liver Int 2015;35:2203–17. https://doi.org/10.1111/liv.12903.

[64] Unger RH. Lipid overload and overflow: metabolic trauma and the metabolic syndrome. Trends Endocrinol Metab 2003;14:398–403. https://doi.org/10.1016/j.tem.2003.09.008.

[65] Blüher M, Mantzoros CS. From leptin to other adipokines in health and disease: facts and expectations at the beginning of the 21st century. Metabolism 2015;64:131–45. https://doi.org/10.1016/j.metabol.2014.10.016.

[66] Yadav A, Kataria MA, Saini V, Yadav A. Role of leptin and adiponectin in insulin resistance. Clin Chim Acta 2013;417:80–4. https://doi.org/10.1016/j.cca.2012.12.007.

[67] Bulló M, García-Lorda P, Peinado-Onsurbe J, Hernández M, Del Castillo D, Argilés JM, et al. TNFalpha expression of subcutaneous adipose tissue in obese and morbid obese females: relationship to adipocyte LPL activity and leptin synthesis. Int J Obes Relat Metab Disord J Int Assoc Study Obes 2002;26:652–8. https://doi.org/10.1038/sj.ijo.0801977.

[68] Hirashima Y, Tsuruzoe K, Kodama S, Igata M, Toyonaga T, Ueki K, et al. Insulin down-regulates insulin receptor substrate-2 expression through the phosphatidylinositol 3-kinase/Akt pathway. J Endocrinol 2003;179:253–66. https://doi.org/10.1677/joe.0.1790253.

[69] Rui L, Yuan M, Frantz D, Shoelson S, White MF. SOCS-1 and SOCS-3 block insulin signaling by ubiquitin-mediated degradation of IRS1 and IRS2. J Biol Chem 2002;277:42394–8. https://doi.org/10.1074/jbc.C200444200.

[70] Shimomura I, Matsuda M, Hammer RE, Bashmakov Y, Brown MS, Goldstein JL. Decreased IRS-2 and increased SREBP-1c lead to mixed insulin resistance and sensitivity in livers of lipodystrophic and ob/ob mice. Mol Cell 2000;6:77–86.

[71] Taniguchi CM, Ueki K, Kahn CR. Complementary roles of IRS-1 and IRS-2 in the hepatic regulation of metabolism. J Clin Invest 2016;126:4387. https://doi.org/10.1172/JCI90689.

[72] Cho H, Mu J, Kim JK, Thorvaldsen JL, Chu Q, Crenshaw EB 3rd, et al. Insulin resistance and a diabetes mellitus-like syndrome in mice lacking the protein

kinase Akt2 (PKB beta). Science 2001;292:1728–31. https://doi.org/10.1126/science.292.5522.1728.

[73] George S, Rochford JJ, Wolfrum C, Gray SL, Schinner S, Wilson JC, et al. A family with severe insulin resistance and diabetes due to a mutation in AKT2. Science 2004;304:1325–8. https://doi.org/10.1126/science.1096706.

[74] Coughlan KA, Valentine RJ, Ruderman NB, Saha AK. Nutrient Excess in AMPK Downregulation and Insulin Resistance. J Endocrinol Diabetes Obes 2013;1:1008.

[75] Lee Y, Kim E-K. AMP-activated protein kinase as a key molecular link between metabolism and clockwork. Exp Mol Med 2013;45:e33–e33. https://doi.org/10.1038/emm.2013.65.

[76] Jeon S-M. Regulation and function of AMPK in physiology and diseases. Exp Mol Med 2016;48:e245. https://doi.org/10.1038/emm.2016.81.

[77] Valentine RJ, Coughlan KA, Ruderman NB, Saha AK. Insulin inhibits AMPK activity and phosphorylates AMPK $Ser^{485/491}$ through Akt in hepatocytes, myotubes and incubated rat skeletal muscle. Arch Biochem Biophys 2014;562:62–9. https://doi.org/10.1016/j.abb.2014.08.013.

[78] Kharroubi AT. Diabetes mellitus: The epidemic of the century. World J Diabetes 2015;6:850. https://doi.org/10.4239/wjd.v6.i6.850.

[79] Kahn SE, Hull RL, Utzschneider KM. Mechanisms linking obesity to insulin resistance and type 2 diabetes. Nature 2006;444:840–6. https://doi.org/10.1038/nature05482.

[80] Younossi Z, Anstee QM, Marietti M, Hardy T, Henry L, Eslam M, et al. Global burden of NAFLD and NASH: Trends, predictions, risk factors and prevention. Nat Rev Gastroenterol Hepatol 2018;15:11–20. https://doi.org/10.1038/nrgastro.2017.109.

[81] Brunt EM, Wong VW-S, Nobili V, Day CP, Sookoian S, Maher JJ, et al. Nonalcoholic fatty liver disease. Nat Rev Dis Prim 2015;1:15080. https://doi.org/10.1038/nrdp.2015.80.

[82] Younossi ZM, Koenig AB, Abdelatif D, Fazel Y, Henry L, Wymer M. Global epidemiology of nonalcoholic fatty liver disease-Meta-analytic assessment of prevalence, incidence, and outcomes. Hepatology 2016;64:73–84. https://doi.org/10.1002/hep.28431.

[83] Yki-Jarvinen H. Non-alcoholic fatty liver disease as a cause and a consequence of metabolic syndrome. Lancet Diabetes Endocrinol 2014;2:901–10. https://doi.org/10.1016/S2213-8587(14)70032-4.

[84] Sayiner M, Younossi ZM. Identifying patients at risk from nonalcoholic fatty liver-related hepatocellular carcinomas. Hepatic Oncol 2016;3:101–3. https://doi.org/10.2217/hep-2016-0002.

[85] Asrani SK, Devarbhavi H, Eaton J, Kamath PS. Burden of liver diseases in the

world. J Hepatol 2019;70:151–71. https://doi.org/10.1016/j.jhep.2018.09.014.

[86] Targher G, Bertolini L, Padovani R, Rodella S, Tessari R, Zenari L, et al. Prevalence of nonalcoholic fatty liver disease and its association with cardiovascular disease among type 2 diabetic patients. Diabetes Care 2007;30:1212–8. https://doi.org/10.2337/dc06-2247.

[87] Adams LA, Lymp JF, St Sauver J, Sanderson SO, Lindor KD, Feldstein A, et al. The natural history of nonalcoholic fatty liver disease: a population-based cohort study. Gastroenterology 2005;129:113–21. https://doi.org/10.1053/j.gastro.2005.04.014.

[88] El-Serag HB, Rudolph KL. Hepatocellular carcinoma: epidemiology and molecular carcinogenesis. Gastroenterology 2007;132:2557–76. https://doi.org/10.1053/j.gastro.2007.04.061.

[89] Hester D, Golabi P, Paik J, Younossi I, Mishra A, Younossi ZM. Among Medicare Patients With Hepatocellular Carcinoma, Non-alcoholic Fatty Liver Disease is the Most Common Etiology and Cause of Mortality. J Clin Gastroenterol 2020;54:459–67. https://doi.org/10.1097/MCG.0000000000001172.

[90] Bataller R, Brenner DA. Liver fibrosis. J Clin Invest 2005;115:209–18. https://doi.org/10.1172/JCI24282.

[91] Mittal S, El-Serag HB, Sada YH, Kanwal F, Duan Z, Temple S, et al. Hepatocellular Carcinoma in the Absence of Cirrhosis in United States Veterans is Associated With Nonalcoholic Fatty Liver Disease. Clin Gastroenterol Hepatol 2016;14:124-31.e1. https://doi.org/10.1016/j.cgh.2015.07.019.

[92] Yasui K, Hashimoto E, Komorizono Y, Koike K, Arii S, Imai Y, et al. Characteristics of patients with nonalcoholic steatohepatitis who develop hepatocellular carcinoma. Clin Gastroenterol Hepatol 2011;9:428–33; quiz e50. https://doi.org/10.1016/j.cgh.2011.01.023.

[93] Lequoy M, Gigante E, Couty JP, Desbois-Mouthon C. Hepatocellular carcinoma in the context of non-alcoholic steatohepatitis (NASH): Recent advances in the pathogenic mechanisms. Horm Mol Biol Clin Investig 2020:1–18. https://doi.org/10.1515/hmbci-2019-0044.

[94] Nair S, Mason A, Eason J, Loss G, Perrillo RP. Is obesity an independent risk factor for hepatocellular carcinoma in cirrhosis? Hepatology 2002;36:150–5. https://doi.org/10.1053/jhep.2002.33713.

[95] Lagiou P, Kuper H, Stuver SO, Tzonou A, Trichopoulos D, Adami HO. Role of diabetes mellitus in the etiology of hepatocellular carcinoma. J Natl Cancer Inst 2000;92:1096–9. https://doi.org/10.1093/jnci/92.13.1096.

[96] Gerber L, Otgonsuren M, Mishra A, Escheik C, Birerdinc A, Stepanova M, et al. Non-alcoholic fatty liver disease (NAFLD) is associated with low level of physical activity: a population-based study. Aliment Pharmacol Ther

2012;36:772–81. https://doi.org/10.1111/apt.12038.

[97] Jensen T, Abdelmalek MF, Sullivan S, Nadeau KJ, Green M, Roncal C, et al. Fructose and sugar: A major mediator of non-alcoholic fatty liver disease. J Hepatol 2018;68:1063–75. https://doi.org/10.1016/j.jhep.2018.01.019.

[98] Park EJ, Lee JH, Yu GY, He G, Ali SR, Holzer RG, et al. Dietary and Genetic Obesity Promote Liver Inflammation and Tumorigenesis by Enhancing IL-6 and TNF Expression. Cell 2010;140:197–208. https://doi.org/10.1016/j.cell.2009.12.052.

[99] Day CP, James OFW. Steatohepatitis: A tale of two “hits”? Gastroenterology 1998;114:842–5. https://doi.org/10.1016/S0016-5085(98)70599-2.

[100] Friedman SL, Neuschwander-Tetri BA, Rinella M, Sanyal AJ. Mechanisms of NAFLD development and therapeutic strategies. Nat Med 2018;24:908–22. https://doi.org/10.1038/s41591-018-0104-9.

[101] Lomonaco R, Ortiz-Lopez C, Orsak B, Webb A, Hardies J, Darland C, et al. Effect of adipose tissue insulin resistance on metabolic parameters and liver histology in obese patients with nonalcoholic fatty liver disease. Hepatology 2012;55:1389–97. https://doi.org/10.1002/hep.25539.

[102] Mitsuyoshi H, Yasui K, Harano Y, Endo M, Tsuji K, Minami M, et al. Analysis of hepatic genes involved in the metabolism of fatty acids and iron in nonalcoholic fatty liver disease. Hepatol Res 2009;39:366–73. https://doi.org/10.1111/j.1872-034X.2008.00464.x.

[103] He J, Lee JH, Febbraio M, Xie W. The emerging roles of fatty acid translocase/CD36 and the aryl hydrocarbon receptor in fatty liver disease. Exp Biol Med (Maywood) 2011;236:1116–21. https://doi.org/10.1258/ebm.2011.011128.

[104] Samuel VT, Liu Z-X, Wang A, Beddow SA, Geisler JG, Kahn M, et al. Inhibition of protein kinase Cepsilon prevents hepatic insulin resistance in nonalcoholic fatty liver disease. J Clin Invest 2007;117:739–45. https://doi.org/10.1172/JCI30400.

[105] Postic C, Girard J. Contribution of de novo fatty acid synthesis to hepatic steatosis and insulin resistance: lessons from genetically engineered mice. J Clin Invest 2008;118:829–38. https://doi.org/10.1172/JCI34275.

[106] Lambert JE, Ramos-Roman MA, Browning JD, Parks EJ. Increased de novo lipogenesis is a distinct characteristic of individuals with nonalcoholic fatty liver disease. Gastroenterology 2014;146:726–35. https://doi.org/10.1053/j.gastro.2013.11.049.

[107] Donnelly KL, Smith CI, Schwarzenberg SJ, Jessurun J, Boldt MD, Parks EJ. Sources of fatty acids stored in liver and secreted via lipoproteins in patients with nonalcoholic fatty liver disease. J Clin Invest 2005;115:1343–51. https://doi.org/10.1172/JCI23621.

[108] Li S, Brown MS, Goldstein JL. Bifurcation of insulin signaling pathway in rat liver: mTORC1 required for stimulation of lipogenesis, but not inhibition of gluconeogenesis. Proc Natl Acad Sci U S A 2010;107:3441–6. https://doi.org/10.1073/pnas.0914798107.

[109] Kammoun HL, Chabanon H, Hainault I, Luquet S, Magnan C, Koike T, et al. GRP78 expression inhibits insulin and ER stress-induced SREBP-1c activation and reduces hepatic steatosis in mice. J Clin Invest 2009;119:1201–15. https://doi.org/10.1172/JCI37007.

[110] Garcia D, Hellberg K, Chaix A, Wallace M, Herzig S, Badur MG, et al. Genetic Liver-Specific AMPK Activation Protects against Diet-Induced Obesity and NAFLD. Cell Rep 2019;26:192-208.e6. https://doi.org/10.1016/j.celrep.2018.12.036.

[111] Donadon V, Balbi M, Zanette G. Hyperinsulinemia and risk for hepatocellular carcinoma in patients with chronic liver diseases and Type 2 diabetes mellitus. Expert Rev Gastroenterol Hepatol 2009;3:465–7. https://doi.org/10.1586/egh.09.41.

[112] Aleksandrova K, Boeing H, Nothlings U, Jenab M, Fedirko V, Kaaks R, et al. Inflammatory and metabolic biomarkers and risk of liver and biliary tract cancer. Hepatology 2014;60:858–71. https://doi.org/10.1002/hep.27016.

[113] Chettouh H, Fartoux L, Aoudjehane L, Wendum D, Claperon A, Chretien Y, et al. Mitogenic insulin receptor-A is overexpressed in human hepatocellular carcinoma due to EGFR-mediated dysregulation of RNA splicing factors. Cancer Res 2013;73:3974–86. https://doi.org/10.1158/0008-5472.CAN-12-3824.

[114] Benabou E, Salame Z, Wendum D, Lequoy M, Tahraoui S, Merabtene F, et al. Insulin receptor isoform A favors tumor progression in human hepatocellular carcinoma by increasing stem/progenitor cell features. Cancer Lett 2019;450:155–68. https://doi.org/10.1016/j.canlet.2019.02.037.

[115] Belfiore A, Frasca F, Pandini G, Sciacca L, Vigneri R. Insulin receptor isoforms and insulin receptor/insulin-like growth factor receptor hybrids in physiology and disease. Endocr Rev 2009;30:586–623. https://doi.org/10.1210/er.2008-0047.

[116] Malaguarnera R, Sacco A, Voci C, Pandini G, Vigneri R, Belfiore A. Proinsulin binds with high affinity the insulin receptor isoform A and predominantly activates the mitogenic pathway. Endocrinology 2012;153:2152–63. https://doi.org/10.1210/en.2011-1843.

[117] Martinez-Quetglas I, Pinyol R, Dauch D, Torrecilla S, Tovar V, Moeini A, et al. IGF2 Is Up-regulated by Epigenetic Mechanisms in Hepatocellular Carcinomas and Is an Actionable Oncogene Product in Experimental Models. Gastroenterology 2016;151:1192–205. https://doi.org/10.1053/j.gastro.2016.09.001.

[118] Tanaka S, Wands JR. Insulin receptor substrate 1 overexpression in human

hepatocellular carcinoma cells prevents transforming growth factor beta1-induced apoptosis. Cancer Res 1996;56:3391–4.

[119] Boissan M, Beurel E, Wendum D, Rey C, Lecluse Y, Housset C, et al. Overexpression of insulin receptor substrate-2 in human and murine hepatocellular carcinoma. Am J Pathol 2005;167:869–77. https://doi.org/10.1016/S0002-9440(10)62058-5.

[120] Yoshikawa H, Matsubara K, Qian GS, Jackson P, Groopman JD, Manning JE, et al. SOCS-1, a negative regulator of the JAK/STAT pathway, is silenced by methylation in human hepatocellular carcinoma and shows growth-suppression activity. Nat Genet 2001;28:29–35. https://doi.org/10.1038/ng0501-29.

[121] Calvisi DF, Ladu S, Gorden A, Farina M, Conner EA, Lee J-S, et al. Ubiquitous activation of Ras and Jak/Stat pathways in human HCC. Gastroenterology 2006;130:1117–28. https://doi.org/10.1053/j.gastro.2006.01.006.

[122] Niwa Y, Kanda H, Shikauchi Y, Saiura A, Matsubara K, Kitagawa T, et al. Methylation silencing of SOCS-3 promotes cell growth and migration by enhancing JAK/STAT and FAK signalings in human hepatocellular carcinoma. Oncogene 2005;24:6406–17. https://doi.org/10.1038/sj.onc.1208788.

[123] Morzyglod L, Cauzac M, Popineau L, Denechaud P-D, Fajas L, Ragazzon B, et al. Growth factor receptor binding protein 14 inhibition triggers insulin-induced mouse hepatocyte proliferation and is associated with hepatocellular carcinoma. Hepatology 2017;65:1352–68. https://doi.org/10.1002/hep.28972.

[124] Vinciguerra M, Veyrat-Durebex C, Moukil MA, Rubbia-Brandt L, Rohner-Jeanrenaud F, Foti M. PTEN down-regulation by unsaturated fatty acids triggers hepatic steatosis via an NF-kappaBp65/mTOR-dependent mechanism. Gastroenterology 2008;134:268–80. https://doi.org/10.1053/j.gastro.2007.10.010.

[125] Lebeaupin C, Vallée D, Hazari Y, Hetz C, Chevet E. Endoplasmic reticulum stress signalling and the pathogenesis of non-alcoholic fatty liver disease. J Hepatol 2018;69:927–47. https://doi.org/10.1016/j.jhep.2018.06.008.

[126] Nakagawa H, Umemura A, Taniguchi K, Font-Burgada J, Dhar D, Ogata H, et al. ER stress cooperates with hypernutrition to trigger TNF-dependent spontaneous HCC development. Cancer Cell 2014;26:331–43. https://doi.org/10.1016/j.ccr.2014.07.001.

[127] Walter P, Ron D. The Unfolded Protein Response: From Stress Pathway to Homeostatic Regulation. Science (80-) 2011;334:1081 LP – 1086. https://doi.org/10.1126/science.1209038.

[128] Ozcan U, Cao Q, Yilmaz E, Lee A-H, Iwakoshi NN, Ozdelen E, et al. Endoplasmic reticulum stress links obesity, insulin action, and type 2 diabetes. Science 2004;306:457–61. https://doi.org/10.1126/science.1103160.

[129] Koliaki C, Szendroedi J, Kaul K, Jelenik T, Nowotny P, Jankowiak F, et al. Adaptation of hepatic mitochondrial function in humans with non-alcoholic fatty liver is lost in steatohepatitis. Cell Metab 2015;21:739–46. https://doi.org/10.1016/j.cmet.2015.04.004.

[130] Feldstein AE, Canbay A, Angulo P, Taniai M, Burgart LJ, Lindor KD, et al. Hepatocyte apoptosis and fas expression are prominent features of human nonalcoholic steatohepatitis. Gastroenterology 2003;125:437–43. https://doi.org/10.1016/s0016-5085(03)00907-7.

[131] Cazanave SC, Mott JL, Bronk SF, Werneburg NW, Fingas CD, Meng XW, et al. Death receptor 5 signaling promotes hepatocyte lipoapoptosis. J Biol Chem 2011;286:39336–48. https://doi.org/10.1074/jbc.M111.280420.

[132] Inokuchi-Shimizu S, Park EJ, Roh YS, Yang L, Zhang B, Song J, et al. TAK1-mediated autophagy and fatty acid oxidation prevent hepatosteatosis and tumorigenesis. J Clin Invest 2014;124:3566–78. https://doi.org/10.1172/JCI74068.

[133] Wiseman H, Halliwell B. Damage to DNA by reactive oxygen and nitrogen species: role in inflammatory disease and progression to cancer. Biochem J 1996;313 (Pt 1:17–29. https://doi.org/10.1042/bj3130017.

[134] Ohnishi S, Ma N, Thanan R, Pinlaor S, Hammam O, Murata M, et al. DNA damage in inflammation-related carcinogenesis and cancer stem cells. Oxid Med Cell Longev 2013;2013:387014. https://doi.org/10.1042/bj3130017.

[135] Yuan D, Huang S, Berger E, Liu L, Gross N, Heinzmann F, et al. Kupffer Cell-Derived Tnf Triggers Cholangiocellular Tumorigenesis through JNK due to Chronic Mitochondrial Dysfunction and ROS. Cancer Cell 2017;31:771-789.e6. https://doi.org/10.1016/j.ccell.2017.05.006.

[136] Canli O, Nicolas AM, Gupta J, Finkelmeier F, Goncharova O, Pesic M, et al. Myeloid Cell-Derived Reactive Oxygen Species Induce Epithelial Mutagenesis. Cancer Cell 2017;32:869-883.e5. https://doi.org/10.1016/j.ccell.2017.11.004.

[137] Daugherity EK, Balmus G, Al Saei A, Moore ES, Abi Abdallah D, Rogers AB, et al. The DNA damage checkpoint protein ATM promotes hepatocellular apoptosis and fibrosis in a mouse model of non-alcoholic fatty liver disease. Cell Cycle 2012;11:1918–28. https://doi.org/10.4161/cc.20259.

[138] Schults MA, Nagle PW, Rensen SS, Godschalk RW, Munnia A, Peluso M, et al. Decreased nucleotide excision repair in steatotic livers associates with myeloperoxidase-immunoreactivity. Mutat Res 2012;736:75–81. https://doi.org/10.1016/j.mrfmmm.2011.11.001.

[139] Hussain SP, Raja K, Amstad PA, Sawyer M, Trudel LJ, Wogan GN, et al. Increased p53 mutation load in nontumorous human liver of wilson disease and hemochromatosis: oxyradical overload diseases. Proc Natl Acad Sci U S A 2000;97:12770–5. https://doi.org/10.1073/pnas.220416097.

[140] Kwong M, Kan YW, Chan JY. The CNC basic leucine zipper factor, Nrf1, is essential for cell survival in response to oxidative stress-inducing agents. Role for Nrf1 in gamma-gcs(l) and gss expression in mouse fibroblasts. J Biol Chem 1999;274:37491–8. https://doi.org/10.1074/jbc.274.52.37491.

[141] Xu Z, Chen L, Leung L, Yen TSB, Lee C, Chan JY. Liver-specific inactivation of the Nrf1 gene in adult mouse leads to nonalcoholic steatohepatitis and hepatic neoplasia. Proc Natl Acad Sci U S A 2005;102:4120–5. https://doi.org/10.1073/pnas.0500660102.

[142] Csak T, Ganz M, Pespisa J, Kodys K, Dolganiuc A, Szabo G. Fatty acid and endotoxin activate inflammasomes in mouse hepatocytes that release danger signals to stimulate immune cells. Hepatology 2011;54:133–44. https://doi.org/10.1002/hep.24341.

[143] Parthasarathy G, Revelo X, Malhi H. Pathogenesis of Nonalcoholic Steatohepatitis: An Overview. Hepatol Commun 2020;4:478–92. https://doi.org/10.1002/hep4.1479.

[144] Hossain M, Kubes P. Innate immune cells orchestrate the repair of sterile injury in the liver and beyond. Eur J Immunol 2019;49:831–41. https://doi.org/10.1002/eji.201847485.

[145] Sutti S, Albano E. Adaptive immunity: an emerging player in the progression of NAFLD. Nat Rev Gastroenterol Hepatol 2020;17:81–92. https://doi.org/10.1038/s41575-019-0210-2.

[146] Tosello-Trampont A-C, Landes SG, Nguyen V, Novobrantseva TI, Hahn YS. Kuppfer cells trigger nonalcoholic steatohepatitis development in diet-induced mouse model through tumor necrosis factor-alpha production. J Biol Chem 2012;287:40161–72. https://doi.org/10.1074/jbc.M112.417014.

[147] Huang W, Metlakunta A, Dedousis N, Zhang P, Sipula I, Dube JJ, et al. Depletion of liver Kupffer cells prevents the development of diet-induced hepatic steatosis and insulin resistance. Diabetes 2010;59:347–57. https://doi.org/10.2337/db09-0016.

[148] Pan J, Ou Z, Cai C, Li P, Gong J, Ruan XZ, et al. Fatty acid activates NLRP3 inflammasomes in mouse Kupffer cells through mitochondrial DNA release. Cell Immunol 2018;332:111–20. https://doi.org/10.1016/j.cellimm.2018.08.006.

[149] Reid DT, Reyes JL, McDonald BA, Vo T, Reimer RA, Eksteen B. Kupffer Cells Undergo Fundamental Changes during the Development of Experimental NASH and Are Critical in Initiating Liver Damage and Inflammation. PLoS One 2016;11:e0159524. https://doi.org/10.1371/journal.pone.0159524.

[150] Chen J, Liang B, Bian D, Luo Y, Yang J, Li Z, et al. Knockout of neutrophil elastase protects against western diet induced nonalcoholic steatohepatitis in mice by regulating hepatic ceramides metabolism. Biochem Biophys Res Commun 2019;518:691–7. https://doi.org/10.1016/j.bbrc.2019.08.111.

[151] Rensen SS, Bieghs V, Xanthoulea S, Arfianti E, Bakker JA, Shiri-Sverdlov R, et al. Neutrophil-derived myeloperoxidase aggravates non-alcoholic steatohepatitis in low-density lipoprotein receptor-deficient mice. PLoS One 2012;7:e52411. https://doi.org/10.1371/journal.pone.0052411.

[152] van der Windt DJ, Sud V, Zhang H, Varley PR, Goswami J, Yazdani HO, et al. Neutrophil extracellular traps promote inflammation and development of hepatocellular carcinoma in nonalcoholic steatohepatitis. Hepatology 2018;68:1347–60. https://doi.org/10.1002/hep.29914.

[153] Kremer M, Hines IN, Milton RJ, Wheeler MD. Favored T helper 1 response in a mouse model of hepatosteatosis is associated with enhanced T cell-mediated hepatitis. Hepatology 2006;44:216–27. https://doi.org/10.1002/hep.21221.

[154] Bhattacharjee J, Kirby M, Softic S, Miles L, Salazar-Gonzalez R-M, Shivakumar P, et al. Hepatic Natural Killer T-cell and CD8+ T-cell Signatures in Mice with Nonalcoholic Steatohepatitis. Hepatol Commun 2017;1:299–310. https://doi.org/10.1002/hep4.1041.

[155] Ghazarian M, Revelo XS, Nohr MK, Luck H, Zeng K, Lei H, et al. Type I Interferon Responses Drive Intrahepatic T cells to Promote Metabolic Syndrome. Sci Immunol 2017;2. https://doi.org/10.1126/sciimmunol.aai7616.

[156] Koo S-Y, Park E-J, Lee C-W. Immunological distinctions between nonalcoholic steatohepatitis and hepatocellular carcinoma. Exp Mol Med 2020. https://doi.org/10.1038/s12276-020-0480-3.

[157] Wu J, Li J, Salcedo R, Mivechi NF, Trinchieri G, Horuzsko A. The proinflammatory myeloid cell receptor TREM-1 controls Kupffer cell activation and development of hepatocellular carcinoma. Cancer Res 2012;72:3977–86. https://doi.org/10.1158/0008-5472.CAN-12-0938.

[158] Malehmir M, Pfister D, Gallage S, Szydlowska M, Inverso D, Kotsiliti E, et al. Platelet GPIbalpha is a mediator and potential interventional target for NASH and subsequent liver cancer. Nat Med 2019;25:641–55. https://doi.org/10.1038/s41591-019-0379-5.

[159] Wolf MJ, Adili A, Piotrowitz K, Abdullah Z, Boege Y, Stemmer K, et al. Metabolic activation of intrahepatic CD8+ T cells and NKT cells causes nonalcoholic steatohepatitis and liver cancer via cross-talk with hepatocytes. Cancer Cell 2014;26:549–64. https://doi.org/10.1016/j.ccell.2014.09.003.

[160] Rakhra K, Bachireddy P, Zabuawala T, Zeiser R, Xu L, Kopelman A, et al. CD4(+) T cells contribute to the remodeling of the microenvironment required for sustained tumor regression upon oncogene inactivation. Cancer Cell 2010;18:485–98. https://doi.org/10.1016/j.ccr.2010.10.002.

[161] Kang T-W, Yevsa T, Woller N, Hoenicke L, Wuestefeld T, Dauch D, et al. Senescence surveillance of pre-malignant hepatocytes limits liver cancer development. Nature 2011;479:547–51. https://doi.org/10.1038/nature10599.

[162] Ma C, Kesarwala AH, Eggert T, Medina-Echeverz J, Kleiner DE, Jin P, et al. NAFLD causes selective CD4(+) T lymphocyte loss and promotes hepatocarcinogenesis. Nature 2016;531:253–7. https://doi.org/10.1038/nature16969.

[163] Shalapour S, Lin X-J, Bastian IN, Brain J, Burt AD, Aksenov AA, et al. Inflammation-induced IgA+ cells dismantle anti-liver cancer immunity. Nature 2017;551:340–5. https://doi.org/10.1038/nature24302.

[164] Cai L, Zhang Z, Zhou L, Wang H, Fu J, Zhang S, et al. Functional impairment in circulating and intrahepatic NK cells and relative mechanism in hepatocellular carcinoma patients. Clin Immunol 2008;129:428–37. https://doi.org/10.1016/j.clim.2008.08.012.

[165] Schnabl B, Brenner DA. Interactions between the intestinal microbiome and liver diseases. Gastroenterology 2014;146:1513–24. https://doi.org/10.1053/j.gastro.2014.01.020.

[166] Le Roy T, Llopis M, Lepage P, Bruneau A, Rabot S, Bevilacqua C, et al. Intestinal microbiota determines development of non-alcoholic fatty liver disease in mice. Gut 2013;62:1787–94. https://doi.org/10.1136/gutjnl-2012-303816.

[167] Leung C, Rivera L, Furness JB, Angus PW. The role of the gut microbiota in NAFLD. Nat Rev Gastroenterol Hepatol 2016;13:412–25. https://doi.org/10.1038/nrgastro.2016.85.

[168] Wigg AJ, Roberts-Thomson IC, Dymock RB, McCarthy PJ, Grose RH, Cummins AG. The role of small intestinal bacterial overgrowth, intestinal permeability, endotoxaemia, and tumour necrosis factor alpha in the pathogenesis of non-alcoholic steatohepatitis. Gut 2001;48:206–11. https://doi.org/10.1136/gut.48.2.206.

[169] Miele L, Valenza V, La Torre G, Montalto M, Cammarota G, Ricci R, et al. Increased intestinal permeability and tight junction alterations in nonalcoholic fatty liver disease. Hepatology 2009;49:1877–87. https://doi.org/10.1002/hep.22848.

[170] Loomba R, Seguritan V, Li W, Long T, Klitgord N, Bhatt A, et al. Gut Microbiome-Based Metagenomic Signature for Non-invasive Detection of Advanced Fibrosis in Human Nonalcoholic Fatty Liver Disease. Cell Metab 2019;30:607. https://doi.org/10.1016/j.cmet.2019.08.002.

[171] Dapito DH, Mencin A, Gwak G-Y, Pradere J-P, Jang M-K, Mederacke I, et al. Promotion of hepatocellular carcinoma by the intestinal microbiota and TLR4. Cancer Cell 2012;21:504–16. https://doi.org/10.1016/j.ccr.2012.02.007.

[172] Chavez-Talavera O, Tailleux A, Lefebvre P, Staels B. Bile Acid Control of Metabolism and Inflammation in Obesity, Type 2 Diabetes, Dyslipidemia, and Nonalcoholic Fatty Liver Disease. Gastroenterology 2017;152:1679-1694.e3. https://doi.org/10.1053/j.gastro.2017.01.055.

[173] Wang X, Fu X, Van Ness C, Meng Z, Ma X, Huang W. Bile Acid Receptors and Liver Cancer. Curr Pathobiol Rep 2013;1:29–35. https://doi.org/10.1007/s40139-012-0003-6.

[174] Jansen PLM. Endogenous bile acids as carcinogens. J Hepatol 2007;47:434–5. https://doi.org/10.1016/j.jhep.2007.06.001.

[175] Chiang JYL. Bile acid metabolism and signaling in liver disease and therapy. Liver Res 2017;1:3–9. https://doi.org/10.1016/j.livres.2017.05.001.

[176] Angulo P, Kleiner DE, Dam-Larsen S, Adams LA, Bjornsson ES, Charatcharoenwitthaya P, et al. Liver Fibrosis, but No Other Histologic Features, Is Associated With Long-term Outcomes of Patients With Nonalcoholic Fatty Liver Disease. Gastroenterology 2015;149:389-97.e10. https://doi.org/10.1053/j.gastro.2015.04.043.

[177] Seki E, De Minicis S, Osterreicher CH, Kluwe J, Osawa Y, Brenner DA, et al. TLR4 enhances TGF-beta signaling and hepatic fibrosis. Nat Med 2007;13:1324–32. https://doi.org/10.1038/nm1663.

[178] Jiang JX, Chen X, Fukada H, Serizawa N, Devaraj S, Torok NJ. Advanced glycation endproducts induce fibrogenic activity in nonalcoholic steatohepatitis by modulating TNF-alpha-converting enzyme activity in mice. Hepatology 2013;58:1339–48. https://doi.org/10.1002/hep.26491.

[179] Wang X, Zheng Z, Caviglia JM, Corey KE, Herfel TM, Cai B, et al. Hepatocyte TAZ/WWTR1 Promotes Inflammation and Fibrosis in Nonalcoholic Steatohepatitis. Cell Metab 2016;24:848–62. https://doi.org/10.1016/j.cmet.2016.09.016.

[180] Schwimmer JB, Celedon MA, Lavine JE, Salem R, Campbell N, Schork NJ, et al. Heritability of nonalcoholic fatty liver disease. Gastroenterology 2009;136:1585–92. https://doi.org/10.1053/j.gastro.2009.01.050.

[181] Wagenknecht LE, Scherzinger AL, Stamm ER, Hanley AJG, Norris JM, Chen Y-DI, et al. Correlates and heritability of nonalcoholic fatty liver disease in a minority cohort. Obesity (Silver Spring) 2009;17:1240–6. https://doi.org/10.1038/oby.2009.4.

[182] Speliotes EK, Yerges-Armstrong LM, Wu J, Hernaez R, Kim LJ, Palmer CD, et al. Genome-wide association analysis identifies variants associated with nonalcoholic fatty liver disease that have distinct effects on metabolic traits. PLoS Genet 2011;7:e1001324. https://doi.org/10.1371/journal.pgen.1001324.

[183] Palmer ND, Musani SK, Yerges-Armstrong LM, Feitosa MF, Bielak LF, Hernaez R, et al. Characterization of European ancestry nonalcoholic fatty liver disease-associated variants in individuals of African and Hispanic descent. Hepatology 2013;58:966–75. https://doi.org/10.1002/hep.26440.

[184] Romeo S, Kozlitina J, Xing C, Pertsemlidis A, Cox D, Pennacchio LA, et al. Genetic variation in PNPLA3 confers susceptibility to nonalcoholic fatty liver disease. Nat Genet 2008;40:1461–5. https://doi.org/10.1038/ng.257.

[185] Huang Y, He S, Li JZ, Seo Y-K, Osborne TF, Cohen JC, et al. A feed-forward loop amplifies nutritional regulation of PNPLA3. Proc Natl Acad Sci U S A 2010;107:7892–7. https://doi.org/10.1073/pnas.1003585107.

[186] Pirazzi C, Valenti L, Motta BM, Pingitore P, Hedfalk K, Mancina RM, et al. PNPLA3 has retinyl-palmitate lipase activity in human hepatic stellate cells. Hum Mol Genet 2014;23:4077–85. https://doi.org/10.1093/hmg/ddu121.

[187] BasuRay S, Smagris E, Cohen JC, Hobbs HH. The PNPLA3 variant associated with fatty liver disease (I148M) accumulates on lipid droplets by evading ubiquitylation. Hepatology 2017;66:1111–24. https://doi.org/10.1002/hep.29273.

[188] Luukkonen PK, Nick A, Holtta-Vuori M, Thiele C, Isokuortti E, Lallukka-Bruck S, et al. Human PNPLA3-I148M variant increases hepatic retention of polyunsaturated fatty acids. JCI Insight 2019;4. https://doi.org/10.1172/jci.insight.127902.

[189] Liu Y-L, Patman GL, Leathart JBS, Piguet A-C, Burt AD, Dufour J-F, et al. Carriage of the PNPLA3 rs738409 C >G polymorphism confers an increased risk of non-alcoholic fatty liver disease associated hepatocellular carcinoma. J Hepatol 2014;61:75–81. https://doi.org/10.1016/j.jhep.2014.02.030.

[190] Singal AG, Manjunath H, Yopp AC, Beg MS, Marrero JA, Gopal P, et al. The effect of PNPLA3 on fibrosis progression and development of hepatocellular carcinoma: a meta-analysis. Am J Gastroenterol 2014;109:325–34. https://doi.org/10.1038/ajg.2013.476.

[191] Schulze K, Imbeaud S, Letouze E, Alexandrov LB, Calderaro J, Rebouissou S, et al. Exome sequencing of hepatocellular carcinomas identifies new mutational signatures and potential therapeutic targets. Nat Genet 2015;47:505–11. https://doi.org/10.1038/ng.3252.

[192] Kozlitina J, Smagris E, Stender S, Nordestgaard BG, Zhou HH, Tybjaerg-Hansen A, et al. Exome-wide association study identifies a TM6SF2 variant that confers susceptibility to nonalcoholic fatty liver disease. Nat Genet 2014;46:352–6. https://doi.org/10.1038/ng.2901.

[193] Mahdessian H, Taxiarchis A, Popov S, Silveira A, Franco-Cereceda A, Hamsten A, et al. TM6SF2 is a regulator of liver fat metabolism influencing triglyceride secretion and hepatic lipid droplet content. Proc Natl Acad Sci U S A 2014;111:8913–8. https://doi.org/10.1073/pnas.1323785111.

[194] Petta S, Miele L, Bugianesi E, Camma C, Rosso C, Boccia S, et al. Glucokinase regulatory protein gene polymorphism affects liver fibrosis in non-alcoholic fatty liver disease. PLoS One 2014;9:e87523. https://doi.org/10.1371/journal.pone.0087523.

[195] Mancina RM, Dongiovanni P, Petta S, Pingitore P, Meroni M, Rametta R, et al. The MBOAT7-TMC4 Variant rs641738 Increases Risk of Nonalcoholic Fatty Liver Disease in Individuals of European Descent. Gastroenterology 2016;150:1219-1230.e6. https://doi.org/10.1053/j.gastro.2016.01.032.

[196] Gellert-Kristensen H, Nordestgaard BG, Tybjaerg-Hansen A, Stender S. High Risk of Fatty Liver Disease Amplifies the Alanine Transaminase-Lowering Effect of a HSD17B13 Variant. Hepatology 2020;71:56–66. https://doi.org/10.1002/hep.30799.

[197] Ma Y, Belyaeva O V, Brown PM, Fujita K, Valles K, Karki S, et al. 17-Beta Hydroxysteroid Dehydrogenase 13 Is a Hepatic Retinol Dehydrogenase Associated With Histological Features of Nonalcoholic Fatty Liver Disease. Hepatology 2019;69:1504–19. https://doi.org/10.1002/hep.30350.

[198] Abul-Husn NS, Cheng X, Li AH, Xin Y, Schurmann C, Stevis P, et al. A Protein-Truncating HSD17B13 Variant and Protection from Chronic Liver Disease. N Engl J Med 2018;378:1096–106. https://doi.org/10.1056/NEJMoa1712191.

[199] Kuramoto J, Arai E, Tian Y, Funahashi N, Hiramoto M, Nammo T, et al. Genome-wide DNA methylation analysis during non-alcoholic steatohepatitis-related multistage hepatocarcinogenesis: comparison with hepatitis virus-related carcinogenesis. Carcinogenesis 2017;38:261–70. https://doi.org/10.1093/carcin/bgx005.

[200] Cheung O, Puri P, Eicken C, Contos MJ, Mirshahi F, Maher JW, et al. Nonalcoholic steatohepatitis is associated with altered hepatic MicroRNA expression. Hepatology 2008;48:1810–20. https://doi.org/10.1002/hep.22569.

[201] Hsu S-H, Wang B, Kota J, Yu J, Costinean S, Kutay H, et al. Essential metabolic, anti-inflammatory, and anti-tumorigenic functions of miR-122 in liver. J Clin Invest 2012;122:2871–83. https://doi.org/10.1172/JCI63539.

[202] Gougelet A, Sartor C, Bachelot L, Godard C, Marchiol C, Renault G, et al. Antitumour activity of an inhibitor of miR-34a in liver cancer with beta-catenin-mutations. Gut 2016;65:1024–34. https://doi.org/10.1136/gutjnl-2014-308969.

[203] Matthews DR, Hosker JP, Rudenski AS, Naylor BA, Treacher DF, Turner RC. Homeostasis model assessment: insulin resistance and beta-cell function from fasting plasma glucose and insulin concentrations in man. Diabetologia 1985;28:412–9. https://doi.org/10.1007/bf00280883.

[204] Sasso M, Beaugrand M, de Ledinghen V, Douvin C, Marcellin P, Poupon R, et al. Controlled attenuation parameter (CAP): a novel VCTE guided ultrasonic attenuation measurement for the evaluation of hepatic steatosis: preliminary study and validation in a cohort of patients with chronic liver disease from various causes. Ultrasound Med Biol 2010;36:1825–35. https://doi.org/10.1016/j.ultrasmedbio.2010.07.005.

[205] Reeder SB, Hu HH, Sirlin CB. Proton density fat-fraction: a standardized MR-based biomarker of tissue fat concentration. J Magn Reson Imaging 2012;36:1011–4. https://doi.org/10.1002/jmri.23741.

[206] Bedossa P. Utility and appropriateness of the fatty liver inhibition of progression (FLIP) algorithm and steatosis, activity, and fibrosis (SAF) score

in the evaluation of biopsies of nonalcoholic fatty liver disease. Hepatology 2014;60:565–75. https://doi.org/10.1002/hep.27173.

[207] Tang A, Cloutier G, Szeverenyi NM, Sirlin CB. Ultrasound Elastography and MR Elastography for Assessing Liver Fibrosis: Part 1, Principles and Techniques. AJR Am J Roentgenol 2015;205:22–32. https://doi.org/10.2214/AJR.15.14552.

[208] Pennisi G, Celsa C, Giammanco A, Spatola F, Petta S. The Burden of Hepatocellular Carcinoma in Non-Alcoholic Fatty Liver Disease: Screening Issue and Future Perspectives. Int J Mol Sci 2019;20. https://doi.org/10.3390/ijms20225613.

[209] Anstee QM, Reeves HL, Kotsiliti E, Govaere O, Heikenwalder M. From NASH to HCC: current concepts and future challenges. Nat Rev Gastroenterol Hepatol 2019;16:411–28. https://doi.org/10.1038/s41575-019-0145-7.

[210] Ogle LF, Orr JG, Willoughby CE, Hutton C, McPherson S, Plummer R, et al. Imagestream detection and characterisation of circulating tumour cells - A liquid biopsy for hepatocellular carcinoma? J Hepatol 2016;65:305–13. https://doi.org/10.1016/j.jhep.2016.04.014.

[211] Mundi MS, Velapati S, Patel J, Kellogg TA, Abu Dayyeh BK, Hurt RT. Evolution of NAFLD and Its Management. Nutr Clin Pract 2020;35:72–84. https://doi.org/10.1002/ncp.10449.

[212] Kim DW, Talati C, Kim R. Hepatocellular carcinoma (HCC): beyond sorafenib-chemotherapy. J Gastrointest Oncol 2017;8:256–65. https://doi.org/10.21037/jgo.2016.09.07.

[213] Llovet JM, Ricci S, Mazzaferro V, Hilgard P, Gane E, Blanc J-F, et al. Sorafenib in advanced hepatocellular carcinoma. N Engl J Med 2008;359:378–90. https://doi.org/10.1056/NEJMoa0708857.

[214] Personeni N, Pressiani T, Rimassa L. Lenvatinib for the treatment of unresectable hepatocellular carcinoma: evidence to date. J Hepatocell Carcinoma 2019;6:31–9. https://doi.org/10.2147/JHC.S168953.

[215] Personeni N, Pressiani T, Santoro A, Rimassa L. Regorafenib in hepatocellular carcinoma: latest evidence and clinical implications. Drugs Context 2018;7:212533. https://doi.org/10.7573/dic.212533.

[216] Gurzov EN, Tran M, Fernandez-Rojo MA, Merry TL, Zhang X, Xu Y, et al. Hepatic oxidative stress promotes insulin-STAT-5 signaling and obesity by inactivating protein tyrosine phosphatase N2. Cell Metab 2014;20:85–102. https://doi.org/10.1016/j.cmet.2014.05.011.

[217] Grohmann M, Wiede F, Dodd GT, Gurzov EN, Ooi GJ, Butt T, et al. Obesity Drives STAT-1-Dependent NASH and STAT-3-Dependent HCC. Cell 2018;175:1289-1306.e20. https://doi.org/10.1016/j.cell.2018.09.053.

[218] Zabolotny JM, Bence-Hanulec KK, Stricker-Krongrad A, Haj F, Wang Y, Minokoshi Y, et al. PTP1B regulates leptin signal transduction in vivo. Dev

Cell 2002;2:489–95. https://doi.org/10.1016/s1534-5807(02)00148-x.

[219] Asante-Appiah E, Kennedy BP. Protein tyrosine phosphatases: the quest for negative regulators of insulin action. Am J Physiol Endocrinol Metab 2003;284:E663-70. https://doi.org/10.1152/ajpendo.00462.2002.

[220] Elchebly M, Payette P, Michaliszyn E, Cromlish W, Collins S, Loy AL, et al. Increased insulin sensitivity and obesity resistance in mice lacking the protein tyrosine phosphatase-1B gene. Science 1999;283:1544–8. https://doi.org/10.1126/science.283.5407.1544.

[221] Delibegovic M, Zimmer D, Kauffman C, Rak K, Hong E-G, Cho Y-R, et al. Liver-specific deletion of protein-tyrosine phosphatase 1B (PTP1B) improves metabolic syndrome and attenuates diet-induced endoplasmic reticulum stress. Diabetes 2009;58:590–9. https://doi.org/10.2337/db08-0913.

[222] Gonzalez-Rodriguez A, Valdecantos MP, Rada P, Addante A, Barahona I, Rey E, et al. Dual role of protein tyrosine phosphatase 1B in the progression and reversion of non-alcoholic steatohepatitis. Mol Metab 2018;7:132–46. https://doi.org/10.1016/j.molmet.2017.10.008.

[223] Wu JJ, Roth RJ, Anderson EJ, Hong E, Lee M, Choi CS, et al. Mice lacking MAP kinase phosphatase-1 have enhanced MAP kinase activity and resistance to diet-induced obesity 2006:61–73. https://doi.org/10.1016/j.cmet.2006.05.010.

[224] Flach RJR, Qin H, Zhang L, Bennett AM. Loss of mitogen-activated protein kinase phosphatase-1 protects from hepatic steatosis by repression of cell death-inducing DNA fragmentation factor A (DFFA)-like effector C (CIDEC)/fat-specific protein 27. J Biol Chem 2011;286:22195–202. https://doi.org/10.1074/jbc.M110.210237.

[225] Lawan A, Zhang L, Gatzke F, Min K, Jurczak MJ, Al-Mutairi M, et al. Hepatic mitogen-activated protein kinase phosphatase 1 selectively regulates glucose metabolism and energy homeostasis. Mol Cell Biol 2015;35:26–40. https://doi.org/10.1128/MCB.00503-14.

[226] Tsujita E, Taketomi A, Gion T, Kuroda Y, Endo K, Watanabe A, et al. Suppressed MKP-1 is an independent predictor of outcome in patients with hepatocellular carcinoma. Oncology 2005;69:342–7. https://doi.org/10.1159/000089766.

[227] Yang B, Tan Y, Sun H, Fan J, Tang Z, Ji Y. Higher intratumor than peritumor expression of DUSP6/MKP-3 is associated with recurrence after curative resection of hepatocellular carcinoma. Chin Med J (Engl) 2014;127:1211–7.

[228] Emanuelli B, Eberle D, Suzuki R, Kahn CR. Overexpression of the dual-specificity phosphatase MKP-4/DUSP-9 protects against stress-induced insulin resistance. Proc Natl Acad Sci U S A 2008;105:3545–50. https://doi.org/10.1073/pnas.0712275105.

[229] Liu J, Ni W, Xiao M, Jiang F, Ni R. Decreased expression and prognostic role

of mitogen-activated protein kinase phosphatase 4 in hepatocellular carcinoma. J Gastrointest Surg 2013;17:756–65. https://doi.org/10.1007/s11605-013-2138-0.

[230] Shen Z, Zhang C, Qu L, Lu C, Xiao M, Ni R, et al. MKP-4 suppresses hepatocarcinogenesis by targeting ERK1/2 pathway. Cancer Cell Int 2019;19:61. https://doi.org/10.1186/s12935-019-0776-3.

[231] Ye P, Xiang M, Liao H, Liu J, Luo H, Wang Y, et al. Dual-Specificity Phosphatase 9 Protects Against Nonalcoholic Fatty Liver Disease in Mice Through ASK1 Suppression 2019;69:76–93. https://doi.org/10.1002/hep.30198.

[232] Wu Y-K, Hu L-F, Lou D-S, Wang B-C, Tan J. Targeting DUSP16/TAK1 signaling alleviates hepatic dyslipidemia and inflammation in high fat diet (HFD)-challenged mice through suppressing JNK MAPK. Biochem Biophys Res Commun 2020;524:142–9. https://doi.org/10.1016/j.bbrc.2020.01.037.

[233] Wu L, Liu Y, Zhao Y, Li M, Guo L. Targeting DUSP7 signaling alleviates hepatic steatosis, inflammation and oxidative stress in high fat diet (HFD)-fed mice via suppression of TAK1. Free Radic Biol Med 2020. https://doi.org/10.1016/j.freeradbiomed.2020.04.009.

[234] Huang Z, Wu LM, Zhang JL, Sabri A, Wang SJ, Qin GJ, et al. Dual Specificity Phosphatase 12 Regulates Hepatic Lipid Metabolism Through Inhibition of the Lipogenesis and Apoptosis Signal–Regulating Kinase 1 Pathways. Hepatology 2019;70:1099–118. https://doi.org/10.1002/hep.30597.

[235] Ye P, Liu J, Xu W, Liu D, Ding X, Le S, et al. Dual-Specificity Phosphatase 26 Protects Against Nonalcoholic Fatty Liver Disease in Mice Through Transforming Growth Factor Beta–Activated Kinase 1 Suppression. Hepatology 2019;69:1946–64. https://doi.org/10.1002/hep.30485.

[236] Wang D, Han S, Peng R, Jiao C, Wang X, Han Z, et al. DUSP28 contributes to human hepatocellular carcinoma via regulation of the p38 MAPK signaling. Int J Oncol 2014;45:2596–604. https://doi.org/10.3892/ijo.2014.2653.

[237] Sanchez-Pareja A, Clement S, Peyrou M, Spahr L, Negro F, Rubbia-Brandt L, et al. Phosphatase and tensin homolog is a differential diagnostic marker between nonalcoholic and alcoholic fatty liver disease. World J Gastroenterol 2016;22:3735–45. https://doi.org/10.3748/wjg.v22.i14.3735.

[238] Horie Y, Suzuki A, Kataoka E, Sasaki T, Hamada K, Sasaki J, et al. Hepatocyte-specific Pten deficiency results in steatohepatitis and hepatocellular carcinomas. J Clin Invest 2004;113:1774–83. https://doi.org/10.1172/JCI20513.

[239] Stiles B, Wang Y, Stahl A, Bassilian S, Lee WP, Kim Y-J, et al. Liver-specific deletion of negative regulator Pten results in fatty liver and insulin hypersensitivity [corrected]. Proc Natl Acad Sci U S A 2004;101:2082–7. https://doi.org/10.1073/pnas.0308617100.

[240] Luo X, Liao R, Hanley KL, Zhu HH, Malo KN, Hernandez C, et al. Dual Shp2 and Pten Deficiencies Promote Non-alcoholic Steatohepatitis and Genesis of Liver Tumor-Initiating Cells. Cell Rep 2016;17:2979–93. https://doi.org/10.1016/j.celrep.2016.11.048.

[241] Bahri MA, Warnock G, Plenevaux A, Choquet P, Constantinesco A, Salmon E, et al. Performance evaluation of the General Electric eXplore CT 120 micro-CT using the vmCT phantom. Nucl Instruments Methods Phys Res Sect A Accel Spectrometers, Detect Assoc Equip 2011;648:S181–5. https://doi.org/10.1016/j.nima.2010.11.178.

[242] Caldwell S, Ikura Y, Dias D, Isomoto K, Yabu A, Moskaluk C, et al. Hepatocellular ballooning in NASH. J Hepatol 2010;53:719–23. https://doi.org/10.1016/j.jhep.2010.04.031.

[243] Love MI, Huber W, Anders S. Moderated estimation of fold change and dispersion for RNA-seq data with DESeq2. Genome Biol 2014;15:550. https://doi.org/10.1186/s13059-014-0550-8.

[244] Zhu A, Ibrahim JG, Love MI. Heavy-tailed prior distributions for sequence count data: removing the noise and preserving large differences. Bioinformatics 2019;35:2084–92. https://doi.org/10.1093/bioinformatics/bty895.

[245] Singh P, Dejager L, Amand M, Theatre E, Vandereyken M, Zurashvili T, et al. DUSP3 Genetic Deletion Confers M2-like Macrophage-Dependent Tolerance to Septic Shock. J Immunol 2015;194:4951–62. https://doi.org/10.4049/jimmunol.1402431.

[246] Lievens D, von Hundelshausen P. Platelets in atherosclerosis. Thromb Haemost 2011;106:827–38. https://doi.org/10.1160/TH11-08-0592.

[247] Parlee SD, Lentz SI, Mori H, MacDougald OA. Quantifying size and number of adipocytes in adipose tissue. Methods Enzymol 2014;537:93–122. https://doi.org/10.1016/B978-0-12-411619-1.00006-9.

[248] Gabay C, Kushner I. Acute-phase proteins and other systemic responses to inflammation. N Engl J Med 1999;340:448–54. https://doi.org/10.1056/NEJM199902113400607.

[249] Gao B, Tsukamoto H. Inflammation in Alcoholic and Nonalcoholic Fatty Liver Disease: Friend or Foe? Gastroenterology 2016;150:1704–9. https://doi.org/10.1053/j.gastro.2016.01.025.

[250] Van Herck MA, Weyler J, Kwanten WJ, Dirinck EL, De Winter BY, Francque SM, et al. The Differential Roles of T Cells in Non-alcoholic Fatty Liver Disease and Obesity. Front Immunol 2019;10:82. https://doi.org/10.3389/fimmu.2019.00082.

[251] Kazankov K, Jorgensen SMD, Thomsen KL, Moller HJ, Vilstrup H, George J, et al. The role of macrophages in nonalcoholic fatty liver disease and nonalcoholic steatohepatitis. Nat Rev Gastroenterol Hepatol 2019;16:145–59.

https://doi.org/10.1038/s41575-018-0082-x.

[252] Engin A. Non-Alcoholic Fatty Liver Disease. In: Engin AB, Engin A, editors. Obes. Lipotoxicity, Cham: Springer International Publishing; 2017, p. 443–67. https://doi.org/10.1007/978-3-319-48382-5_19.

[253] Vesselinovitch SD, Koka M, Mihailovich N, Rao K V. Carcinogenicity of diethylnitrosamine in newborn, infant, and adult mice. J Cancer Res Clin Oncol 1984;108:60–5. https://doi.org/10.1007/BF00390974.

[254] Tolba R, Kraus T, Liedtke C, Schwarz M, Weiskirchen R. Diethylnitrosamine (DEN)-induced carcinogenic liver injury in mice. Lab Anim 2015;49:59–69. https://doi.org/10.1177/0023677215570086.

[255] Nakai H, Fuess S, Storm TA, Muramatsu S, Nara Y, Kay MA. Unrestricted hepatocyte transduction with adeno-associated virus serotype 8 vectors in mice. J Virol 2005;79:214–24. https://doi.org/10.1128/JVI.79.1.214-224.2005.

[256] Yu L-X, Yan H-X, Liu Q, Yang W, Wu H-P, Dong W, et al. Endotoxin accumulation prevents carcinogen-induced apoptosis and promotes liver tumorigenesis in rodents. Hepatology 2010;52:1322–33. https://doi.org/10.1002/hep.23845.

[257] Hoffstedt J, Arner E, Wahrenberg H, Andersson DP, Qvisth V, Löfgren P, et al. Regional impact of adipose tissue morphology on the metabolic profile in morbid obesity. Diabetologia 2010;53:2496–503. https://doi.org/10.1007/s00125-010-1889-3.

[258] Weyer C, Foley JE, Bogardus C, Tataranni PA, Pratley RE. Enlarged subcutaneous abdominal adipocyte size, but not obesity itself, predicts type II diabetes independent of insulin resistance. Diabetologia 2000;43:1498–506. https://doi.org/10.1007/s001250051560.

[259] Engin A. The Pathogenesis of Obesity-Associated Adipose Tissue Inflammation. In: Engin AB, Engin A, editors. Obes. Lipotoxicity, Cham: Springer International Publishing; 2017, p. 221–45. https://doi.org/10.1007/978-3-319-48382-5_9.

[260] Stolarczyk E. Adipose tissue inflammation in obesity: a metabolic or immune response? Curr Opin Pharmacol 2017;37:35–40. https://doi.org/10.1016/j.coph.2017.08.006.

[261] Arguello G, Balboa E, Arrese M, Zanlungo S. Recent insights on the role of cholesterol in non-alcoholic fatty liver disease. Biochim Biophys Acta 2015;1852:1765–78. https://doi.org/10.1016/j.bbadis.2015.05.015.

[262] Kotzka J, Müller-Wieland D, Roth G, Kremer L, Munck M, Schürmann S, et al. Sterol regulatory element binding proteins (SREBP)-1a and SREBP-2 are linked to the MAP-kinase cascade. J Lipid Res 2000;41:99–108.

[263] Kotzka J, Knebel B, Haas J, Kremer L, Jacob S, Hartwig S, et al. Preventing phosphorylation of sterol regulatory element-binding protein 1a by MAP-

kinases protects mice from fatty liver and visceral obesity. PLoS One 2012;7:e32609. https://doi.org/10.1371/journal.pone.0032609.

[264] Czech MP, Tencerova M, Pedersen DJ, Aouadi M. Insulin signalling mechanisms for triacylglycerol storage. Diabetologia 2013;56:949–64. https://doi.org/10.1007/s00125-013-2869-1.

[265] Koska J, Stefan N, Permana PA, Weyer C, Sonoda M, Bogardus C, et al. Increased fat accumulation in liver may link insulin resistance with subcutaneous abdominal adipocyte enlargement, visceral adiposity, and hypoadiponectinemia in obese individuals. Am J Clin Nutr 2008;87:295–302. https://doi.org/10.1093/ajcn/87.2.295.

[266] Biddinger SB, Hernandez-Ono A, Rask-Madsen C, Haas JT, Alemán JO, Suzuki R, et al. Hepatic insulin resistance is sufficient to produce dyslipidemia and susceptibility to atherosclerosis. Cell Metab 2008;7:125–34. https://doi.org/10.1016/j.cmet.2007.11.013.

[267] Haas JT, Miao J, Chanda D, Wang Y, Zhao E, Haas ME, et al. Hepatic insulin signaling is required for obesity-dependent expression of SREBP-1c mRNA but not for feeding-dependent expression. Cell Metab 2012;15:873–84. https://doi.org/10.1016/j.cmet.2012.05.002.

[268] Semple RK, Sleigh A, Murgatroyd PR, Adams CA, Bluck L, Jackson S, et al. Postreceptor insulin resistance contributes to human dyslipidemia and hepatic steatosis. J Clin Invest 2009;119:315–22. https://doi.org/10.1172/JCI37432.

[269] Jing Z-T, Liu W, Xue C-R, Wu S-X, Chen W-N, Lin X-J, et al. AKT activator SC79 protects hepatocytes from TNF-α-mediated apoptosis and alleviates d-Gal/LPS-induced liver injury. Am J Physiol Liver Physiol 2019;316:G387–96. https://doi.org/10.1152/ajpgi.00350.2018.

[270] Li C, Li Y, He L, Agarwal AR, Zeng N, Cadenas E, et al. PI3K/AKT signaling regulates bioenergetics in immortalized hepatocytes. Free Radic Biol Med 2013;60:29–40. https://doi.org/10.1016/j.freeradbiomed.2013.01.013.

[271] Oliveira AG, Araújo TG, Carvalho B de M, Rocha GZ, Santos A, Saad MJA. The Role of Hepatocyte Growth Factor (HGF) in Insulin Resistance and Diabetes. Front Endocrinol (Lausanne) 2018;9:503. https://doi.org/10.3389/fendo.2018.00503.

[272] Chen H. Nutrient mTORC1 signaling contributes to hepatic lipid metabolism in the pathogenesis of non-alcoholic fatty liver disease. Liver Res 2020;4:15–22. https://doi.org/10.1016/j.livres.2020.02.004.

[273] Xu A, Wang B, Fu J, Qin W, Yu T, Yang Z, et al. Diet-induced hepatic steatosis activates Ras to promote hepatocarcinogenesis via CPT1α. Cancer Lett 2019;442:40–52. https://doi.org/10.1016/j.canlet.2018.10.024.

[274] Lokau J, Schoeder V, Haybaeck J, Garbers C. Jak-Stat Signaling Induced by Interleukin-6 Family Cytokines in Hepatocellular Carcinoma. Cancers (Basel) 2019;11. https://doi.org/10.3390/cancers11111704.

[275] He G, Yu G-Y, Temkin V, Ogata H, Kuntzen C, Sakurai T, et al. Hepatocyte IKKbeta/NF-kappaB inhibits tumor promotion and progression by preventing oxidative stress-driven STAT3 activation. Cancer Cell 2010;17:286–97. https://doi.org/10.1016/j.ccr.2009.12.048.

[276] Yin L, Chang C, Xu C. G2/M checkpoint plays a vital role at the early stage of HCC by analysis of key pathways and genes. Oncotarget 2017;8:76305–17. https://doi.org/10.18632/oncotarget.19351.

[277] Gao D, Nong S, Huang X, Lu Y, Zhao H, Lin Y, et al. The effects of palmitate on hepatic insulin resistance are mediated by NADPH Oxidase 3-derived reactive oxygen species through JNK and p38MAPK pathways. J Biol Chem 2010;285:29965–73. https://doi.org/10.1074/jbc.M110.128694.

[278] Arab JP, Karpen SJ, Dawson PA, Arrese M, Trauner M. Bile acids and nonalcoholic fatty liver disease: Molecular insights and therapeutic perspectives. Hepatology 2017;65:350–62. https://doi.org/10.1002/hep.28709.